Conte, Giuseppe (2000) An experimental study for the characterisation of gas/liquid flow splitting at T-junctions. PhD thesis, University of Nottingham.

University of Nottingham

School of Chemical, Environmental and Mining Engineering

An Experimental Study for the Characterisation of Gas/Liquid Flow Splitting at T-junctions

By

Giuseppe Conte (Laurea)

Thesis submitted to the University of Nottingham for the degree of
Doctor of Philosophy
October 2000

To my mother, my grandmother and my sister

Acknowledgements

In the first place, I would like to express my gratitude to Prof. Barry Azzopardi. His guidance and his trust also outside of the supervision of this work have given me uncommon opportunities. I thank him for leading me with the strength of his example rather than by plain authority. Special thanks also to my second supervisor, Dr John Hills for his acute criticism and invaluable help during the writing up.

Thank you to the staff of the Chem. Eng. Workshop. Each of the gentlemen and ladies involved with technical issues have been, at different stages of this experience, essential for the progressive achievements that have led to this result.

Many thanks to all the colleagues of Research Rooms 6, 8 and B8 that have finished and started the experience of a Ph.D. during my permanence at Nottingham University. I wish them all well in their future. Thanks also to the people visiting for shorter projects that I have made friends with and to the students that I have supervised for Undergraduate and M. Eng. Research Projects. In particular Aarti, Jon and Tim.

Thank you to the friends that I have made at Lincoln Hall of Residence. The warden, Dr Joanne Wright and all the fellow tutors have made my life and studies in Nottingham a more meaningful experience and have contributed to building the equilibrium that I needed in the final stages.

Thank you to my mates back in Italy who have always been in touch and always ready to change plans for my visits back home. In particular I would like to thank my friends Davide, Flavio, Gianluca and Ottavio with whom I have continued to share a path of growth, even though so far apart.

I am grateful to Samantha, just for being there and for her support, especially during the writing up period explosively mixed with my job-hunting campaign. I would like to express all my esteem and appreciation and the belief that she will achieve and deserve all her ambitious targets.

May I thank my close family in the persons of my mother Rosa, my grandmother Luisa and my sister Tina to whom I dedicate this work and the four years that have led to it. Without their example, understanding and encouragement this would never have been possible. Many thanks also to my uncles, aunts and cousins.

Finally, I should not and would never forget to thank my loved father Alfonso, who is elsewhere looking upon our lives. Perhaps in the glory of God, certainly in a place in my heart from where, from time to time, strength, humility and passion come to drive all my best actions and give place to those achievements that mean so much to me. In name of his memory I should always feel compelled to excel.

Abstract

In two-phase gas/liquid flow, the phenomenon of maldistribution of the phases occurring downstream of a splitting T-junction has been the topic of investigation of several authors. The negative consequences of this maldistribution on the operation of downstream unit have often led to the conclusion that T-junctions in two-phase pipelines are to be avoided. However, the large degree of segregation of the phases obtained at the outlets of a T-junction for certain flow rates and geometries, has encouraged Industry and researchers to exploit this simple device as a partial phase separator.

In this work, experiments and interpretations are carried out in two experimental rigs, one with a horizontal main pipe (0.127 ID) and the other with a vertical main pipe (0.076). These consist of measurement of the split characteristic and, in the case of horizontal annular flow, of film thickness.

Comparison with predictive models is carried out for the horizontal geometry. For the vertical main pipe experiments, interpretation and semi-empirical correlations are proposed to fit a large database including the present data and previous findings.

Chapter III - Experiments in horizontal geometry 68

List of Figures

Chapter I

Chapter II

Chapter III

Figure III.2.12: *Effect of phase split on film thickness at the inlet to the T-junction, 12.5 cm upstream of its centre.* U_{gs}*=24.5,* U_{ls}*=0.278 m/s.*

Figure III.2.13: *Logarithmic diagram of film distribution at the inlet to the T-junction, 12.5 cm upstream of its centre.* U_{gs}*=24.5,* U_{ls}*=0.278 m/s*

Figure III.2.14: *Effect of phase split on film thickness at the side outlet of the T-junction, 12.5 cm downstream of its centre.* U_{gs}*=24.5,* U_{ls}*=0.278 m/s*

Figure III.2.15: *Effect of phase split on film thickness at run outlet from the T-junction, 12.5 cm downstream of its centre.* U_{gs}*=24.5,* U_{ls}*=0.278 m/s.*

Figure III.2.16: *Particular of the film thickness distribution at the downstream corner of the T, in the run leg.* U_{gs}*=24.5,* U_{ls}*=0.278 m/s.*

Figure III.2.17: *Film thickness distribution around pipe circumference for a constant gas superficial velocity of 16.5 m/s, at the inlet to the T-junction.*

Figure III.2.18: *Film thickness distribution around pipe circumference for a constant liquid superficial velocity of 0.136 m/s, at the inlet to the T-junction.*

Figure III.2.19: *Film thickness distribution around pipe circumference for a constant liquid superficial velocity of 0.136 m/s, at the inlet to the T-junction. Logarithmic plot, showing the inversion of thickness trend from the bottom (centre of plot) to the top of pipe.*

Figure III.2.20: *Film thickness distribution around pipe circumference for a constant liquid superficial velocity of 0.136 m/s, at the side arm outlet of the junction.*

Figure III.2.21: *Film thickness distribution around pipe circumference for a constant gas superficial velocity of 16.5 m/s, at the side arm outlet of the junction.*
Figure III.2.22: *Film thickness distribution around pipe circumference for a constant liquid superficial velocity of 0.136 m/s, at the run arm outlet of the junction.*

Chapter IV

Chapter V

Chapter I

Two-phase flow in a pipe and the T-junction problem.

T-junctions are commonly used in industry as flow splitters, either singly or combined in series as a manifold. When a gas/liquid mixture splits at a T-junction, the possible impact of phase maldistribution on downstream units is the reason why there has been significant interest in the fluid dynamics of this particular geometry. The problem was initially tackled for the case of manifolds in pipelines carrying a single-phase fluid (Gardel, 1957), in order to predict the pressure drops and the distribution of mass flow rates which occur.

However, multiphase flow is commonly encountered in power generation, chemical and oil industries and the behaviour of these flows at T-junctions is significantly more complex and will form the subject of this study.

In such flow there is an additional problem to be solved. As well as pressure drop and overall flow split, there is the problem of predicting the distribution of the phases after the split because of phase maldistribution, which usually occurs. Due to several physical and geometrical factors (difference of momentum of the two phases, inter-phase drag, gravity, junction geometry, etc.), the qualities of the two-phase mixtures in the side arm and the downstream run differ from each other and from that in the feed branch (upstream of the T). This maldistribution can lead to malfunction of equipment downstream of the junction, and it needs to be carefully predicted. More recently, there has been an interest in taking advantage of the maldistribution to use the T-junction as a partial phase separator and, also from this perspective, it is important to predict the extent of the maldistribution. A complete overview of the possible applications can be found in Roberts (1994), Rea (1998) and Azzopardi (1999).

The remainder of this chapter presents the general two-phase T-junction problem, after a brief introduction to two-phase flow patterns, which are known to affect the operation of a T-junction.

Chapter II will present a survey of experiments and predictive models aimed to the understanding of phenomena occurring at a T-junction when a gas/liquid mixture splits through it.

Chapter III focuses on the experiments carried out in the case of annular flow approaching a T-junction with all legs in a horizontal plane and 0.127 m ID pipe. These consist of flow split and film thickness distribution measurements.

Chapter IV contains a comparison between the experimental results and models.

Chapter V contains the results of split experiments carried out in a 0.076m ID T-junction with a vertical main pipe. The results are analysed together with a wider database to understand trends and propose modelling and correlations.

Chapter VI presents a final overview with conclusions and areas of investigation for future work.

I.1 Flow patterns.

When a gas-liquid mixture flows in a pipe, it has been observed that the interface between the two phases can assume different features depending on variables such as inlet flow rates, fluids pair, pipe diameter, etc. This is relevant to the split of the phases at a T-junction because the topology of the flow will influence the likelihood of each phase to be diverted in the side arm or to continue downstream in the run. These configurations of the flow are called flow patterns and by means of experimental observation the following classification of flow patterns is made.

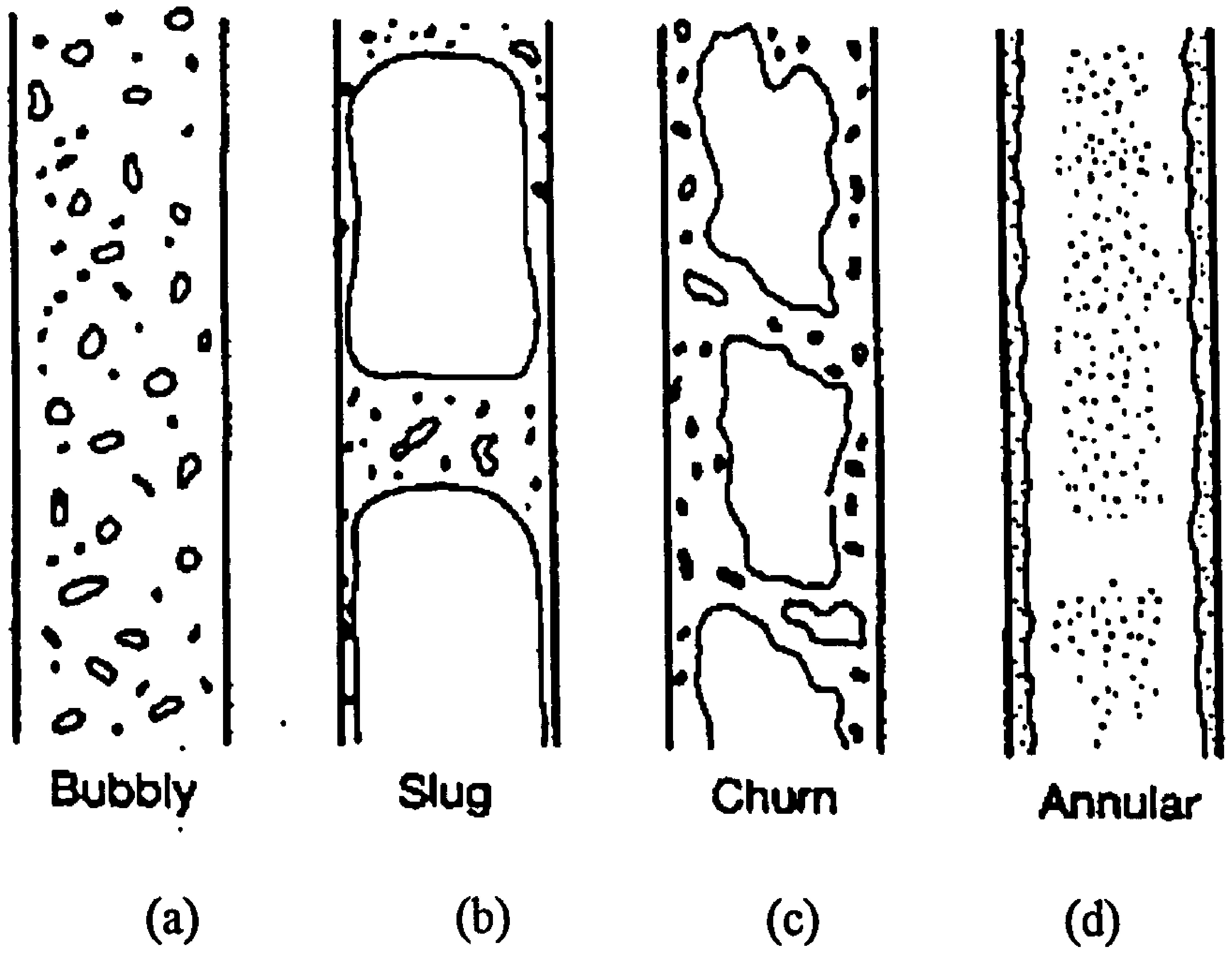

Figure I.1.1: *Flow Patterns in vertical upflow.*

In the case of a vertical pipe with co-current, upward flow, the sequence observed is shown in Figure I.1.1, in which we can consider the ratio between gas and liquid flow rate increasing from left to right.

For low values of this ratio *bubbly flow* (Figure I.1.1a) is observed. The main feature is the stability of such a flow in which bubbles of approximately uniform diameter are carried throughout the liquid.

As the ratio is increased we can also expect an increase in the bubble diameter, and the possibility of coalescence between two bubbles moving in the same neighbourhood. The qualitative change in the flow occurs when many bubbles coalesce to give larger bubbles occupying almost the entire diameter of the tube. This regime is known as *slug flow* (Figure I.1.1b). The bubbles are separated from the wall by a thin liquid film and between two gas bubbles it is possible to observe a liquid slug entraining gas from the gas bubble's wake. It should be pointed out that slug flow does not occurr in large diameter pipes and no gas entrainment is observed in the liquid slugs, for small diameter pipes

From this change in the pattern, a tendency is initiated for the gas and the liquid to travel separately and this leads to the *annular flow* (Figure I.1.1d) passing through a chaotic behaviour known as *churn flow* (I.1.1c). In the latter a churning motion of irregularly shaped portions of both the fluids is observed, in the former two well defined zones are identifiable:

1) Liquid film adjacent to the wall possibly entraining gas bubbles

2) Gas core flowing in the remaining part of the tube entraining liquid droplets.

Those droplets are caused by break-up of waves on the surface of the film. Some authors (Taitel *et al.*, 1980) regard churn flow as a zone of adjustment of the two phases to create the slug flow pattern. In this sense churn flow would not be regarded as a real flow-pattern although it can develop for a considerable number of diameters of the pipe.

Furthermore, if starting from annular flow conditions the gas flow rate is decreased, for a certain gas flow rate the liquid film starts flooding the pipe in some sections in a chaotic fashion: the churn flow regime appears. This description as a flooding condition rather than an entrance effect for the slug flow regime shows that the churn flow regime must be considered a flow pattern in addition to the others described above.

For co-current flow in a horizontal pipe, the situation changes because the main direction of motion is no longer coincident with that of gravity: the vertical direction is not an axis of symmetry for the flow. Alves (1954) classified the types of patterns, Figure I.1.2. Reasoning again in terms of growing gas flow rate, the following sequence can be observed.

For low flow rates the flow is defined as *bubbly* but in this case the bubbles are confined to a zone near the top of the pipe. As the gas flow rate increases, the bubbles become bigger and their coalescence leads to a flow regime known as *plug flow*. The next qualitative change occurs when a continuous gas layer is formed in the

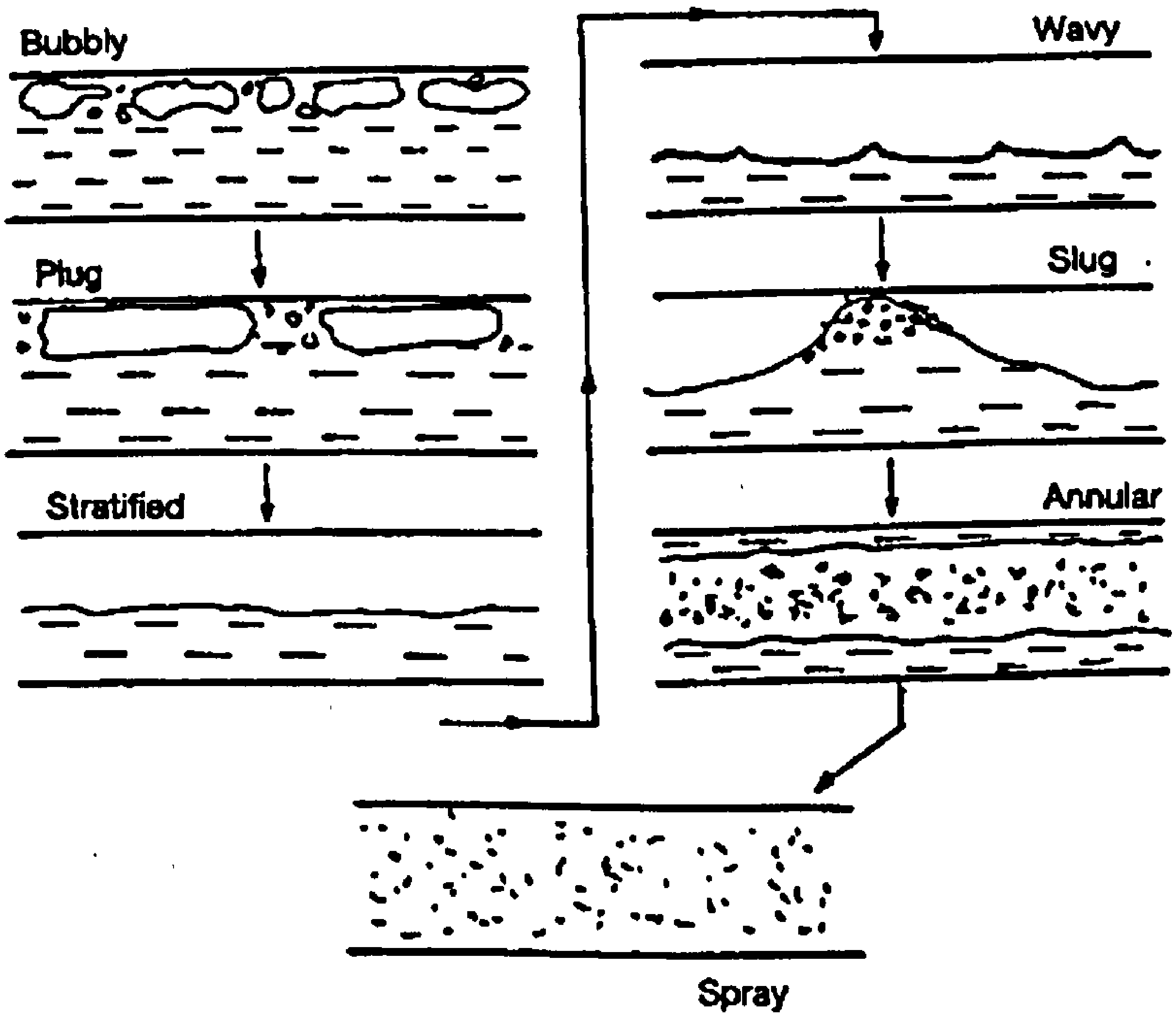

Figure I.1.2: *Flow Patterns in horizontal two-phase flow.*

upper part of the pipe as consequence of the plugs joining and we can speak of *stratified flow*.

A further increase in the gas flow rate leads to the formation of waves on the liquid surface due to the shear stress exerted by the gas phase on the liquid. This is *wavy flow*. As the waves become high enough to touch the top of the pipe, the *slug flow* is reached. For higher gas flow rates, *annular flow* takes place, basically with the same feature described in the case of vertical pipe with the only difference that the liquid film will be thicker at the bottom than at the top because of the effect of gravity. If the gas flow rate is very high the thickness of the film becomes negligible and the liquid travels only in the gas core occupying the entire pipe. This is the flow known as *spray* or *mist flow*.

I.2 Flow regime maps.

Collecting the work of several authors it has been possible to draw flow regime (or flow pattern) maps in which the boundaries among different flow regimes are drawn in the $U_{gs} - U_{ls}$ plane.

The difficulty in doing this consists in the gradual transition from one flow regime to another and in the subjectivity of the interpretation of a flow pattern as belonging to one class or to the other on the boundary between two of them. Furthermore, flow pattern maps are dependent on the pair of fluids as well as on the pipe diameter and operating pressure.)

Apart from visual observation, some authors propose more objective criteria. For instance, Barnea *et al.* (1980) and Costigan & Whalley (1997) used a conductance probe technique to measure void fraction to support visual observation.

VUoTo

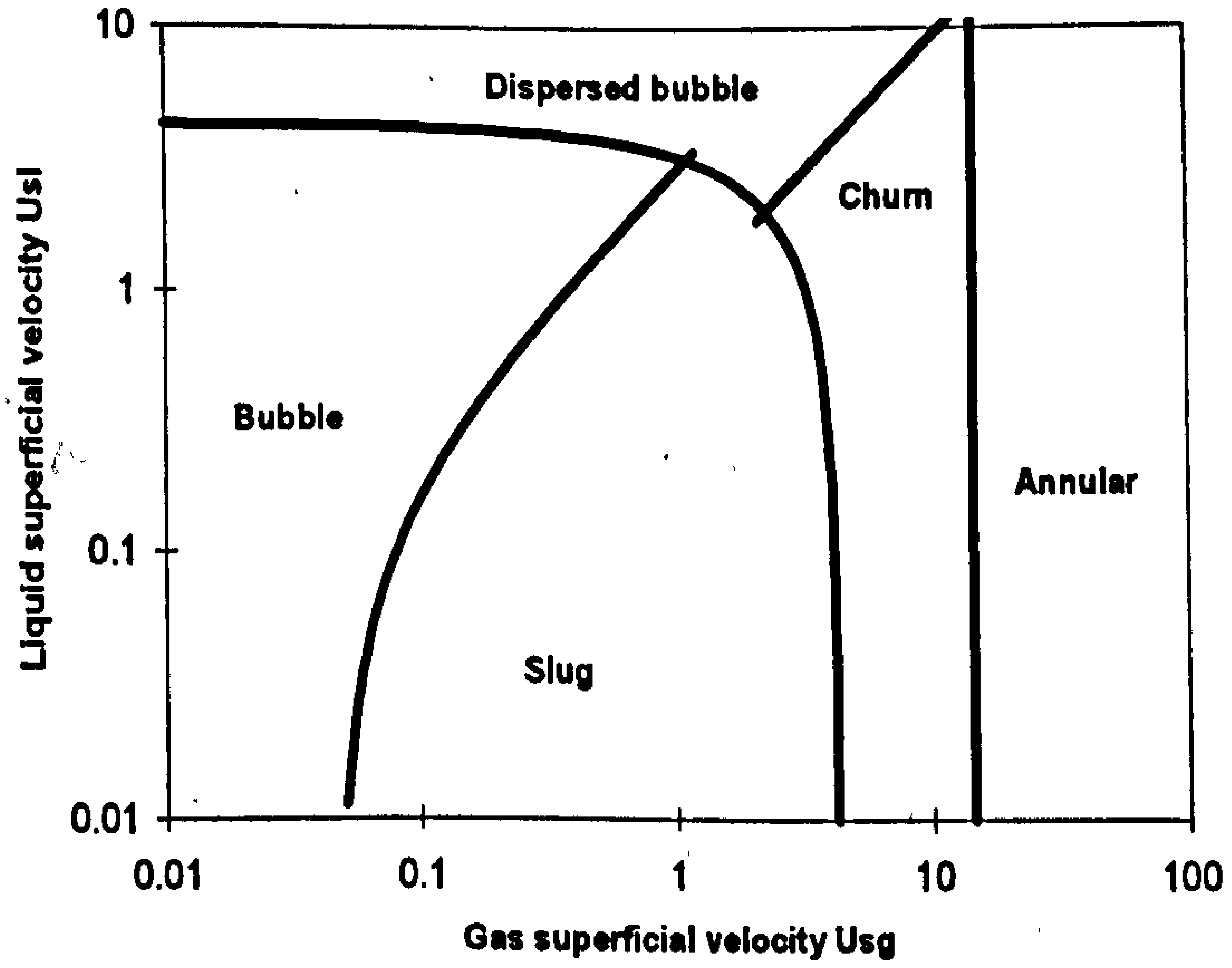

Figure I.2.1: *Flow pattern map in vertical upflow for air/water in a 0.076m ID pipe, atmospheric pressure. Prediction by Taitel et al. (1980)*

Semi-theoretical predictions of the boundaries between flow patterns have been been developed by Taitel *et al.* (1980) for vertical pipes and Taitel & Dukler (1976) for horizontal pipes. These are illustrated for a vertical pipe 0.076m ID (Figure I.2.1) and a horizontal pipe 0.127m ID (Figure I.2.2). Both are considered at atmospheric pressure, to show predictions for the diameters employed in the experiments described in chapters V and III respectively.

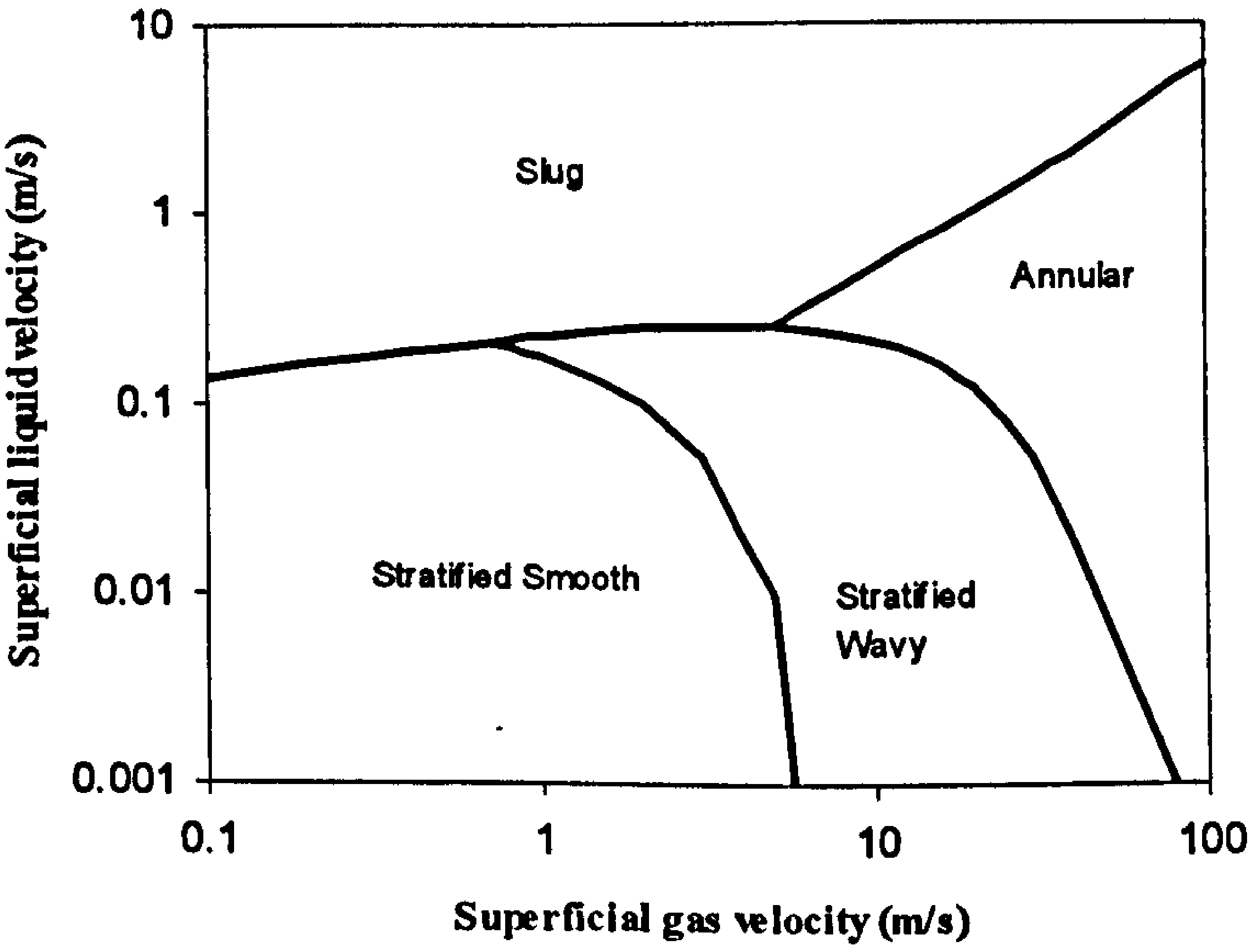

Figure I.2.2: *Flow pattern map for horizontal air/water flow in a 0.127 m ID pipe, atmospheric pressure. Prediction by Taitel & Dukler (1976).*

I.3 The T-junction problem.

A complete description of two-phase flow in a T-junction requires the parameters shown fig I.3.1: $\dot{M}_1$, x_1, $\dot{M}_2$, x_2, $\dot{M}_3$, x_3, $\Delta p_{1\text{-}2}$, $\Delta p_{1\text{-}3}$, D_1, D_2, D_3 and the angles θ, β, ϕ (main pipe orientation, side arm orientation against main pipe and against horizontal direction). $\dot{M}$ is the mass flux, x the quality, Δp the pressure drop and D the branch diameter. Suffixes 1, 2 and 3 indicate the inlet, run and side branch respectively.

As already mentioned in section I.1, the flow pattern in the inlet branch strongly affects the behaviour of the phases at the T.

This highlights the practical problems of developing a general model for such systems since it is not possible to write a general constitutive equation, bearing in mind the variability of the interaction between the two phases. From this, two different ways to deal with the problem follow.

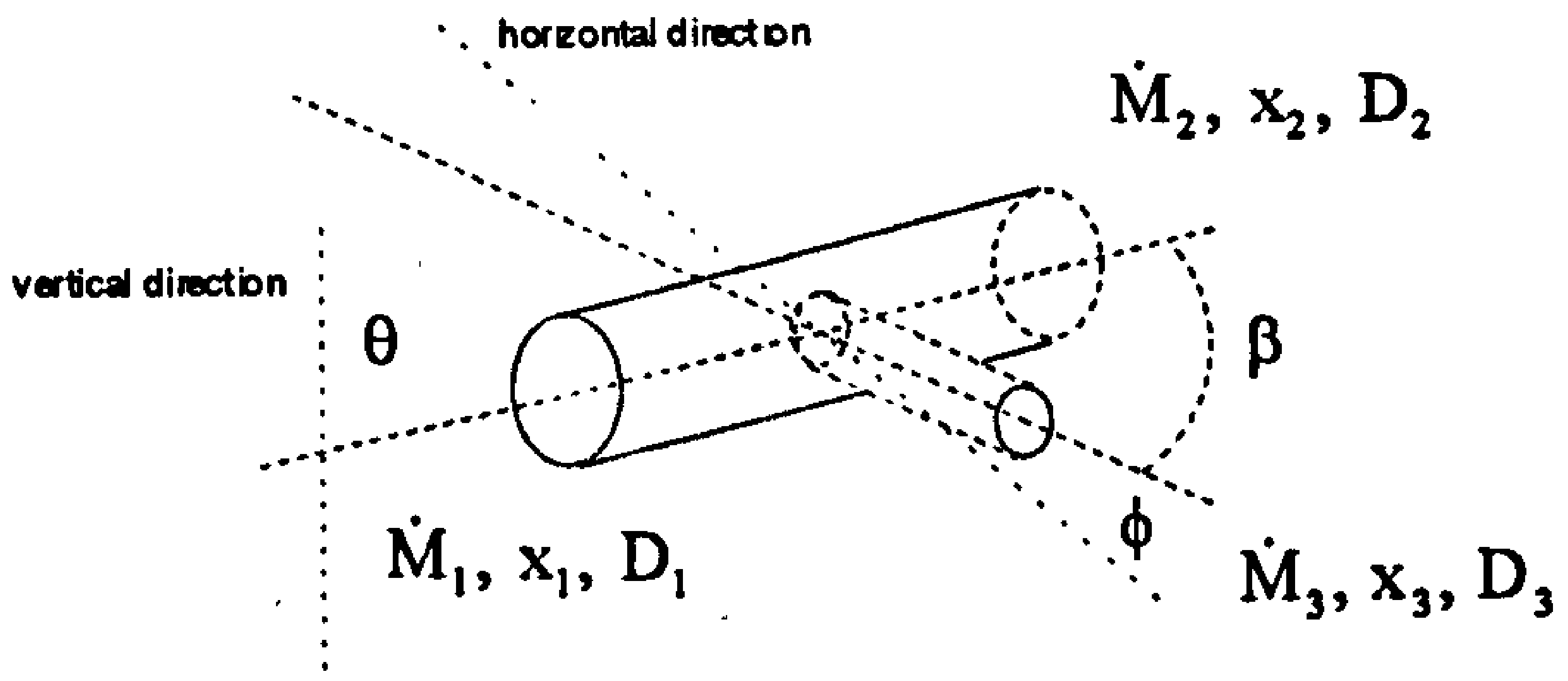

Figure I.3.1: *Parameters involved in the T-junction problem.*

Some authors, maintaining the idea of writing a differential balance, write the constitutive equations considering the interaction between the two phases and its dependence on the flow patterns so as to produce a model whose validity is restricted to a particular class of inlet flow pattern. Then, the integration of the velocity field for both the phases gives the global mass balance and the quality downstream from the T. In this approach, microscopic measurements are often needed. This is called the "two-fluid" approach (e.g.: Lahey 1990; Issa & Oliveira 1994, etc.).

The other approach is global in itself in the sense that macroscopic balances are written around the junction and the problem is closed by writing an equation for the phase split on the basis of some basic physical and geometrical ideas and using the available experimental data. More specifically, as formally pointed out by Saba & Lahey (1984), once the pair of fluids and junction geometry are fixed, the following variables define the problem:

$$\dot{M}_1, \dot{M}_2, \dot{M}_3, x_1, x_2, x_3, \Delta p_{1\text{-}2} \text{ and } \Delta p_{1\text{-}3}.$$

Three of these will be known, for example: $\dot{M}_1$, x_1 and $\Delta p_{1\text{-}3}$ and 5 equations are needed to close the problem. The available equations are:

Mass balance for the mixture:

$$\dot{M}_1 A_1 = \dot{M}_2 A_2 + \dot{M}_3 A_3 \qquad [I.3.1]$$

Mass balance for the gas component:

$$\dot{M}_1 x_1 A_1 = \dot{M}_2 x_2 A_2 + \dot{M}_3 x_3 A_3 \qquad [I.3.2]$$

Mixture linear momentum balance for the branch and for the run:

$$\Delta p_{1\text{-}3} = (p_1 - p_{1J}) + (\Delta p_{1\text{-}3})_J + (p_{3J} - p_3) \qquad [I.3.3]$$

$$\Delta p_{1\text{-}2} = (p_1 - p_{1J}) + (\Delta p_{1\text{-}2})_J + (p_{2J} - p_2) \qquad [I.3.4]$$

where both reversible (p_i-p_{iJ}) and irreversible ($(\Delta p_{ij})_J$) pressure drops could be calculated via empirical correlations using two-phase multipliers (Chisholm, 1967 and 1973, Saba & Lahey, 1982) and loss coefficients (Gardel, 1957).

To obtain closure of the problem, a fifth equation (the split equation) is needed and here several authors propose various approaches. Results are restricted to a particular flow pattern in this case too (e.g.: Saba & Lahey 1984; Lahey 1990, Lahey *et al.*, 1985). In general, all the models and correlations which do not account for the structural effects of flow pattern, fail in the prediction of the phase redistribution outside of the range of parameters they are based on.

In Chapter II we shall outline the current knowledge in this field from the experimental results to the different ways of modelling such systems.

In the next two sections of this Chapter, the standard nomenclature and the typical way of representing experiments are presented.

I.4 Split data

There are two traditional ways of plotting experimental data of phase split:

1) Fraction of incoming liquid diverted in the branch ($L' = \dot{M}_{L3} / \dot{M}_{L1}$) vs. the same property of the gas ($G' = \dot{M}_{G3} / \dot{M}_{G1}$)
2) Quality ratio x_3/x_1 vs. mass flux ratio $\dot{M}_3 / \dot{M}_1$ between the incoming and the branch streams (split ratio).

The first type of diagram (Figure I.4.1), allows immediate identification of the zone of liquid and gas dominating flow split. It is a "square" diagram and on the left side of the diagonal line, the points where liquid extraction in the side arm is dominating are located. The diagonal itself is the line of even separation and the

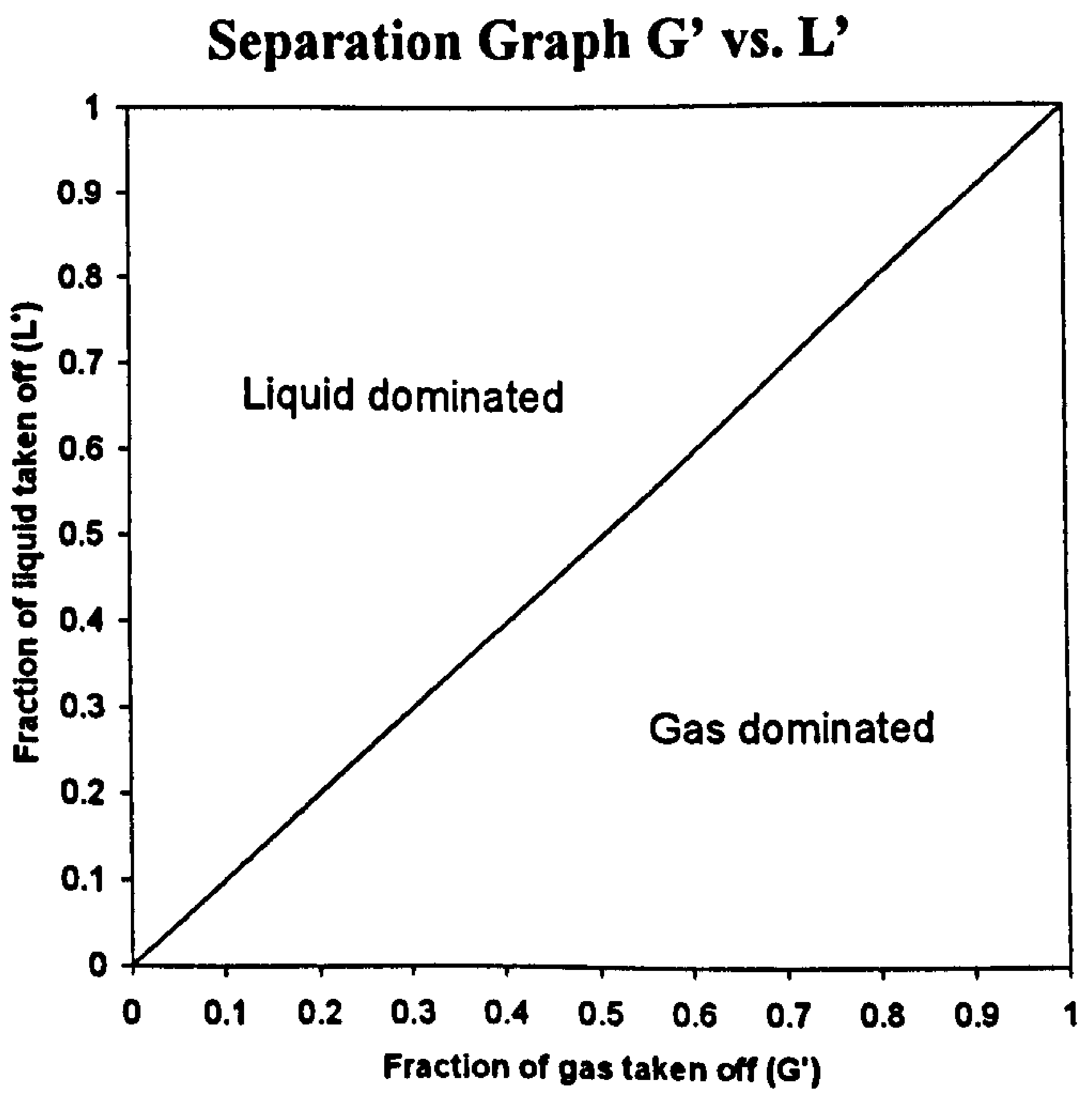

Figure I.4.1: *Square diagram for the split characteristic. Liquid diverted fraction (L') vs. gas diverted fraction (G').*

points at gas dominated separation are on the right side of it. The abscissa axis is the curve of no gas extraction and the ordinate is the line of no liquid extraction. The remaining two sides of the square give total gas (G'=1) and liquid (L'=1) separation.

In the second representation (x_3/x_1 vs. $\dot{M}_3/\dot{M}_1$, Figure I.4.2) the abscissa axis ($x_3/x_1=0$) gives the points with no gas extraction. The horizontal line for $x_3/x_1=1$ substitutes the line at 45° in the previous graph ($x_3=x_1$, even separation).

The hyperbola given by the equation $\dot{M}_3 x_3 = \dot{M}_1 x_1$ is the line of total gas extraction. The physical validity of this curve is restricted by the inlet conditions: when $x_3=1$, the horizontal line $x_3/x_1=1/x_1$ (depending on inlet quality) intersects the hyperbola for $\dot{M}_3/\dot{M}_1=x_1$. On that horizontal line only gas is extracted, all of it on the point of intersection with the hyperbola of total gas extraction. The advantage of this "inlet-dependent" representation, is the visualisation of a minimum or a maximum which will show respectively the maximum liquid or gas separation (since the minimum will appear below and the maximum above the line of even separation $x_3=x_1$).

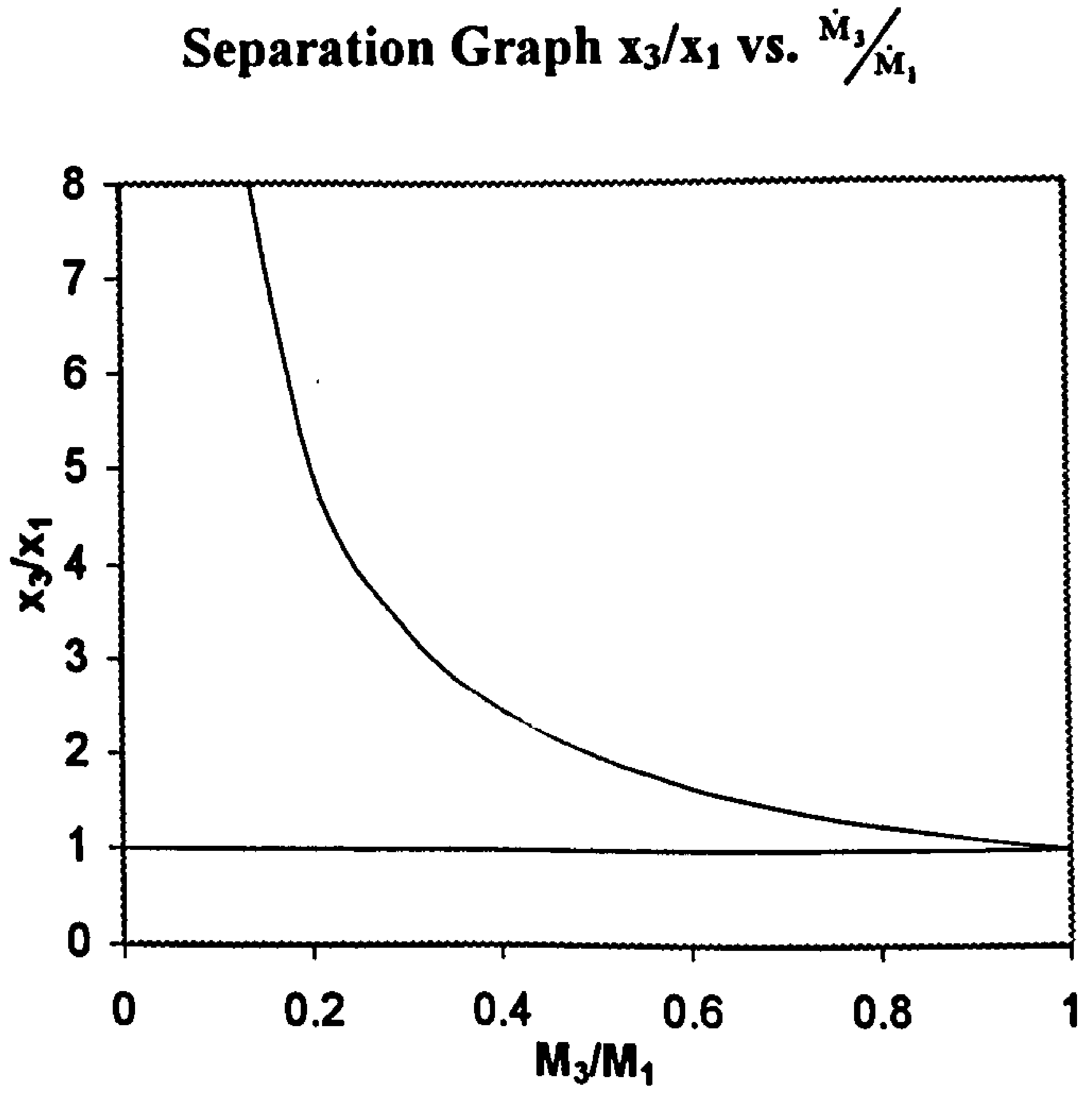

Figure I.4.2: *Alternative diagram for the representation of split characteristic. Side/inlet quality ratio vs. side/inlet flow rate ratio.*

I.5 Pressure drops at the junction.

Pressure drop measurements at the junction generally show a loss between inlet and side arm and a recovery into the run. Although frictional losses occur, since part of the flow is diverted in the branch, the velocity of the mixture in the run is reduced. In the single-phase case, this leads to a pressure recovery by the Bernoulli effect. In two phase-flow, the Bernoulli equation cannot be used in its global form. Nevertheless, the same behaviour is observed in two-phase flow. After a certain length downstream from the junction, the pressure profiles in the side and the run branches will recover their linear shape. The pressure drops $(\Delta p_{12})_j$ and $(\Delta p_{13})_j$ are given by the difference of pressure between the inlet pressure profile and the two outlet profiles, after they have recovered their steady nature, extrapolated to the junction (Figure I.8).

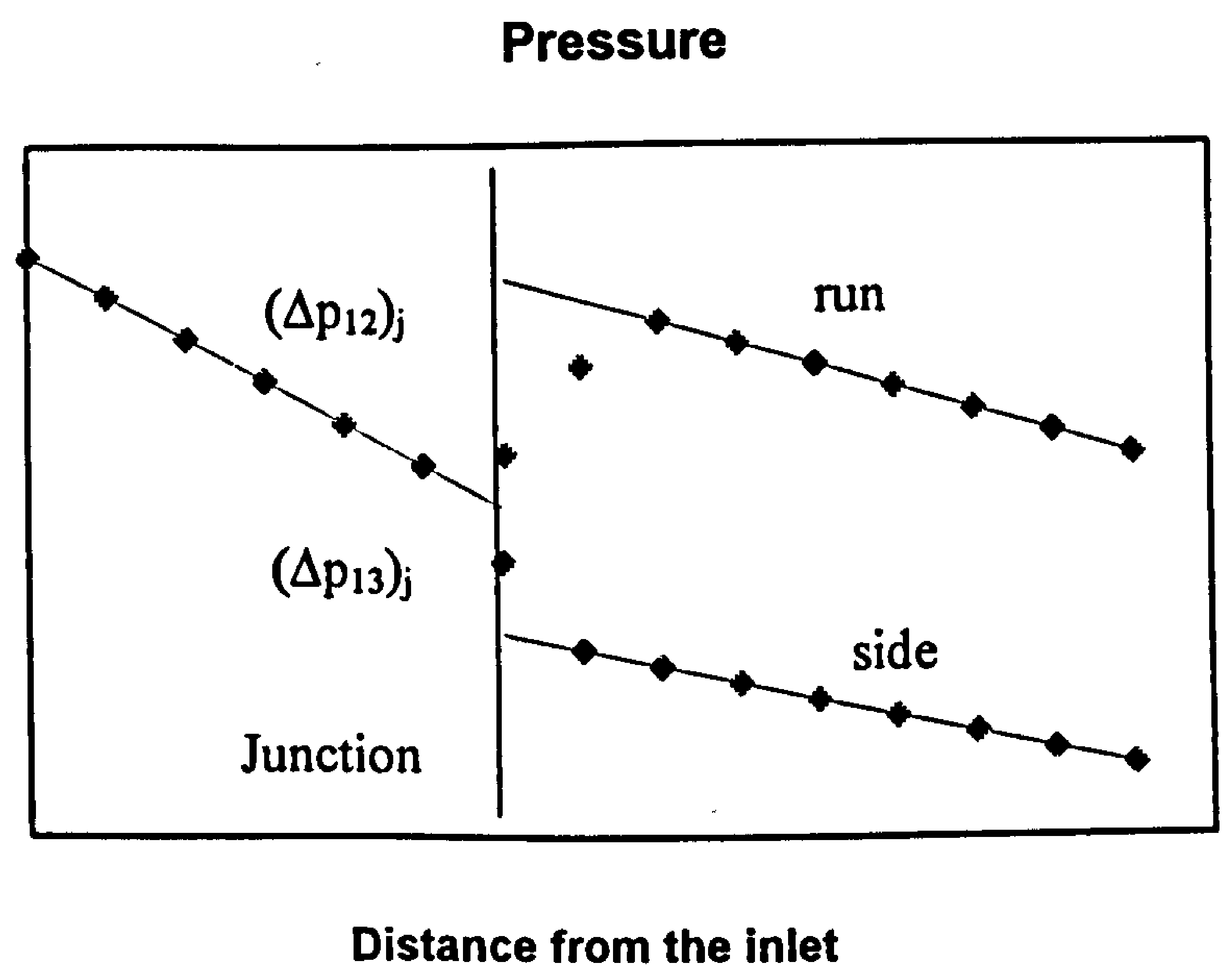

Figure I.V.1: *Diagram for the representation of pressure profiles at T-junctions. Pressure vs. axial distance from the inlet.*

Chapter II

Literature review

Introduction

In this chapter the current knowledge on the problem of two-phase flow splitting at T-junctions will be outlined. In choosing a structure for this discussion, several possibilities of cataloguing data and modelling are available. A first, obvious level of classification is through the main geometry, i.e. the orientation of the main pipe. Although, theoretically, there are infinite pipe inclinations, the cases of interest are reduced to 0° (horizontal) and 90^0 (vertical) inclinations to the horizontal plane. The cases of horizontal and vertical T-junctions have traditionally been tackled separately. Exceptions are found in the works of Saba & Lahey (1984) and Azzopardi & Whalley (1982). Suu (1992) compared his data from vertical bubble flow, to those obtained in horizontal pipes by Collier (1976) and Rubel *et al.* (1988).

Some authors (Peng, 1994; Muller and Reimann, 1991) arrange data taking into account the effect of various geometrical and physical parameters, as listed in section I.3 (e.g.: pipe diameter, diameter ratio, side arm inclination, fluids properties, etc.).

Alternatively, it is possible to attempt a systematic presentation of data in terms of conditions at the inlet to the T (Azzopardi, 1999). To make a coherent comparison of data, these inlet conditions should describe in the most comprehensive way the geometry, physical properties of the fluids and operating conditions. In this sense, for example, an inlet condition expressed in terms of inlet mass flux (kg/m^{2}s) and quality would be more descriptive than one in terms of mass flow rate (kg/s) and quality. The former would allow comparison of data obtained for different pipe diameters or section geometries. Given the number and the complexity of the parameters that describe the problem, the specification of the most general 'inlet condition' is not an easy operation.

A global way of describing the flow at the inlet is through its flow pattern. The advantage of this is that we can reduce the categories of data to the very few flow patterns observed in the vertical and horizontal geometries. Also, this research is concerned with the behaviour of gas/liquid mixtures at vertical and horizontal T-junctions and many patterns observed in a horizontal pipe can be assimilated to the vertical cases. This would help reducing the traditional distinction between these two cases and, possibly, operate a better synthesis.

Many predictive methods are derived by mutual exchange between the interpretations obtained studying these two geometries. Also, as will be discussed, the most successful models are those that are based on the flow pattern approaching the junction. This is because flow patterns have a strong influence on the split of phases (Azzopardi & Baker, 1981; Azzopardi & Whalley, 1982). These are all reasons why an arrangement of available data and modelling by flow patterns seems the most appropriate.

There are disadvantages in the fact that the classification of a flow pattern as belonging to one category or the other always contains an element of subjectivity, in a more or less wide band about the boundaries between two of them. Also, not all authors observe or report the flow pattern approaching the T, requiring hypotheses on the regime by locating their inlet conditions on flow pattern maps.

Nonetheless, it is believed that this approach is the most suitable to the nature of this work. The presentation is structured starting from the results obtained in the vertical main geometry, where fewer flow patterns exist. Results in the horizontal main geometry will follow with a systematic attempt at comparing them to the previous case, when flow patterns can be assimilated to those observed in vertical pipes. Where appropriate, reference will be made to side arm parameters such as inclination and diameter ratio as well as to fluid properties and other geometrical and physical features.

A review of models developed follows using the same scheme. It is also underlined that, with reference to the side/main diameter ratio, the term 'regular T-junction' is used to indicate those cases where side and main branches have the same diameter and 'reduced T-junction' otherwise. Unless otherwise stated, the pair of fluid used in the experiments described below is air/water. Finally, in this review as in the subsequent experiments and interpretations, the cases of concern are those where the side arm is horizontal at an angle of 90° to the main pipe (square T-junctions).

II.1 Experimental

II.1.1 Vertical annular flow

Most data in vertical T-junctions have been collected in the annular flow regime (Azzopardi & Whalley, 1982; Azzopardi, 1988; Charron & Whalley, 1995; Azzopardi, 1994). In this regime, the interpretation and modelling of the split of the phases is most successful for both vertical and horizontal geometry. The consolidated argument is that the momentum of the phases plays an important role in determining the amount of each phase diverted into the side arm. The liquid phase is distributed between a slow film at the wall and liquid drops. The drops travel at a velocity similar to the gas phase (Azzopardi & Teixeira, 1994; Azzopardi & Zaidi, 1998) hence, their momentum will be much higher than that of the gas (high velocity, low density) and the liquid film (low velocity, high density). This momentum will be opposed to the pressure differential in the side arm and to the centripetal force and under-pressure created by the fluids turning 90° into the branch (Oranje, 1973; Hong, 1978). These considerations explain the fact that the split behaviour, when annular flow approaches a T-junction, varies from liquid to gas dominated, depending on the degree of break up of the waves and entrainment of the liquid phase. An important work in this area is that of Hewitt & Govan (1990) who accurately predicted the increase of entrained fraction with gas velocity, above a certain threshold (transitional velocity).

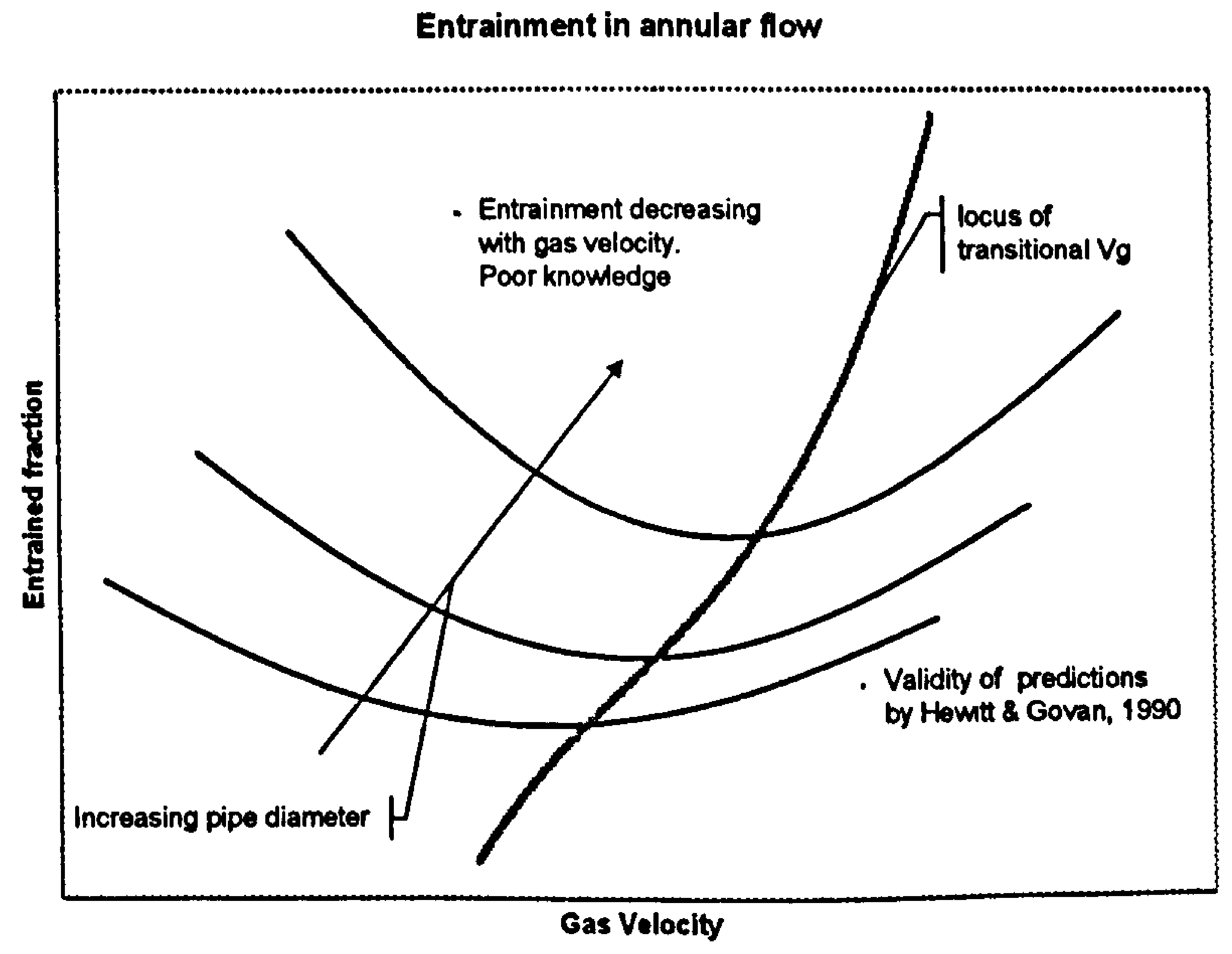

Figure II.1.1: *Sketch of the trends of entrained fraction in vertical annular flow.*

Below this threshold the entrained fraction decreases when gas velocity is increased and the knowledge is poor (Verbeeck *et al.*, 1992). The transitional velocity increases with pipe diameter and so does the entrained fraction (Azzopardi, 1994). This behaviour is schematically represented in Figure II.1.1.

Overall, entrained fraction can vary from few percent to 100%, for mist flow and no entrainment to 60% entraiment might cover the cases where split data have been taken. This explains the variety of split behaviours in annular flow at small gas take off. For increasing gas inlet flow rate, the general trend is in the direction of decreasing liquid take off for the same gas take off (Figure II.1.2). This can be explained in terms of an increase of gas momentum and entrained fraction of liquid in the main flow. For higher take off, other phenomena occur. In the cases of gas dominated splits at lower take off, a steep increase of liquid diverted fraction is often observed for small variations of gas take off as sketched in Figure II.1.2 in correspondence of the change of slope. This is related to several additional mechanisms feeding the phases to the side arm.

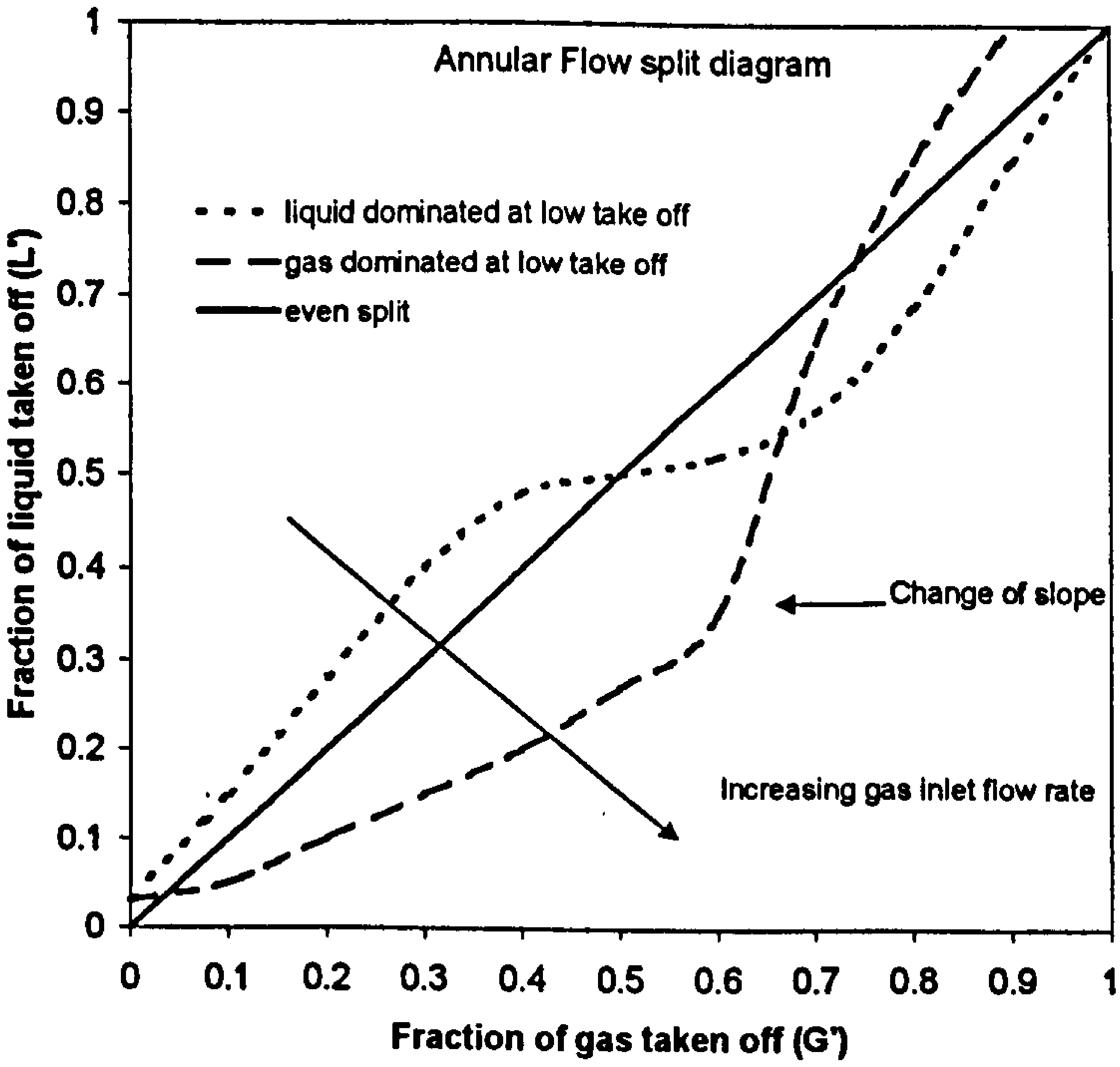

Figure II.1.2: *Types of split occurring for vertical annular flow*

When the amount of gas taken off is large enough, the gas velocity in the run falls below the flooding point. Large waves detach from the liquid film to flood the run pipe and be drawn back into the side arm, Azzopardi (1988). These waves also capture the liquid drops initially carrying straight past the junction. For large diameters this last effect is less important as flooding is manifested by means of waves which do not occupy the full pipe cross sectional area. Furthermore, the entrained liquid fraction will be larger than in the corresponding cases at smaller diameter, Azzopardi (1994). For the cases showing liquid dominated split at low take off, another mechanism was observed before the occurrence of flooding. The pressure recovery in the run arm, due to the loss of convective momentum through the side arm, causes the film travelling on the wall opposite to the branch opening to slow down, Azzopardi & Purvis (1987). The film eventually will stop and a liquid collar on the wall opposite to the side opening has been observed feeding the side arm with liquid. This phenomenon is referred to as 'film stop'. At lower take off, Charron and Whalley (1995) give some evidence of the existence of an opposite transfer mechanism, where liquid recirculates in the side arm to be ejected and carried up in the run.

Accordingly to the above observation on the trends at low take off, Azzopardi & Whalley (1982) obtained good predictions by assuming that the liquid was diverted only from the wall film. They also imposed that both phases come from a common segment of the pipe subtended to the side arm, as already observed in single-phase flow by McNown (1954). This idea has been modified in several ways to obtain better predictions and details will be given in the section dedicated to modelling. Their experiments were carried out in a vertical T-junction with the main tube of 0.032m ID and three different side tubes of 0.00635, 0.0127 and 0.019m ID. Inlet conditions were: $4.4<U_{gs}<43.5$ m/s and $0.016<U_{ls}<0.11$ m/s at a pressure of 1.5 bar. The split behaviour was investigated at low take off and trends were similar to what has been described in a previous paragraph. An increase of side arm diameter caused a small increase of diverted liquid. Azzopardi (1984) later studied this effect using part of the database of Azzopardi & Whalley (1982). The author argued that a smaller opening resulted in a shorter path of the liquid film under the influence of the pressure differential in the side arm. This is confirmed also by the experiments of Zetzmann (1984) in the slug/churn flow regimes, where the length of the path is changed by varying the branch angle to the main pipe (angle β in Figure I.3.1).

An interesting effect at low take off is represented by the occurrence of a liquid take off threshold before any gas is fed to the side arm. This is due to the fact that a certain amount of liquid must be withdrawn from the film before the gas becomes available to the side arm opening.

Charron & Whalley (1995) used a cotton threads visualisation technique to locate the dividing streamlines for single-phase gas flow at a 0.032m ID, regular T-junction, for several split ratios. Inlet conditions for the two-phase flow experiments were in the range $13<U_{gs}<59$ m/s and $0.004<U_{ls}<0.097$ m/s at a pressure of 1.5 bar. Here, the term 'dividing streamline' indicates the streamline in each vertical plane, ending in the downstream corner of the T. This divides the streamlines going to the branch from those carrying straight on to the run arm. Charron & Whalley (1995) observed that the diverted gas came from a convex portion of the pipe cross section and not a segment (Figure II.1.3).

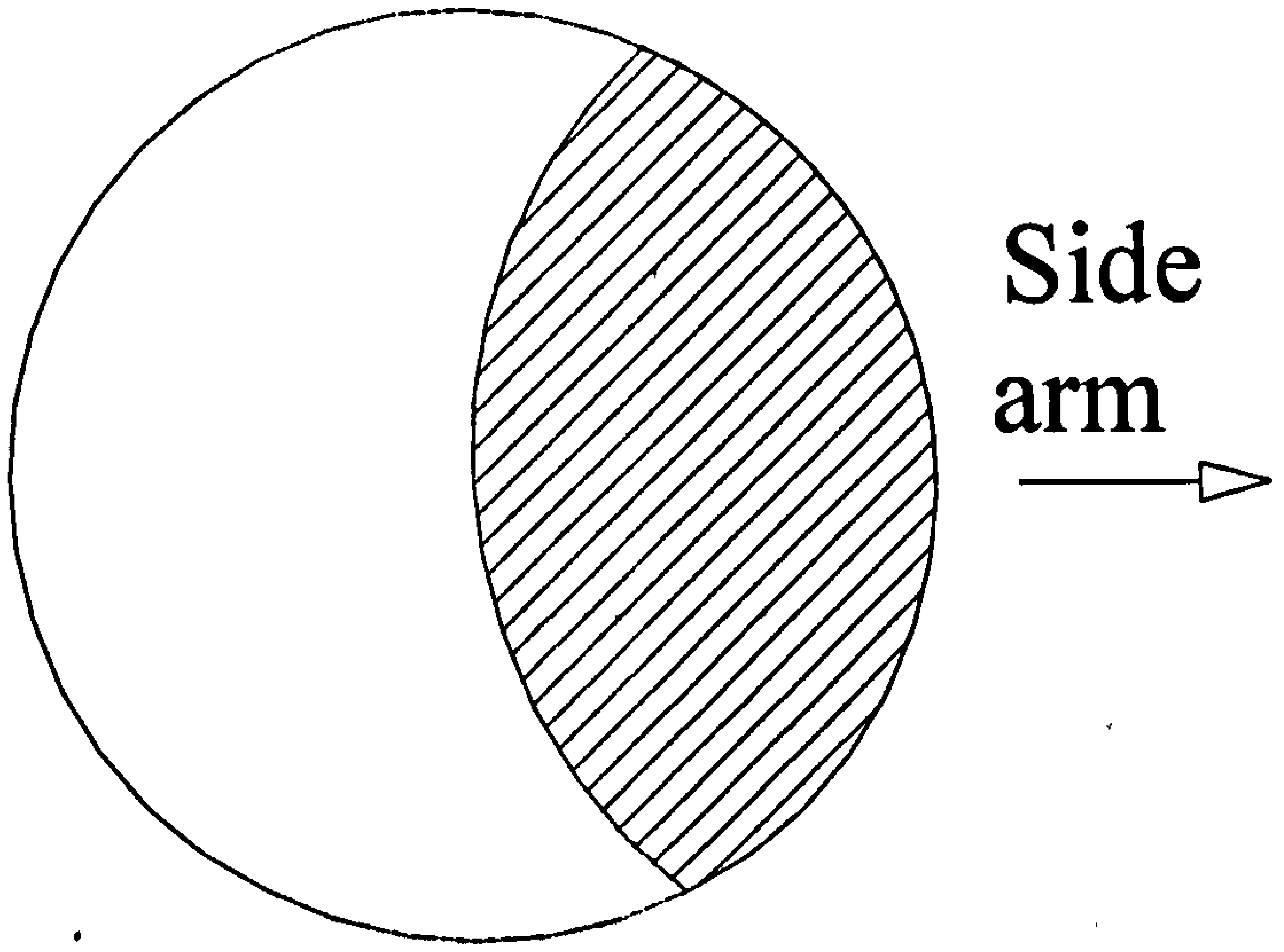

Figure II.1.3: *main pipe cross section. Dashed area is the zone from where gas is taken off accordingly to the experiments of Charron and Whalley (1995): a convex portion of pipe rather than a circular section.*

In fact, it would be expected that the larger portion of phases be taken off the centre of the side arm horizontal diameter. Later we will discuss models, earlier than Charron & Whalley's work which contain an assumption of such shapes of the zones from where the phases are diverted (the so called 'zones of influence').

It is known that the geometry downstream of the T can influence the split of the phases. Azzopardi (1994) carried out experiments in a 0.127m ID regular, square T-junction with a vertical main pipe ($22<U_{gs}<40$ m/s; $0.006<U_{ls}<0.02$ m/s; P=1.0 bar). The author observed that with a run arm length of 14D, the liquid film which was not diverted into the branch, flowed upward on the wall near to the side opening and downwards on the wall opposite. This happened after the up-flowing film reached the top of run leg before the 90° bend of the experimental arrangement. This falling film encounters the upflowing annular flow and eventually forms a liquid ridge at the T from where liquid is taken off into the side branch.

II.1.2 Horizontal stratified and annular flows

Although modelling and experiments often treat the cases of stratified and annular flows independently, the transition from stratified to annular flow is very smooth and it is reasonable for some aspects to consider them as belonging to the same class of two phase flow patterns. Stratified flow does not exist in vertical pipes, as it is a consequence of the angle of gravity to the pipe axis. Annular flow in horizontal ducts presents all the features of vertical annular flow but, because of gravity, liquid is drained towards the bottom of the pipe causing asymmetry in the wall film. The liquid film is then thicker at the bottom, which makes it similar in some features to stratified flow. For high liquid velocities, in the stratified flow regime, the presence of large disturbance waves over the base film initiates one of the mechanisms that is believed to be responsible for the formation of the liquid annulus on the pipe wall (Fukano & Ousaka, 1989). For annular flow in large diameter pipes, the film at the bottom is still very thick and a high degree of asymmetry results from the abrupt thinning of the film along the circumferential direction, towards the top of the pipe. This is called semi-annular flow. For the above, many arguments applied for the prediction of annular flow split in vertical pipes can be extended to the horizontal case if all the effects due to asymmetry are taken into account. In this, understanding the split of stratified flow is of great help.

However, it should be strongly highlighted that the physical reasons for the formation of a liquid annulus at the pipe wall are conceptually different for the two geometries and still a matter of lively debate (Laurinat *et al.*, 1985; Fukano & Ousaka, 1989; Hurlburt & Newell, 2000). Vertical annular up-flow occurs when the gas drag magnitude is such to keep an up-flowing film at the wall against gravity, since the liquid will segregate towards the zones where the gas velocity is smaller.

In the horizontal case, gravity must be overcame in a direction perpendicular to that of the main flow, hence, drag forces are originated only by secondary flows

(Laurinat *et al.*, 1985). Other reasons can intervene and are believed to be more effective in originating horizontal annular flow such as the already mentioned pumping action of disturbance waves (Fukano and Ousaka, 1989) and the entrainment and deposition of liquid droplets.

Because of the large database, conditions are tabulated in Table II.1.1. For the stratified flow regime there is a distinction between smooth and wavy surface of the interface between the two phases. The latter is accompanied by liquid entrainment and the same arguments based on liquid drops' momentum apply in the discussion of split characteristics.

In analogy with vertical annular flow, for the case of horizontal regular T-junctions, both in stratified and annular flow, a threshold of liquid take-off before any gas is diverted is observed. This is due to the head of liquid at the bottom of the main pipe. Because of it, liquid is driven into the side arm even when the momentum of the liquid film is large enough for it to go straight past the junction, against the centripetal force created by the 90° turn of the gas phase (Azzopardi & Rea, 1999). This effect disappears for reduced T-junctions when the film depth is smaller than the vertical distance between the bottom of main and side branches. In these cases, when the flow is stratified, a threshold of gas take off can be observed instead (Wren *et al*, 1999; Walters *et al.*, 1998).

Indirect mechanisms of liquid take off are somewhat similar to those discussed for vertical pipes. Film stop is observed in some conditions. Also, the sudden rise of liquid take off is often caused by the transition of the liquid film flow in the run leg from supercritical (Fr>1) to subcritical (Fr<1) regime. Here the Froude number is defined by $Fr = U_{lf}/\sqrt{gD}$ (U_{lf} being the liquid film velocity and g the acceleration of gravity). When this occurs, a hydraulic jump is observed in the run leg. This consists of a zone of gas entrainment where the liquid depth rises to allow for its smaller velocity. When the hydraulic jump reaches the T-junction, for large gas take-off, liquid is driven from it to the side arm (Azzopardi & Smith, 1992), giving to the split characteristic similar features to those shown in vertical annular flow when flooding occurs. When the main flow is annular this zone assumes the features of a highly turbulent mixing area followed by a slugging flow. Overall, as in the vertical case, the split characteristic can show liquid as well as gas dominated maldistribution. More phenomena are involved in the horizontal case, as discussed below.

The increase of liquid superficial velocity at the inlet causes the liquid film to travel faster and data show a decrease of the fraction of liquid taken off (Hong, 1978; Shoham *et al.*, 1987; Azzopardi & Memory, 1989; Rea & Azzopardi, 1999). The trend observed when gas superficial velocity is increased is more complex. There, the drag of the gas on the liquid layer acts in the direction of lowering the liquid depth at the bottom and causes the entrained fraction to increase. In contrast, the shape of the liquid film becomes more symmetrical and available to the side opening. For this reason, several trends can be observed depending on which of the above factors are dominating. The small diameter pipe data by Hong (1978, D=0.0095 m) and Stacey *et al.* (2000, D=0.005m), show an increase of liquid take off with gas flow rate. This is more marked in the stratified to annular transition, where the effect of increasing symmetry is dominating. Although entrainment would increase, given the small diameter it is expected that the amount of it would be small. For large diameter pipe such as the data of Riemann *et al.* (1988, D=0.05 m), the flow is very likely to be semi-annular, hence very asymmetric and similar to stratified. Again, data show that the symmetry effect overcomes the increase of entrained fraction and the trend is even more markedly in the direction of increasing liquid take off with gas flow rate. The data of Buell *et al.* (1994) for an intermediate diameter (D=0.032 m) show the opposite trend. In this case, it might be argued that when the pipe diameter is small enough to give a highly symmetric annular flow but large enough for entrainment to be significant, increasing gas flow rate affects entrainment much more than the symmetry, unless a stratified to annular transition is involved. This is similar to the trend consistently observed in the vertical geometry where the averaged distribution of the film is perfectly symmetrical.

The above can be used also to understand why, in the case of regular T-junctions and for several pipe diameters, a comparison of annular flow data with the same superficial momenta of the phases $\rho_i U_{is}^2$ (i=g,l) show a higher liquid take off for the smaller diameters (Hong, 1978; Buell *et al.*, 1994; Stacey *et al.*, 2000).

With reference to diameter ratio, an interesting feature is found in the work of Walters *et al.* (1998).. Their data in a 0.038 m main pipe diameter T-junction, showed the expected reduction of liquid take off when the diameter ratio was reduced from 1 to 0.5. As mentioned above, this could be caused by the step that the liquid has to leap to be diverted from the bottom of the main pipe, where most of the film flows.

Also, analogously to the vertical case, the liquid film is exposed for a shorter length to the pressure differential in the side arm. However, when diameter ratio was further reduced to 0.2, an increase in liquid take off was observed. This might be due to the higher gas velocity in the side arm and hence, by Bernoulli, lower n pressure.

Data from Reimann *et al.* (1988), Rubel and co-workers (1988,1994) for steam/water mixtures and Peng (1994) show results compatible with the above discussion.

II.1.3 Vertical Bubbly flow

Bubbly flow in vertical pipes has been investigated by Azzopardi & Whalley (1982), Azzopardi & Baker (1981), Suu (1992). The trend in split data shows the dominance of gas take-off. This can be explained by the usual momentum based reasoning. In bubbly flow, the gas bubbles are dispersed in a liquid continuum, moving at a velocity slightly higher than that of the liquid under the action of the Archimedean lift. Because of the higher density of the liquid, its momentum is much higher than that of gas. Hence, gas is preferentially taken off and liquid is likely to be diverted from the slow layer near the pipe wall.

II.1.4 Vertical Slug and Churn flows

A number of authors have investigated the split of low void fraction, two-phase flow (Chadwick, 1965; Azzopardi & Whalley, 1982; Zetzmann, 1984; Honan & Lahey, 1981; Davis & Fungtamasan, 1990; Hewitt *et al.*, 1990; Azzopardi *et al.*, 1994; Suu, 1992). As specified in the previous chapter, slug flow is characterized by the presence of long, bullet shaped Taylor bubbles in a liquid continuum, separated by liquid slugs eventually entraining gas from the bubble's wake. The split of such flows is generally liquid dominated. Azzopardi *et al.* (1994) observed that the gas is diverted into the side arm as a portion of the Taylor bubble is torn off its main body when it is deformed by the lateral pull and split by the falling film from the run arm. The general trend shows an increase of gas take off when the gas inlet flow rate is reduced. A much smaller effect is observed by varying the inlet liquid flow rate.

Suu (1992) reports gas dominated split in his slug flow regime data. This is probably due to the fact that his results were obtained in a region of slug flow very close to the boundary with bubbly flow. In those conditions, Taylor bubbles are relatively short and the entrainment from the bubble's wake into the liquid slugs is very efficient. This gives place to the preferential gas take-off for the reasons discussed in the paragraph regarding vertical bubbly flow.

The behaviour in the churn flow regime is more complex. For high liquid flow rates (Hewitt *et al.*, 1990; Azzopardi and Whalley, 1982), the separation is gas dominated. This is somewhat similar to what happens in annular flow. Again the occurrence of flooding in the run pipe would explain the observed increase of liquid fraction in the side arm at larger take off.

Data from the works of Honan & Lahey (1981), Zetzmann (1984) and Davis & Fungtamasan (1990) are in line with the features discussed above.

The experiments of Chadwick (1965) for steam/water mixtures were produced as tests for a reactor refuelling machine at full scale. The T-junction had a connecting rod placed opposite to the side arm and data in the high gas take off region show an increase in vapour take off with vapour flow rate.

II.1.5 Non-annular horizontal flows.

The knowledge in horizontal flow patterns other than stratified and annular is much more restricted. No data has been reviewed in the plug flow regime and the only works in horizontal bubbly flow are those from Collier (1976), and Mudde *et al.* (1993). The latter carried out experiments in a large diameter T-junction (0.23 m ID) where the T was placed very close to a 90° bend coming off a vertical inlet where bubbly flow was generated. Suu (1992) compared his vertical bubbly flow data with those by Collier (1976) which reported gas dominated separation. Suu (1992) claims good qualitative comparison.

More data have been generated in the slug flow regime. Johansen (1979), Saba & Lahey (1984), Fairhurst (1986), Katsaounis (1987, vertical upward side arm), Reimann *et al* (1988). The most recent work is from Arirachakaran (1997) in a 0.051 m ID regular T-junction. He regarded the slug flow as composed of sequences of annular and bubbly or liquid single-phase flow applying to this the 'dam-break' concept. This is based on the idea that liquid enters the side arm from the liquid slug because of its hydrostatic head, similarly to the pouring of liquid from a break in a dam. Split is generally gas dominated. An explanation for this can be given by the usual momentum argument. Gas and liquid will be moving at roughly the same velocity, so the lower momentum gas will be easily taken off. Whilst increasing liquid flow rate gives consistently a reduction in liquid take off, increasing the gas velocity generates a less uniform behaviour, switching to opposite trends as gas take off moves from low to high values. More specifically liquid take off increases with gas velocity at high take off and reduces when take off is low. It might be argued that when gas flow rate is increased, the local liquid velocity in the slug and in the annular section is also increased. Hence, whilst a more symmetrical film will enhance liquid take off from the annular portions, less liquid would be taken off from the slugs. These two mechanisms could have different weight in the low and high take off regime. In support of this, Arirachakaran (1997) observes that as gas take off increases the proportion of total liquid diverted that is taken off from the slugs reduces drastically.

Table II.1.1: Sources of reviewed data for two phase flow at T-junctions.

Author(s) and year	Fluids	Diameter (m)	Main pipe orientation	Pattern(s)	U_{gs} (m/s)	U_{ls} (m/s)	Pressure (bar)	Diameter ratio (-)
Chadwick (1965)	Steam/water	0.13	Vertical	Slug/Churn	1.8 – 6.4	1.25 – 1.6	69	0.58
Oranje (1973)	natural gas/ condensate	0.076	Horizontal	Stratified Annular	3 - 14	0.00018	30	0.67 1
Collier (1976)	air/water	0.038	Horizontal	Stratified Annular	0.8 – 18.5	0.066 – 0.13	3	0.67
Hong (1978)	air/water or air/0.005 – 0.01 Pas liquids	0.0095	Horizontal	Stratified Annular	9 - 43	0.0023 – 0.047	1.2 – 1.6	1
Johansen (1979)	air/water	0.051	Horizontal	Slug Stratified Annular	1.22 – 27.4	0.00457 – 0.0122		1
Honan & Lahey (1981)	air/water	0.038	Vertical	Slug/Churn	0.8 - 14	1.35 – 2.7	1.5	1
Azzopardi & Whalley (1982)	air/water	0.032	Vertical and Horizontal	Annular Churn Bubbly	4.4- 43.5	0.016- 0.11	1.5	0.2 0.4 0.6
Saba & Lahey (1984)	air/water	0.038	Horizontal	Stratified Slug	0.8 – 6.5	1.35 – 2.7	1.3 – 1.9	1
Zetzmann (1984)	air/water	0.024 0.05 0.1	Vertical	Churn Annular				0.5 1

Table II.1 Continued

Fairhurst (1986)	air/water	0.054	Horizontal	Slug	1.25	5.5		1
Katsaounis (1987)	air/water	0.203	Horizontal	Stratified Slug	0.08 - 2	0.025 – 0.1	1	0.26
Shoham *et al* (1987)	air/water	0.051	Horizontal	Stratified Annular	2.7 - 26	0.011 – 0.055	3	1
Reimann *et al* (1988)	air/water steam/water	0.05	Horizontal	Stratified Slug Annular	1 - 40	0.05 - 7	6 - 100	0.084 0.2 0.52 1
Azzopardi *et al* (1988)	air/water	0.032	Vertical	Annular	4.4 – 43.5	0.011 – 0.16	1.5	1
Davis & Fungtamasan (1990)	air/water	0.05	Vertical	Bubbly Slug Churn				0.5 1
Hewitt *et al.* (1990)	air/water	0.032	Vertical	Slug Churn	2.2-11.7	0.8-2.4	3-4.4	0.6 1
Arirachakaran (1990)	air/water	0.051	Horizontal	Slug	0.59 – 0.47	0.3 – 1.2	1	1
Azzopardi & Memory (1989) Azzopardi & Smith (1992)	air/water	0.038	Horizontal	Stratified Annular	0.7 - 31	0.008 – 0.078	1.5 - 3	0.33 0.67 1
Suu (1992)	air/water	0.021	Vertical	Bubbly Slug	0.07-0.32	0.81	2.38	1
Mudde *et al* (1993)	air/water	0.23	Horizontal	Stratified	0.01 – 0.19	0.5 – 1.5	1	0.43
Azzopardi *et al.* (1994)	air/water	0.076	Vertical	Slug	0.2-1.2	0.09-0.4	1.0	1
Charron & Whalley (1995)	air/water	0.032	Vertical	Annular	13-59	0.004-0.097	1.5	1
Peng (1994) Peng *et al* (1996)	Steam/water	0.026	Horizontal	Stratified Annular			1.1 – 2.1	0.5 0.82 1
Buell *et al* (1994) Walters *et al* (1998)	air/water	0.038	Horizontal	Stratified Annular	2.7 - 40	0.002 – 0.18	1.5 – 3	0..206 0.5 1
Rea & Azzopardi (1999) Wren *et al* (1999)	air/water	0.127	Horizontal	Stratified Annular	4 - 43	0.0045 – 0.558	1	0.6 – 1
Stacey *et al* (2000)	air/water	0.005	Horizontal	Annular	46 - 60	0.1 - 0.2	1.5	1

II.2 Modelling and comparison with experiments.

II.2.1 Introduction

The split of two-phase flow at T-junctions is very complex. The variables involved and the two main approaches used in modelling were briefly introduced in section. I.3. In the following a more detailed discussion on this aspect will be given before presentation of the works.

Saba & Lahey (1984) treated the problem as one-dimensional and carried out an analysis of the degree of freedom of the system in macroscopic terms. This is detailed in section I.3 and requires the determination of a 'characteristic equation' of the system, which in our case is the split characteristic. Some authors propose a form for this equation based on physical observations and/or empirically fitted to experimental data (e.g.: Azzopardi & Whalley, 1982; Zetzmann, 1984; Azzopardi, 1989). Others write an additional balance equation for example to predict the location of the dividing streamline (e.g.: Shoham *et al.*, 1987; Hwang *et al* ,1988; Ballyk *et al.*, 1990; Ma *et al,* 1991).

A different approach is that introduced by McCreery (1984) and later discussed and developed for the case of bubbly flow by Lemonnier & Harvieu (1987). The work of McCreery (1984) was extended by McCreery & Banerjee (1990) who considered the case of annular and annular-mist flow and solved the two-dimensional potential flow for the gas bulk and used a Lagrangian frame to calculate droplet trajectories. The paper by Lemonnier & Harvieu (1987) represents the link that encouraged the general philosophy behind this last kind of approach, the so called 'two-fluid' approach, which flourished with the advance in computer technology.

The argument is that the fifth equation, as a necessity to make the number of equations equal to that of unknown macroscopic variables, ends up being not more meaningful or simpler than empirical correlation. Furthermore, this equation often contains adjustable parameters (sometimes of non-realistic magnitude) and does not take into account the segregation phenomena from a mechanistic point of view.

A more rational approach is to write the differential mass balances and the 2-D or 3-D vector momentum balances. The closure problem will require the introduction of an interaction law between the phases, often pattern dependent. Solution is more often than not numerical (Lahey, 1990; Issa & Oliveira, 1991, Adechy & Issa, 1999).

From the above one can conclude that the two-fluid approach has built in a model for the flow approaching the junction. However, the fifth equation approach requires this knowledge as well, either from experiments or two-phase flow modelling in a straight pipe. In this sense, any two-phase pipe flow model is a necessary precursor of a split model. From this it is evident that modelling is very flow-pattern dependent hence, the papers discussed will be sorted by flow patterns and, for annular flow, a review of the models for the flow approaching the T will be given. Concepts are often applicable to both vertical and horizontal main geometry. For this reason, models will be presented in a common frame and the suitability of each approach to one main geometry or the other pointed out.

II.2.2 Horizontal annular flow models

As already mentioned in section II.1.2, the mechanism by which the liquid film is kept at the top of the pipe circumference in horizontal annular flow is not of trivial nature. Gravity acting downwards causes the liquid film to drain to the bottom of the pipe and some phenomenon must be invoked to justify the occurrence of horizontal annular flow. Butterworth (1974) recognised four possible mechanisms:

1) surface tension
2) circumferential secondary flow
3) spreading action of the disturbance waves
4) entrainment and deposition of drops from and to the liquid film

The first mechanism has never been investigated, as it would be relevant only for small diameter pipes for which no detailed experimental work is available.

Circumferential secondary flow was invoked by Laurinat *et al* (1985). Because of the non uniform roughness of the gas-liquid interface, secondary flows are induced in the circumferential direction. The shearing action of this flow is believed by some authors to be the primary reason for liquid holding on the pipe wall against gravity. Although Flores *et al* (1995) in their experimental study show the existence of this secondary flow, Jayanti *et al* (1989), calculated that its order of magnitude is far too small to justify it as the dominant mechanism. Nevertheless, **Laurinat *et al* (1995)** obtain very good predictions of the data of Laurinat (1982) in a 0.0508 m ID horizontal pipe using the predominance of secondary flows. Furthermore, all subsequent analysis by later authors builds on the same mathematical form of equations that are presented below.

As in most cases the model was built in the hypotheses of very thin films (h/D<<1) and this allows writing the balance equations in Cartesian co-ordinates. If the x co-ordinate is the circumferential one, for x=0 at the top of the pipe, y the radial distance from the wall and z the direction of flow, the components of the momentum balance on a film element Rdxdydz can be written as:

$$-\frac{1}{R}\frac{\partial p}{\partial \bar{x}}+\frac{\partial \tau_{xy}}{\partial y}+\frac{1}{R}\frac{\partial \tau_{xx}}{\partial \bar{x}}-\rho_l g \sin \bar{x}=0 \qquad [\text{II.2.1}]$$

$$-\frac{\partial p}{\partial y}-\rho_l g \cos \bar{x}=0 \qquad [\text{II.2.2}]$$

$$\frac{\partial \tau_{yz}}{\partial y}+\frac{1}{R}\frac{\partial \tau_{xz}}{\partial \bar{x}}=0 \qquad [\text{II.2.3}]$$

This holds in the hypothesis of negligible averaged velocity components in the radial and circumferential directions in comparison to the axial one.

Integrating the y component across the thickness of the film [0,h] gives the pressure distribution in the film as composed of the pressure at the interface and the hydrostatic component. The interface pressure can be related to the pressure in the gas phase and the radius of curvature of the film via the liquid surface tension. Manipulation and assumption of negligible surface tension contribution yields to the non-dimensional equations:

$$\frac{\partial \tau_{yz}^{+}}{\partial y^{+}}+\frac{1}{R^{+}}\frac{\partial \tau_{xz}^{+}}{\partial \bar{x}}=0 \qquad [\text{II.2.4}]$$

$$\frac{\partial \tau_{yx}^{+}}{\partial y}+\frac{1}{R^{+}}\frac{\partial \tau_{xx}^{+}}{\partial \bar{x}}-\frac{1}{R^{+}Fr}\sin \bar{x}-\frac{1}{R^{+2}Fr}\cos \bar{x}\frac{dh^{+}}{d\bar{x}}=0 \qquad [\text{II.2.5}]$$

The other equation needed is the mass balance on the liquid film in the circumferential direction:

$$\frac{1}{R^+}\frac{\partial \Gamma_x^+}{\partial \bar{x}} = r_D^+ - r_A^+ \qquad [II.2.6]$$

here R^+ is the radius, Γ_x^+ the circumferential film flow rate, r_D^+ and r_a^+ the rates of deposition and atomisation respectively and Fr is the Froude number for the gas $Fr=U_{gs}/(gD)^{0.5}$. The terms of the equations are made non-dimensional by using the kinematic viscosity of the liquid and a friction velocity $u^*=(\tau_s/\rho_l)^{0.5}$, τ_s being the smooth wall stress for the gas phase.

Multiple integration of II.2.4-5 along the y co-ordinate reduces τ_{yz} and τ_{yx} to their interfacial values. For these values and for the rates of liquid atomisation and deposition, empirical correlations are used (Cherimisinoff & Davis, 1979; Darling & McManus, 1969; Dallman, 1978; Laurinat, 1982 respectively). By definition $\tau_{xx}^+ = \overline{u'^{+2}}$ hence, the authors interpreted u' as the angular deviations of the main flow and assumed the normal stress to scale with the square of the mean local axial velocity $\bar{w} = \Gamma_z / h$. Omitting from now onwards the superscript '+' for non dimensional variables:

$$\tau_{xx} = -C_1 \bar{w}^2 \qquad [II.2.7]$$

whilst τ_{xz} was assumed to scale with its derivative:

$$\tau_{xz} = C_2 \frac{d\bar{w}^2}{dx}. \qquad [II.2.8]$$

Finally the system of ordinary differential equations for the circumferential variation is:

$$I_1(C_3 + C_4\Gamma_z) + \frac{C_2}{R} I_2 \frac{d^2\bar{w}^2}{d\bar{x}^2} = \Gamma_z \qquad [II.2.9]$$

$$I_1 C_5 \bar{\tau}_i \sin\bar{x} - \frac{I_2}{R} C_1 \frac{d\bar{w}^2}{d\bar{x}} - \frac{I_2}{RFr}\left(\sin\bar{x} + \frac{\cos\bar{x}}{R}\frac{dh}{dx}\right) = \Gamma_x \qquad [II.2.10]$$

$$\frac{1}{R}\frac{d\Gamma_x}{d\overline{x}} = r_D - r_A \qquad [II.2.11]$$

The constants C_i (i=1...5) derive from the assumption made on the various terms of the equation and I_1 and I_2 are integrals coming from manipulations of equations contained in Laurinat's paper. This system describes the circumferential variation of $\overline{w}$,h and Γ_x when the following boundary conditions are imposed:

$$\overline{x} = 0 \Rightarrow \Gamma_x = 0; \frac{d\overline{w}^2}{d\overline{x}} = 0 \qquad [II.2.12]$$

$$\overline{x} = \pi \Rightarrow \frac{d\overline{w}^2}{d\overline{x}} = 0 \qquad [II.2.13]$$

Because of the second order derivative of the average axial velocity, a condition is needed either on h or $\overline{w}$. For example the knowledge of h(0).

It must be highlighted that the system II.2.9-11 contains all the relevant terms in the hypotheses of validity of the form of the Reynolds stresses.

The equations where simplified assuming that the dispersion term is negligible (C_2=0). All constants and the rates of atomisation and deposition are adjusted according to empirical findings apart from C_5, which represents the magnitude of the term due to secondary flow. This was considered dominant and the constant adjusted to fit experiments in a 0.051 m ID horizontal pipe. The expressions used for entrainment and deposition relegated this term to a secondary role in determining the film distribution.

Lin *et al* (1985) used the same model of Laurinat *et al* (1985) for their data in a 0.0269 m ID horizontal pipe. There, using the net droplet exchange model of Butterworth (1974), they show that inclusion of the circumferential drag due to secondary gas flow as proposed by Laurinat, is crucial to correctly predict film thickness at the top. Again, wave spreading mechanism is not considered important and the magnitude of secondary flow, imposed to fit data.

The same approach is followed by **Hurlburt and Newell (2000)** who, starting from the findings of Laurinat, simplified the problem by introducing a symmetry parameter defined by the ratio between the average thickness h_{avg} and the thickness at the bottom h_0. We shall go in the details of this model, as this will be employed in Chapter IV to carry out comparison with the data of Chapter III. Williams (1996) plotted his symmetry parameter against the gas Froude number. The author observes that this would account only for the effect of gas flow rate on the degree of symmetry. Liquid flow rate is then included by plotting the symmetry parameter against $(\dot{m}_g/\dot{m}_l)^{0.5}Fr$. Such a plot of data from several authors and pipe diameters (0.025-0.095 m) shows a drastic reduction of scatter.

Laurinat's equations are simplified neglecting the dispersion term together with circumferential shear and atomisation and deposition. This implies that the circumferential velocity is zero. The normal stress term is assumed dominating on the static pressure gradient due to the variation of film thickness and equations II.2.4 and II.2.5 are reduced to:

$$\frac{\partial \tau_{yz}^{+}}{\partial y^{+}} = 0 \qquad [II.2.14]$$

$$\frac{\partial \tau_{xx}^{+}}{\partial \overline{x}} - \frac{1}{Fr}\sin\overline{x} = 0 \qquad [II.2.15]$$

Equation II.2.14 implies that the axial shear stress is independent of radial position and equal to its interfacial value. If the normal Reynolds stress τ_{xx}^{+} is assumed to be only a function of h^{+}, then, equation II.2.15 can be written as:

$$\frac{d\tau_{xx}^{+}}{dh^{+}} = -\frac{\sin(\overline{x})}{Fr_{\tau_s}\dfrac{dh^{+}}{d\overline{x}}} \qquad [II.2.16]$$

By plotting the RHS of equation II.2.16 as a function of h^{+}, from the experiments of Dallman (1978), the author obtains the following function for $\tau_{xx}^{+}(h^{+})$:

$$\tau_{xx}^{+} = -\tau_{xx,max}^{+}\left[1 - \exp\left(-\frac{h^{+}-6}{18}\right)\right] \qquad [II.2.17]$$

and, by substituting II.2.17 in II.2.15, the problem is reduced to the ordinary, uncoupled differential equation for the dimensionless thickness:

$$-\frac{\tau_{xx,max}}{18}\exp\left(-\frac{h^{+}-6}{18}\right)\frac{dh^{+}}{d\bar{x}}-\frac{1}{Fr}\sin\bar{x}=0 \qquad [II.2.18]$$

Equation I.2.18 can be solved analytically for h^{+} and the solution depends on the boundary condition given by the dimensionless film thickness at the pipe bottom h_{o}^{+}:

$$\frac{h^{+}-6}{h_{o}^{+}-6}=\frac{\ln[\alpha-\beta(\cos\bar{x}-1)]}{\ln\alpha} \qquad [II.2.19]$$

where:

$$h^{+}=\frac{h}{\nu_{l}}\left(\frac{\tau_{s}}{\rho_{l}}\right)^{0.5} \qquad [II.2.20]$$

$$\alpha=\exp\left(-\frac{h_{o}}{12}\right) \qquad [II.2.21]$$

$$\beta=\frac{1}{\tau_{xx,max}Fr_{\tau_{s}}} \qquad [II.2.22]$$

$$Fr_{\tau_{s}}=\frac{\tau_{s}}{\rho_{l}gR} \qquad [II.2.23]$$

and τ_{s} is the shear for single phase flow of the gas in a smooth tube, used to render the equations non-dimensional:

$$\tau_{s}=0.023\,Re_{gs}^{-0.2}\,\rho_{g}U_{gs}^{2} \qquad [II.2.24]$$

The other equation needed is the mass balance for the liquid phase:

$$\dot{m}_{lf}=\dot{m}_{l}-\dot{m}_{lE} \qquad [II.2.25]$$

were the subscripts l, f and E refer respectively to liquid, film and entrained quantities and the entrained fraction is considered a known parameter. The local average liquid velocity is correlated and depending on the film thickness. Hence, its determination is coupled to the solution of equation II.2.18.

Rather than by imposing the film thickness at the bottom, the problem is closed by implementing the empirical correlation mentioned above for the symmetry parameter h_{avg}/h_o. This is correlated to the dimensionless number $(\dot{m}_g/\dot{m}_l)^{0.5}Fr$. Here, h_{avg} is the average film thickness:

$$h_{avg} = \frac{1}{\pi}\int_0^{\pi} h(\bar{x})d\bar{x} \quad [II.2.26]$$

and the empirical correlation proposed by Hurlburt & Newell (2000) is:

$$\frac{h_{avg}}{h_o} = \frac{4}{3\pi}\left(\frac{h_o}{D}\right)^{0.5} + 0.9\left[1 - \exp\left(-\frac{(\dot{m}_g/\dot{m}_l)^{0.5}Fr}{90}\right)\right] \quad [II.2.27]$$

Hence, once the inlet conditions are given and fixed a value for h_o, the value of h_{avg}/h_o is calculated through equation II.2.27 and, because a theoretical expression of this ratio can be obtained from II.2.26, depending on $\tau_{xx,max}$, the value of this constant can be found for any fixed h_0. The film distribution is given by II.2.19, for the value of h_o that gives a correct mass balance (equation II.2.25), once the axial shear stress correlation (equation II.2.28) and the average axial velocity correlation (equation II.2.29) are implemented (Asali *et al*, 1985; Henstock & Hanratty, 1976). These are as follows:

$$\frac{\tau_i}{\tau_s} - 1 = 10\left[1 - \exp\left(-\frac{\phi h_i^+}{250}\right)\right] \quad [II.2.28]$$

and

$$\frac{W_{avg}}{u_i^*} = \left[\left(1.5 \left(h_i^+ \right)^{0.111} \right)^{-2} + \left(9.5 \left(h_i^+ \right)^{0.111} \right)^{-2} \right]^{-0.5} \qquad [II.2.29]$$

where

$$\phi = \frac{\mu_l}{\mu_g} \left(\frac{\rho_g}{\rho_l} \right)^{0.5} \qquad [II.2.30]$$

$$h_i^+ = \frac{h u_i^*}{\nu_l} \qquad [II.2.31]$$

$$u_i^* = \left(\frac{\tau_i}{\rho_l} \right)^{0.5} \qquad [II.2.32]$$

Also, a model for the entrained fraction is needed to carry out the mass balance on the liquid. The author assumed this to be known.

Results of the model show deterioration of the agreement with the data of Laurinat (1982) when the symmetry parameter is low, closer to stratified conditions.

Fukano & Ousaka (1989) made experiments in a 0.026 m ID horizontal or near horizontal pipe. They tested the model of Laurinat against their data and found non-convergence of the model for velocities U_{gs}<30 m/s and/or U_{ls}>0.06 m/s, although Lin *et al* (1985) found solution using different correlations. Also, no solution could be found when the top of the pipe was dry, towards stratified flow. The argument of the authors is that the magnitude of the circumferential drag necessary to obtain good agreement with data was unrealistic. This is currently supported by the investigations of Jayanti *et al* (1989).

The authors assumed the wave spreading mechanism, interpreted as pumping action of the disturbance waves, to be dominating. This is due to the difference of pressure rise when stagnation occurs at the rear of the wave, between the top and the bottom of the pipe. Since the wave on the base film is faster at the bottom, the negative pressure gradient will move liquid towards the top against gravity. Once the wave has gone past, liquid drains down at the back of it. The process is unsteady but the authors assumed that there is an average film distribution based on the observation that the time interval between the transit of two waves is smaller than the characteristic time for the liquid to drain at the bottom. The equations are the same used by Laurinat but the circumferential drag is neglected and the pumping action is included by modelling the normal stress as proportional to the pressure difference between the crest and the rear of the wave. In dimensional terms:

$$\tau_{xx} = -C_1 \Delta p = \frac{-C_1 \rho_g \left[\left(w_{gr} - c_D \right)^2 - \left(w_{gc} - c_D \right)^2 \right]}{4} \qquad [II.2.33]$$

where c_D is the wave velocity and w_{gr} and w_{gc} are the gas axial velocities at the rear and crest of the wave.

The constant C_1 was calculated by iteration when convergence of the film distribution was obtained. The authors claim very good agreement with data and obtain solutions also for those cases when the wall is dry at the top. The quality of results is as good as Laurinat's when both models give convergence.

Fisher and Pearce (1978) and **James *et al* (1987)** dealt with models dominated by mass transfer (i.e., entrainment and deposition of drops).

II.2.3 Annular and stratified flows

Azzopardi & Whalley (1982) were the earliest authors to propose a predictive method for the split of vertical annular flow. Their experiments at low take off and small liquid inlets, showed a weak dependence of split characteristic on the gas flow rate. The authors argued that given the high Reynolds number for the gas phase in all the database, the shape of the gas velocity profile is independent of the inlet flow rate. If the fraction of liquid film taken off depends only on the shape of the gas streamlines, then for the same proportion of gas taken off in the side arm, the same amount of liquid will be diverted, whatever the inlet gas flow rate.

Data were plotted as fraction of diverted gas versus the apparent angle θ over which the film is extracted:

$$\theta = \frac{2\pi * \text{side water flowrate}}{\text{Total film flowrate}} \qquad [II.2.34]$$

Because it was found that this relationship was linear, the authors assumed that the phases were both taken off from a common segment of the pipe cross section and hence the relationship between this angle θ and the fraction of diverted gas is:

$$G' = \frac{1}{2\pi}(\theta - \sin\theta) \quad [II.2.35]$$

and for the liquid

$$L' = \frac{\theta}{2\pi}(1 - E) \quad [II.2.36]$$

Because of the linear relationship between θ and the gas mass flow rate in the side arm, this angle was interpreted as composed of the sum of an angle A (i.e. the physical angle subtended by the side arm to the axis of the main pipe, Figure II.2.1) plus a term linear in the gas mass flow rate in the side arm. The latter is expected to increase as the side arm diameter increases and the model is independent from the mass flow rates at the inlet.

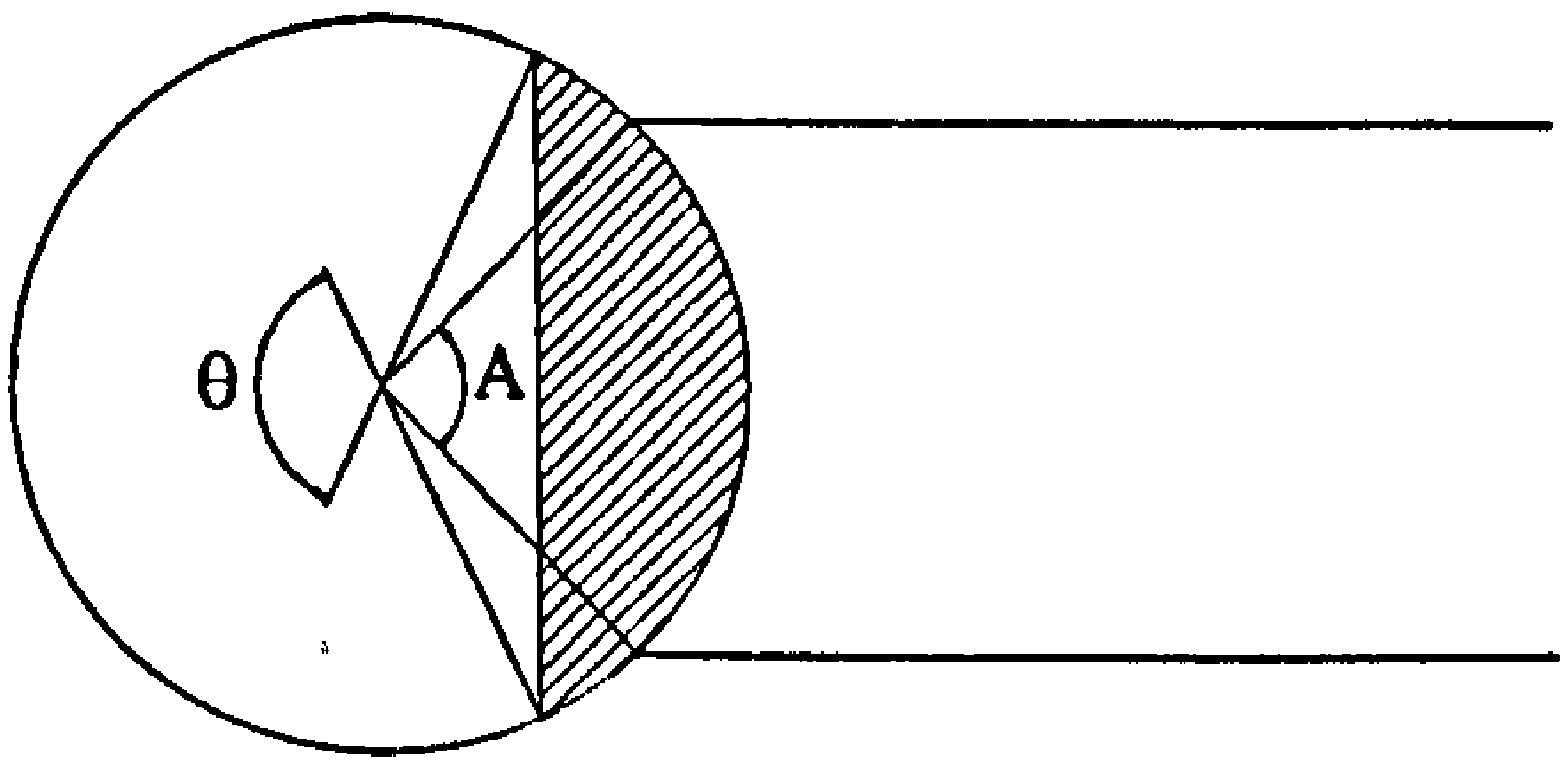

Figure II.2.1: *sketch showing the concept of common segment for phases take off in annular flow. Azzopardi & Whalley (1982).*

An empirical improvement to take into account the effect of diameter ratio was introduced by Azzopardi (1984). This is based on the idea that the smaller the side diameter, the higher will be the probability of the liquid film going past the junction without entering the side arm. This was empirically correlated by the definition of a correction factor K:

$$K = 1.2 * \left(\frac{d_3}{d_1} \right)^{0.4} \quad [II.2.37]$$

and, taking into account the liquid entrainment, the fraction of liquid taken off becomes:

$$L' = K \frac{\theta}{2\pi} (1 - E) \quad [II.2.38]$$

Where K physically represents the ratio between the apparent angle θ for the case of regular T and the same angle for the case of reduced T-junction. E is the entrained fraction and accounts for the fact that the droplets are not diverted in the side arm because of their large momentum. For each G', θ can be calculated from equation II.2.35.

Azzopardi (1989) developed this method further by accounting for indirect mechanisms of liquid take-off such as film stop and flooding.

The fraction of gas to be diverted for the occurrence of film stop is evaluated by writing the extended Bernoulli equation between inlet and run outlet for the mixture and the liquid film. The loss coefficient at the T appearing in the dissipation term of the Bernoulli equation for the mixture is imposed using the single-phase flow correlation from Gardel (1959).

This yields:

$$G_{fs}^{i} = 0.715 - \sqrt{0.493 - 0.633 \frac{\rho_l U_{l1}^2}{\rho_g U_{g1}^2} + \frac{1.266D}{\rho_g U_{g1}^2}} \quad [II.2.39]$$

Here D is the dissipation term in the Bernoulli equation for the liquid film. No indication for its magnitude was available and it was assumed zero giving an underestimate of the critical gas take off for the conservative case.

Once film stop occurs, there is an extra-entrainment of liquid depending on the way the shear of the gas acts on the liquid. This is fitted by the equation:

$$L'_{extra} = (1 - L^* - E)\sqrt{\frac{G'^2}{1 - 2G' - 2G'^2}} \qquad [II.2.40]$$

where L^* is the direct take off obtained using equation II.2.38 and E is the entrained fraction.

Occurrence of flooding is calculated using the flooding equation of Wallis (1961):

$$\sqrt{U_l^*} + \sqrt{U_g^*} = 0.88 \qquad [II.2.41]$$

The non-dimensional velocities are:

$$U_i^* = U_{is2}\left(\frac{\rho_i}{(\rho_l - \rho_g)gD}\right)^{0.5} \qquad i=l,g \qquad [II.2.42]$$

When $U_{ls2}=0$, the gas velocity in the run can be calculated from equation II.2.41 and the critical gas take off is:

$$G'_{flood} = 1 - \frac{U_{gs2}^{flood}}{U_{gs1}^{flood}} \qquad [II.2.43]$$

As flooding can occur with or without previous appearance of film stop, the expression for the amount of liquid available to fall back will be different in the two cases. If film stop does not occur, then, since the entrained liquid is caught by the flooding waves, all the liquid which is not taken off directly is involved in flooding (Azzopardi, 1988). Hence:

$$U_{ls2} = \frac{\dot{M}_{l1} - \dot{M}_l^*}{\rho_l A_l} \quad [II.2.44]$$

where A_l is the cross sectional area of the mean pipe and $\dot{M}_l^*$ is the liquid taken off by the direct take off mechanism.

If film stop occurs, then only the entrained fraction, which is seen to deposit on the pipe wall after the junction, is available to fall back:

$$U_{ls2} = \frac{\dot{M}_{lE}}{\rho_l A_l} \quad [II.2.45]$$

The superficial velocity of liquid falling back is given for each case by II.2.44-45 (depending on the case) subtracted of the liquid carried up and calculated from II.2.41 for each gas split.

Very good agreement with experiments is achieved for the vertical data of Azzopardi (1988) in a 0.032 m ID regular square T-junction, using the prediction of entrainment by Govan *et al.* (1988) and the film distribution model by Asali (1984). The reasoning is extended to the case of horizontal pipes. There flooding does not occur and different relationships are needed for entrainment, film distribution and local film flow rate which is not uniform around the pipe circumference. Film flow rate was considered uniform in the first approximation. The equation of Dallman *et al* (1984) was used for liquid entrainment and film distribution was predicted by using the model of Laurinat *et al.* (1984). This allowed comparison with the horizontal data of Hong (1978), Shoham *et al* (1987) and Azzopardi *et al* (1988). Significant under prediction is shown with the data of Hong (1978) in a 0.0095m ID T-junction. For such small pipes, as discussed in the experimental section, liquid take off is enhanced by the symmetry of the film and entrainment is presumably lower then what is predicted by the equation of Dallman *et al* (1984) for larger pipes. However, the trend is correct. Good prediction was shown with the data of Shoham *et al* (1987) and Azzopardi *et al.* (1988). Discrepancies are attributed to the assumption of uniform film flow rate. The author claims better agreement with the data by Azzopardi & Whalley (1982) if the measured liquid flow rate variation is fed into the model.

Roberts *et al* (1995) further developed this model to test it in the transition between stratified and annular flow for the case of a horizontal 0.127 ID T-junction exploring the semi-annular flow region. The idea of direct take off from a common segment and that of film stop were applied considering the film to be composed of a stratified layer at the bottom, up to a certain angle, and a film of uniform thickness along the rest of the pipe circumference. The angle covered by the stratified layer was estimated by using the correlations for fraction of wetted wall by Hamersma & Hart (1987) or Hart *et al* (1989) whilst entrained fraction was according with the correlation of Williams (1986). Hamersma et Hart (1987) also give a correlation for the void fraction. Alternatively, void fraction was imposed using the correlation of Lockhart & Martinelli (1949).

At the lowest gas flow rates, best fit of the data was observed using the fraction of wetted wall of Hamersma & Hart (1987) with the void fraction from Lockhart & Martinelli (1949). As gas flow rate was increased, better prediction was given by Hamersma's own void fraction correlation. This also gives the best fit when liquid flow rate is increased but liquid take-off is significantly over predicted. This was attributed to the small, unrealistic values of entrained fraction given by Williams (1986). Also, very good agreement was obtained with the data of Azzopardi (1988) on the stratified-annular boundary by using the wetted wall fraction from Hart *et al* (1989). Finally, for the data in stratified flow by Shoham *et al* (1987), best predictions showed when Hamersma's wetted wall and Lockart & Martinelli's void fraction were imposed.

Overall, in the case of small liquid hold-up stratified, semi-annular and annular flow, the enhancement of Azzopardi (1989) by Roberts *et al.* (1995) satisfactorily models the phase split showing good applicability, independently of pipe diameter. Nonetheless, the windows of validity of each assumption on fraction of wetted wall, entrainment and void fraction show that better knowledge is to be achieved to predict them more reliably in a wide range of inlet conditions. For the highest liquid flow rates, both in stratified and annular flow, scale assumes a more significant role in modelling.

For stratified flow, Rea & Azzopardi (1999) took this into account by using their experimental data and feeding them into the model by Shoham *et al.* (1987) discussed further below.

Roberts *et al* (1997), who recognized the importance of accurately predicting the liquid film distribution, also considered the effect of scale. The authors extended the model of Azzopardi (1989) to the horizontal annular flow regime. As already pointed out in the section regarding experiments, the degree of asymmetry of the liquid film is more marked for larger diameter pipes and models accounting for different mechanism by which the liquid is held on the top of the pipe give very different predictions. In particular the authors used the model of film distribution of Fukano & Ousaka (1989) invoking the mechanism of pumping action of the disturbance waves due to the normal stress gradient. The film thickness at the bottom is imposed by using the empirical correlation from Sekoguchi *et al* (1982) obtained for the case of a 0.026 m ID pipe and extended to any diameter in the following manner:

$$h_0^+ = 846 \frac{D}{D_{ref}} \frac{Re_{lf}^{0.44}}{Re_{sg}^{0.59}} \qquad [II.2.46]$$

where D_{ref}=0.026 m and Re_{lf} and R_{sg} are the Reynolds number for the liquid film and the gas respectively. The non dimensional height is normalized by u^*/ν_l where ν_l is the liquid kinematic viscosity and friction velocity $u^*=(\tau_i/\rho_l)^{0.5}$. Convergence and the determination of the constant appearing in the expression for the normal stress in the circumferential direction, τ_{xx} is obtained by imposing the entrained fraction by Laurinat *et al* (1984) and iterating until the value of this constant is compatible with that entrained fraction

After this was implemented in the model of Azzopardi (1989), results were compared with experiments obtained for pipe diameters of 0.032 and 0.038 m for horizontal, vertical upward and downward orientations of the side arm (Azzopardi & Whalley, 1982; Azzopardi, 1988; Azzopardi & Smith, 1992). Agreement is improved significantly in all cases, especially when film stop occurs and it is calculated on the basis of a varying film flow rate. For the upward side arm case, liquid take off is over-predicted and this could be attributed to the fact that the liquid falling back from the side arm when gas take off is not large enough, is not accounted for.

Similarly, Azzopardi & Rea (1999) attempted better predictions for larger diameter pipes (0.127 m) using the model of Hurlburt (1997) for the circumferential film distribution. They further developed the correlation for the thickness at the bottom proposed by Roberts *et al.* (1997) using more available data and showing that dependence on the square of the pipe diameter better fits experimental data:

$$h_0^+ = 846\left(\frac{D}{D_r}\right)^2 \frac{Re_{lf}^{0.44}}{Re_{gs}^{0.59}} \qquad [II.2.47]$$

The prediction over-estimated the height for the largest available diameter (0.095 m) and this relationship was also used to close the problem instead of the empirical fit of $\frac{h_{avg}}{h_0} = f\left(\frac{\dot{M}_g^2}{\dot{M}_l^2}Fr\right)$ used by Hurlburt.

Results obtained using the entrained fraction by Dallman *et al* (1979) and Williams *et al* (1996) gave better qualitative results as opposed to the uniform film assumption of Azzopardi (1989) although liquid take off was under predicted. Quantitative agreement could be obtained if a smaller entrained fraction was imposed.

Because of the implementation of a film thickness distribution, split could be calculated also for different orientations of the side arm. Again, only qualitative comparison was satisfying as the liquid take off was over predicted.

The approach of other authors often seeks the determination of the surface envelope of the dividing streamlines for each longitudinal section of the inlet pipe, parallel to the plane of the T. In an implicit manner, this is contained also in the basic model of Azzopardi & Whalley (1982) and throughout the above models where such surface is, for both phases, a plane individuated by the segment from where the fluids are diverted (subtended by the angle θ).

Shoham *et al.* (1987), for example, developed their model for horizontal annular and stratified flow. They neglect entrainment of the liquid and still assume a planar shape for the surface envelope of the dividing streamlines (Figure II.2.2). For the annular flow case, the film was assumed to be symmetrical which makes this model particularly suitable for vertical annular flow. The height h for stratified flow and the thickness δ for annular flow are both calculated by the model of Taitel & Dukler (1976). This implies writing a momentum balance for each phase and imposing equal pressure drops for the two phases. Estimation of the friction factor for the evaluation of the wall and interfacial stresses is required.

Initially, the authors propose a simple geometrical model depending on the normalised height of the film in the stratified flow (h/D) and normalised film thickness in the annular flow (δ/D). As in Azzopardi & Whalley (1982), the two phases are assumed to come from the same segment and the split characteristic is obtained by moving this segment across the pipe section. This model shows some features encountered in the experiments such as the shape of the separation curves and, for annular inlet flow, the existence of a liquid fraction intake threshold for any gas to be extracted. Also, the annular flow case degenerates into the geometrical model of Azzopardi & Whalley (1982) when $\delta/D \sim 0$.

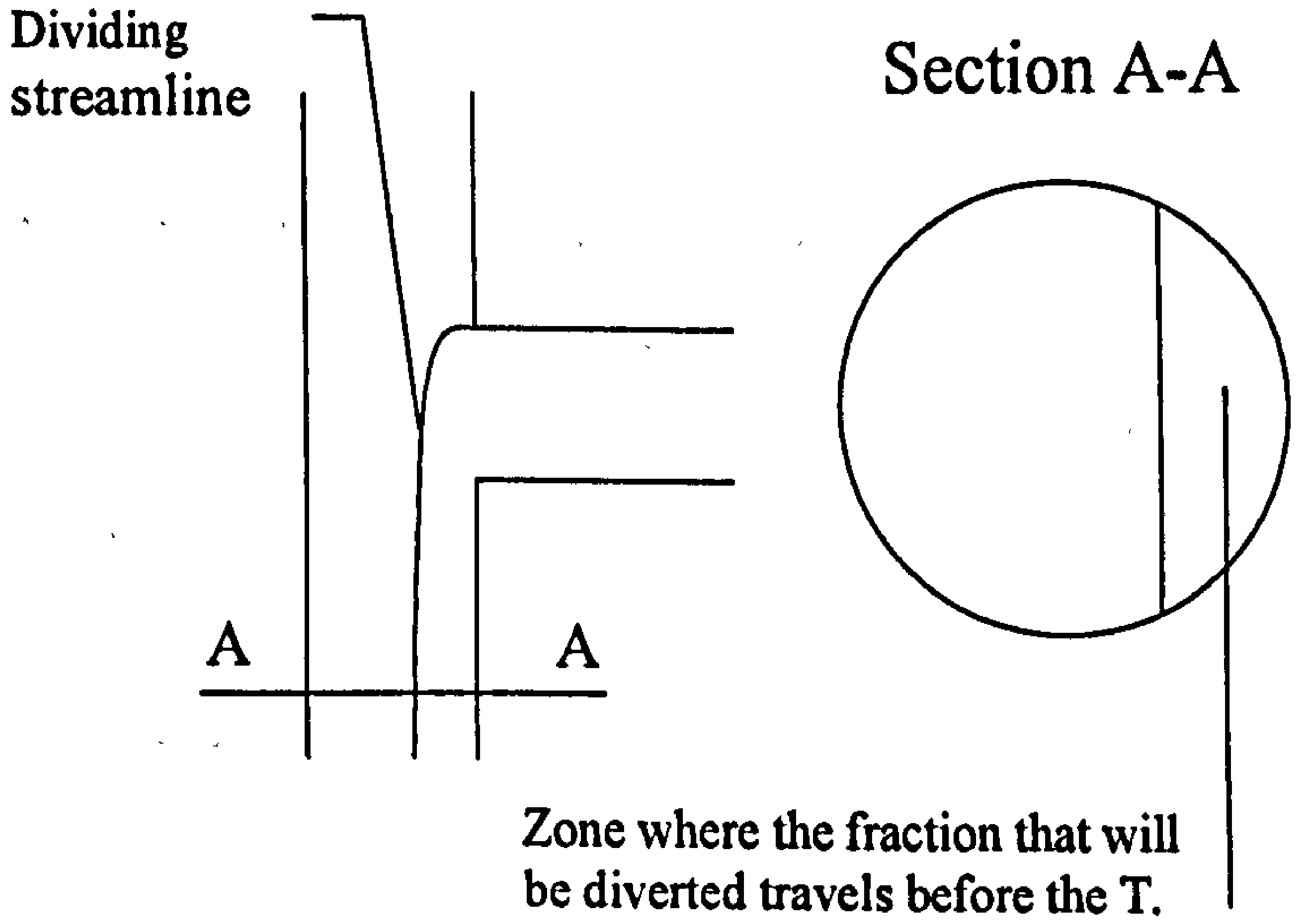

Fig II.2.2: *Sketch showing the model by Shoham et al (1987).*

The authors then improved the model on the basis of the take off mechanism reported by Hong (1978) proposing that the liquid film is affected by a net centripetal force. This is due to the turn of the gas phase into the side arm. The hypotheses of coincidence of the dividing streamlines for the two phases is removed and as a gas dividing streamline (i.e.: G') is imposed, the corresponding dividing streamline is calculated for the liquid (i.e.: L').

The trajectory of the gas streamline is assumed to be an arc of circumference and the radius of curvature r_0 can then be calculated. The net centripetal force is expressed as (Banerjee *et al,* 1961; Whalley, 1980):

$$f_c = \frac{\rho_l v_l^2 - \rho_g v_g^2}{\rho_l r_0} \qquad [II.2.48]$$

Where v is the local velocity of the phases depending on the flow regime and on the film height in the stratified case and film thickness in the annular case. It is also function of the superficial velocity of the phases. The law of radial motion for the liquid will be obtained solving the differential equation:

$$\ddot{r} = f_c - k\dot{r} \qquad [II.2.49]$$

containing the viscous damping action of the liquid. This allows the position of the dividing streamline for the liquid and the displacement of the segment of liquid take-off from the imposed gas segment to be calculated. From this, the fraction of liquid taken off, L', can be determined.

The authors claim very good agreement with data in the annular flow regime. However, if the correlation by Wallis (1969) was used to calculate the interfacial friction factor, quantitative agreement was poor. If δ/D is used as an adjustable parameter, also quantitative agreement could be achieved but the film thicknesses required were not realistic.

In the stratified wavy flow pattern, a constant value of the interfacial friction factor as proposed by Cohen & Hanratty (1968) is used (f_i=0.009) giving satisfactory results.

In stratified smooth flow the authors reasonably assume the friction factors to be close to the smooth wall ones. This leads to film heights lower than the ones needed to obtain good agreement with experiments.

An attempt to enhance this model was made by **Rea & Azzopardi (1999)** who tested its predictive capability by imposing the measured values of film height in the stratified flow regime obtained from their experiments in a 0.127 m ID T-junction. This also affected the damping factor k in equation II.2.49, which is inversely proportional to the height, and the void fraction as it was calculated from the experimental shape of the gas-liquid interface. This indirectly tested the predictions of Taitel & Dukler (1978).

An additional feature introduced by Rea and Azzopardi (1999) deals with the behaviour in the low take off region. Following the mechanism proposed by Arirachakaran (1990) who studied slug flow, the authors argue that for low take off, the mechanism dominating liquid diversion in the side arm is gravity driven when the wall supporting the layer is removed at the side opening. This is analogous to a 'dam-break', where a negative pressure wave propagates in the liquid causing it to pour out of the rupture. The area per unit depth that is diverted by this mechanism is given by:

$$A_{div} = \frac{8w_0^3 t_r}{27g} \qquad [II.2.50]$$

where t_r is the residence time of the liquid across the side arm opening, g is the acceleration of gravity and $w_0=\sqrt{gh_0}$ is the velocity of propagation of the negative pressure wave, h_0 being the liquid height at the centre.

These modifications significantly improve the prediction of Shoham's original model in the case of large diameter pipes, highlighting the poor account taken of scale effect by the stratified flow model of Taitel & Dukler (1978). This last model consistently over predicts film height larger than 0.02 m. Scale effect is important also in introducing the 'dam-break' mechanism, as film asymmetry is more marked for larger pipes and the observed initial increase of liquid take off is predicted. Still, agreement is poor at large take off where film stop might occur, as it is not accounted for. The occurrence of a hydraulic jump in the run leg, discussed in the review of experiments is still lacking of any modelling and high liquid take off can not be correctly predicted.

Shoham ***et al*** **(1987)** extended the same model to the case of reduced T-junctions. This is achieved in a straightforward manner by considering that the smaller diameter in the side arm will cause the liquid to travel across the side opening in a shorter time. Hence less liquid is taken off. On the other hand, because of the smaller radius of curvature in the gas dividing streamline, the centripetal force is of larger magnitude. In both cases a decrease in the predicted liquid take off is calculated. This fits in a satisfactory way the data in the stratified flow but underestimates liquid take off for the annular case, where no significant variation is observed for diameter ratios between 1 and 0.5. In this latter case the authors suggest to use the previous model. This might be due to the fact that the model only considers the under-pressure caused by the gas turning into the T and does not allow for the increase of pressure differential in the side due to the higher velocity of the gas as it travels in a smaller duct. As already mentioned Walters *et al* (1998) find in fact that liquid take off increases when the diameter ratio is brought from 0.5 to 0.2 in their 0.038m ID data.

Penmatcha *et al.* (1996) and **Marti & Shoham (1997)** further refine the model of Shoham *et al* (1987) to account for diameter ratio and side arm inclinations in the stratified flow regime. In particular Penmatcha *et al* (1996) concentrates on downward and Marti & Shoham (1997) includes upward inclinations. The most interesting feature though is that the authors abandon the criterion whereby the net centripetal force caused by the gas turning into the T is responsible for the split of the phases. The approach is based on momentum balances written for each phase along the respective dividing streamline. The driving force responsible for the split is then the pressure drop towards the side arm imposed by the known fraction of gas travelling into it plus gravity (depending on pipe inclination) and elevation (i.e.: the distance between the bottom of main pipe and side arm). The last two are both zero for the case of horizontal side arm and negligible for the gas phase whilst the elevation is not significant for downward inclinations.

The momentum balance written for the generic phase is:

$$\frac{\partial p}{\partial y} + \rho_i g \sin\phi + \rho_i \frac{\partial u_i}{\partial t} + \rho_i g \frac{\partial z}{\partial y} = 0 \quad i=g,l \qquad [II.2.51]$$

z is the elevation, y the radial distance, ϕ the side arm inclination positive upward and g is the acceleration of gravity

Integration of the momentum equations for the gas gives:

$$\Delta p_g = -2\rho_g u_g^2 \frac{Y_g^2}{X_g^2} \quad [II.2.52]$$

which can be substituted into the result yielded by the integration for the liquid phase:

$$\left(\frac{2\rho_l u_l^2}{X_l^2}\right) y_l^2 + \left(\frac{\Delta p_g}{Y_g} + \rho_l g \sin\phi\right) y_l + \rho_l g z = 0 \, [II.2.53]$$

where X_i is the axial distance in correspondence of the side arm opening and Y_i is the radial distance of the dividing streamline before it starts turning towards the stagnation point (i=l,g) on the downstream corner of the T.

With regard to comparison with data, it must be pointed out that the experimental campaign was carried out for the same main pipe diameter of 0.051m as in Shoham *et al* (1987) but with a round edged T. The same inlet conditions give higher liquid take off than what was obtained in the earlier work but no assumption is made over the corner geometry in the model.

Comparisons for the horizontal side arm and regular T are qualitatively good if the measured hold up is introduced rather than using the prediction of Taitel & Dukler (1978). This particularly under predicted for larger heights.

Yet another line of analysis is the approach by Shoukri and co-workers (1988-97). **Ballyk & Shoukri (1990)** developed a model for annular flow in a horizontal regular T-junction to test against the experiments by Ballyk *et al.* (1988).

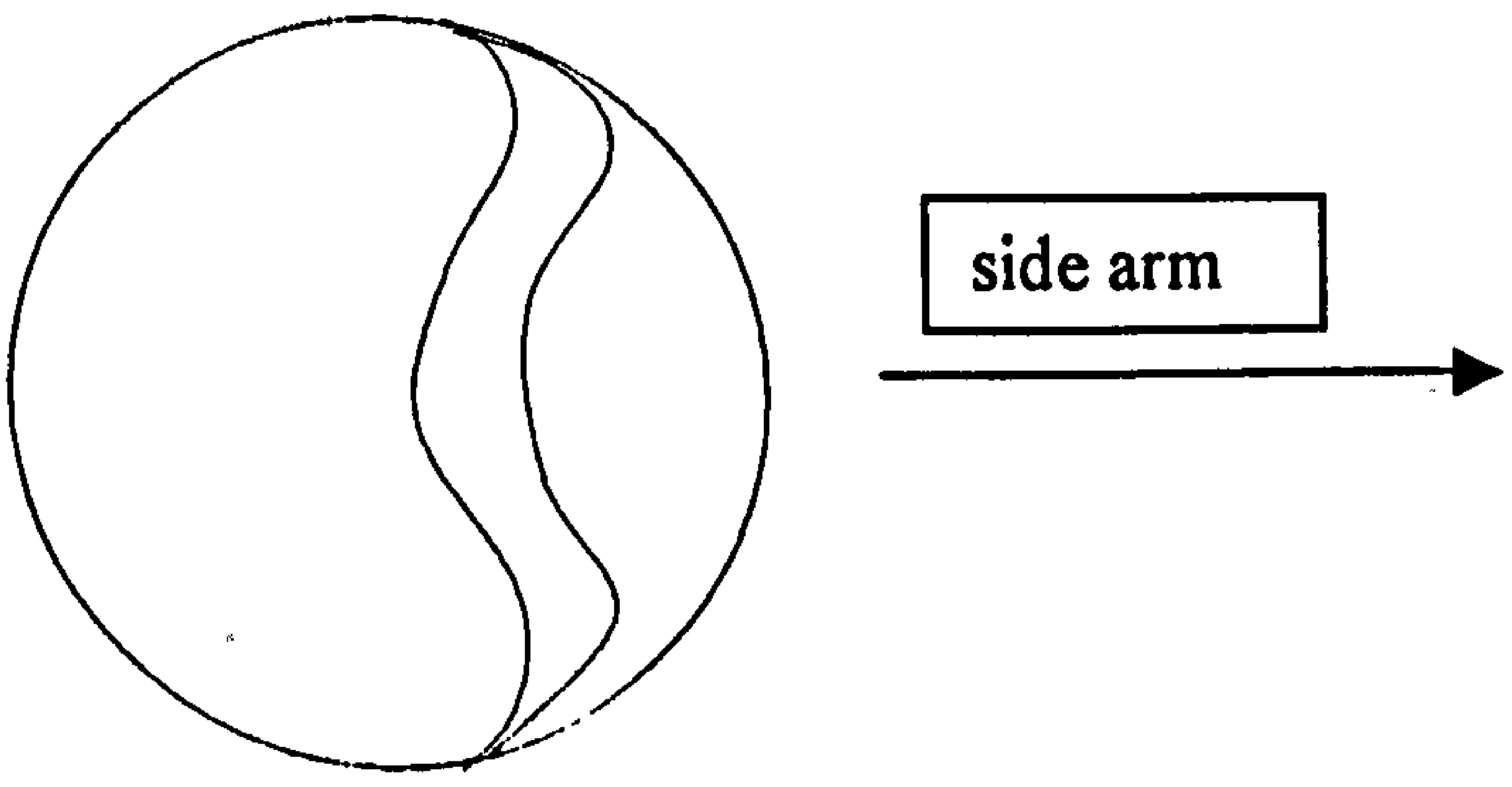

Figure II.2.3: *Non-planar 'zones of influence' from the model of Ballyk et al (1990) and Peng & Shoukri (1997).*

They also used the concept of dividing streamline and were the first to account for its dependence on the elevation of the horizontal plane. In other words, the dividing streamlines for the flow in two horizontal parallel planes, are not the same.

Figure II.2.3 shows the inlet pipe cross section and the shape of the surface dividing the diverted fraction from the remaining stream.

Because of the high velocity of the phases in annular flow, the flow is supposed to be dominated by inertial and pressure forces so that Euler's equation can be written in the junction domain for each phase uncoupled from the other (no interaction term). Peng & Shoukri (1997) improved this by considering also a gravitational term to include the case of inclined side arm:

$$\begin{aligned} &\mathrm{div}\,\underline{u} = 0 \\ &u_x \frac{\partial u_x}{\partial x} + u_y \frac{\partial u_x}{\partial y} = -\frac{1}{\rho}\frac{\partial p}{\partial x} \\ &u_x \frac{\partial u_y}{\partial x} + u_y \frac{\partial u_y}{\partial y} = -\frac{1}{\rho}\frac{\partial p}{\partial y} + g\sin\theta \\ &\mathrm{curl}\,\underline{u} = 0 \end{aligned} \qquad [II.2.54]$$

where x is the direction of the flow and y is the direction of the side branch.

The system of equations is solved imposing that the velocity has component only in the x direction equal for the gas to the mean gas velocity and for the liquid to the wall film velocity.

The two pressure derivatives are modelled as follows:

1) $\frac{\partial p}{\partial x}$ imposing that the irreversible pressure recovery $(\Delta p_{12})_J$ changes linearly along the observed length over which steady, linear pipe loss is reached again.

2) $\frac{\partial p}{\partial y}$ is modelled assuming it is zero at the wall opposite to the junction and linear in the distance from the wall, again normalised on the development length of the branch pressure change.

The calculation is made at different elevations and iterated with different starting points until the streamline ends on the intersection of side and main pipes downstream from the T (so obtaining a dividing streamline).

In this way the zones of influence are bound by a non planar surface. As reasonable, the zone from which the phases are taken off is wider in line with the midpoint of the side branch vertical diameter (Figure II.2.3). The quality of the streams is obtained by imposing a film profile as experimentally measured by Lin *et al* (1985) in the work of Ballyk & Shoukri (1990) and the model by Peng (1994) following Butterworth (1984) in the more recent work by Peng & Shoukri. This consists of a film mass conservation equation, the triangular relationship (Hewitt & Hall-Taylor, 1978) and the momentum equation for the film as reduced by Butterworth (1974):

$$\frac{d\Gamma}{d\theta}+R\left(\dot{M}_e-\dot{M}_d\right)=0 \qquad \text{film continuity}$$

$$\Gamma=\int_0^h \rho u_x dy \qquad \text{triangular relationship} \qquad [II.2.55]$$

$$(\mu+\nu)\frac{\partial^2 u_x}{\partial y^2}+g\sin\theta=0 \qquad \text{momentum equation}$$

were ν is the turbulent diffusivity, R the radius, Γ is the circumferential film flow rate, θ the circumferential angle, h is the film thickness and $\dot{M}_e$ and $\dot{M}_d$ the entrainment and deposition fluxes from and to the liquid film surface. Empirical correlations for entrainment and deposition are used (Lin *et al*, 1985; Laurinat *et al*, 1985; Hutchinson *et al*, 1973).

Results were compared with the experiments of Peng *et al.* (1996) and Ballyk *et al.* (1988) for horizontal, 45° and 90° downward branch orientation. Prediction was good as long as the gas velocity was not too large. There, prediction was poor especially for the downward cases. The authors give explanation for this by the fact that the annular model is a very simple one, not taking into account that for very high gas velocity, the film becomes symmetrical again. A definite weakness of the model is the necessity of a predicted or measured value of the pressure drops at the junction. In fact, the model showed to be quite sensitive to the chosen value of the development length before linear pressure drop started in the side arm and values were adjusted for best fit of data.

Hart *et al.* (1991) modelled flow split to fit their low hold-up data ($\varepsilon_l<0.06$) and although the approach is independent of flow pattern, many hypotheses used in its development strongly rely on the low value of ε_l. This restricts its applicability to stratified, annular and annular-mist flow.

The model is called the *Double Stream Model.* This is obtained writing the extended Bernoulli equation for each phase in the inlet-to-run and inlet-to-arm streams. Subtracting the former from the latter:

$$\text{Gas} \quad (p_2-p_3)_g+\frac{1}{2}\rho_g g\left(u_{g2}^2-u_{g3}^2\right)+\rho_g g\left(z_{g2}-z_{g3}\right)=\frac{1}{2}\rho_g u_{g1}^2\left(k_{13}-k_{12}\right)$$

[II.2.56]

$$\text{Liquid} \quad (p_2-p_3)_l+\frac{1}{2}\rho_l g\left(u_{l2}^2-u_{l3}^2\right)+\rho_l g\left(z_{l2}-z_{l3}\right)=\frac{1}{2}\rho_l u_{l1}^2\left(k'_{13}-k'_{12}\right)$$

[II.2.57]

where k are the loss coefficients for the gas and k' for the liquid phase, the subscripts have the conventional meaning in two-phase flow at T-junctions and u is the root mean square of axial velocity that by definition is:

$$u=\sqrt{\frac{<v^3>}{<v>}} \quad \text{[II.2.58]}$$

The equality of pressure drops for the two phases is imposed, i.e.: $(p_2\text{-}p_3)_g = (p_2\text{-}p_3)_l$ which subtracting equation II.2.57 from II.2.56 and dividing by $\frac{1}{2}\rho_l u_{l1}^2$ gives:

$$\frac{\rho_g u_{g1}^2}{\rho_l u_{l1}^2}\left(\frac{u_{g2}^2}{u_{g1}^2}-\frac{u_{g3}^2}{u_{g1}^2}\right)-\left(\frac{u_{l2}^2}{u_{l1}^2}-\frac{u_{l3}^2}{u_{l1}^2}\right)+\frac{2g}{u_{l1}^2}\left[\frac{\rho_g}{\rho_l}\left(z_{g2}-z_{g3}\right)-\left(z_{l2}-z_{l3}\right)\right]= \qquad \text{[II.2.59]}$$
$$=\frac{\rho_g u_{g1}^2}{\rho_l u_{l1}^2}\left(k_{13}-k_{12}\right)-\left(k'_{13}-k'_{12}\right)$$

Similarity of the velocity profiles in both phases and in all branches is then imposed and this allows writing the ratio of the mean squares within the same phase as the square of the mean. The different shapes of velocity profile will remain only in the factor defined by the authors as the ratio of kinetic energies of gas and liquid in the inlet pipe (the shape factor is eliminated by division):

$$\kappa = \frac{\rho_g u_{g1}^2}{\rho_l u_{l1}^2} = \frac{\beta_g \rho_g < v_{g1} >^2}{\beta_l \rho_l < v_{l1} >^2} \quad [II.2.60]$$

Finally, imposing the equality of the differences of loss coefficients 1-2 and 1-3 for the two phases calculated as proposed by Gardel (1957), the system gives a linear correlation for G' and L' parametric in κ and a dimensionless number λ:

$$L' = \lambda + \kappa(G' - \lambda) \quad [II.2.61]$$

$$\lambda = \frac{1}{2}\left(1 + k_{12} - k_{13}\right) \quad [II.2.62]$$

Note that κ is known once the liquid hold-up at the inlet is estimated as in Hart *et al.* (1989).

Prediction is very good as opposed to the model by Shoham *et al.* (1987). This last model was obtained in different flow conditions and underestimates the degree of separation for the data collected in this paper. On the other hand it gives better information on the shape of the separation curve. Comparison with Roberts *et al* (1995) is interesting as it considers the same hold up of liquid. The quantitative agreement with data is comparable in the two cases but the model of Roberts *et al.* (1995), which does not fall into a linear relationship, picks very well some trends that a linear model can not predict.

II.2.4 Models independent of flow patterns

Saba & Lahey (1984), who formalized the necessity of a fifth equation, propose a linear momentum balance for the gas phase in the branch to fit their data in slug flow obtained in a horizontal, regular T-junction with 0.038 m ID. The differential momentum balance gas phase was written as:

$$-\varepsilon_g \frac{dp}{dz} = \varepsilon_g F_d + \varepsilon_g \rho_g u_g \frac{du_g}{dz} + \varepsilon_g F_w + \rho_g g \varepsilon_g \sin\phi \quad [II.2.63]$$

where ε_g is the gas void fraction, F_d and F_w are the volumetric interfacial and wall drag forces on the gas and ϕ is the angle formed by the side branch with the horizontal direction (ϕ=0 for the treated case of a horizontal T-junction). This equation is then integrated along a streamline ending in the side branch. Many two-phase flow correlations are used to evaluate the pressure drop terms in the macroscopic momentum equations for the run and for the side arm

Comparisons with the data collected show good agreement if the hypothesis of homogeneous flow is made (i.e.: $u_l = u_g$) especially for high split ratios. The same features are observed if comparison is made with the data by Honan & Lahey (1981). Data by Collier (1976) are well predicted by the hypothesis of slip flow (gas and liquid average velocities are not equal: non homogeneous flow), using a void fraction parameter as an adjustable quantity. This is in agreement with the fact that Collier's data were obtained in annular flow conditions.

Hwang *et al* (1988) obtained the split equation by calculating the dividing streamlines. They were the earliest to consider distinct zones of influence for the two phases. To determine the position of the dividing streamlines, they write Euler's equation in the local system of co-ordinates (s,n) for the generic streamline:

$$\frac{\partial p}{\partial s} = -\rho_k u_k \frac{\partial u_k}{\partial s} + F_{D_{k,s}} \qquad [II.2.64]$$

$$\frac{\partial p}{\partial n} = \rho_k u_k \frac{u_k^2}{R_k} + F_{D_{k,n}} \qquad [II.2.65]$$

Where, k identifies the phase, $F_{Dk,s}$ and $F_{Dk,n}$ are the components along s and n of the drag force exerted on the phase k and R_k is the radius of curvature of the streamline appearing in the expression of the centrifugal force acting as an effect of the curved path of the fluid element. These equations are considered in a point where a streamline for the gas phase crosses with a streamline for the liquid phase, i.e.: the stagnation point for both dividing streamlines. The dynamic equilibrium between the two phases is imposed as equality of the resultant of the volumetric forces acting on the two phases, leading to algebraic relationships to calculate the angle between two streamlines. To obtain the split of the phases, the authors calculate this angle at the stagnation point and then impose a functional shape to the streamlines as:

$$\frac{y}{\delta_k} = 1 - \left(1 - \frac{\eta}{D_3}\right)^{m_k} \qquad [II.2.66]$$

where (y,η) is the co-ordinates system in Figure II.2.4.

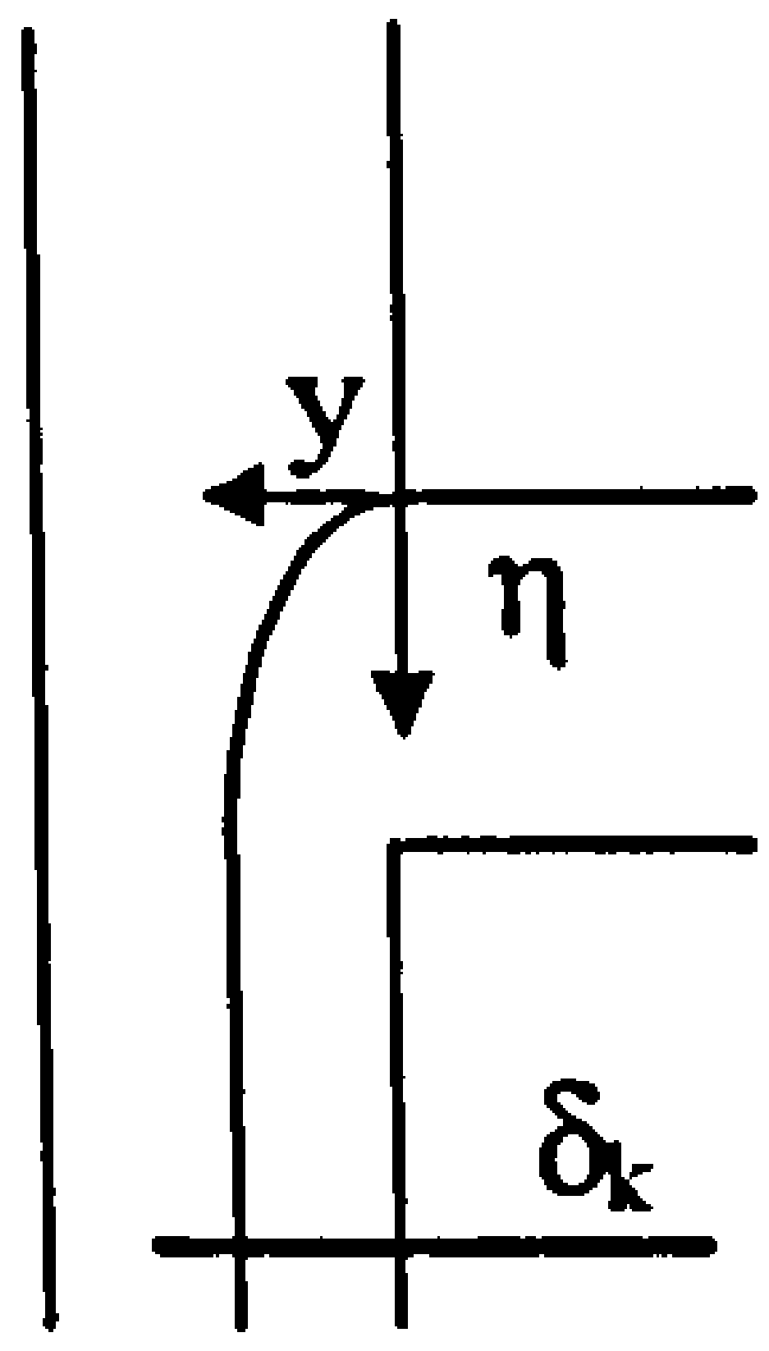

Figure II.2.4: *System of co-ordinates in the model by Hwang et al (1988).*

The idea is to use a known separation of the phases to calculate m_k as an adjustable parameter that best fits the experimental data. Simplified equations can be written for separated flows where the drag of each phase on the other can be neglected. In this, although the approach allows dealing with any flow pattern, this (flow pattern) must be known and fed into the model to determine the split of the phases.

Finally those ideas are extended to the case of β (angle between main pipe and side branch) different from 90°. The authors propose that as β increases from 0° to 180°, the pressure drop at the junction between inlet and side branch increases, hence the centrifugal component must increase to compensate it and the radius of curvature of the dividing streamline decreases. Again they propose a shape for the two cases of $0 \leq \beta < 90$ and $90 < \beta \leq 180$ containing an adjustable parameter.

Comparison with data was made for stratified, annular and bubbly flow from the works of Azzopardi & Baker (1981), Zetzmann (1984), Saba & Lahey (1984), Seeger *et al* (1986) and Hwang (1986). The authors claim that 97% of these data are predicted within 25%. However, data in the bubbly regime by Zetzmann (1984) were quite visibly outside of this range.

The work by **Ma *et al.* (1990)** is in the class of approach of the fifth equation (Saba & Lahey, 1984). They propose the energy conservation equation written in a two-dimensional, horizontal control volume bounded by the wall opposite to the junction and the three pipe diameters (Figure II.2.5). Hypothesis of constant internal energy in the control volume is made so that the only terms in the energy balance are the pressure and kinetic ones. As for the momentum balances, the equations are written for both phases and then summed to eliminate the exchange terms. If by Q we indicate the volumetric flow rate, summing the energy balances allows eliminating the interfacial energy transfer terms:

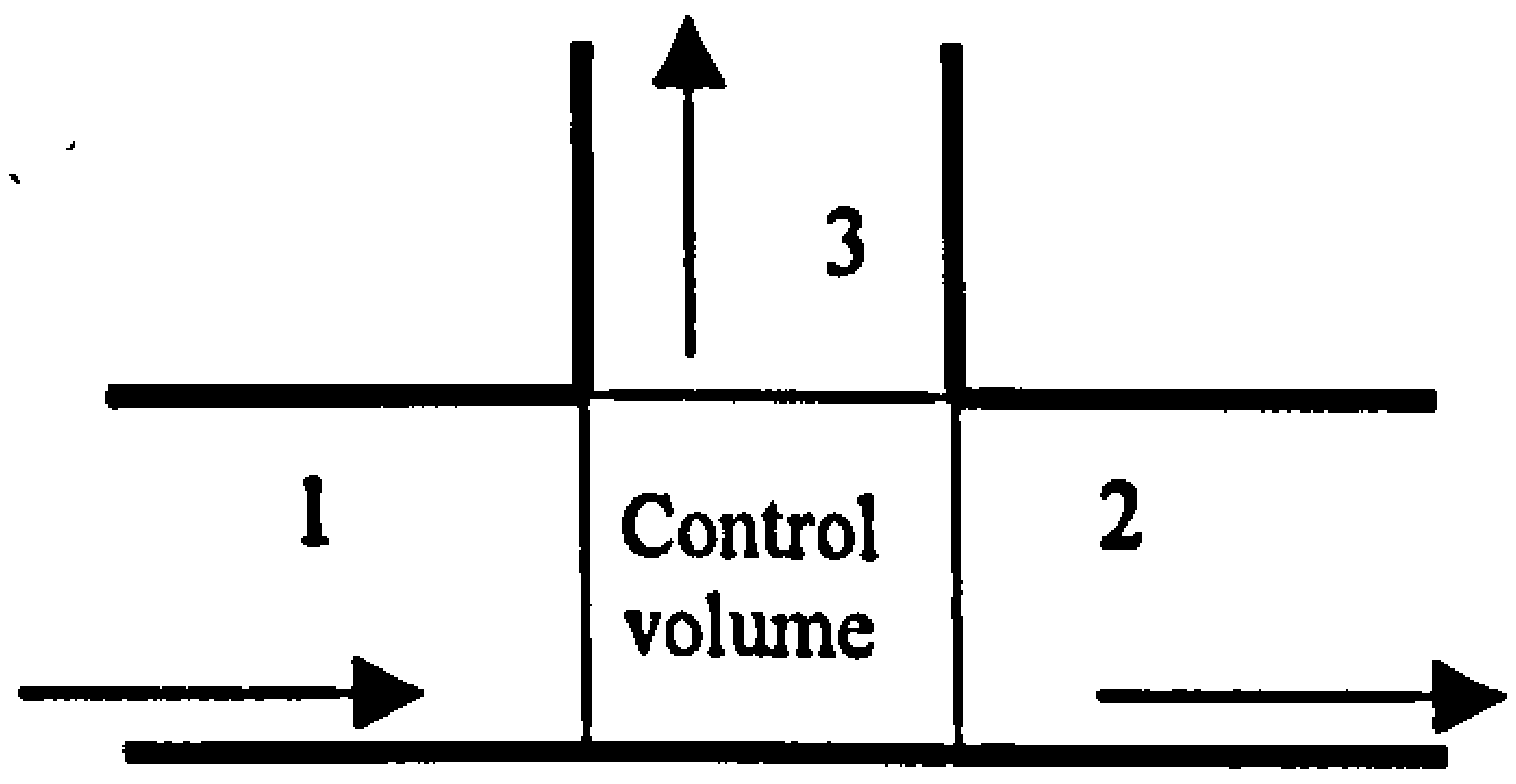

Figure II.2.5: *Control volume and standard nomenclature for the model by Ma et al (1991).*

$$-P_1Q_1 + P_2Q_2 + P_3Q_3 - (u_{1g}^2/2)\rho_{1g}Q_{1g} + (u_{2g}^2/2)\rho_{2g}Q_{2g} + (u_{3g}^2/2)\rho_{3g}Q_{3g} - (u_{1l}^2/2)\rho_{1l}Q_{1l} + (u_{2l}^2/2)\rho_{2l}Q_{2l} + (u_{3l}^2/2)\rho_{3l}Q_{3l} = 0$$

[II.2.67]

A homogeneous model is employed to provide the information about void fraction. It is assumed that the mixture density:

$$\bar{\rho} = \varepsilon_g \rho_g + (1 - \varepsilon_g)\rho_l \qquad [II.2.68]$$

and

$$\bar{\rho} = \frac{\dot{M}_g + \dot{M}_l}{Q_g + Q_l} \qquad [II.2.69]$$

which gives the relationship between mixture density and void fraction:

$$\varepsilon_g = \frac{\bar{\rho} - \rho_l}{\rho_g - \rho_l}. \qquad [II.2.70]$$

This again, restricts the applicability of the model to the cases where a homogeneous model is plausible.

Comparison is made against data in the literature showing quite good agreement with the data by Saba & Lahey (1984) and Lahey (1988) in case of water-air mixtures. For the data by Ballyk *et al.* (1988) taken for water steam two-phase flow, agreement is quite poor as expected from the assumption of constant internal energy, which does not hold in this case.

Of a different nature is the approach of **Lahey *et al* (1987)**. The authors develop the ideas present in Azzopardi & Whalley (1982) obtaining the closure to the problem using expressions for the probability of the phases to be extracted in the side arm depending on the position. Probability functions are proposed and the integral of the local velocity weighted on the probability function for the phase "i", will give the quantity of phase extracted.

In a cylindrical system of co-ordinates (r,ϕ,z) the probability functions are written as the ratio between local driving force in the side arm and local momentum of the phase (i.e.: the tendency of the fluid to carry straight in the run arm).

The authors write the probability of the liquid phase to be taken off as:

$$P_l = P_{l/g} P_g + P_{l/lo}(1 - P_g) \qquad [II.2.71]$$

where:

P_g = probability of the gas phase to be extracted.

$P_{l/g}$ = conditional probability of liquid to be extracted together with the gas.

$P_{l/l0}$ = conditional probability of the liquid to be extracted when no gas is extracted.

And:

$$P_g(r,\phi,z)=K_1\left(\frac{P(r,\phi,z)-P_{3J}}{\rho_g U_{gz}^2(r,\phi,z)}\right) \qquad [II.2.72]$$

$$P_{l/g}(r,\phi,z)=K_2\left(\frac{\rho_g U_{gz}^2(r,\phi,z)}{\rho_l U_{lz}^2(r,\phi,z)}\right) \qquad [II.2.73]$$

$$P_{l/l_0}(r,\phi,z)=K_4\left(\frac{\left(\delta(\phi_3)\big/D_3\right)^{2.5}}{\frac{\dot{M}_3(1-x_3)}{\rho_l A_3\sqrt{gD_3}}\left(\frac{\rho_l}{\rho_l-\rho_g}\right)^{0.5}}\right) \qquad [II.2.74]$$

The expression of P_{l/l_0} reflects the fact that this quantity is expected to depend on the film thickness δ at the angle ϕ_3 where the side arm is located. This expression is recommended for annular and stratified flow.

The amount of phases taken off can then be calculated from the following equations:

$$\dot{M}_{l3}=\int_{-\infty}^{+\infty}\int_{0}^{2\pi R}\int_{0}\left\{P_l(r,\phi,z)\rho_l U_{lz}^2(r,\phi,z)\left[1-\varepsilon_g(r,\phi,z)\right]\right\}dr\,d\phi\,dz \qquad [II.2.75]$$

$$\dot{M}_{g3}=\int_{-\infty}^{+\infty}\int_{0}^{2\pi R}\int_{0}\left\{P_g(r,\phi,z)\rho_g U_{gz}^2(r,\phi,z)\varepsilon_g(r,\phi,z)\right\}dr\,d\phi\,dz \qquad [II.2.76]$$

Correlations are used for the pressure drops containing terms of irreversible losses for which Gardel (1957) and Saba & Lahey (1984) suggest empirical values.

This analysis degenerates into the split equations [II.2.34-35] suggested by Azzopardi & Whalley (1982) when the probability functions are calculated for annular flow in the case of low take off.

In the high take off extreme, for churn, turbulent flow, the model is in agreement with data by Saba & Lahey (1984). Predictions are checked against the experiments of Zetzmann showing good agreement for high split ratio.

II.2.5 Two fluid approach – models for bubbly flow.

One reason why two-fluid models are not easy to employ is the fact that they require the knowledge of the interface between the two phases where the interaction law should be applied. For the case of bubbly flow, this can be obtained quite easily through reasonable approximation.

In the paper by **Lemonnier & Harvieu (1987)**, the problem is treated for bubbly flow in a 2-D Eulerian frame. The flow is assumed to be inertia dominated. This allows the problem to be solved in terms of potential flow for the carrier (liquid) phase. Single bubbles can then be superimposed to the carrier flow and trajectories calculated by a momentum balance containing the interaction law. This would also model segregation phenomena.

The model is guided by the experimental observation that the flow at the T is of two types. These have in common the eddy in the side arm on the wall opposite to the flow direction (eddy bounded by the curve D_1B in Figure II.2.6). The difference between the two types of flow is that depending on the withdrawn flow rate, a secondary eddy is originated in the run arm downstream of the junction and opposite to the side arm opening (Figure II.2.6). This is caused by the pressure recovery in the run. As the withdrawn fraction increases, the layer flowing in the run arm encounters an opposite pressure gradient. When the gradient intensity is strong enough, the layer detaches forming the downstream eddy.

The two eddies are calculated as follows. For the run eddy, a function is guessed for an intensity of single layer singularities source on the AC boundary in Figure II.2.6. The side eddy is considered a potential constant pressure region and a shape of the eddy boundary is guessed. Imposing stagnation in D_2 and the continuity of the velocity field in D_1 closes the problem. These conditions allow defining the intensity function, whilst an iterative procedure allows calculating the side eddy boundary imposing at each calculation a new eddy boundary satisfying the condition of tangency to the velocity (obtained in the previous iteration) in D_1. An analysis is made, showing the weak dependence of the results from the chosen shape of the intensity function.

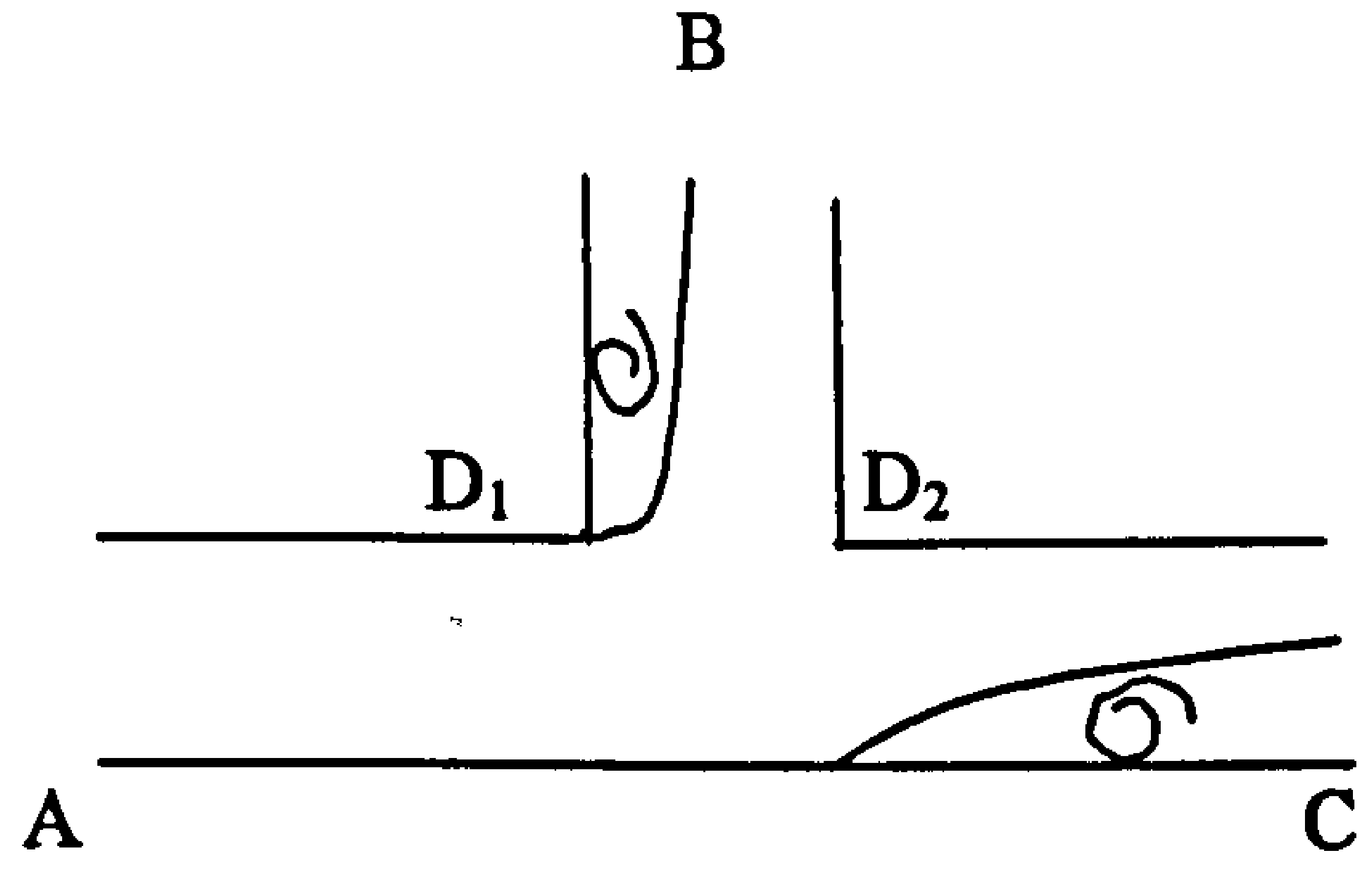

Figure II.2.6: *Model of Lemonnier & Harvieu (1987).*

The validity of the model for the carrier phase was checked with the hydrogen bubbles visualisation technique. The shape of eddies is predicted very well within the uncertainties of the experimental technique. Also, comparisons are made with the irreversible pressure drop in the branch as calculated by a sudden expansion model and the experiments by Gardel (1970), showing very good agreement.

The momentum balance on the bubbles is made imposing that the bubble diameter stays constant. The pressure distribution of the carrier potential flow around the spherical bubble is calculated. Buoyancy and drag force complete the balance. The drag force is modelled using a drag coefficient $C_D(Re)$. Reynolds number is high enough to assume $C_D=0.44$ (as from standard correlation).

Results of simulations show very good agreement with experimental data by Zetzmann (1984).

The approach used by Lahey (1990) who also uses a two-fluids model, treats the problem very thoroughly. The author first models the phase distribution in vertical up flow and down flow in the bubbly regime and then performs prediction of phase distribution and pressure drop at a T-junction. The model contains the continuity and momentum equation for the two phases written considering them as two interpenetrating continua:

$$\frac{D\varepsilon_k}{Dt} + \varepsilon_k \underline{\nabla} \cdot \underline{u}_k = 0 \qquad [II.2.77]$$

$$\varepsilon_k \rho_k \frac{D < \underline{u}_k >}{Dt} = \underline{\nabla} \cdot \varepsilon_k \left[\mu_k \underline{\nabla} < \underline{u}_k > - \rho_k \left(< \underline{u}_k ' \underline{u}_k ' > \right) \right] - \varepsilon_k \underline{\nabla} p_k - \varepsilon_k \rho_k \underline{g} + \underline{M}_{ik} +$$
$$- \underline{M}_{wk} - \underline{\tau}_{ki} \cdot \underline{\nabla} \varepsilon_k + \left(p_{ki} - p_k \right) \underline{\nabla} \varepsilon_k$$

[II.2.78]

where, $\underline{u}_k = <\underline{u}_k> + \underline{u}_k'$, i = interface, w = wall and k = l, g. $\underline{M}_{ik}$ and $\underline{M}_{wk}$ are respectively the interfacial and wall shear forces acting on the phase k. The stress tensor $\underline{\tau}$ is in square brackets and contains the Newtonian term involving the viscosity of the phase k (μ_k) and the Reynolds stress depending on the time averaged product of the turbulent fluctuations.

The simplifications introduced are as follows:

$p_k = p$ the two phases have the same pressure

$\underline{\tau}_{ki} = \underline{\tau}_k$ same constitutive law for the stresses in the flow and at the interface between the phases

$p_{gi} = p_g$ in the gas phase the pressure is the same in the bubble and on its surface

$p_{li} - p_l = - (1/4)\, \rho_l (<\underline{u}_g> - <\underline{u}_l>)^2$ inviscid law for the difference of pressure between bulk and interface in the liquid phase.

The third law of dynamics gives:

$$\underline{M}_{ig} = - \underline{M}_{il} = \underline{M}_i \quad [II.2.79]$$

and the force at the interface is decomposed into drag and non-drag forces:

$$\underline{M}_i = \underline{M}_i^{d} + \underline{M}_i^{nd} \quad [II.2.80]$$

The drag force is modelled proportional to the squared time averaged slip velocity through a drag coefficient:

$$\underline{M}_i^{d} = (1/8) \rho_l C_D \left| <\underline{u}_g> - <\underline{u}_l> \right| (<\underline{u}_g> - <\underline{u}_l>)\, A_I''' \quad [II.2.81]$$

The drag coefficient is obtained from the dirty water model (Wallis, 1969) as function of the Reynolds number for the bubble:

$$C_D = \frac{6.3}{Re_b^{0.385}}, \quad Re_b = \frac{\rho_l \left| <\underline{u}_g> - <\underline{u}_l> \right| D_b}{\mu_l} \qquad [II.2.82]$$

If all bubbles are assumed to have the same size, the interfacial area density is given by:

$$A_i''' = 6\varepsilon_g / D_b. \qquad [II.2.83]$$

A non-drag force is the lateral lift force. Drew & Lahey (1987) have derived this force that is proportional to the relative velocity of the dispersed sphere and to the liquid vorticity:

$$\underline{M}_{ig}^{nd} = -C_L \rho_l \varepsilon_g \left(<\underline{u}_{gz}> - <\underline{u}_{lz}> \right) \frac{d<\underline{u}_{lz}>}{dr} \qquad [II.2.84]$$

where z is the axial coordinate and r the radial one. C_L is 0.5 for inviscid flow of a single bubble and decreases with the liquid viscosity. The author uses a value of 0.05 for this parameter.

Finally the wall stress for the gas is imposed to be zero whilst for the liquid phase the friction factor relationship is used:

$$\underline{M}_{wl} = \frac{1}{2} \frac{f}{D} \rho_l <\underline{u}_l> \left| <\underline{u}_l> \right|. \qquad [II.2.85]$$

Turbulence model.

A turbulence model is needed for closure. The turbulence can be present in the continuum phase because of its high Reynolds number. Nevertheless, even when Reynolds number is small, the presence of bubbles can induce turbulence. The bubble-induced turbulent stress tensor can be expressed as (Nigmatulin, 1979):

$$\underline{\underline{\tau}}_l^T = \varepsilon_g \rho_l \left[C_1 \left| <\underline{u}_g> - <\underline{u}_l> \right|^2 \underline{I} + C_2 \left(<\underline{u}_g> - <\underline{u}_l> \right) \left(<\underline{u}_g> - <\underline{u}_l> \right) \right]$$

[II.2.86]

where C$_1$ = 3/20 and C$_2$ = 1/20 (Biesheuvel & van Wijngaarden, 1984).

The author argues that, since the liquid velocity in bubbly flow does peak off the centerline of the pipe, the turbulence model to introduce for the closure of the problem can not be of the k-ε type, based on the eddy diffusivity. Also, a k-ε model does not account for the bubble-induced turbulence.

For the above reason a more global τ-ε model is used on the basis of the one developed for single phase by Launder *et al.* (1975). Without going in details, the final equation for the turbulent stress is of the form:

$$\varepsilon_l \frac{D}{Dt}(<\underline{u}'\underline{u}'>) = \underline{\nabla} \cdot \varepsilon_l \left[\frac{\mu_l}{\rho_l} \underline{\nabla}(<\underline{u}'\underline{u}'>) - (<\underline{u}'\underline{u}'\underline{u}'>) \right] + \varepsilon_l \left(\underline{\underline{P}} + \underline{\underline{\Phi}} - 2\varepsilon \underline{\underline{I}} + \underline{\underline{S}}_i \right)$$

[II.2.87]

Note that whilst ε_l denotes the liquid fraction ε indicates the dissipation of liquid phase turbulence. The tensor $\underline{\underline{P}}$ is the production of turbulence tensor and $\underline{\underline{\Phi}}$ is the pressure-strain tensor, which acts to exchange kinetic energy between the various Reynolds stress tensor components. The interesting feature is constituted by the presence of the tensor $\underline{\underline{S}}_i$, which represents the source of turbulence induced by the bubble. This tensor is modelled as:

$$\underline{\underline{S}}_i = \begin{bmatrix} \frac{4}{5} & 0 & 0 \\ 0 & \frac{3}{5} & 0 \\ 0 & 0 & \frac{3}{5} \end{bmatrix} \frac{1}{4} C_i \frac{\varepsilon_g \left| <\underline{u}_g> - <\underline{u}_l> \right|}{D_b} \qquad \text{[II.2.88]}$$

were C$_i$ is experimentally determined.

Boundary conditions.

Boundary conditions for the momentum equation are placed at the inertial sub layer close to the wall where the logarithmic law of the wall is assumed to be valid as proved in single phase flow. They consist of no normal component and tangential velocity component at the wall given by:

$$\frac{<\underline{u}_l>}{u^*} = 2.5\ln y^* + 5 \qquad [II.2.89]$$

$$y^* = \frac{y^* \rho_l \underline{u}^*}{\mu_l} \qquad \underline{u}^* = \sqrt{\frac{\tau_w}{\rho_l}} \qquad [II.2.90]$$

where y is the distance from the wall. For the τ-ε model, a form of the tensor <$\underline{u}$'$\underline{u}$'> at the wall, for axisymmetric pipe is given by:

$$<\underline{u}'\underline{u}'> = \begin{bmatrix} 5.1 & 0 & 1 \\ 0 & 2.3 & 0 \\ 1 & 0 & 1 \end{bmatrix} (u^*)^2 \qquad [II.2.91]$$

Dissipation at the wall is accounted for by expressing ε as:

$$\varepsilon = \frac{1}{\kappa}\frac{u^*}{y}(u^*) \qquad [II.2.92]$$

where κ is the von Karman constant ($\kappa = 0.435$).

Phase split at a T-junction and comparison with experiments.

Phase split at a T-junction is modelled on the idea of dividing streamlines that can be determined with the 3-D two-fluids model. In this case another non-drag force must be introduced i.e. the virtual mass force, modelled as in Drew & Lahey (1987):

$$\underline{M}_{il}^{nd} = -\underline{M}_{ig}^{nd} = \varepsilon_l \rho_l C_{vv} \left[\frac{D<\underline{u}_g>}{Dt} - \frac{D<\underline{u}_l>}{Dt} \right] \qquad [II.2.93]$$

C_{vv} is the so-called virtual volume coefficient depending on the flow pattern. The lateral lift force was neglected and a drag force between the phases was introduced. Since comparison was made with data in stratified flow by Lahey (1987), away from the junction a drag coefficient C_D(Re, film depth) was used as proposed by Andritsos & Hanratty (1987). In the junction, where the flow is well mixed, bubbly flow drag law was assumed. For this drag law a value of the interfacial area density is needed. This is directly related to the void fraction and is used in the model as an adjustable parameter. The best fit is obtained assuming this parameter given by:

$$A_i''' = 0.88\, A_{is}''' + 0.12\, A_{ib}''' \quad [II.2.94]$$

Were the subscript "b" refers to single bubble and "s" to stratified flow. As predictable this parameter is closer to the one for bubbly flow, the flow being well mixed at the T.

Prediction is made imposing the pressure at the outlets so to have the measured split ratio. The model gives back x_3/x_1. Predictions are very good and it is noted that neglecting virtual mass produces data less close to reality.

A k-ε turbulence model is used instead by **Issa & Oliveira (1994)**. The momentum equations are written for the phase m in view of employing the k-ε turbulence model, introducing an effective viscosity. The generic component of the vector momentum equation is given by:

$$\rho_m \frac{D\varepsilon_m <u_{mi}>}{Dt} = -\varepsilon_m \frac{\partial p}{\partial x_i} + \frac{\partial}{\partial x_j}\left[\varepsilon_m \mu_m^{eff}\left(\frac{\partial <u_{mi}>}{\partial x_j} + \frac{\partial <u_{mj}>}{\partial x_i} - \frac{2}{3}\frac{\partial <u_{mk}>}{\partial x_k}\delta_{ij}\right)\right] +$$
$$+\varepsilon_g \rho_g A_D\left(<u_{ni}> - <u_{mi}>\right) + g_i \varepsilon_m \rho_m + S_{mi}$$

[II.2.95]

where m and n are the two phases, $\delta_{ij}=1$ for $i = j$ and 0 for $i \neq j$. The effective viscosity is defined as the sum of a molecular viscosity plus a turbulent viscosity:

$$\mu^{eff} = \mu + \mu^t \quad [II.2.96]$$

and

$$\mu^t = \rho v^t \quad [II.2.97]$$

will be obtained from the turbulence model. S_{mi} is the i component of the source of momentum in the phase m.

The interaction term is a drag force (third term on the RHS of equation II.2.95) where:

$$A_D = \frac{\frac{3}{4}\left(\rho_l \left| < u_l > - < u_g > \right| C_D\right)}{\rho_g d_b} \quad [II.2.98]$$

The drag coefficient C_D is the one for spherical bubbles modified by an empirical correction factor, depending on void fraction as given by Zuber (1964):

$$C_D = \left(\frac{24}{Re_b}\right)\left(1 + 0.15 Re_b^{0.687}\right) f(\varepsilon_g) \quad [II.2.99]$$

Turbulence model

The transport equations pertaining to the k-ε model are:

$$\rho_l \frac{D\varepsilon_l k}{Dt} = \frac{\partial}{\partial x_j}\left[\varepsilon_l \frac{\mu_l^{eff}}{\sigma_k} \frac{\partial k}{\partial x_j}\right] + \dot{M}_l - \rho_l \varepsilon_l \varepsilon + S_k \quad [II.2.100]$$

$$\rho_l \frac{D\varepsilon_l \varepsilon}{Dt} = \frac{\partial}{\partial x_j}\left[\varepsilon_l \frac{\mu_l^{eff}}{\sigma_\varepsilon} \frac{\partial \varepsilon}{\partial x_j}\right] + \frac{\varepsilon}{k}\left(C_1 \dot{M}_l - C_2 \rho_l \varepsilon_l \varepsilon\right) + S_\varepsilon \quad [II.2.101]$$

where k is the turbulence kinetic energy and ε is its rate of dissipation. $\sigma_k = 1$ and $\sigma_\varepsilon = 1.22$ are the turbulent Schmidt numbers, C_1=1.44 and C_2=1.92.

Note that the equations are written in the liquid phase where we assume the presence of turbulent flow. Here we highlight the fact that account is given for the presence of bubbles in the source terms in the momentum equations and in the equations of the turbulence model. The presence of bubble-induced turbulence is accounted for indirectly.

The eddy diffusivity ν^t is given by:

$$\nu^t = C_\mu k^2/\varepsilon;\ C_\mu = 0.09. \qquad [II.2.102]$$

The source terms in the k-ε model are:

$$S_k = -2A_D(1-C_t)\rho_g\varepsilon_g k - (A_D\rho_g\nu^t)/[\varepsilon_l(<u_{gi}>-<u_{li}>)\partial\varepsilon_g/\partial x_i] \quad [II.2.103]$$

$$S_\varepsilon = -2A_D(1-C_t)\rho_g\varepsilon_g\varepsilon \qquad [II.2.104]$$

where C_t is the ratio between the fluctuating component of velocity in the gas and liquid phase modelled as in Gosman *et al.* (1992).

The source terms in the momentum equations are obtained as:

$$S_{li} = -\frac{2}{3}\rho_l\frac{\partial\varepsilon_l k}{\partial x_i} + \frac{A_D\rho_g\rho_l\nu^t}{\varepsilon_l\rho_l\frac{\partial\varepsilon_g}{\partial x_i}} \qquad [II.2.105]$$

$$S_{gi} = -\frac{2}{3}\rho_g\frac{\partial\varepsilon_g C_t^2 k}{\partial x_i} - \frac{A_D\rho_g\rho_l\nu^t}{\varepsilon_l\rho_l\frac{\partial\varepsilon_g}{\partial x_i}} \qquad [II.2.106]$$

Finally, the effective viscosity for the gas phase is given by $\mu_g^{eff} = \mu_g + \rho_g C_t^2\nu^t$.

Simulations and comparison with experimental data by Popp & Sallet.

The authors make their prediction in a vertical T-junction with a rectangular cross section (0.025 X 0.1 m) as in the experiments by Popp & Sallet (1983). The inlet conditions used are:

Q_{1l}=1.885 10^{-3} m^3/s.

Q_{1g}=4.135 10^{-5} m^3/s

$<\varepsilon_g>_1$=2.08 %

Boundary conditions at the two outlets are zero axial gradient for all variables exception made for the pressure that is linearly interpolated between the T and the outlets. The split ratio is imposed and the phase split is calculated.

Not only is prediction good but also it highlights how the use of a 3-D frame improves results significantly as opposed to 2-D approaches.

II.3 Conclusions to literature review

The review of the literature points out a few strengths and weaknesses in the current capability of predicting two-phase flow at T-junctions. The case of vertical annular flow is efficiently dealt with using the approach of Azzopardi (1989). A simple geometrical model starting from the concept of 'common segment' and prediction of the additional routes of liquid take off, allows accurate predictions of the split characteristic.

Vertical bubbly flow is well tackled by the approach of Issa & Oliveira (1991). There, more sophisticated tools are required. Interaction between the phases, mechanistic modelling of the flow including a model for turbulence and CFD are used to solve the full 3D problem.

If the final aim is a 'recipe' for engineering practice, the simplicity of the former approach becomes a great advantage. Furthermore, it directly deals with the phenomenology of the split mechanism. The latter approach is certainly less 'ready to use' and requires the solution of the full problem. On the other hand, this represents an experiment in itself as the results of simulations can be directly analysed to validate assumptions, giving new hints for the understanding of the problem. In this sense, the T-junction problem is an excellent test-bed to validate general methodologies such as CFD, given its relatively simple geometry.

The success of the model by Azzopardi (1989) makes particularly appealing the attempt to extend the applicability of the concept of common segment to the case of a horizontal pipe. There, the difficulty is in modelling the more complex horizontal annular flow. Particularly, entrained fraction and the relative importance of the known mechanisms for the formation of a liquid annulus against gravity need to be better understood. The attempts of Roberts *et al* (1997) and Azzopardi & Rea (1999) are encouraging although their success is restricted to the range investigated in those works. We will further pursue this attempt in chapter IV. On the other hand, a split mechanism for non-annular flow patterns has never been proposed. There, as shown by Lahey *et al* (1987), predictions based on a more general formulation in terms of probability functions that include the common segment for the case of annular flow, quickly fail. The vertical case is certainly more suitable for this purpose because of its symmetry around the direction of gravity and this approach is carried out in Chapter V.

Chapter III

Experiments in horizontal geometry

Introduction

This chapter presents phase split and film thickness measurements obtained from experiments performed on a 0.127 m ID T-junction. Both the main and side arms of the T-junction were orientated horizontally. Section III.2 describes the apparatus used in further detail and presents the phase split measurements. Section III.3 details the film thickness measurements. All experiments are carried out in the annular or semi-annular flow regime.

III.1 Two-phase flow split

III.1.1 Experimental apparatus

The apparatus used for phase split experiments (Figure III.1.1) was constructed of acrylic resin pipes of 0.127 m ID with a wall thickness of 0.003 m. These are connected to the T-piece test section, which was machined from an acrylic resin cube of length 0.2 m. The corners of the T, where the side arm joins the main tube, are square edged (zero radius of curvature).

A centrifugal blower supplied air to the inlet; the flow rate was metered by using standard orifice plates (0.040 m, 0.060 m, and 0.105 m orifice diameter). The selected orifice plate was mounted on a vertical section of pipe between the blower outlet and the mixing section and different size orifice plates were used depending on the required air flow rate. To minimise the risk of back flow of liquid into the blower, the outlet pipe was shaped in an inverted U, from the blower outlet to the inlet of the mixing unit.

RITORNO FLUSSO

In the mixing unit, the water passes into the pipe through a sinter wall section, fed by three pipes placed at equidistant positions around the circumference of the unit (120° angular separation). The water is delivered by two centrifugal pumps, supplied from a common storage tank and selected on the basis of water flow rate. The flow rate from the small pump is metered by a bank of three rotameters and a magnetic flowmeter is employed for the large pump.

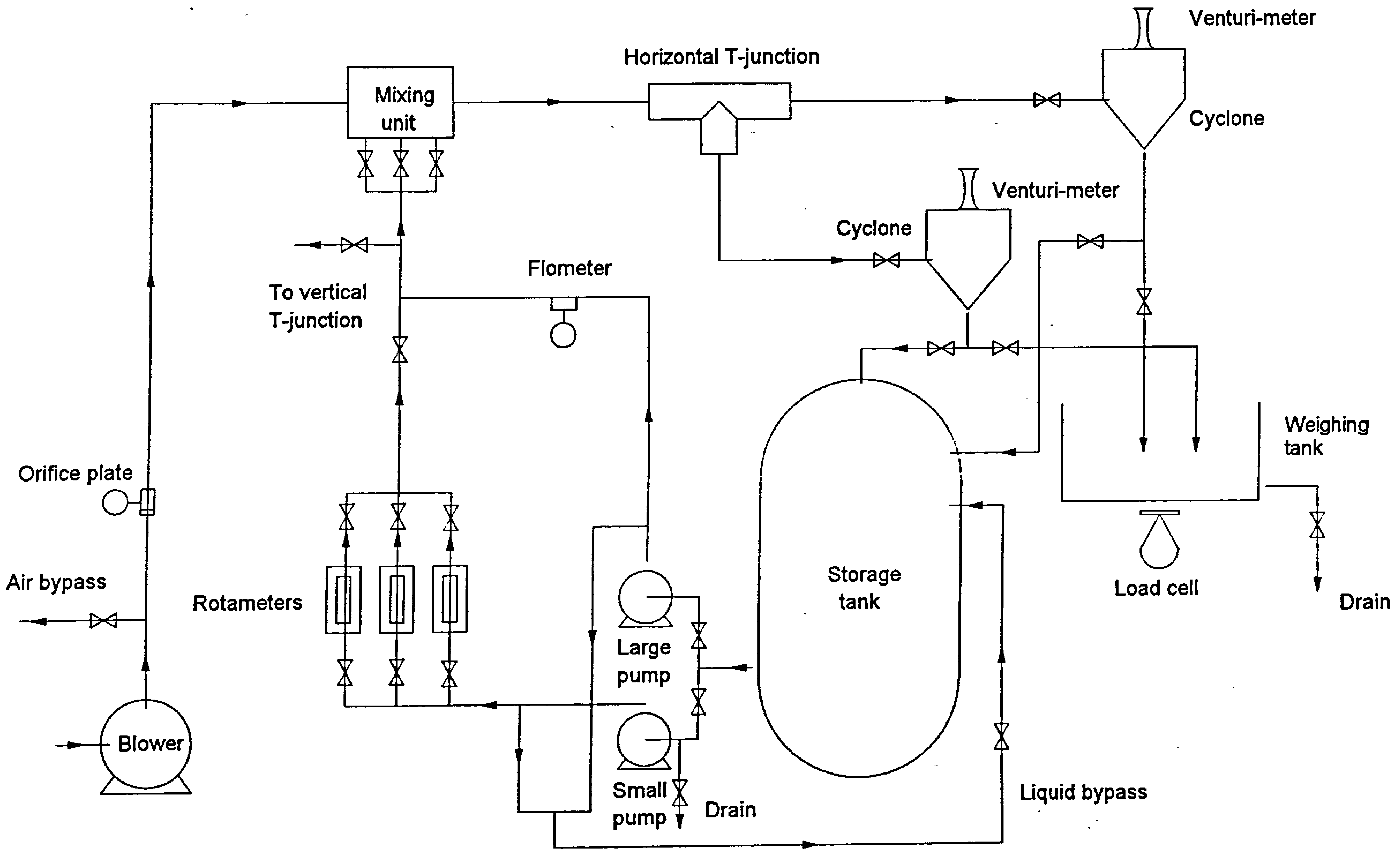

Figure III.1.1: *Sketch of the experimental apparatus.*

The gas flow rate is regulated by means of an air bypass to atmosphere. The liquid flow rate is obtained by adjusting the valves below the rotameters or the magnetic flowmeter, depending upon which pump is in use. A bypass to the storage tank allows the full range of liquid flow rates.

The centre of the junction is 4 m (31D) downstream of the mixing section and short removable portions of pipe are provided around the T in each of the three legs. These pieces are 0.3 m long and are removed to enable insertion of the film thickness test sections. The divided streams flow in the side arm for 2 m and in the run for 2.5 m before encountering butterfly valves that control the resistance. Cyclones are placed at the extremities of the run and side arm to separate the gas and liquid phases.

PRIMA DI INCONTRARE

From each cyclone, the liquid can either be returned to the storage tank or fed to a weigh tank mounted on a load cell for flow rate measurement via timed weighing. Air is discharged to the atmosphere after metering by calibrated orifice plates or Venturi-meters.

SCARICATA

The range of gas and liquid superficial velocities achievable in the facility is shown together with a flow pattern map in Figure III.1.2. The small head that is provided by the blower (0.1 bar) imposes limits on the gas flow rate achievable at high liquid flow rates. This is the reason why the high gas velocity boundary drops at the top of the range of liquid flow rate. At the other extreme, for low liquid velocities, the minimum gas flow rate increases. The shaded area in Figure III.1.2, shows the intersection of the annular flow region and the operating range of the facility; i.e. where experiments in annular flow can be performed.

III.1.2 Experimental procedure

The rig was started up by introducing the gas first to avoid flooding of the air line with water. For this set of experiments, shown in Figure III.1.2, high liquid flow rate was used to maintain annular flow. For this reason the large pump was selected. This was started up with the minimum liquid flow, then both air and water flows were increased to the desired values.

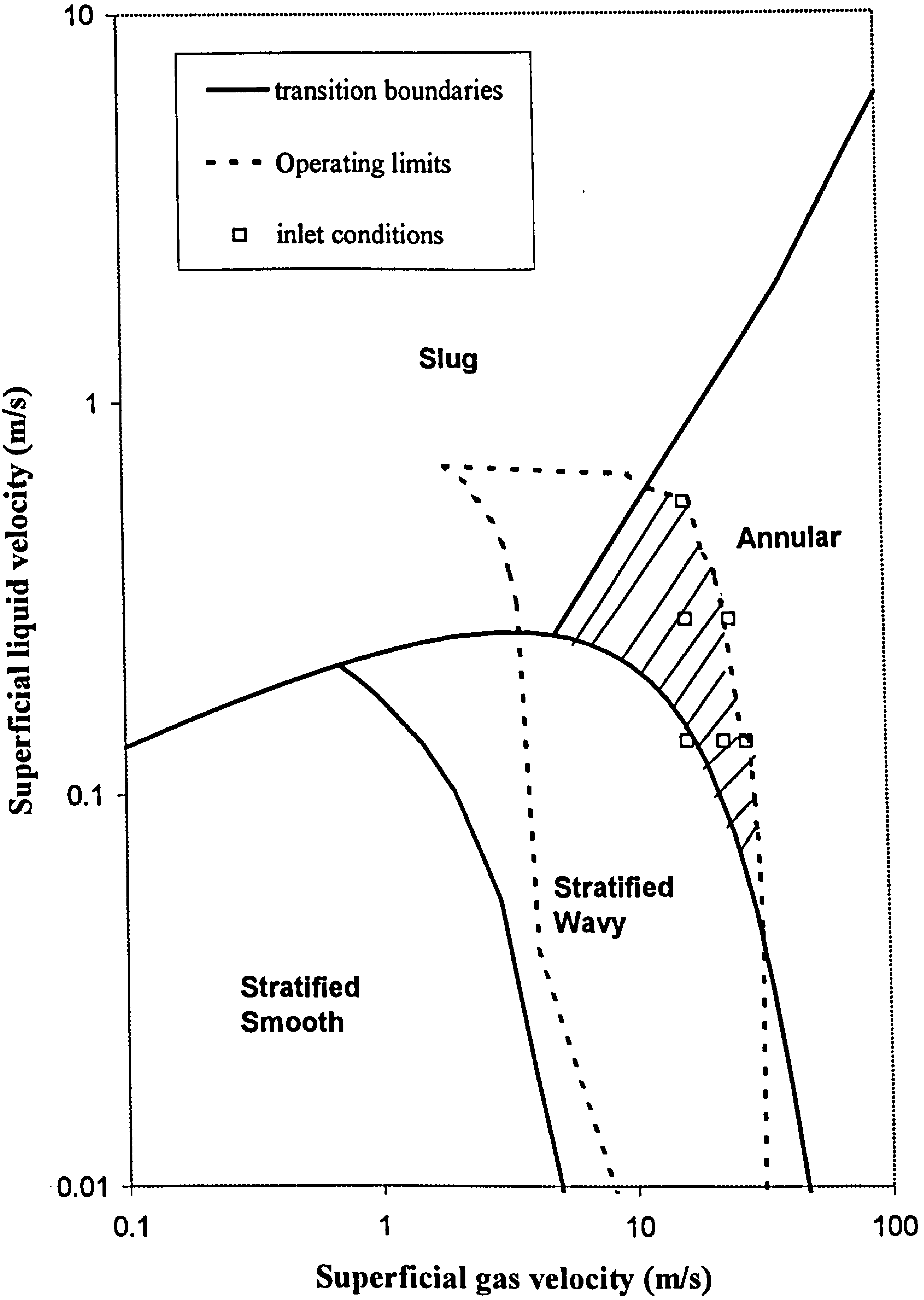

Figure III.1.2: *Flow pattern map from predictions of Taitel & Dukler for a 0.127 ID horizontal pipe, with operating limits and inlet conditions. Log-log scales.*

The gas flow rate needed adjustment after any increase or decrease in water flow rate, due to the small head provided by the blower.

PAGE
MISSING
IN
ORIGINAL

Table III.1.1: *Inlet conditions for phase split runs.*

Run	U_{gs}	U_{ls}
a)	16.5	0.550
b)	16.5	0.278
c)	· 24.5	0.278
d)	16.5	0.136
e)	23.0	0.136
f)	28.1	0.136

All results are plotted on the same diagram in Figure III.1.3. Tabulated data are given in Appendix A.

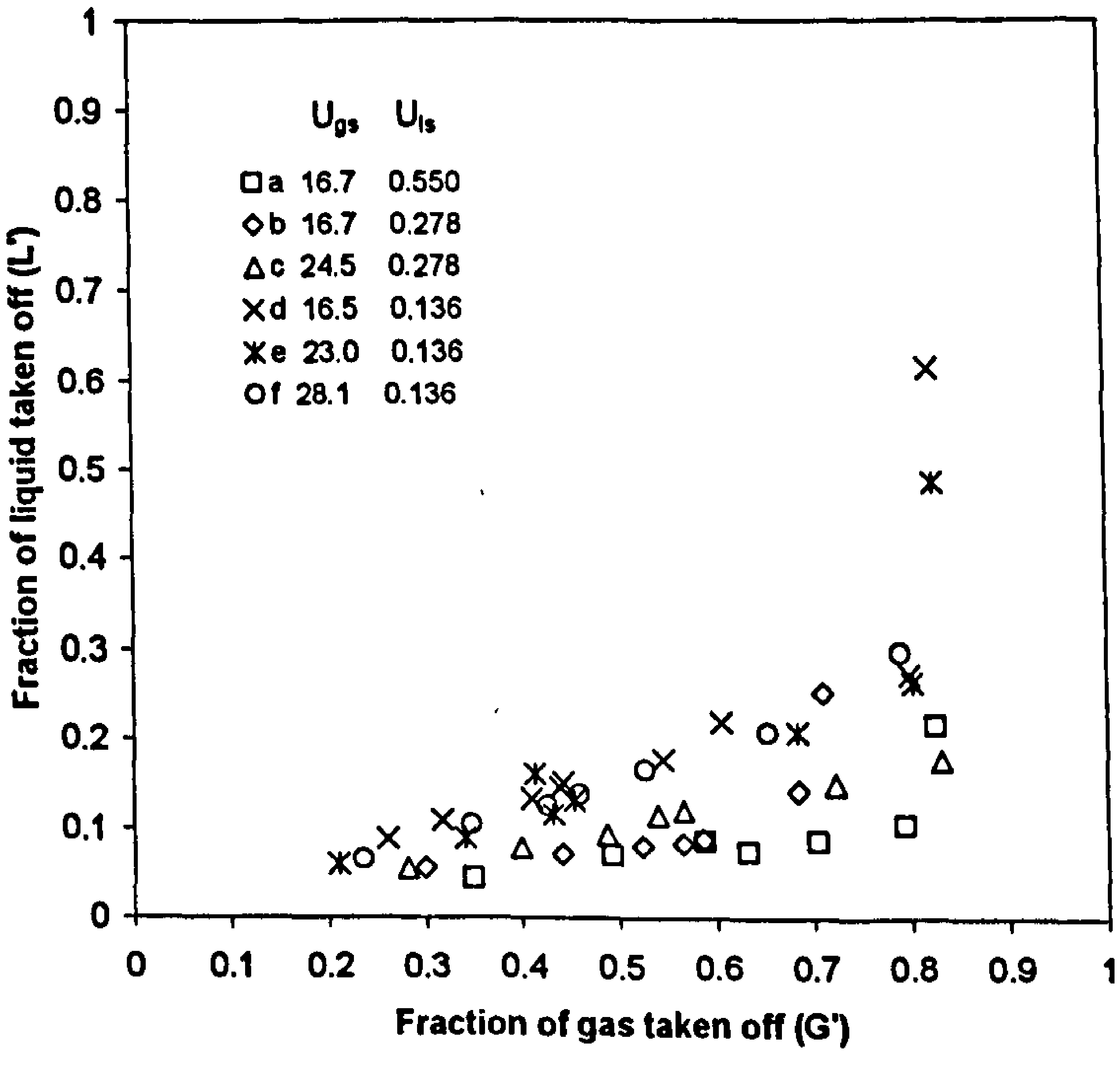

Figure III.1.3: *Split results for the full database in the horizontal, 0.127 ID T-junction.*

Figure III.1.3 shows that split data have been taken in the range 0.21-0.83 of the fraction of gas taken off. Above this limit, the position of the valve on the run would bring the gas flow rate below the set point and outside of the range of operability of the rig. The range of rig operability has been obtained with both valves fully open. Hence, this shifts towards lower gas velocities when resistances are increased.

[illegible] [illegible] [illegible]

Overall, the split of phases is gas dominated, which is in agreement with general trends in the literature. At the largest liquid flow rates, the amount of liquid taken off is very small and hardly increases until 70-80% of the gas is diverted into the side arm. Then the curve rises steeply to the point (1,1), outside of the range of G' investigated.

The effects of inlet liquid and gas flow rates, are shown better in Figures III.1.4-5, where three runs at constant gas and liquid inlets respectively are plotted.

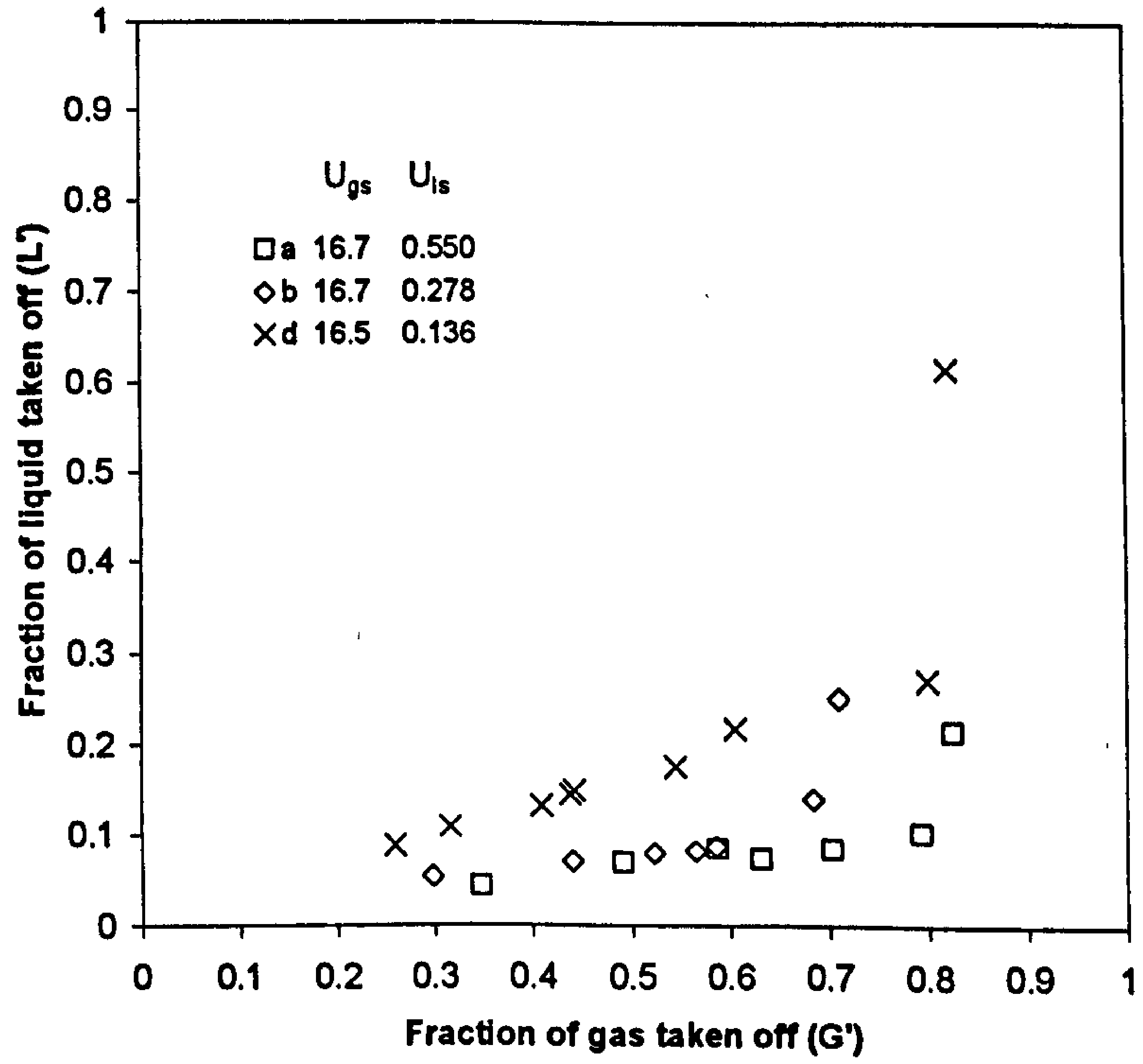

Figure III.1.4: *Split data for a constant gas superficial velocity of 16.5 m/s*

Figure III.1.4 above, shows that with a constant gas superficial velocity at the inlet of 16.5 m/s, a decrease of liquid fraction taken off is observed when the liquid flow rate is increased. This is in agreement with the fact that the superficial momentum of the liquid increases and the pressure differential in the side arm becomes less effective in diverting it.

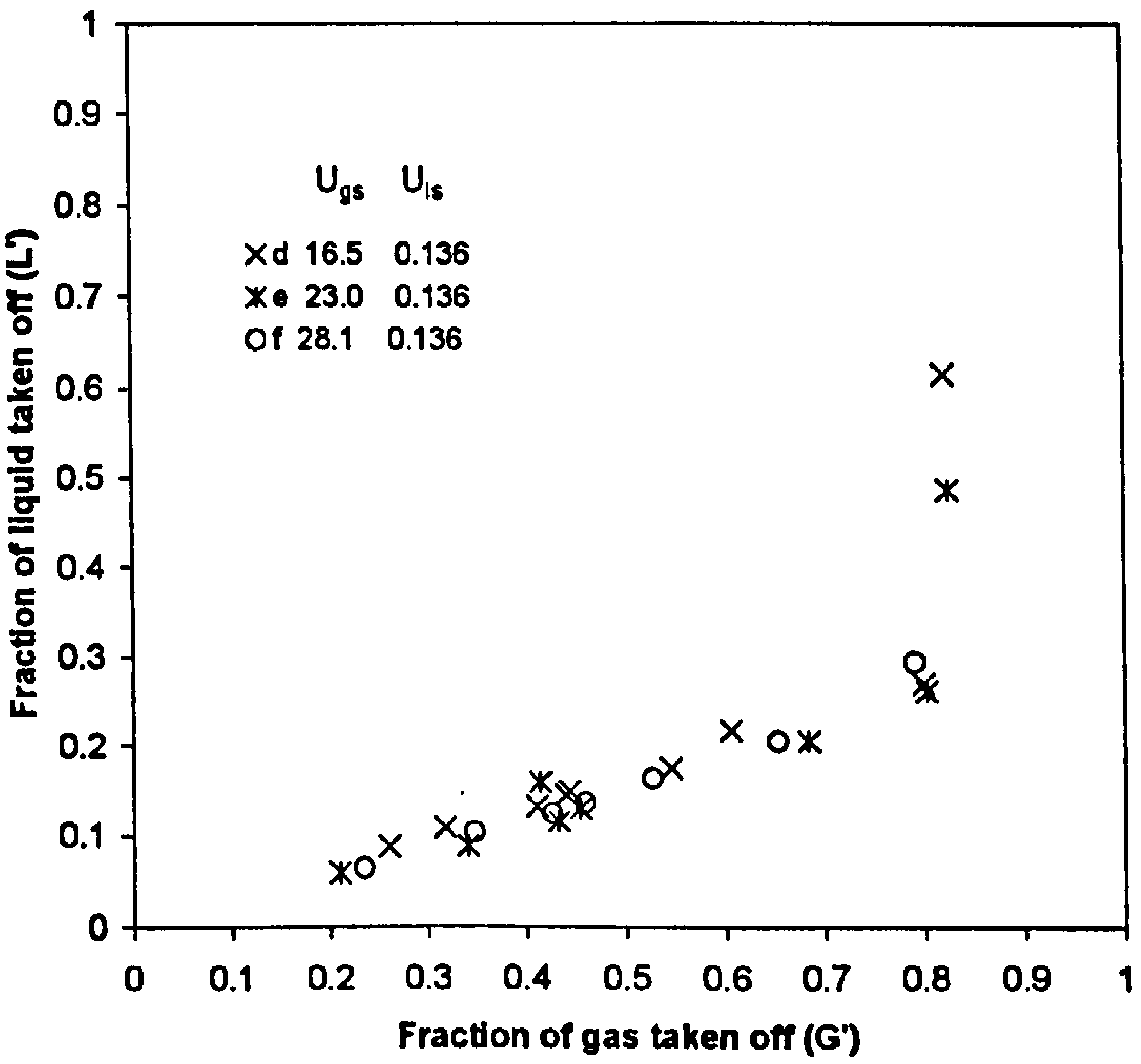

Figure III.1.5: *Split data for a constant liquid superficial velocity of 0.136 m/s*

When liquid superficial velocity is kept constant at 0.136 m/s (Figure III.1.5), no visible effect on the split of the phases is observed by varying the gas flow rate. This is also in agreement with previous findings (Rea, 1998) and confirms that the momentum of the liquid film is the dominant factor. Considering a constant fraction of gas take off, a larger gas inlet means that the gas travels faster in the side arm and hence a stronger pressure differential acts upon it. Split results show that this does not affect liquid take off. This effect will be discussed further in section III.3.

When the split ratio (fraction of incoming mixture diverted to the side arm) was increased, the film at the bottom of the run pipe was seen to become thicker before a hydraulic jump occurred. This happens because of a transition from supercritical ($Fr>1$) to subcritical ($Fr<1$) flow of the film ($Fr = U_{lf}/\sqrt{gD}$). For some conditions the liquid completely filled up the pipe, and when the front of hydraulic jump reached the junction for G'~0.75, this fed a substantial amount of liquid to the side arm, hence increasing steeply L'. Film stop was also observed in the run arm.

III.2 Film thickness measurements

III.2.1 Introduction

As emerged from the literature, phase split mechanism at T-junctions is strongly dependent on flow pattern. In the case of horizontal annular flow, this is characterised by the distribution of the film around the pipe, the entrained fraction, the drop size distribution and the local fluxes of liquid in the film and as drops. If one assumes the hypothesis of Azzopardi & Whalley (1982) is valid, that drops carry on past the junction, attention must be directed to the characterisation of the film. There is evidence in the literature that scale has a strong effect on the film distribution around the pipe circumference (Williams (1990), Laurinat (1982), Dallman (1984)). In fact, models developed for small pipes do not apply to larger ones and this might be due to the relative importance of the several mechanisms proposed to justify the presence of a film at the top of the pipe, against gravity.

Generally, for larger pipes the film is seen to be less symmetric with a stratified-like distribution at the bottom and an abrupt thinning of the film towards the top. The work of Williams (1990) in a 0.0953 m ID horizontal pipe is the only data available which gives film thickness measurements in annular flow for pipes large enough to be of relevance to industry. There, gas velocities are above 30 m/s. In this research, results obtained for the same inlet velocities where split data has been taken (Table III.1.1) are presented. Also, measurements will be performed to characterise the film distribution around the junction, in the three legs of the T, within the T-junction and at the inlet, not far from the mixing section. Also, data are taken for different split ratios at the T to investigate how this affects the behaviour of the liquid film.

III.2.2 The experimental technique

The most widely used technique for film thickness measurements is based on the different impedance of the two media. In particular if the condensed phase is conductive (e.g.: water with dissolved salts), conductance measurements have been employed. Capacitance has been used in other cases (e.g.: oils). As the conductivity of tap water with its concentration of dissolved ions is several orders of magnitude larger than that of air (virtually 0), the CONDUCTANCE MEASUREMENTS former will be employed. Because the circuit works on alternating current, the total impedance Z should be considered. Since the water as a resistance and as a capacitor is under the same potential, we should consider it as a capacitor in parallel with a resistance and the total impedance is:

$$Z = \sqrt{\frac{1}{R^2} + \frac{1}{X_c^2}} \quad \text{[III.2.1]}$$

where for a frequency f and capacitance C, the capacitive reactance is given by $X_c = -1/(2\pi fC)$. For the systems we are dealing with, where $C \sim 10^{-12}$ F, $1/X_c$ becomes negligible compared to the resistive component, even when using conventional 50Hz alternating current, the impedance reduces to its resistive component.

Capacitance probes are used with non-conductive media. In that case, the resistive component is suppressed by the characteristic of the medium.

III.2.3 Typology and design of conductance probes.

As evident from the above, a conductance probe is the arrangement of two electrodes, extremities of a circuit, which is closed by the liquid film bridging between them. There are several ways to arrange the probes and these result in a range of response characteristics of conductance to film thickness and hence measured voltage to film thickness. The basic criteria to determine the optimal arrangement of electrodes are listed below:

HANNO PER RISULTATO

1) A monotonically growing voltage response with film thickness, with a slope that ensures a good degree of confidence in the measurements.
   PENDENZA
2) The characteristic dimensions of the probe should be small enough compared with those of the system to ensure locality of measurement.
3) Non-intrusive geometry, probes should not disturb the flow.
4) Probes must work in the expected range of film thickness.

There are three probe configurations which have been used in the past for film thickness measurement in pipes. These are needle probes, wire probes and flush mounted probes.

Needle probe.

This method DIPENDE DA relies on the contact made between an electrode mounted flush with the pipe surface and the tip of a needle moving across the pipe diameter passing through the fixed electrode. When the tip of the needle is at the gas-liquid interface, the liquid will conduct the signal to the fixed electrode. Because the interface is wavy, it is assumed that the distance between the flush mounted probe and the tip of the needle is equal to the film thickness when the time of contact with liquid is 50% of the total time of measurement.

The advantage of this method is that it is very precise, does not require calibration and is applicable to a wide range of thickness. Furthermore, the local character of measurement is very good. On the other hand, it can be quite intrusive for thin films and it is particularly laborious to operate.

Wires probe.

In this methodology, the electrodes are constituted of two parallel thin wires stretched along CORDE chords of the pipe. As the liquid height varies, the surface of active electrode increases and so the resistance decreases because of the larger area of passage for the electric current. The method relies on calibration depending on geometrical dimensions and conductivity of the medium. The response of this system is fairly linear and can be used for thick films. In fact, the same principle is used in some tank level measurement systems. For thin films it is usually INATTENDIBILE unreliable because of its intrusive nature (i.e.: the formation of a meniscus due to surface tension effects). Also, the local character of measurement depends on the distance between the wires.

Hence, this method has been used widely for the measurement of film height in stratified and slug flow.

Flush mounted pins probe.

This arrangement falls in the general category of flush mounted probes and refers to a particular geometry of the electrodes. The method is used for very thin films typically up to 2 mm. In this case, each electrode is a pin mounted flush with the pipe surface and coupled to another electrode close to it. If care is taken in the mounting of probes, the method is virtually non-intrusive, but because the active surface of the electrodes does not vary with film thickness, the response is not linear when the thickness exceeds a value depending on diameter and separation between the probes. The electric field is very weak away from the pipe surface and has a negligible contribution to the passage of current. The response is initially linear close to the pipe wall (typically up to 2 mm) and then asymptotically flattens SI APPIATISCE to a uniform value. To enlarge the range of measurement, the diameter and separation of pins can be increased. An optimum balance must be struck between range of operability and local character of the measurement. Other common flush mounted probes have concentric electrodes or parallel strips.

The types of probe employed in this study were chosen on the basis of the characteristics described above and visual observations of the flow regime in the inlet pipe. The liquid film in semi-annular flow was observed to be asymmetrical with a thick film at the pipe bottom, which became abruptly IMPROVVISAMENTE much thinner towards the top. For this reason, wire probes were used at the pipe bottom and flush mounted probes at the top. IMP.

III.2.4 Wire probes test section for height measurements at the pipe bottom and its calibration – The 'harp' test section.

The facility used for the measurement of film thickness at the bottom of the pipe is the same employed by Rea (1998), Figure III.2.2 and for ease of denomination, we will refer to it as the 'harp' test section. Five pairs of stainless steel wires are stretched along chords of the pipe cross section. The spacing between two wires of the same pair-probe is of 5 mm and the distance between two analogous wires of two consecutive pairs is of 25 mm, with the central pair symmetrical to the vertical diameter. Wires have a diameter of 0.33 mm and are tightened to a Perspex ring with a depth of 25 mm. To ensure appropriate tension of each wire, a plastic screw is inserted in a threaded hole at the top and bottom of the ring. This has a passing hole, 0.7 mm bore PERFORATO, through its length and a transversal metallic screw of 1 mm pushes the wire against the wall of the passing hole, Figure III.2.3. Particular care had to be taken to avoid the wires snapping ROTTURA on the sides of the metallic screw when they were fitted. Because the flow pattern is annular, precaution had to be taken to eliminate the route PERCORSO for current at the top of the pipe, across the thin film. For this reason, each wire was insulated 15 mm from the upper wall with a synthetic, waterproof coating. IMP.

IL CIRCUITO SI CHIUDE
SOLO IN BASSO

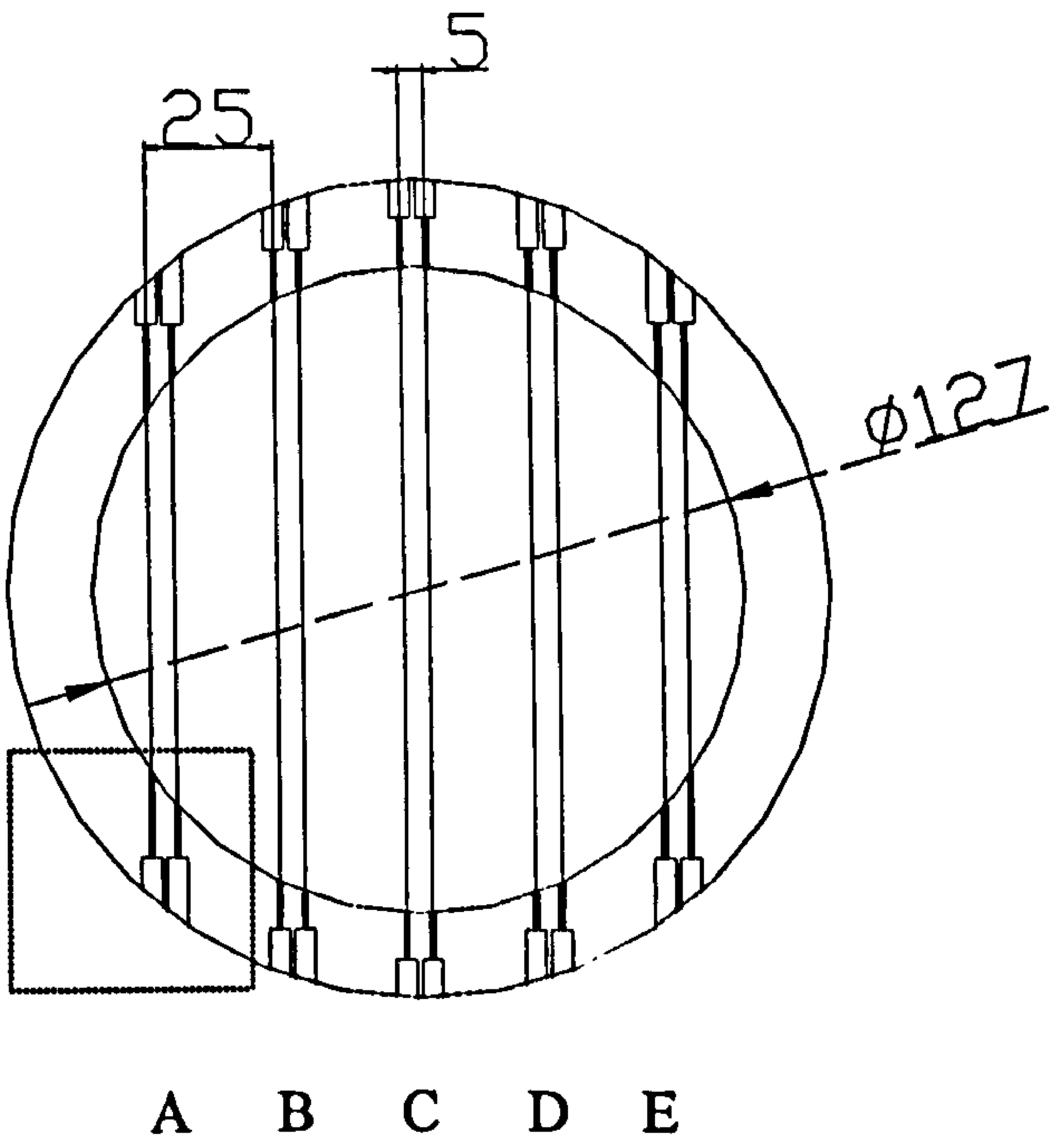

Figure III.2.2: *Sketch of the test section for film thickness measurement at the bottom of pipe (the 'harp') used near the mixing section and in the three legs of the T. The dashed square is enlarged in Figure III.2.3.*

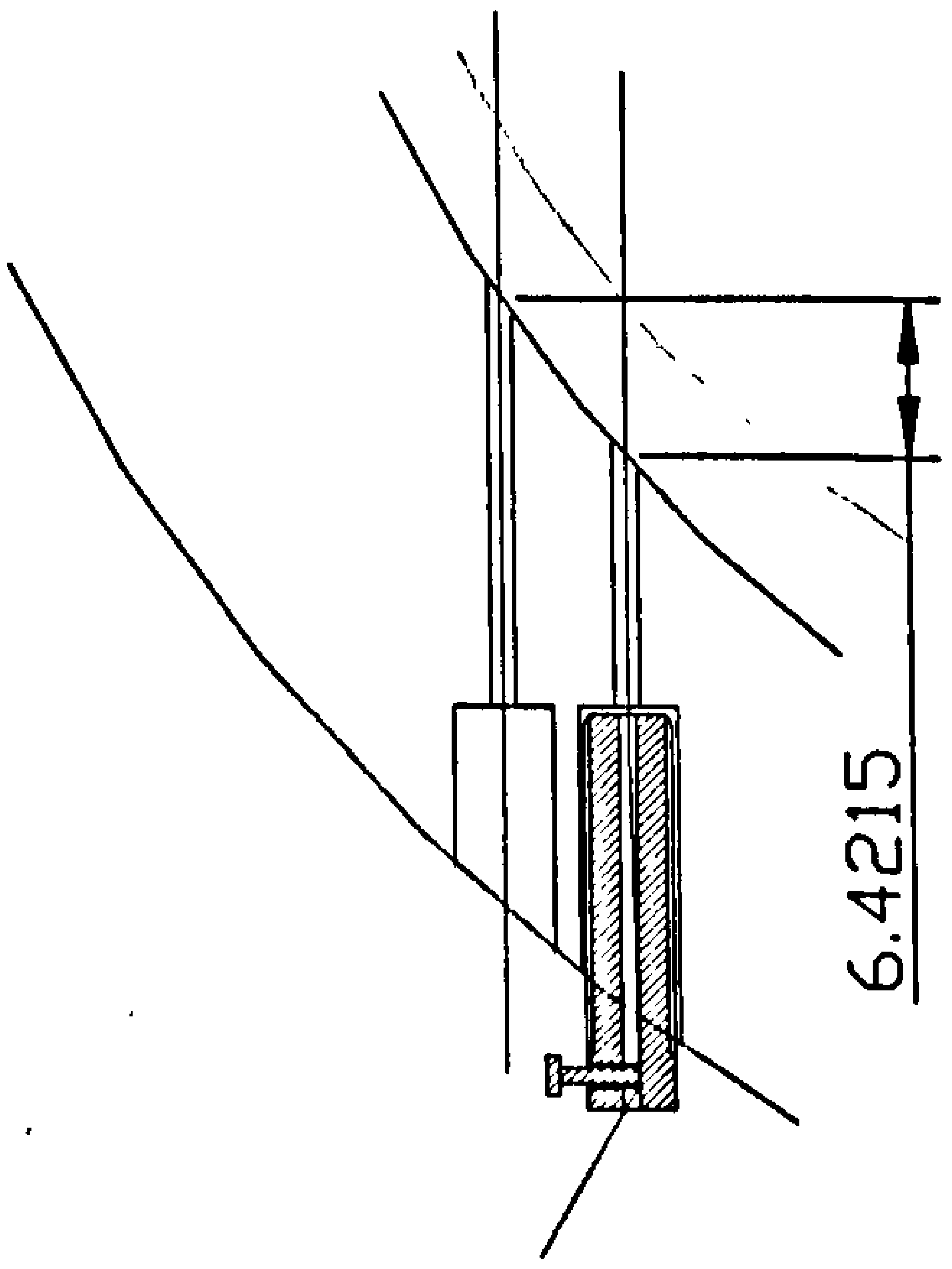

Figure III.2.3: *Particular of Figure III.2.2 in the dashed square showing the system to tight up the wires and the distance between the bottom of two electrodes.*

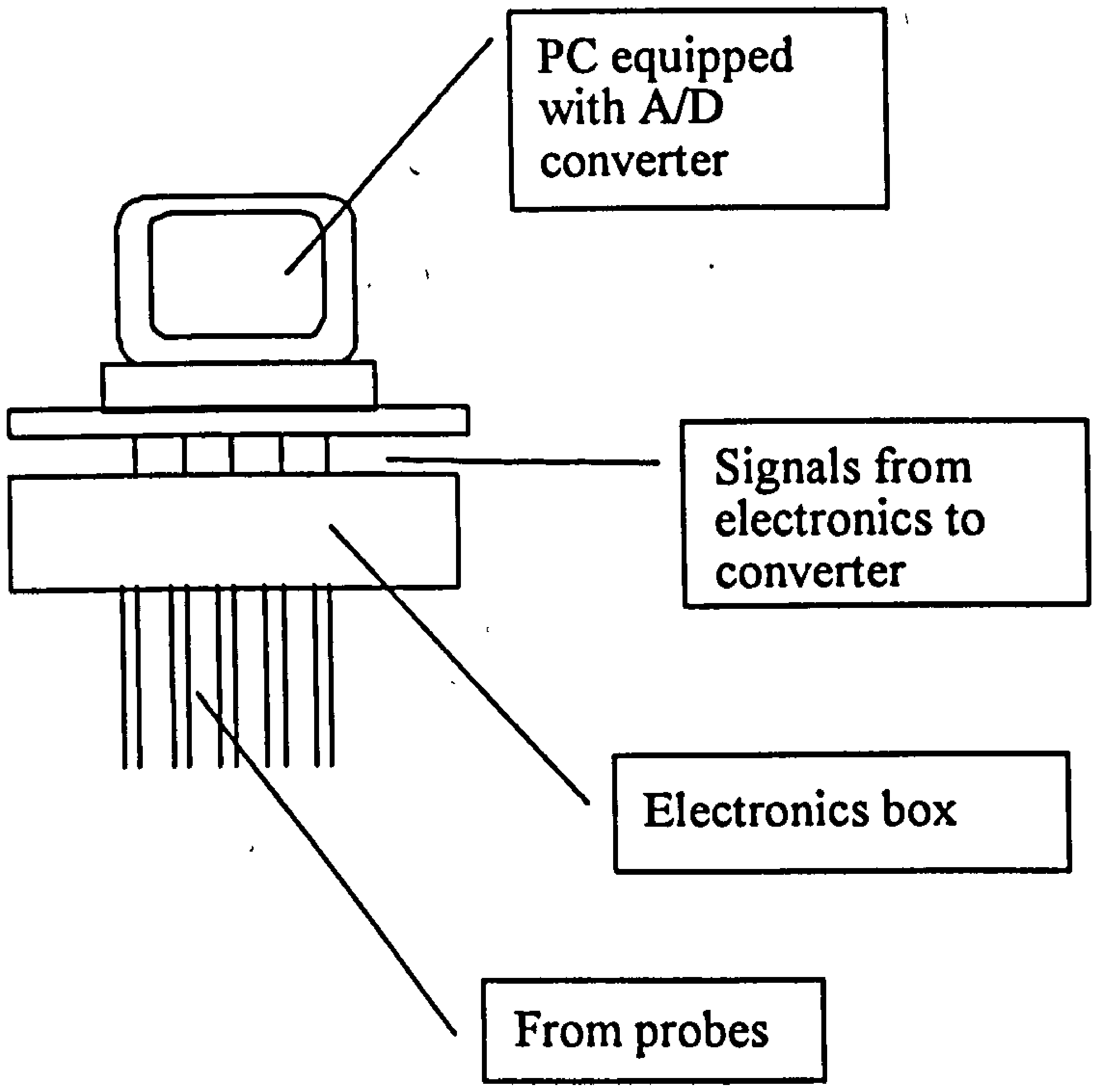

Figure III.2.4: *Sketch of the arrangement for data collection.*

A sketch of the arrangement for collection of data is shown in Figure III.2.4. The voltage is applied and filtered by an electronics box designed at Imperial College, London and used also by Srichai (1996). The signal from 5 probes could be obtained simultaneously and, after filtering, this was fed to a PC equipped with an A/D converter card by Data Translation, DT-VPI. Before calibration, the electronics box was opened and the gains were adjusted to obtain optimal operation in the expected range of heights. The maximum nominal signal processed by the system is 10 V but it was observed to be ~9.7 V for all the channels. However, the A/D converter processes signals up to 10 V and gains were adjusted so that for a height of 50mm at the centre, the signal was 9V. Data processing was partly carried out using HP-Vee 4.0 by Hewlett Packard. Microsoft Excel 97 and FORTRAN programs were used in conjunction with this package.

The system was calibrated by flanging the ring with fitted probes between two short pieces of Perspex pipe. Special screws had to be designed for this operation as well as for the location of the test section in the loop. The extremities were closed with transparent lids to form a cylinder and a graded scale in millimetres was placed from the bottom of the pipe up to 60 mm on both lids. Water was added or removed via a small hole. The cylinder so obtained was held horizontal in a wooden frame and the level was checked by using a spirit level and that the level of water read on the two extremities was the same. On one side, an optical target allowed accurate assessment of the height of liquid from the bottom of the pipe, with a confidence of 1 mm. The signals were recorded for steps of 5 mm simultaneously from the five channels through the A/D converter.

Calibration of the probes at the periphery of the pipe cross section proved more difficult. The curvature of the pipe caused a difference in height of ~6.4 and 2.1 mm between the bottom of the two electrodes for the most external (A & E) and intermediate (B & D) probes respectively, Figures III.2.2-3. Furthermore, the shape of the film during calibration was flat as opposed to the annular flow conditions. However, it is expected that the electrode impinging to the lesser extent in the liquid film would control the resistance across the two electrodes. Hence, calibration was made for the height at the external electrode.

IMP.

IMP

It is known (Williams, 1990) that cross talking among probes can strongly influence the response of such systems. In other words, if measurements from one probe are taken simultaneously to adjacent probes, the response can be affected. For this reason, the probes were calibrated in the same configuration as used in the experiments. In the specific case, the five channels were used simultaneously for the five probes both for calibrations and measurements.

Because the electrical conductivity of water was seen to vary with parameters that will be discussed in section III.2.7, the calibration was carried out with solutions of de-ionised water and sodium chloride of three different conductivities in the experienced range for steps of ~50 µS/cm. By linear interpolation, a calibration curve for each probe at any conductivity in the range could be obtained. Figure III.2.5, shows the calibration lines for the five probes for a conductivity of 612 µS/cm and Figure III.2.6 shows the calibration lines for probe C for three conductivities of 612, 665 and 725 µS/cm.

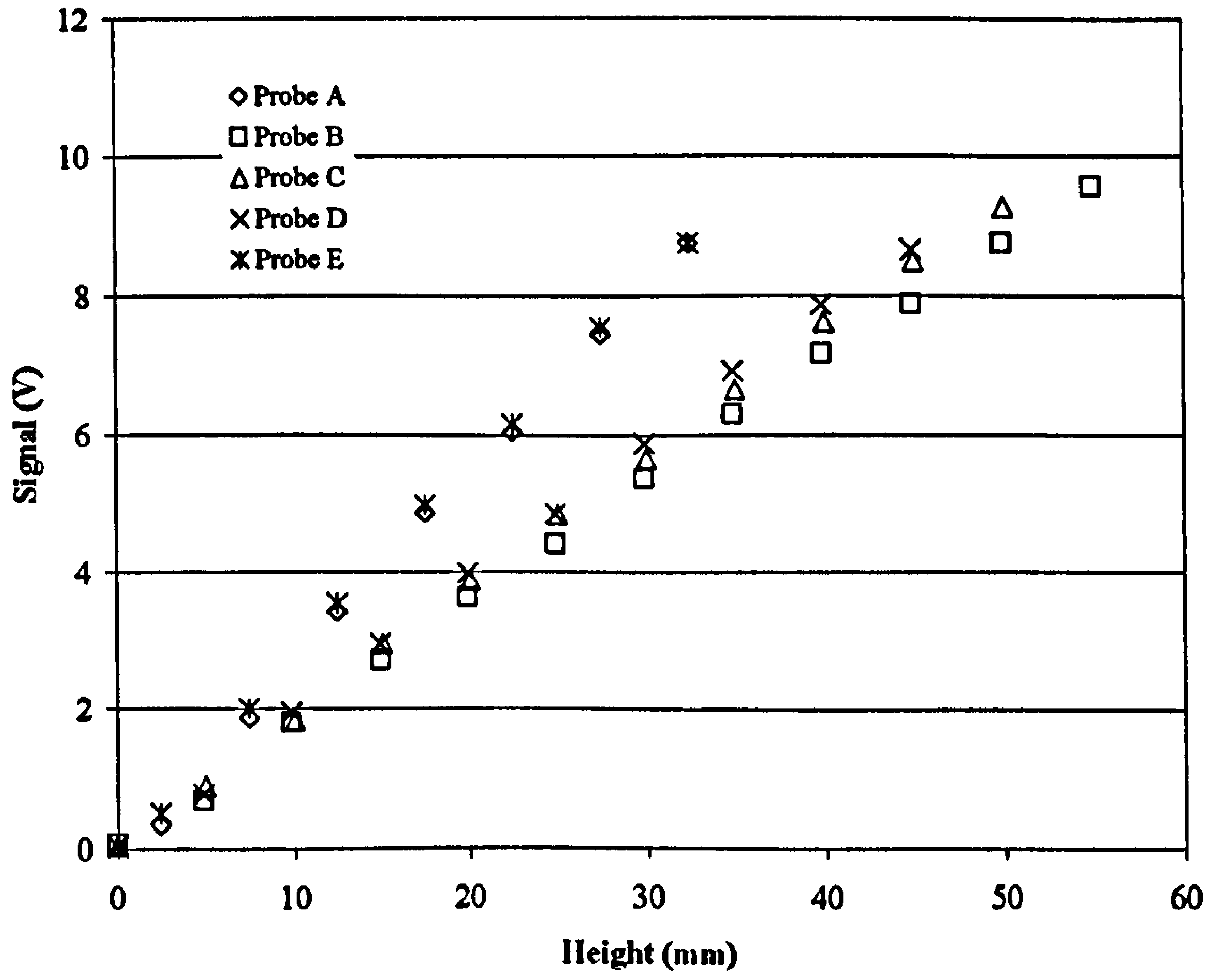

Figure III.2.5: *Calibration lines for the five probes for a conductivity of 612 μS/cm.*

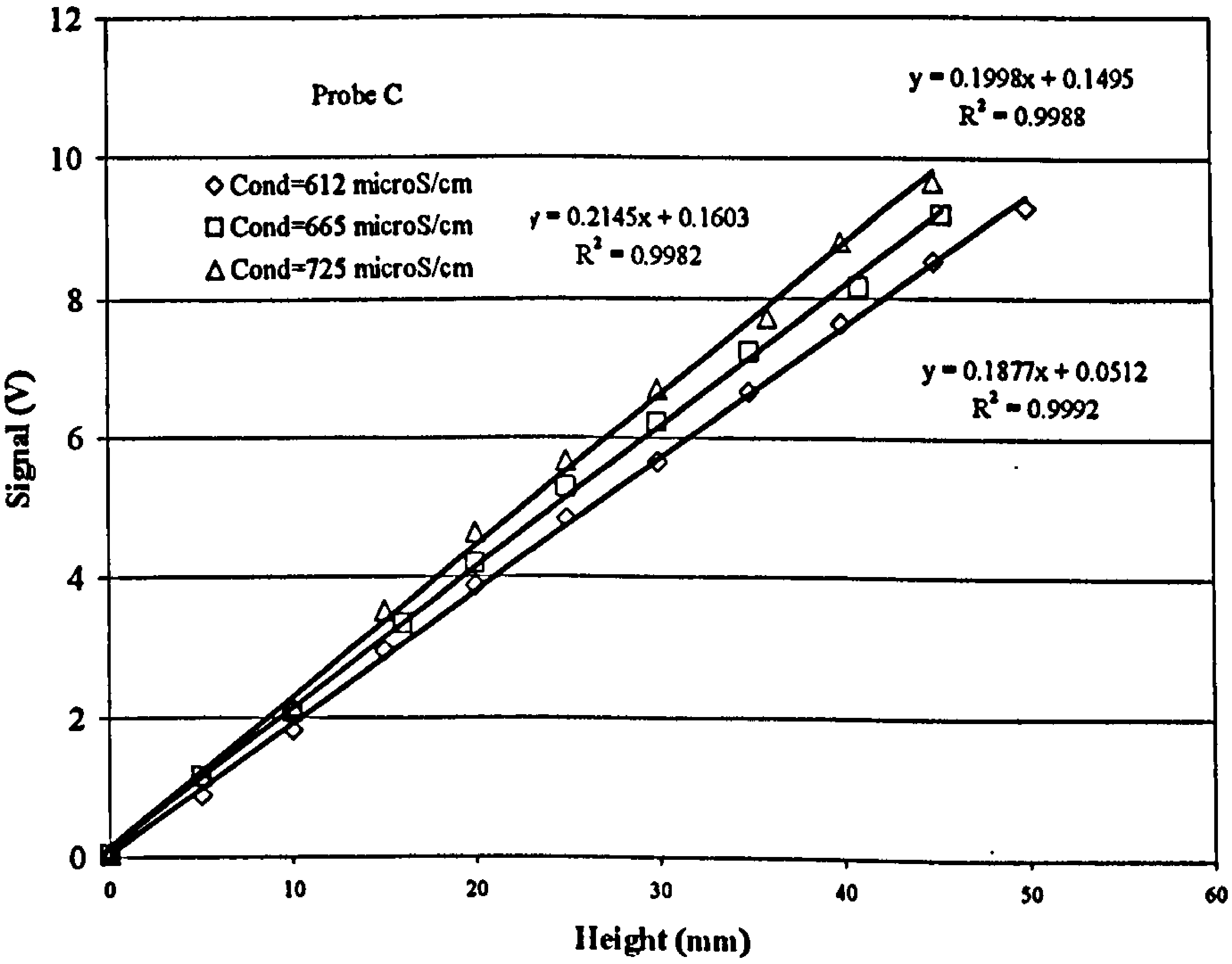

Figure III.2.6: *Calibration lines of probe C for different conductivities.*

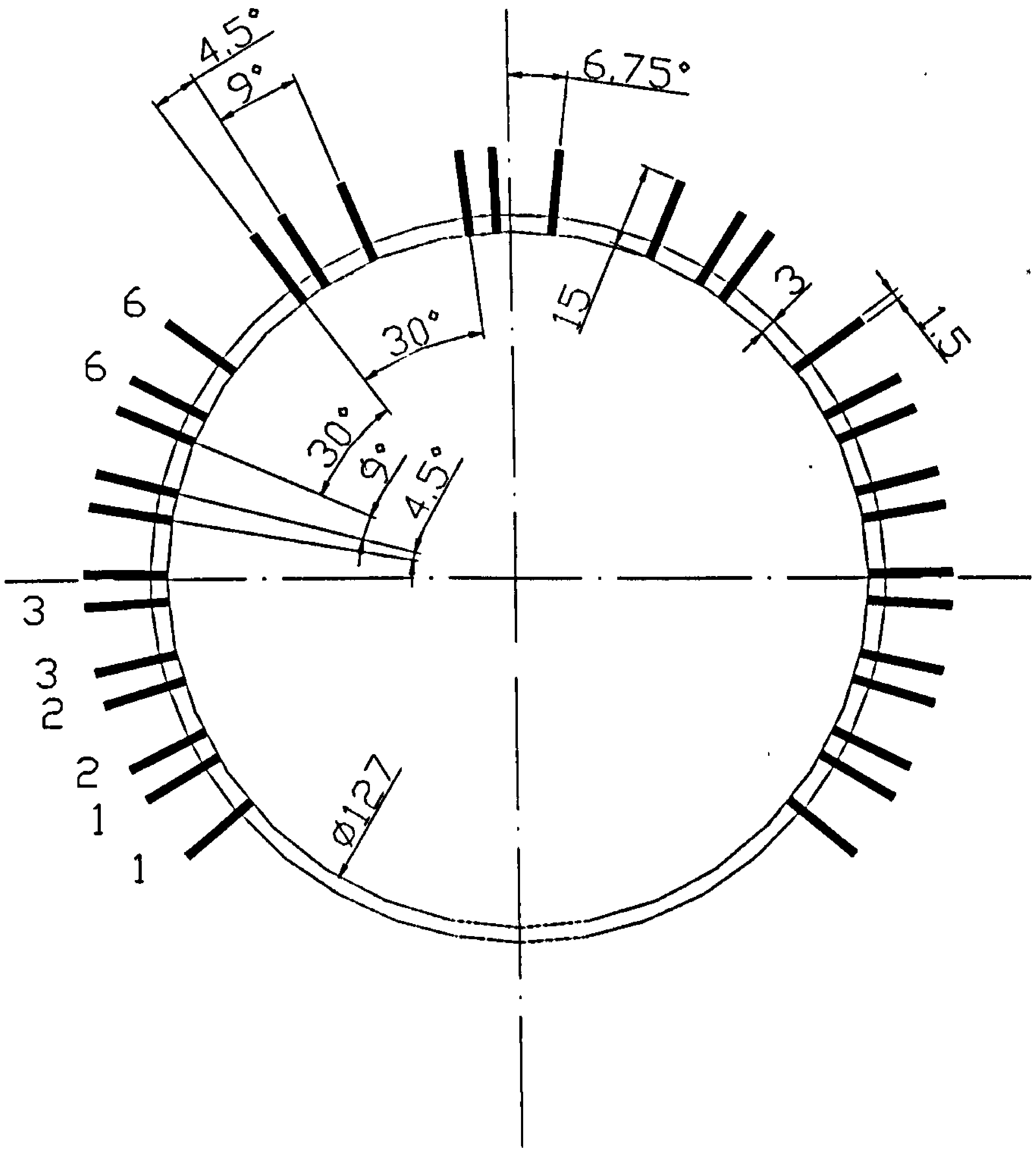

Figure III.2.7: *Cross section view of the test section for film thickness measurements at the top of the pipe (the pins-ring). Linear dimensions are in mm.*

III.2.5 Flush mounted pin probes test section for thickness measurements at the pipe top and its calibration – the pins-ring test section.

The main advantage of flush mounted probes is their non-intrusivity and accuracy for measurement of small thickness. The range extends typically up to 2 mm but using bigger diameter pins and increasing their separation can AMPLIATO widen the range. A limit is imposed as the electrodes have to be sufficiently close to give a good quality local measurement. The measured thickness is assumed to be the value at the mid-point between the centre of the electrodes.

For this reason, two configurations were tried on the same test section, Figure III.2.7. In one configuration, the electrodes are spaced by every 9° and by every 4.5° in the other. The pins were made from 1.5 mm diameter welding rods, made of stainless steel to avoid problems of corrosion. The pins were located at one extremity of a 19 cm long section of Perspex pipe, 2 cm from the male flange. They were glued in precision machined holes with epoxy-resin and mounted flush to the internal surface of the pipe. However, accuracy of the mounting did not allow the electrodes to be perfectly flush and so machining was needed. Because of the different hardness of steel and Perspex, particular attention had to be taken to avoid jamming of the lathe and disruption of the test section.

The series of pins on the two sides of the test section were used by switching the connections to the electronics so that intermediate electrodes could belong to two probes in sequence, one with a spacing of 5 mm (4.5°) and the other of 10 mm (9°). The sequence is shown in Figure III.2.7 (1-1; 2-1; 2-2; 3-2; 3-3...6-6). The three groups of three pins at the very top of the section, 30° apart, were used in the same way but each group was used independently, with no coupling of pins belonging to different groups. A switchboard was built to avoid laborious operations on the test sections and signals were taken individually.

Calibration of this test section required the use of a calibration slot. This was machined out of a block of Perspex in the shape of a solid cylinder with the same diameter as the test section. On one extremity, down to a length of 6 cm, the cylinder was notched progressively for steps of 51°, cutting 0.3, 0.5, 1, 1.5, 2.25, 3 and 5 mm off the original surface in the radial direction (Figure III.2.8). The test section was flanged to a lid on the extremity opposite to the location of pins and placed vertically with the lid at the bottom on a horizontal surface. The slot was slid in the open cavity with the notched extremity at the top. The interstice was filled with water of known conductivity and a handle allowed rotating the slot so that a varying gap of water could be created in front of the probe being calibrated. Calibrations as well as measurements were taken individually, recording the signal probe by probe although the electronics box would have allowed 5 signals to be measured simultaneously. This was a necessity as it was very laborious to calibrate more probes simultaneously given the characteristics of the slot and to avoid the effect of cross talking.

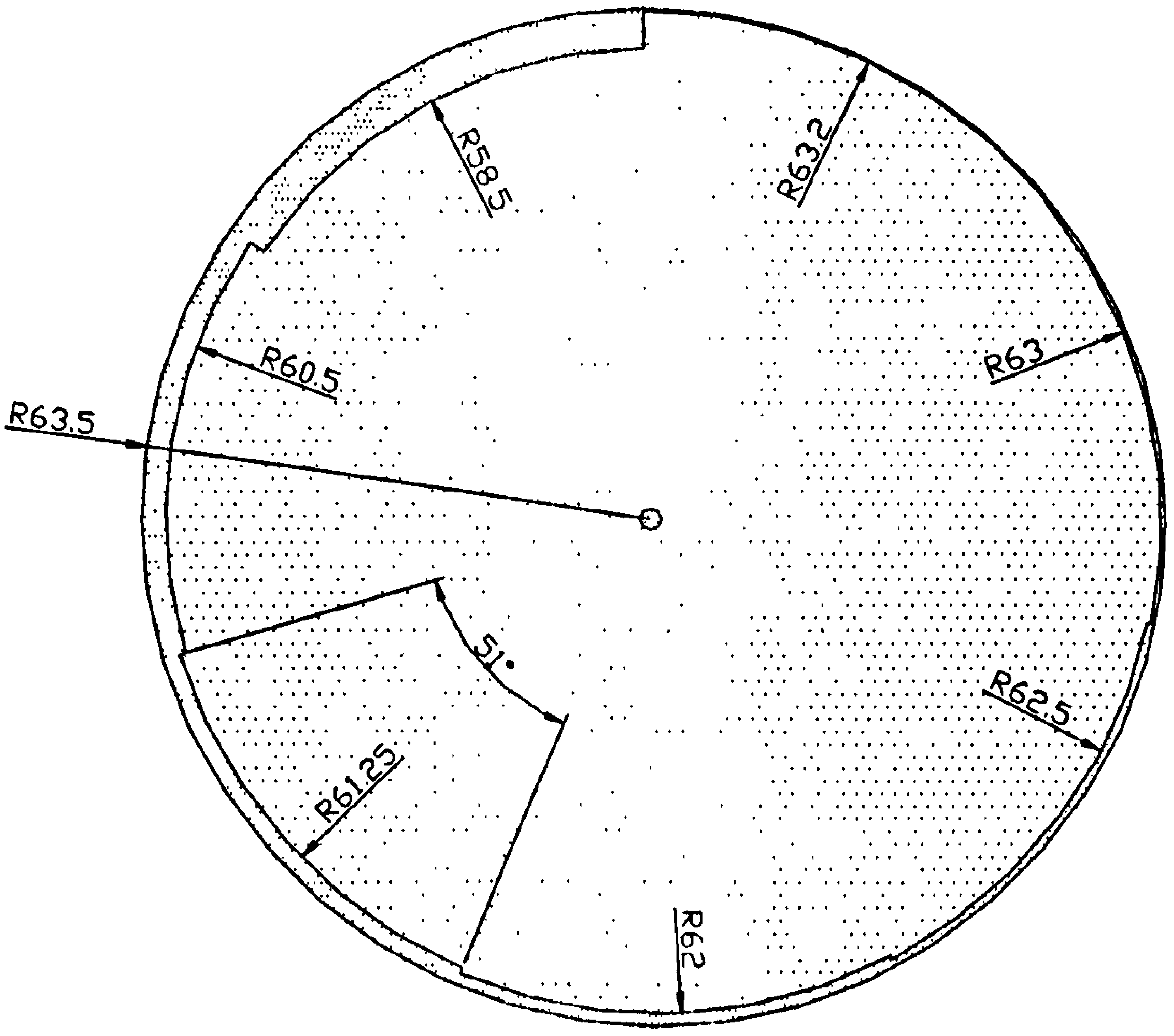

Figure III.2.8: *Top view of the calibration slot for the flush mounted probes test section. The darker shade is the original cylinder, the lighter shade is the upper part of the slot after cutting. Linear dimensions are in mm.*

Because of thermal deformation of the test section, the slot often jammed into the section. A looser tolerance had to be allowed and calibrated cylindrical gauges were placed between the pipe wall and the slot surface to ensure the required liquid gap.

The electronics box, analogous to that used for wire probes, had a nominal voltage of 7.5 V. The gains were regulated so that a signal of 7 V was recorded for a liquid thickness of 5 mm at a water conductivity of 600 μS/cm. In Figure III.2.9 the calibration curves are shown for the two possible combinations of probes (5 and 10 mm spacing) at the top of the pipe. The curve for 5 mm spacing is much steeper for small thickness and becomes quite flat for thicknesses over 1.5 mm. Conversely, although less linear and with a smaller initial slope for very thin films, the calibration curve for 10 mm spacing allows a good degree of confidence up to 2.5 mm. The calibration curves were fitted with polynomial equations 3rd - 5th order for three conductivities, similar to the 'harp' test section.

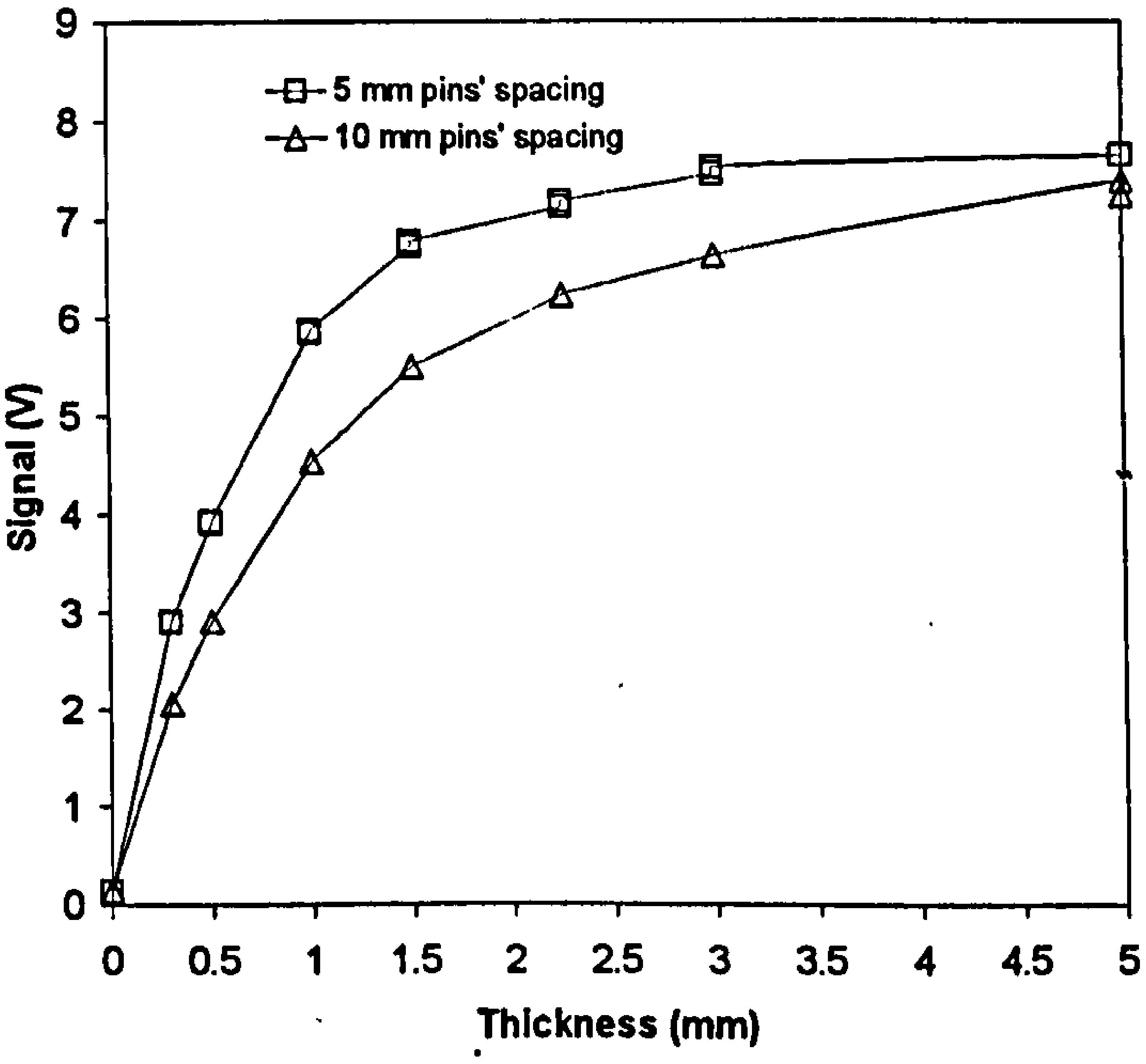

Figure III.2.9: *Calibration curves for flush mounted pin probes showing signal plateau and the effect of electrodes spacing. Conductivity = 600 μS/cm.*

III.2.6 Wire probes test section for height measurements at the T-junction and its calibration.

Another test section was designed for the measurement of film height within the T-junction. A T-block was built with the same dimensions as the one described for the measurement of split data (section III.1.1). Stainless steel wires were fitted in the locations shown in Figure III.2.10. The spacing between the electrodes of a probe was again 5 mm and the probes were 25 mm apart in the radial direction. To avoid the problems experienced with the probes far from the vertical diameter, where the two wires have different lengths due to the pipe curvature, the wires were aligned along the pipe axis (see section C-C of Figure III.2.10-b). An exception was made for the probes in the section B-B, which were placed as in the test section shown in section III.2.4.

The axial separation of probes is 36.75 mm, Figure III.2.10-a. Concern was felt about the impact of the flow disturbances caused by the first electrode of a probe, upon the one downstream. The distance apart is 20 wire diameters. However (dashed circle in Figure III.2.10-a) an extra electrode was added to the central probe of the first row so that comparison between results in the two configurations could be made. Differences were within the experimental error for all inlet conditions.

The electronics box used was the same discussed in III.2.4 and calibration and measurements were taken in sequences of five probes starting from the first row of probes seen by the splitting flow down to the 5th. Finally, the signals from the row B-B were acquired. Calibration was obtained by placing the T on a horizontal plane and closing the three legs, as discussed in III.2.4.

III.2.7 Experimental set-up for film thickness measurements

Particular attention had to be taken in assembling the loop when film thickness measurements were to be made. As the test sections were flanged at some location of the loop, there was concern that irregularities such as gaps and steps could significantly disturb the flow, especially when the film is very thin. Hence, flanges were machined to ensure smooth transition from one section to another. Initially, the measurements at the three legs of the T were taken by placing the combination of pins-ring and harp test sections in sequence, at a distance of 1 cm from each other and 12.5 cm from the centre of the T in the three directions. Because of the directionality of the flanges, when measurements were taken in the run and in the side arm the harp test section was placed before the pins-ring, stream-wise. In this cases the wires at the top could disturb the flow of the thin film, however, both visually and from measurements no such effect could be observed.

The set up for measurements within the T required similar care for the regularity of joints at the flanges.

Another problem that had to be accounted for, was the variation of conductivity of the water in the storage tank. Because of seasonal variations, the water from the tap exhibited values of conductivity between 500 and 650 µS/cm. Also, the conductivity was significantly increased by warming of the water from dissipation of energy at the pump.

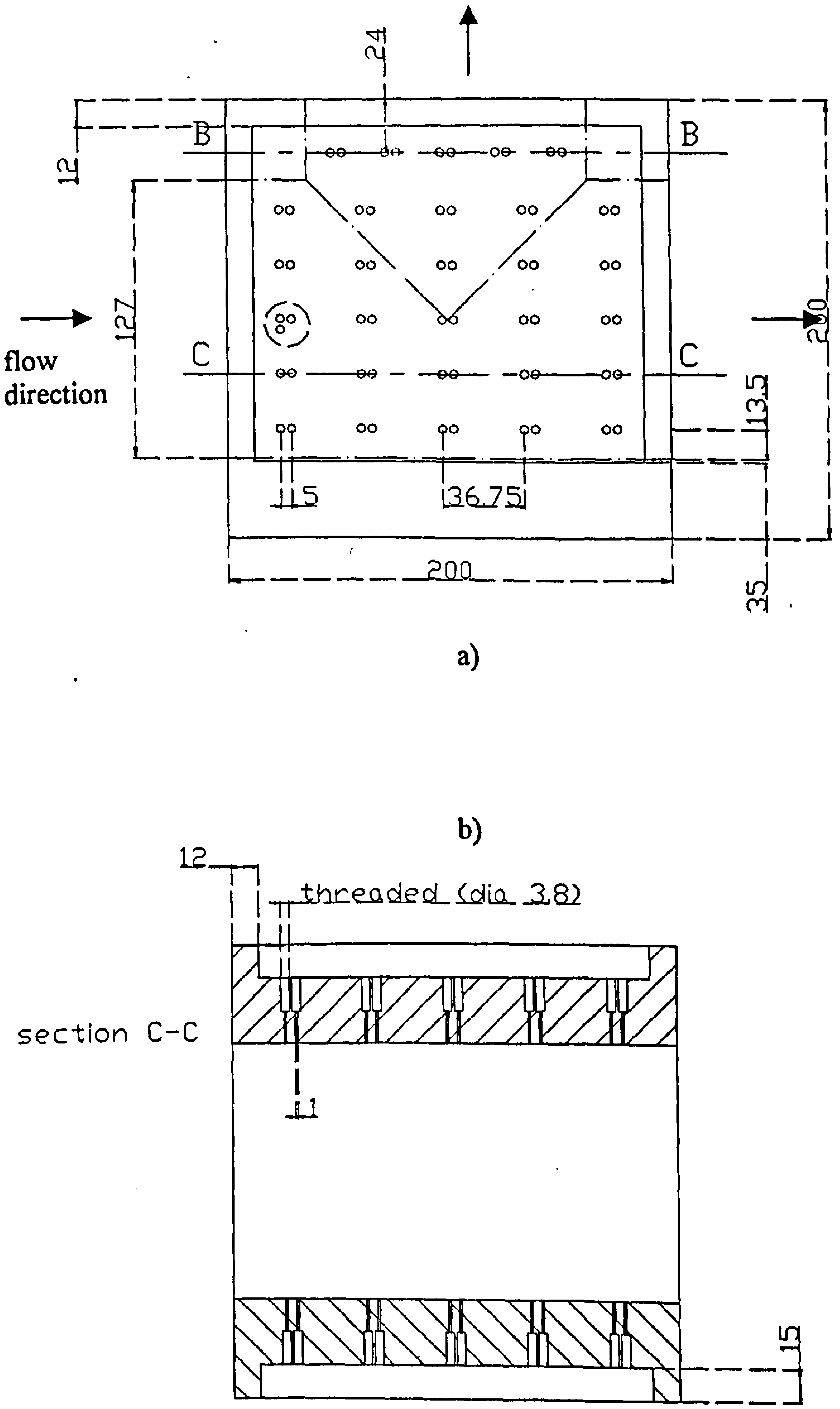

a)

b)

Figure III.2.10: *plant (a) and side section (b) views of the test section for film height measurements in the T. Dimensions are in mm.*

Furthermore, the water became quickly fouled and mineral deposits begun to show, particularly on the wires. To avoid large variations of conductivity within the same experimental run and to reduce fouling of the electrodes, fresh water was fed continuously to the storage tank and discharged through a drain. It was observed that 20 minutes after start-up, the conductivity maintained a constant value with variations of ±5 μS/cm. This was checked throughout each session of experiments by collecting water at ~6 m of pipe length downstream of the measuring station, before it was fed back to the storage tank.

Calibration of the test sections was repeated periodically without any cleaning of the electrodes. It was observed that the variations of the calibration curves caused changes in the film thickness which were well within experimental error. The largest discrepancy recorded was 3.5%.

Conductivity was measured by using a standard conductivity-meter manufactured by WTW (Germany).

III.2.8 Film thickness results from harp and pin-ring test sections.

As already mentioned, measurements were taken for the same inlet conditions as for the split data (Table III.1.1), for 3 split conditions of low, average and high gas take off. It was observed that the split of the phases did not influence significantly the film distribution upstream of the junction, in the section located 12.5 cm (1 diameter) from the centre of the junction.

The examples illustrated below, are representative of all the database. The data is tabulated in appendix A.

Figure III.2.11, shows the film thickness distribution in the three legs of the T for case c) of Table III.1.1 (U_{gs}=24.5, U_{ls}=0.28 m/s) for a fractional gas take off G'=0.52 obtained by keeping both valves downstream of the junction fully open. The abscissa is the angular position of the probes and the convention is anti-clockwise for the observer travelling with the direction of the flow.

As already mentioned, the liquid film at the inlet abruptly changes thickness towards the periphery of the pipe and the film distribution is generally symmetrical.

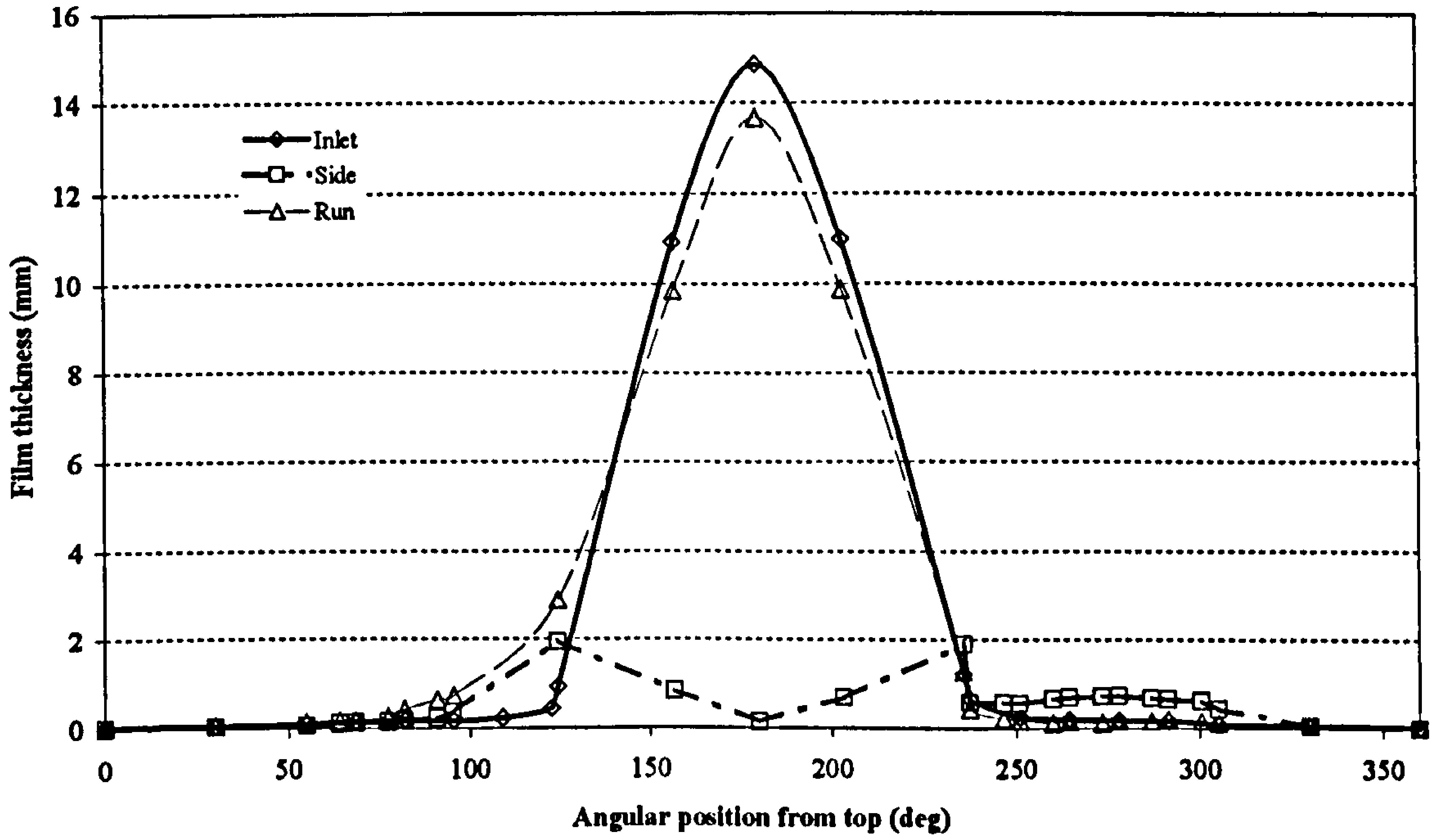

Figure III.2.11: *Film thickness distribution in the three legs of the T for Ugs=24.5, Uls=0.278 m/s. (G',L')=(0.52,0.16) (case C in Table III.1.1).*

The film distribution in the run is non-symmetrical and this is due to the film climbing on the wall of the pipe close to the downstream corner of the T. This is due to the fact that under the pressure differential from the side arm, the film bends towards it and hits the downstream corner and because of its momentum climbs on the pipe wall causing the thicker film observed between 100° and 150° on the run leg curve. Because of the convention, the downstream corner of the T, in the side arm is located at the other end of the graph, around 250°. There, it can be seen that the film is significantly thicker than it was at the inlet.

The effect of phase split on the film distribution for this case can be seen in Figures III.2.12-16 for small, average and large gas take off, for the three legs. Figure III.2.12, shows that no effect of the split of the phases is fed back to the film distribution, even very close to the upstream corner of the junction (0.5D).

The inlet distribution can be better appreciated from Figure III.2.13, where the ordinate axis is plotted in logarithmic scale. The film symmetry is very good and the sudden thinning of the liquid is very visible from the bottom towards the top. The film keeps then fairly constant and drops again towards the very top.

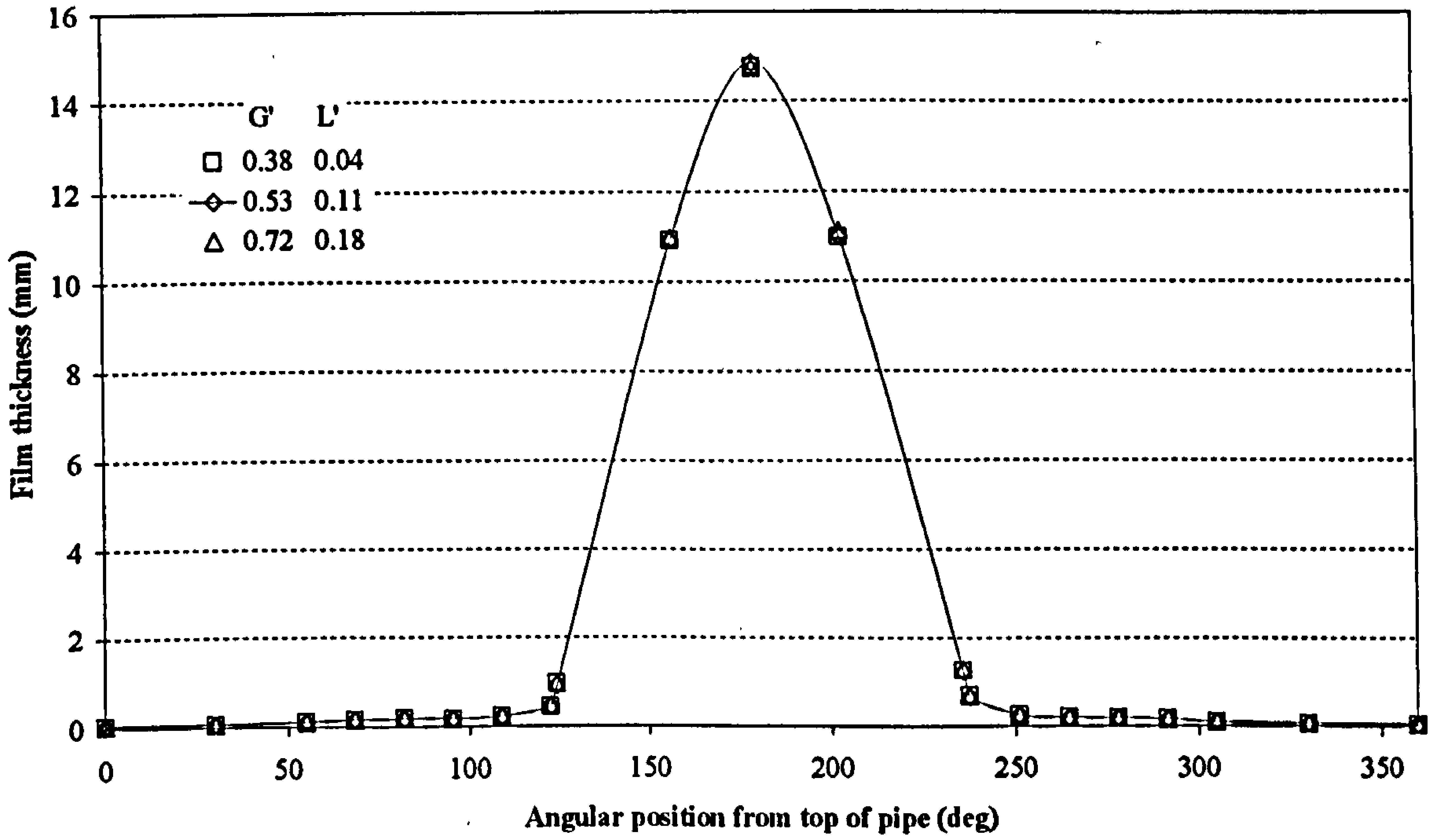

Figure III.2.12: *Effect of phase split on film thickness at the inlet to the T-junction, 12.5 cm upstream of its centre.* $U_{gs}=24.5$, $U_{ls}=0.278$ m/s.

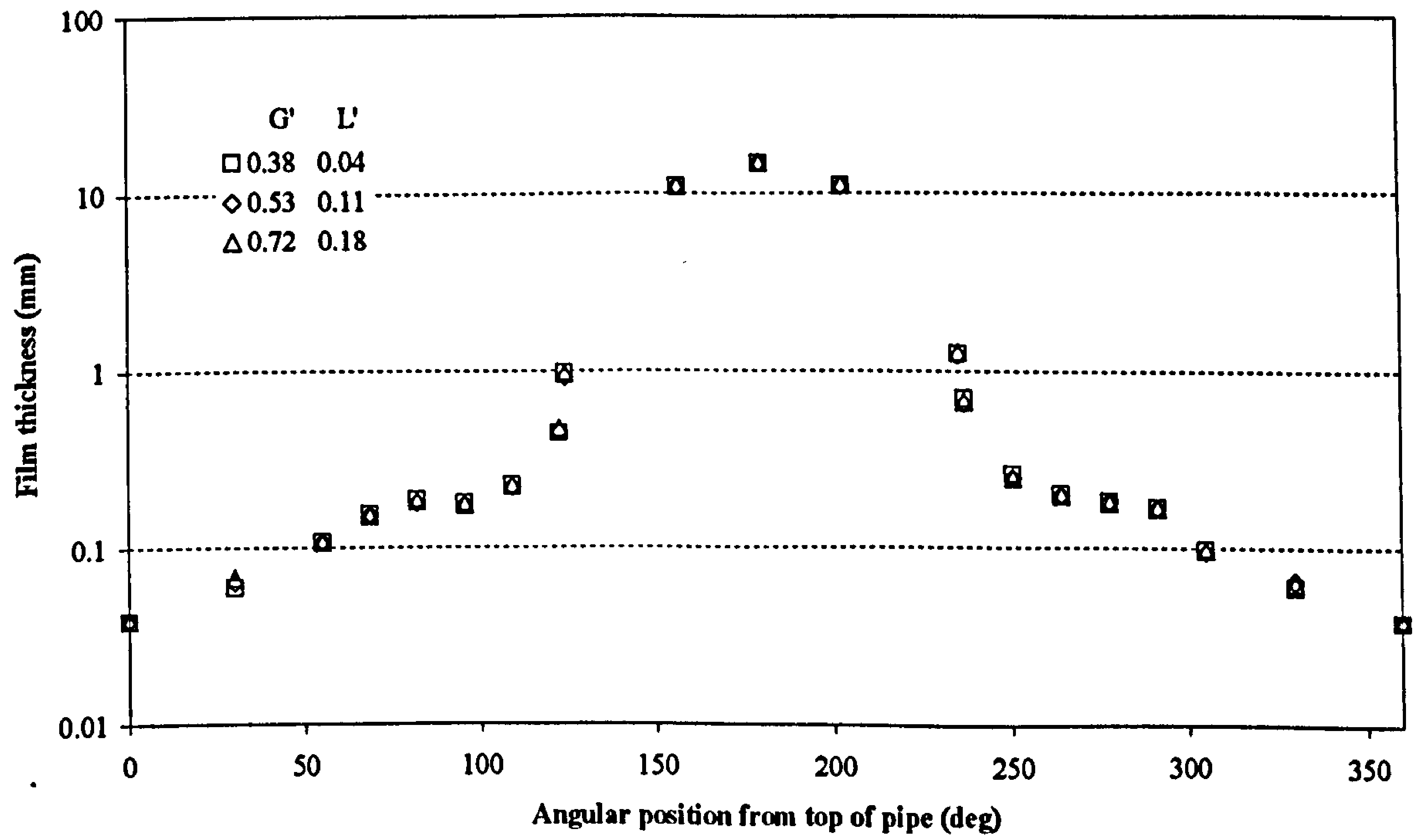

Figure III.2.13: *Logarithmic diagram of film distribution at the inlet to the T-junction, 12.5 cm upstream of its centre.* $U_{gs}=24.5$, $U_{ls}=0.278$ m/s

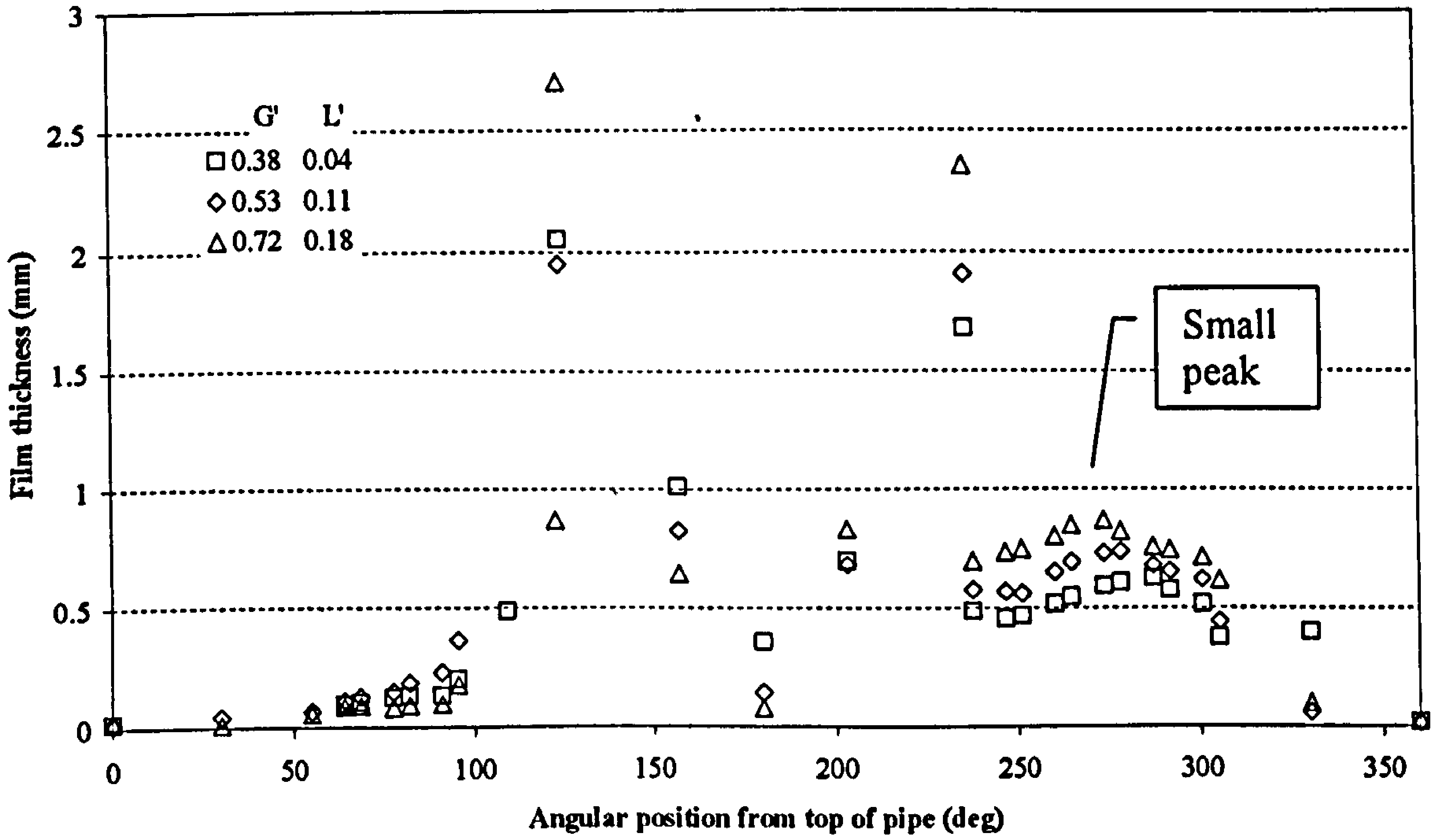

Figure III.2.14: *Effect of phase split on film thickness at the side outlet of the T-junction, 12.5 cm downstream of its centre.* U_{gs}*=24.5,* U_{ls}*=0.278 m/s*

Figure III.2.14, shows the film distribution in the side arm. There, two peaks were visually observed and obtained from the conductance measurements. At the downstream corner of the T, part of the film was seen flowing as a thick rivulet (peak between 200 and 250°), slowly converging towards the bottom of the side arm. Because of its momentum, the remaining film climbed up the wall at the entrance to the side arm against gravity and, for high liquid flow rates or large take off of liquid, turned around the entire pipe circumference. This film moving in the circumferential direction joined the liquid diverted at the upstream corner of the junction to form a liquid ridge (peak between 100° and 150°) from which droplets were entrained in the gas stream. The film thickness at the bottom of the pipe towards its centre was seen to be very small, with the central probe nearly dry for some conditions. Also, there is a smaller, secondary peak moving towards the top of the pipe as the take off decreases (peak between 250 and 300°). In this section of the pipe circumference, the film is observed to become thicker as the diverted fraction increases. This secondary peak is due to the opposing forces of gravity and momentum of the liquid entering the side in the circumferential direction. This would also explain why the location of this maximum is closer to the pipe bottom when more liquid turns into the side arm. It is fair to assume that the velocity of the liquid climbing up to the wall of the side arm is related to its velocity at the inlet. Hence, this does not vary with split ratio and nor does the related driving force towards the pipe top. When a larger volume of liquid is forced on the wall of the downstream corner in the side arm, the action of gravity to drain the liquid is stronger and the maximum moves closer to the bottom. It could be expected that the velocity of the gas has a strong component in the circumferential direction too and, as the fraction of diverted gas increases monotonically with the fraction of liquid, the drag of the gas should increase its effect against gravity. However, experiments suggest that the effect of gravity also overcomes the circumferential drag.

Figure III.2.15 shows the results in the run arm. The thickness at the bottom of the run outlet is seen to decrease when the diverted fraction increases. This trend is reversed towards the downstream corner, in the run arm. In fact, the wire probe at the side of the central one, in the direction of the side arm, already shows a larger thickness for a larger diverted fraction. This can be seen more clearly in the enlarged diagram of Figure III.2.16, below 140°. There, the small but distinct trend of liquid thickening with diverted fraction is evident. Also in this case, the film exhibited a circumferential component of motion. This is due to the turning of the film towards the side arm occurring at the junction. For this reason, when the diverted fraction increases, although less liquid enters the run outlet the film climbing up the wall is thicker because the lateral component of the film velocity is of larger magnitude. Furthermore, the decrease of gas axial velocity in the run due to the larger gas diversion, forces the thin film to slow down and hence become thicker and drain at the bottom, as was observed further down the run arm.

The remaining five data sets can be used to make comparisons of film distribution variation with gas and liquid superficial velocity. In this, it can be useful to plot data on the pipe circumference for better visualisation. On the other hand, because the film thickness towards the top of the pipe is of the order of a millimetre, this represents only few percent of the length scale in the radial direction (63.5 mm). For this reason, when appropriate, data will be plotted again on a rectified diagram, on a logarithmic scale if necessary.

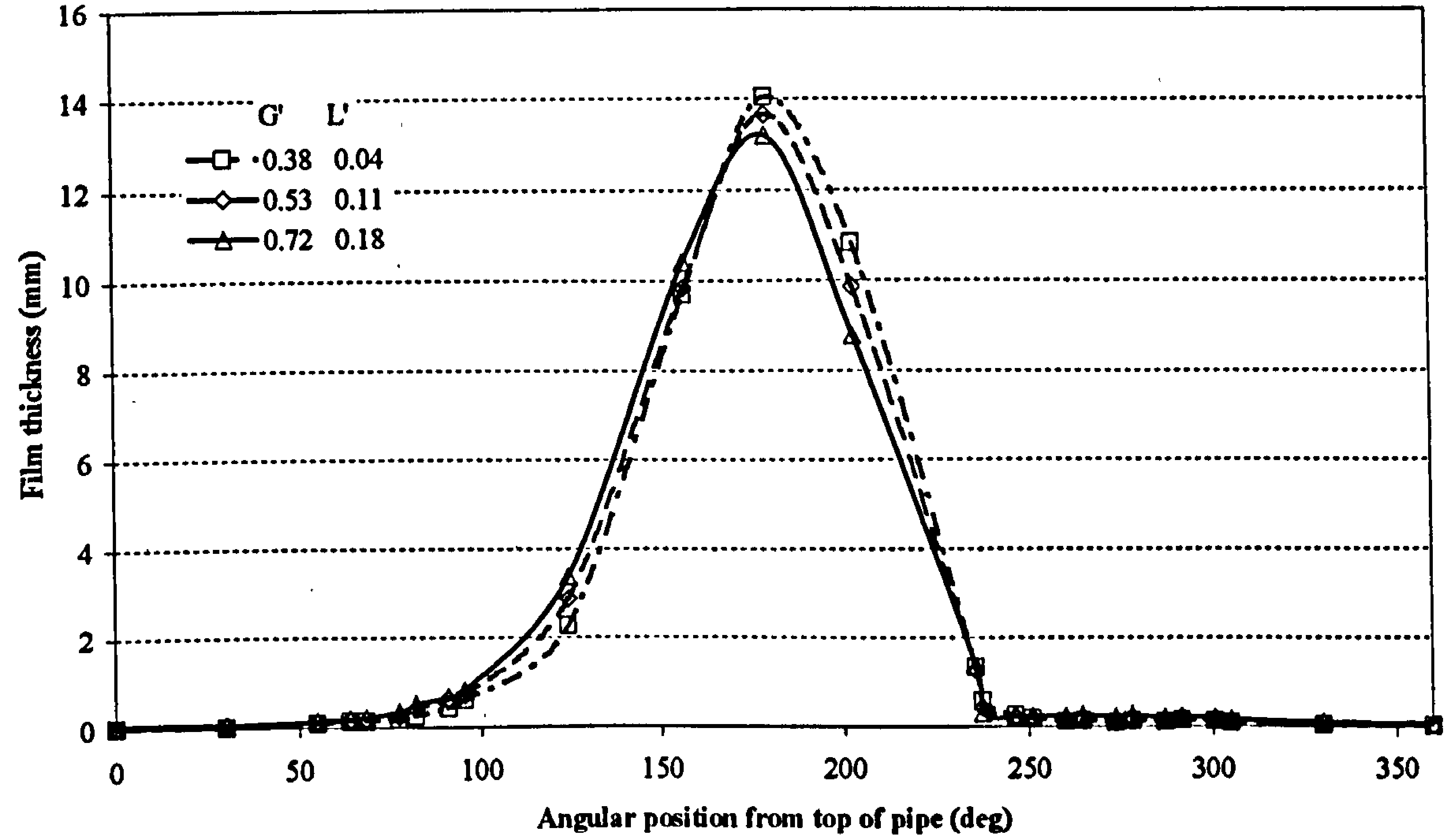

Figure III.2.15: *Effect of phase split on film thickness at run outlet from the T-junction, 12.5 cm downstream of its centre.* U_{gs}*=24.5,* U_{ls}*=0.278 m/s.*

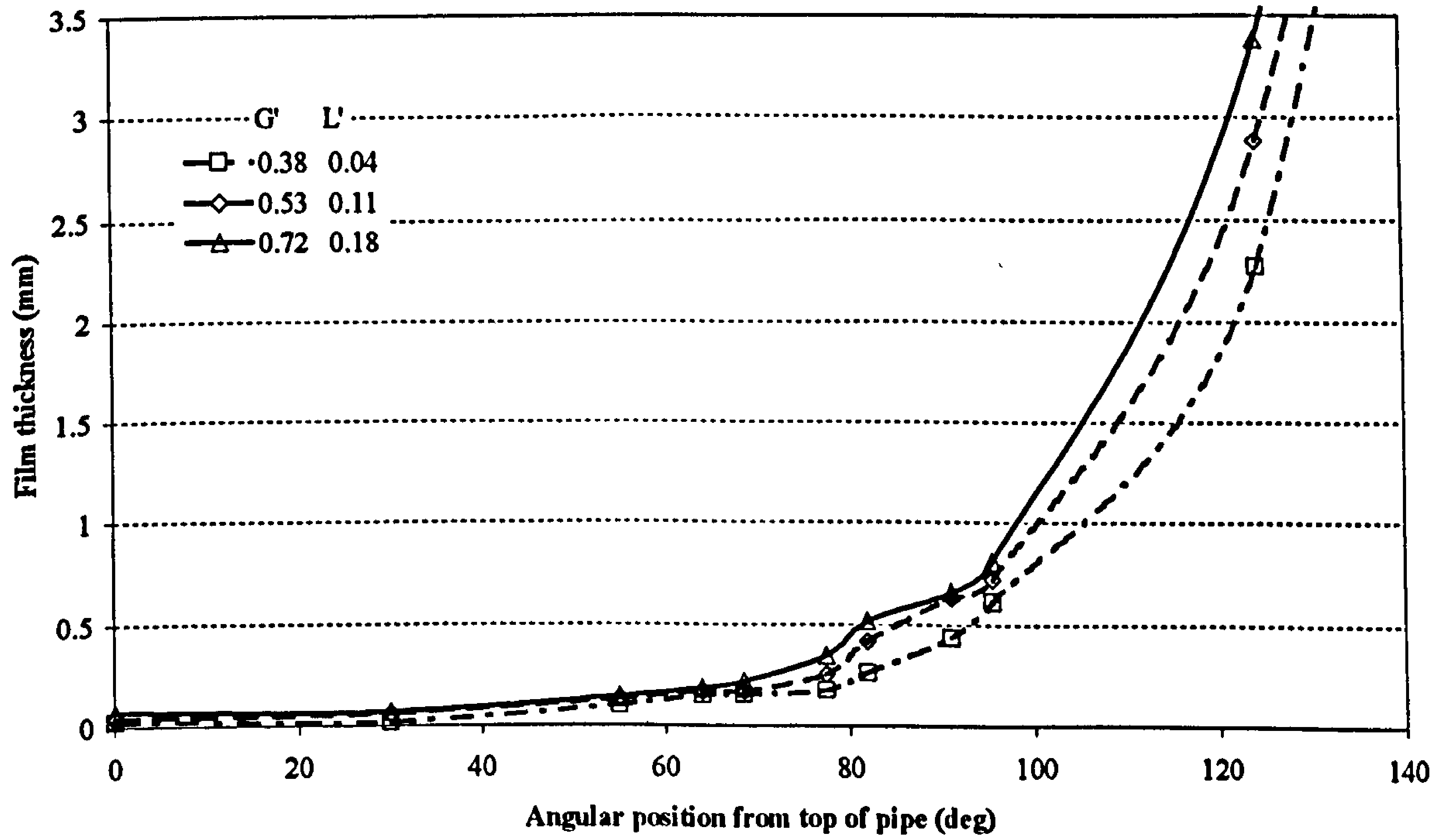

Figure III.2.16: *Particular of the film thickness distribution at the downstream corner of the T, in the run leg.* U_{gs}*=24.5,* U_{ls}*=0.278 m/s.*

Runs a), b) and d) (Figure III.2.17) show the variation of film distribution for varying liquid superficial velocity (0.55, 0.278 and 0.136 m/s respectively) and constant gas velocity of 16.5 m/s.

Surprisingly, the film distribution does not change significantly in the range of flow rates investigated in disagreement with other findings (Rea, 1998, Paras *et al*, 1994). A small trend can be seen in the film becoming thicker towards the top and slightly thinner at the bottom when liquid flow rate is increased. This suggests an influence of the liquid velocity in helping the film to climb up the pipe wall, eventually by the pumping action proposed by Fukano and Ousaka (1989).

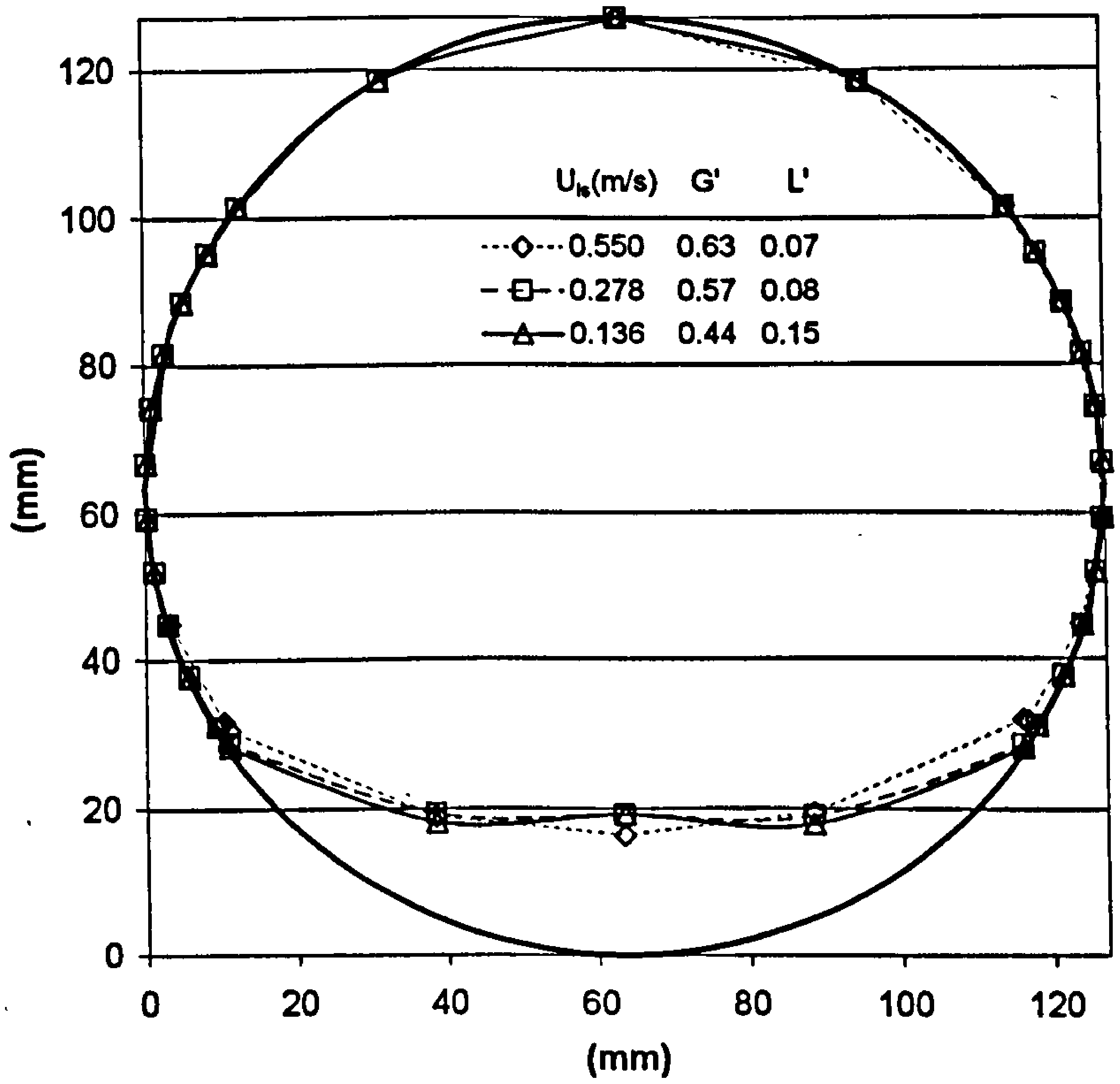

Figure III.2.17: *Film thickness distribution around pipe circumference for a constant gas superficial velocity of 16.5 m/s, at the inlet to the T-junction.*

Figure III.2.18, shows the film distribution for a constant liquid velocity of 0.136 m/s from runs d), e) and f) (U_{gs}=16.5, 23.0 and 28.1 m/s respectively). There, the film at the bottom becomes thinner as gas velocity is increased whilst the film at the top becomes thicker. This data set is plotted again in Figure III.2.19 on a logarithmic scale. There, it is possible to appreciate the inversion of trend of film

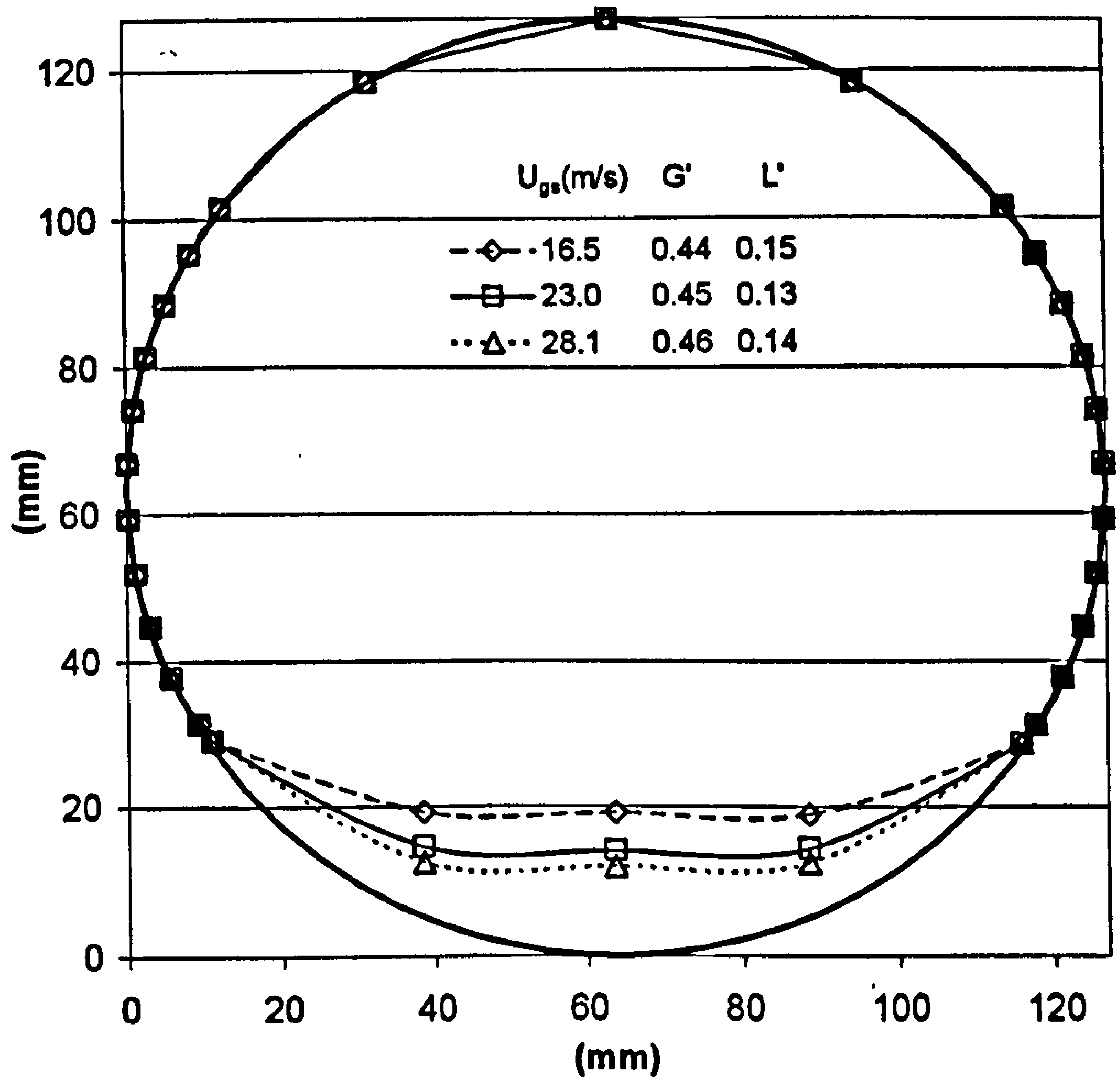

Figure III.2.18: *Film thickness distribution around pipe circumference for a constant liquid superficial velocity of 0.136 m/s, at the inlet to the T-junction.*

thickness with gas velocity due to a larger degree of symmetry around the pipe centre, for larger gas velocity.

For cases b), d), e) and f), a mild peak at the bottom of the pipe is observed, as already reported by Rea (1998).

Comparison of data for the same inlet conditions at the run and side outlet of the T is reported below, Figures III.2.20-23. In Figures III.2.20 and 21, data are plotted for the side arm results on a rectified plot. The results of runs e), f) and d) (Figure III.2.20, U_{ls}=0.136 m/s) show that the distribution in the side arm follows roughly the trend observed at the inlet with thicker film for the smaller gas velocity. The pipe top is dry as visually observed and recorded by the conductance probes.

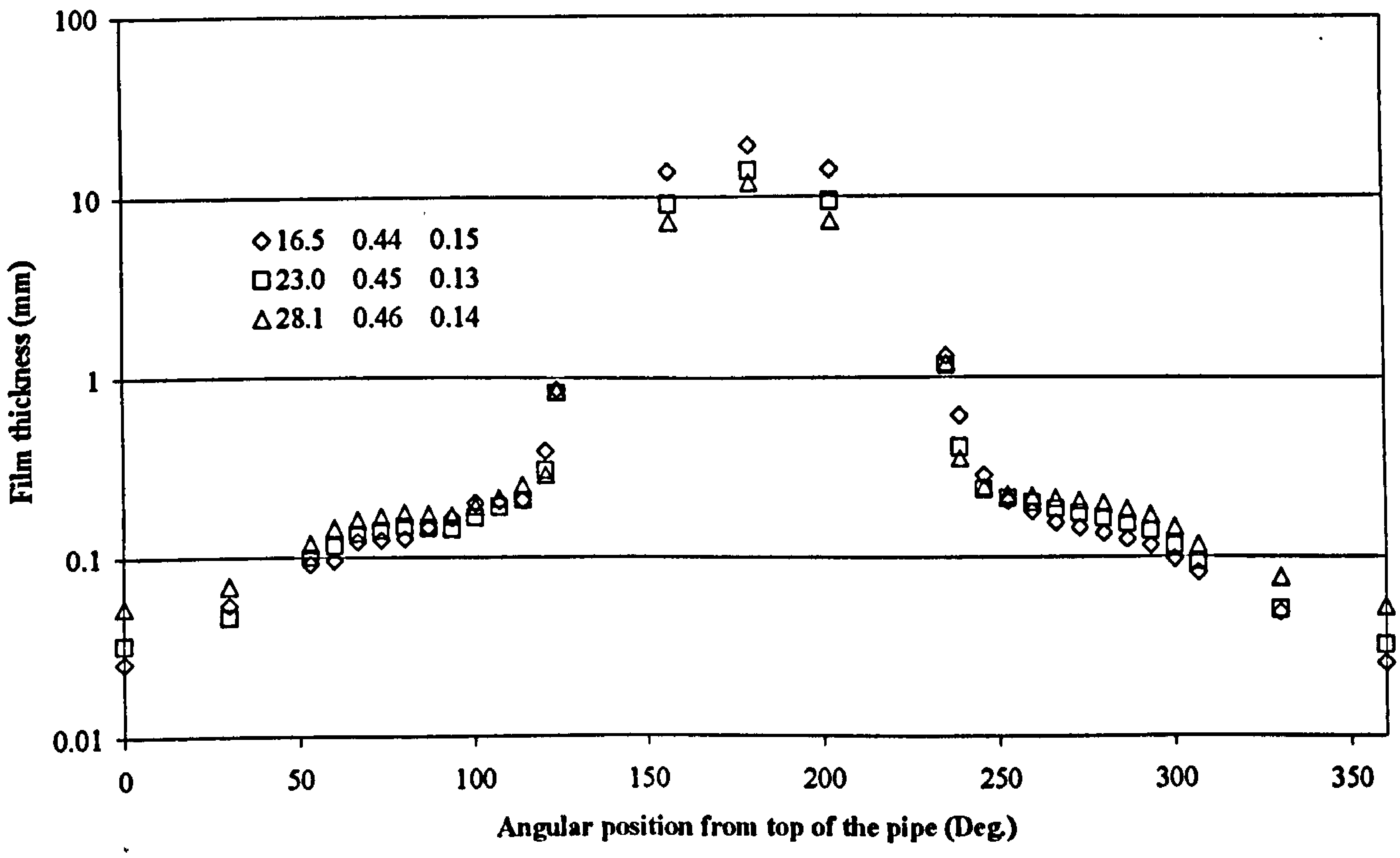

Figure III.2.19: *Film thickness distribution around pipe circumference for a constant liquid superficial velocity of 0.136 m/s, at the inlet to the T-junction. Logarithmic plot, showing the inversion of thickness trend from the bottom (centre of plot) to the top of pipe.*

From Figure III.2.21, no general trend can be argued for cases a), c) and e) for a constant gas inlet. In this case, for the lowest liquid flow rates, the top of the pipe in the side arm is seen to become dry, as visible at the two extremes of the plot. However, for the measurements at the bottom (central part of the rectified plot) it must be borne in mind that the film thickness is of the order of a millimetre on the wire probes, which are calibrated with a degree of confidence of the same order.

The trend in the run arm can be again visualised on a circumferential plot. In Figure III.2.22, for runs d), e) and f) at constant liquid velocity the trend of the inlet is repeated. On the left side of the plot, in correspondence of the downstream corner of the T in the run, the film can be seen to be asymmetrical due to climbing on the pipe circumference.

Finally, in Figure III.2.23, for the case of constant gas inlet of cases a), b) and d) the climbing effect is only slightly visible if at all and the profile appears quite symmetric. This might be due to the small gas flow rate involved and the subsequent

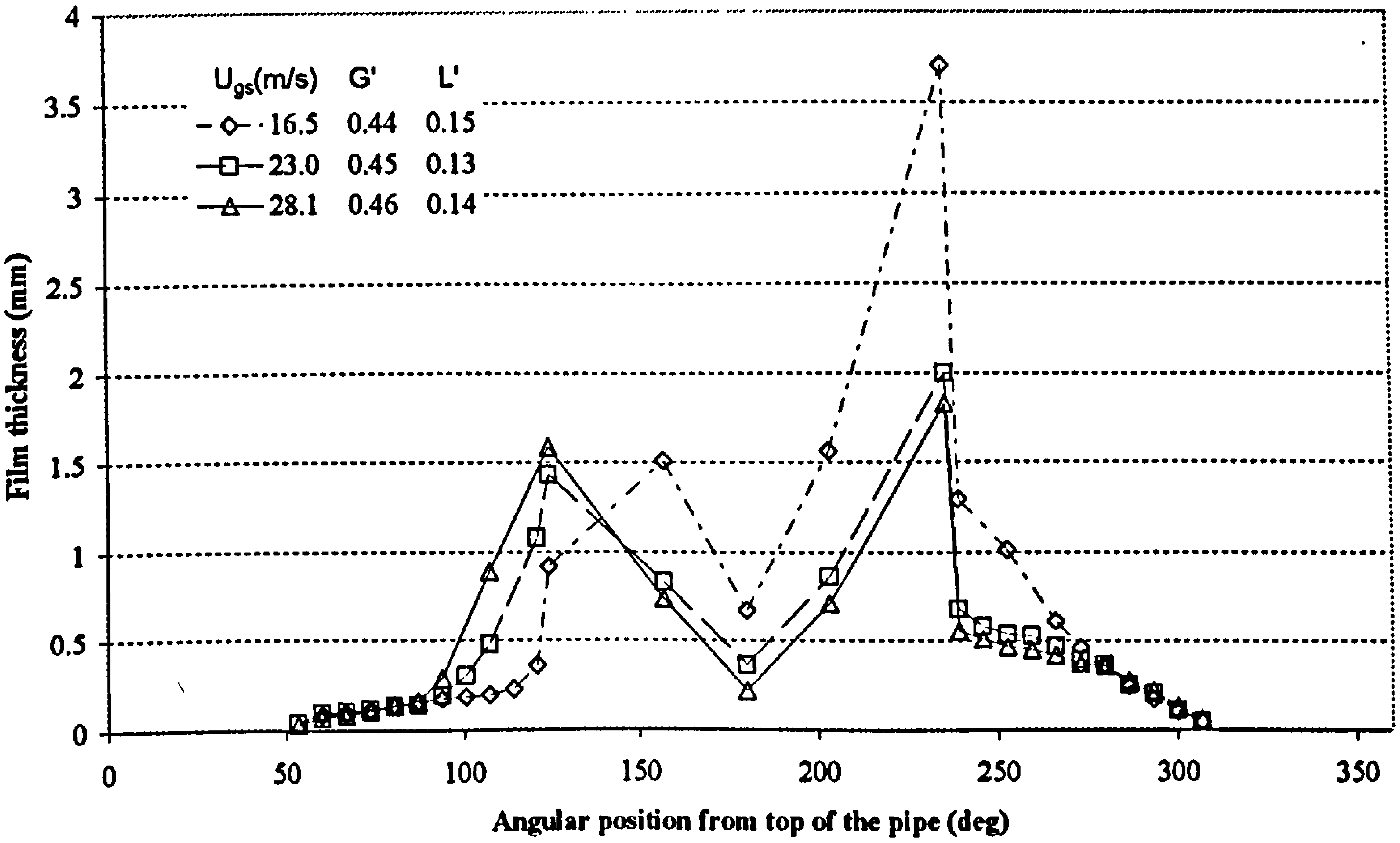

Figure III.2.20: *Film thickness distribution around pipe circumference for a constant liquid superficial velocity of 0.136 m/s, at the side arm outlet of the junction.*

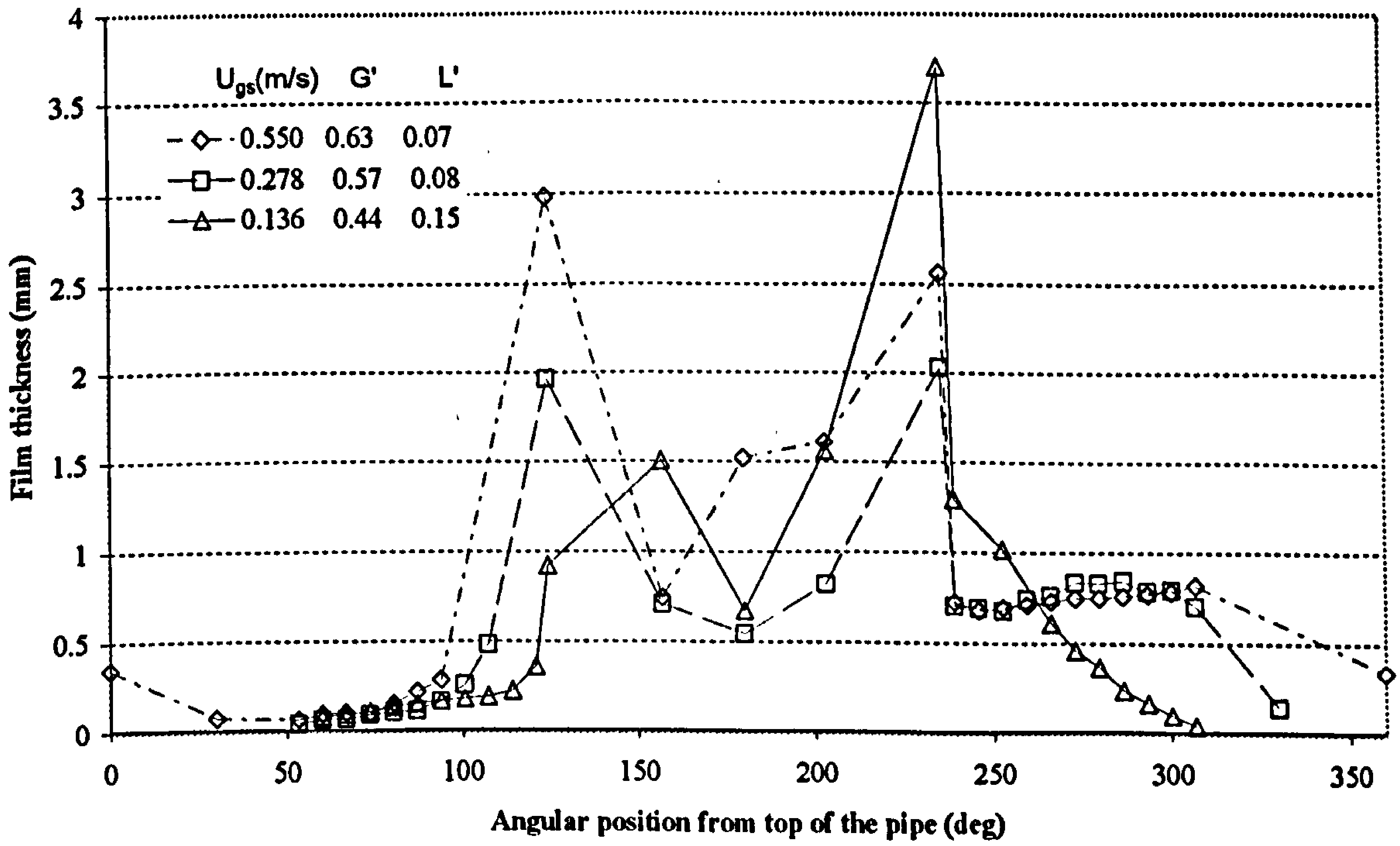

Figure III.2.21: *Film thickness distribution around pipe circumference for a constant gas superficial velocity of 16.5 m/s, at the side arm outlet of the junction.*

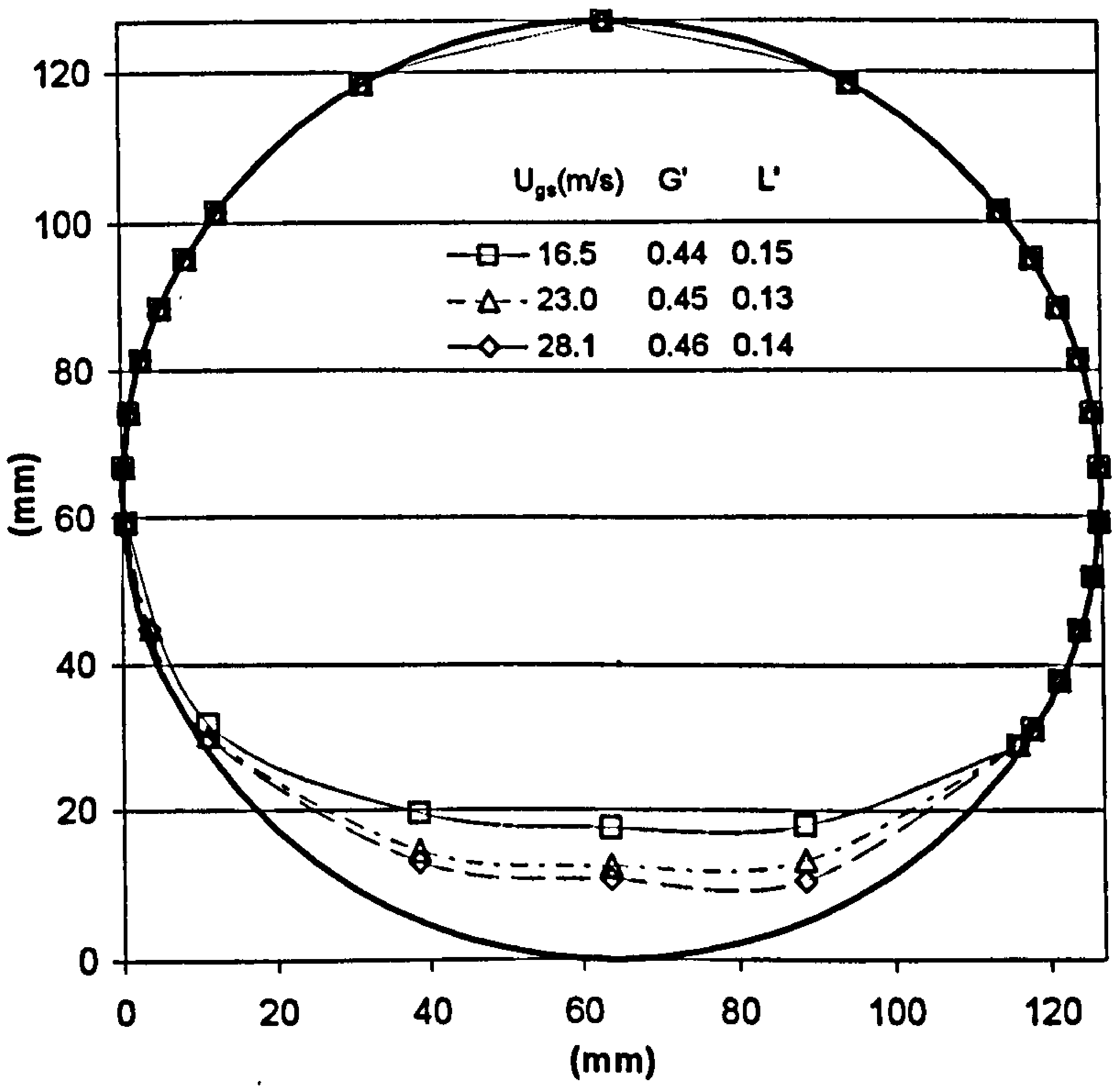

Figure III.2.22: *Film thickness distribution around pipe circumference for a constant liquid superficial velocity of 0.136 m/s, at the run arm outlet of the junction.*

modest magnitude of recirculations in the run. A rectified plot in linear scale better shows the asymmetry, Figure III.2.24.

With regard to the effect of split ratio on film distribution, the trends are within the features discussed for case c) (U_{gs}=24.5 m/s and U_{ls}=0.278 m/s), at the beginning of this section.

Another interesting comparison can be made if the profile close to the feed is compared to the film distribution at the inlet to the T-junction. This can give a feeling of the degree of redistribution towards the fully developed condition. Because the phases are mixed by introducing the liquid as a film through a porous sinter wall and the gas in the axial direction, it is expected that the profile at the feed would be more symmetric. The general trend can be appreciated by plotting the liquid film distribution for case b) (U_{gs}=16.5 m/s and U_{ls}=0.278 m/s) as it was measured 0.9 m downstream of the mixing section and 0.125 m upstream of the centre of the T, Figure III.2.25. The distance between the two measurement locations is about 3 m (23D).

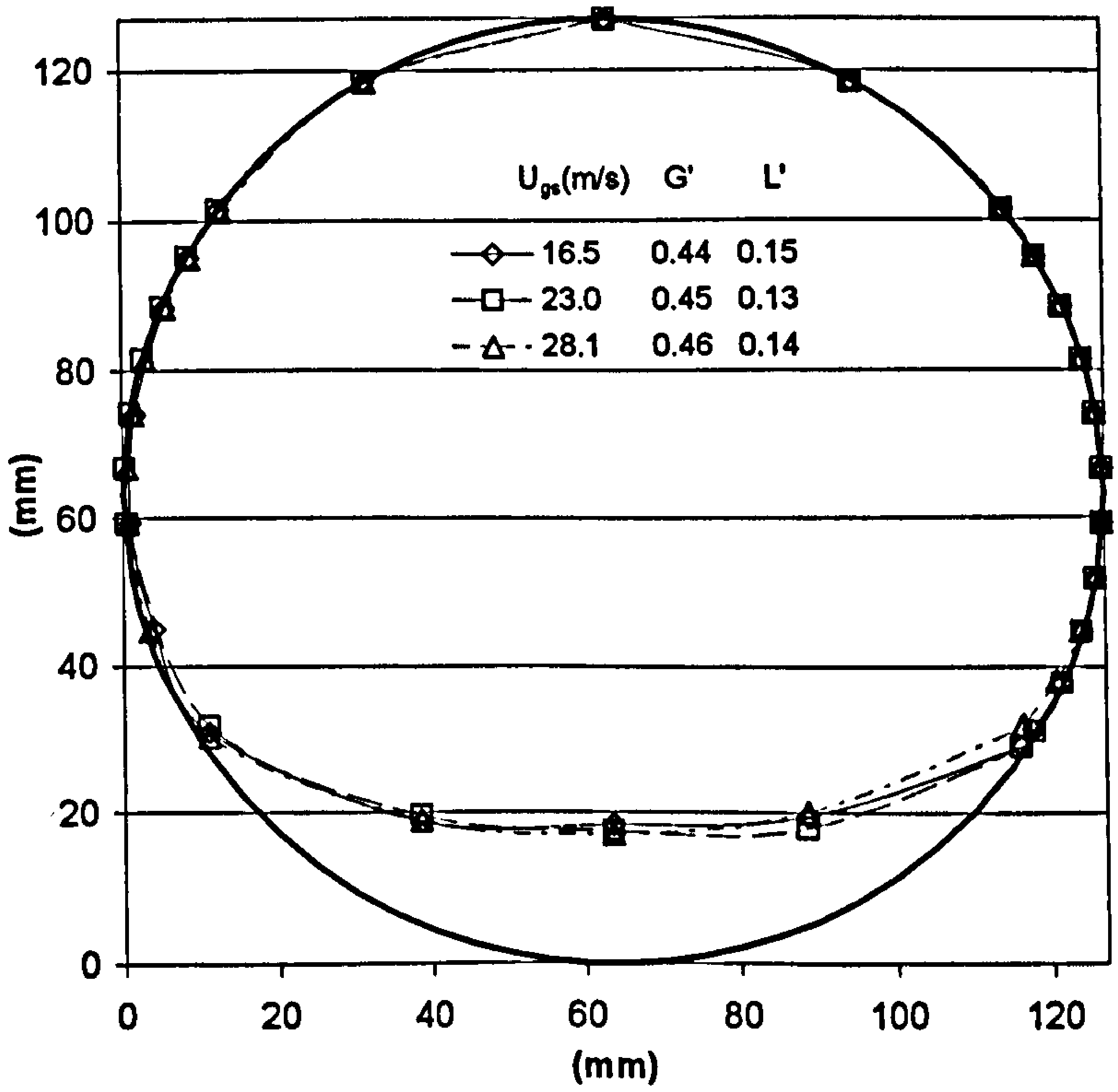

Figure III.2.23: *Film thickness distribution around pipe circumference for a constant gas superficial velocity of 16.5 m/s, at the run arm outlet of the junction.*

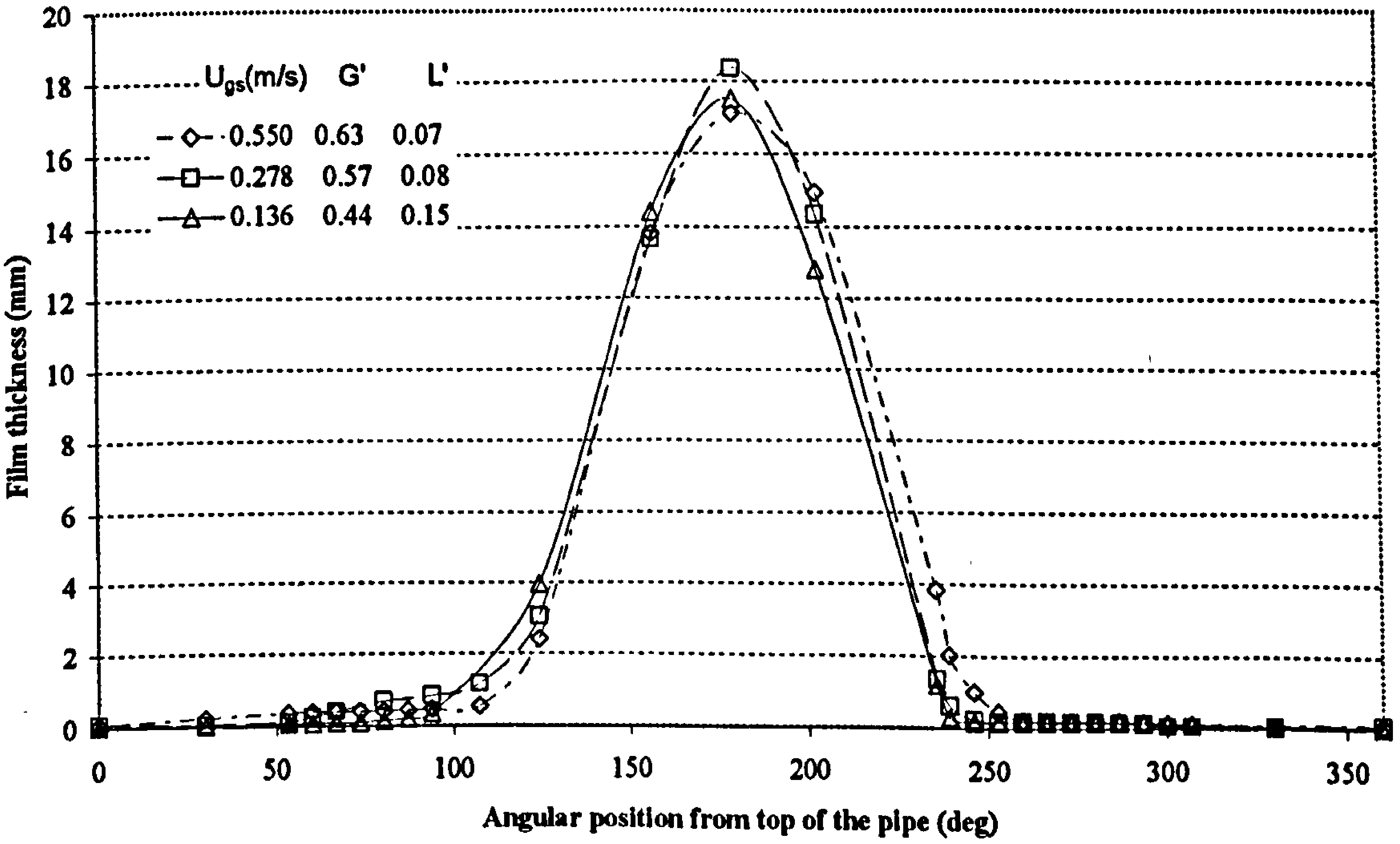

Figure III.2.24: *Film thickness distribution on a rectified plot for a constant gas superficial velocity of 16.5 m/s, at the run arm outlet of the junction. Linear scale.*

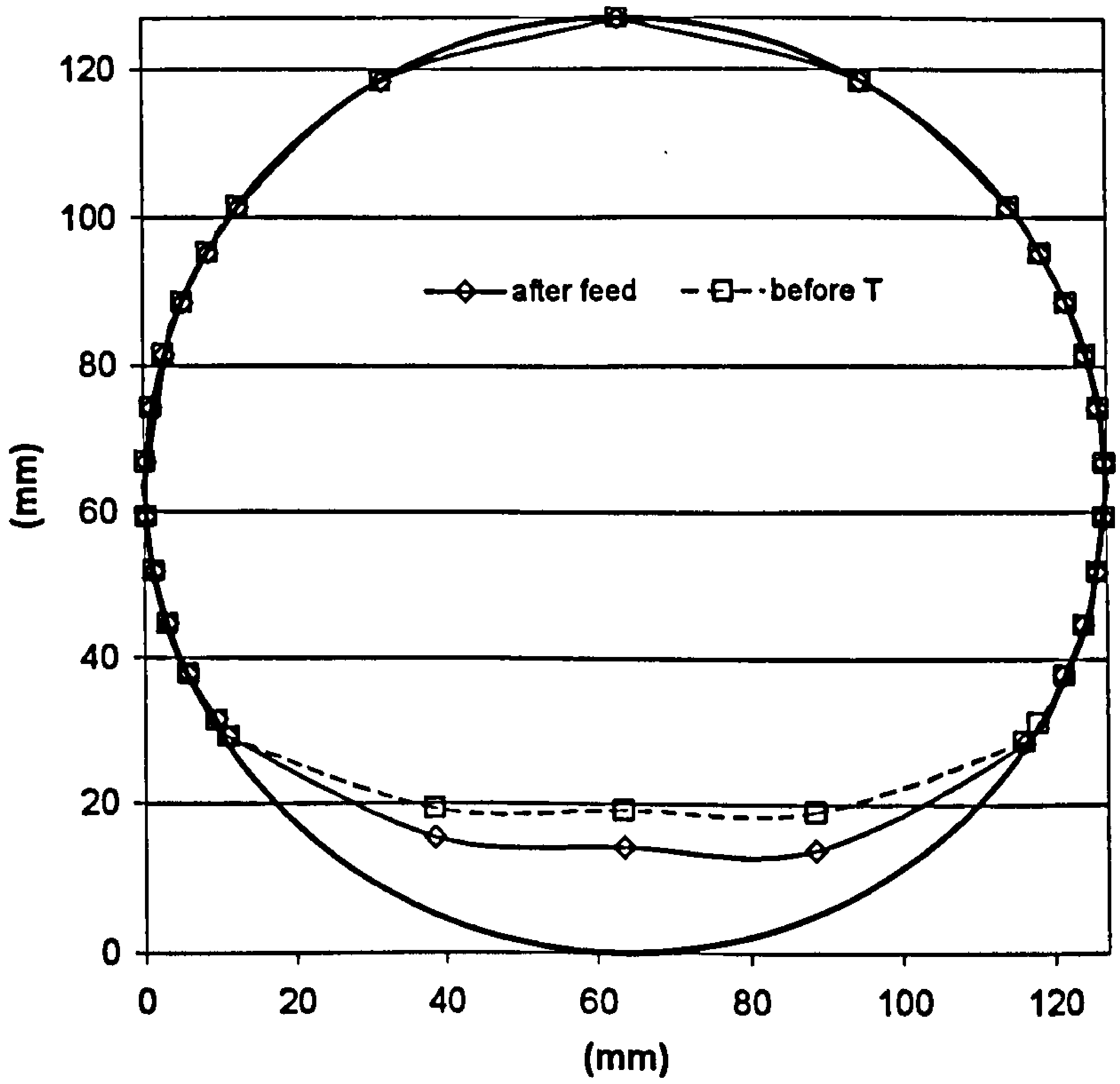

Figure III.2.25: *Film thickness distribution about pipe circumference showing the development of film profile from a section close to the feed to a section before the T junction. Case b), U_{gs}=16.5 m/s, U_{ls}=0.278 m/s.*

Exceptions to this trend can be found for cases a) and c). For both cases, the trend at the top of the pipe is unchanged, with a thicker film close to the feed as it would be appreciated from a rectified, logarithmic plot. However, case a) shows a marked peak at the bottom of the pipe for the measurement at the feed (Figure III.2.27) whilst case c) does not show significant variation of the film distribution at the bottom between feed and inlet to the T (Figure III.2.28).

For case a), the observed peak might be explained by considering that in this case, the largest liquid inlet is fed to the rig and the influence of inlet effect is strongest. There is no apparent explanation for the anomaly of case c).

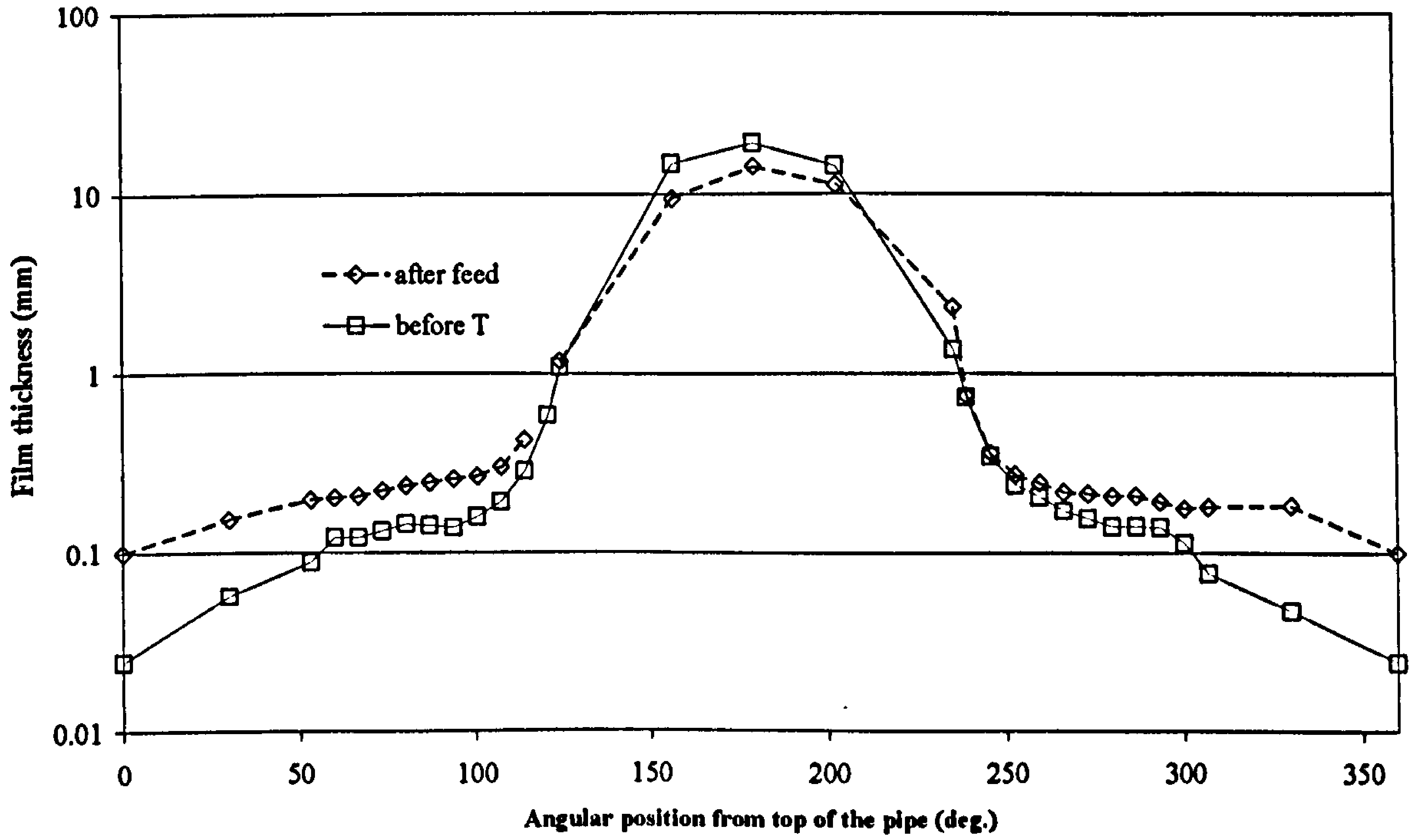

Figure III.2.26: *Film thickness distribution on a rectified plot showing the development of film profile from a section close to the feed to a section before the T junction. Case b), U_{gs}=16.5 m/s, U_{ls}=0.278 m/s. The ordinate scale is logarithmic.*

To conclude this section, we present a comparison of film thickness data with the results obtained by Williams (1990). This was the only case of film thickness data obtained for a pipe diameter comparable with the one used in this work. Run 16 at the lower gas boundary of Williams' work is obtained in a 0.095 m ID pipe at a distance of 260D from the mixing section for U_{gs} = 31.7 m/s and U_{ls} = 0.123 m/s. This can be compared with case f) of the present work (U_{gs} = 28.1 m/s, U_{ls} = 0.136 m/s).

Figure III.2.29 shows the two data sets in logarithmic scale for the semi-circumference with the film thickness normalised against the pipe diameter. Results match fairly well, although the data from Williams is lower than those presently obtained. This can be imputed partly to the difference in inlet conditions particularly in gas flow rate and scale effects. Furthermore, the data from Williams are taken at a distance from the feed of 260 D against the 23 D of the present work. This could be evidence for non-fully developed entrainment and deposition rates at such a small distance from the feed.

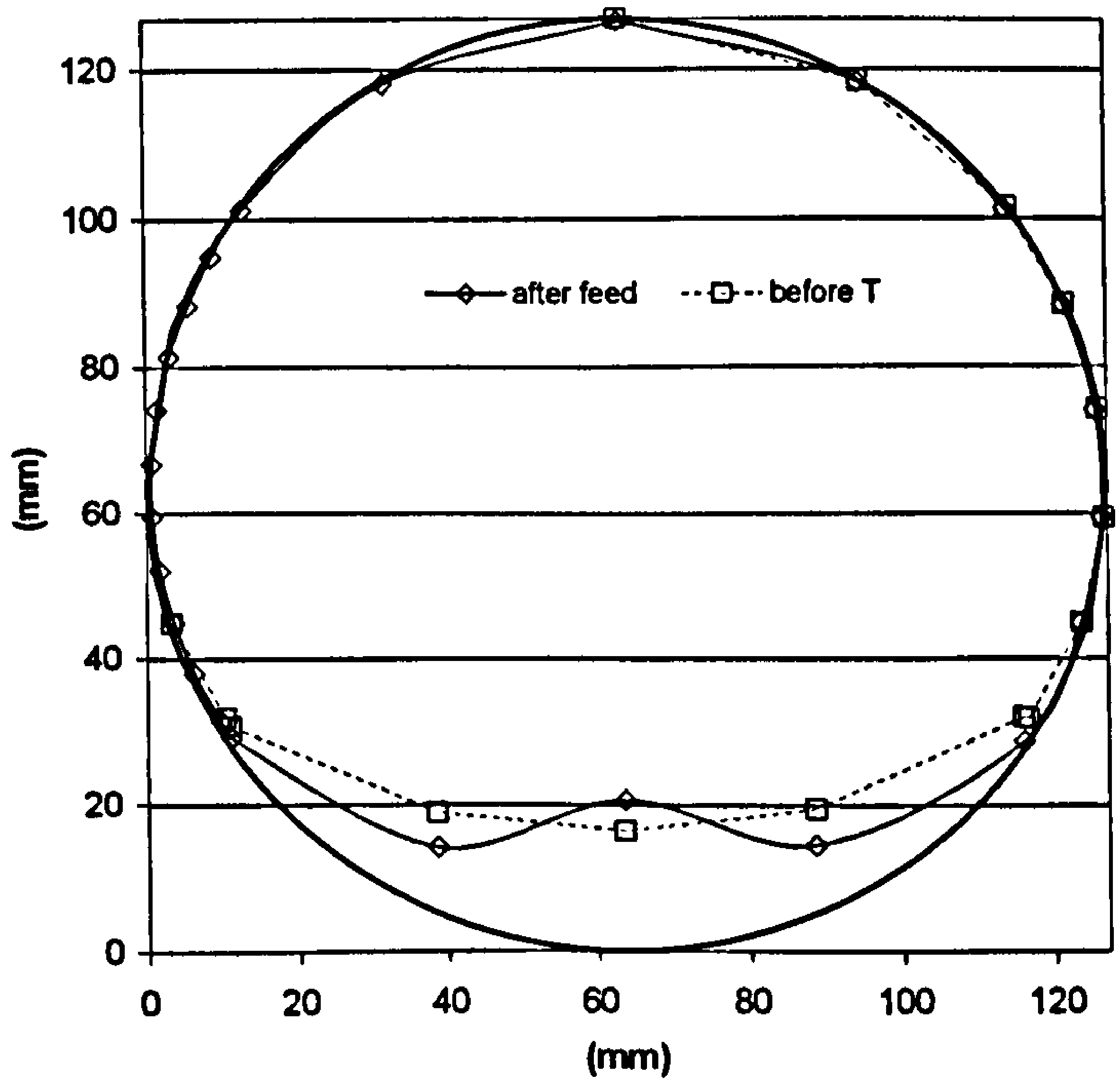

Figure III.2.27: *Film thickness distribution about pipe circumference showing the development of film profile from a section close to the feed to a section before the T junction. Case a), U_{gs}=16.5 m/s, U_{ls}=0.550 m/s. Unusual peak at the pipe bottom.*

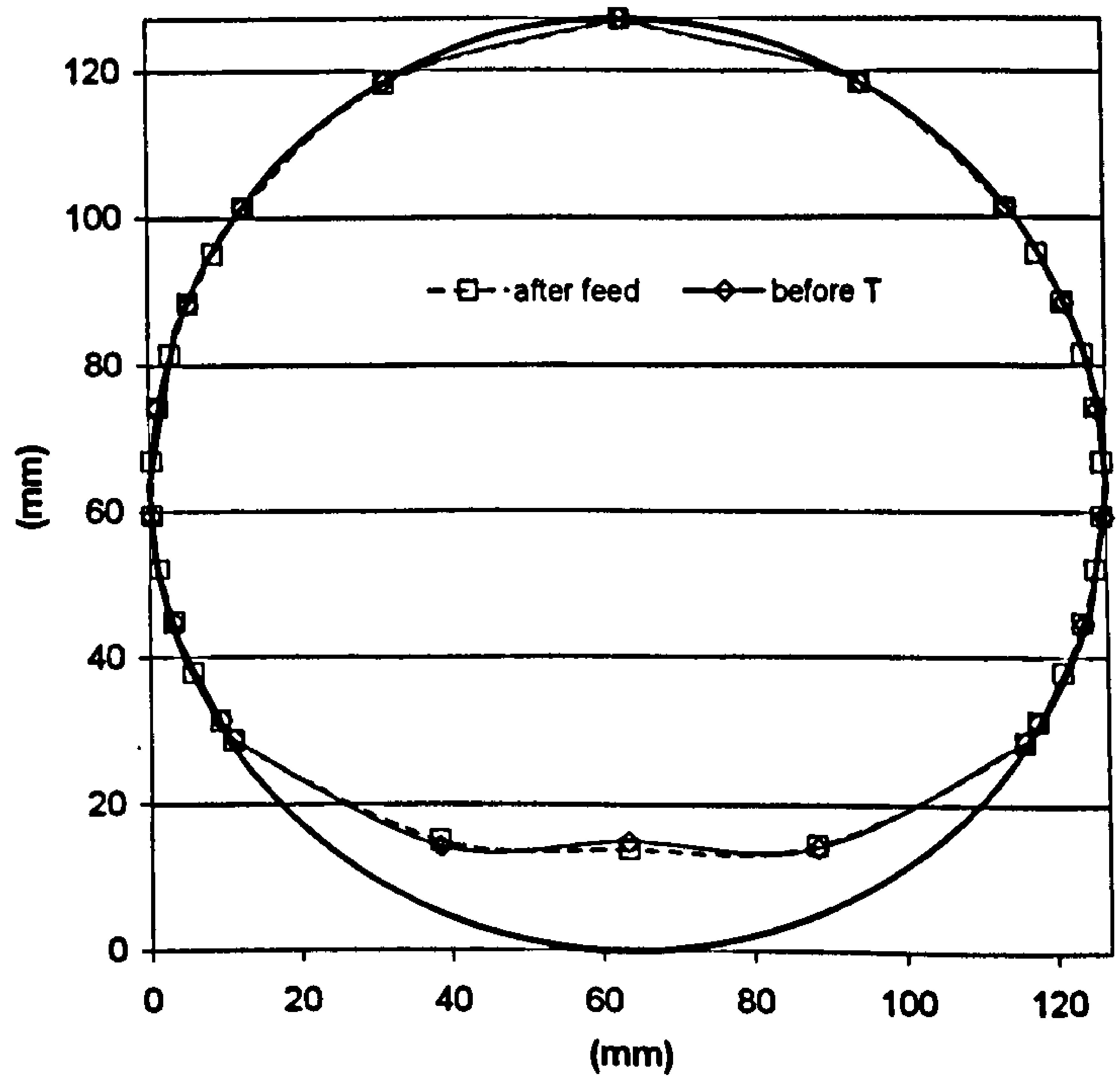

Figure III.2.28: *Film thickness distribution about pipe circumference showing the development of film profile from a section close to the feed to a section before the T junction. Case c), U_{gs}=24.5 m/s, U_{ls}=0.278 m/s. No significant variation at the bottom.*

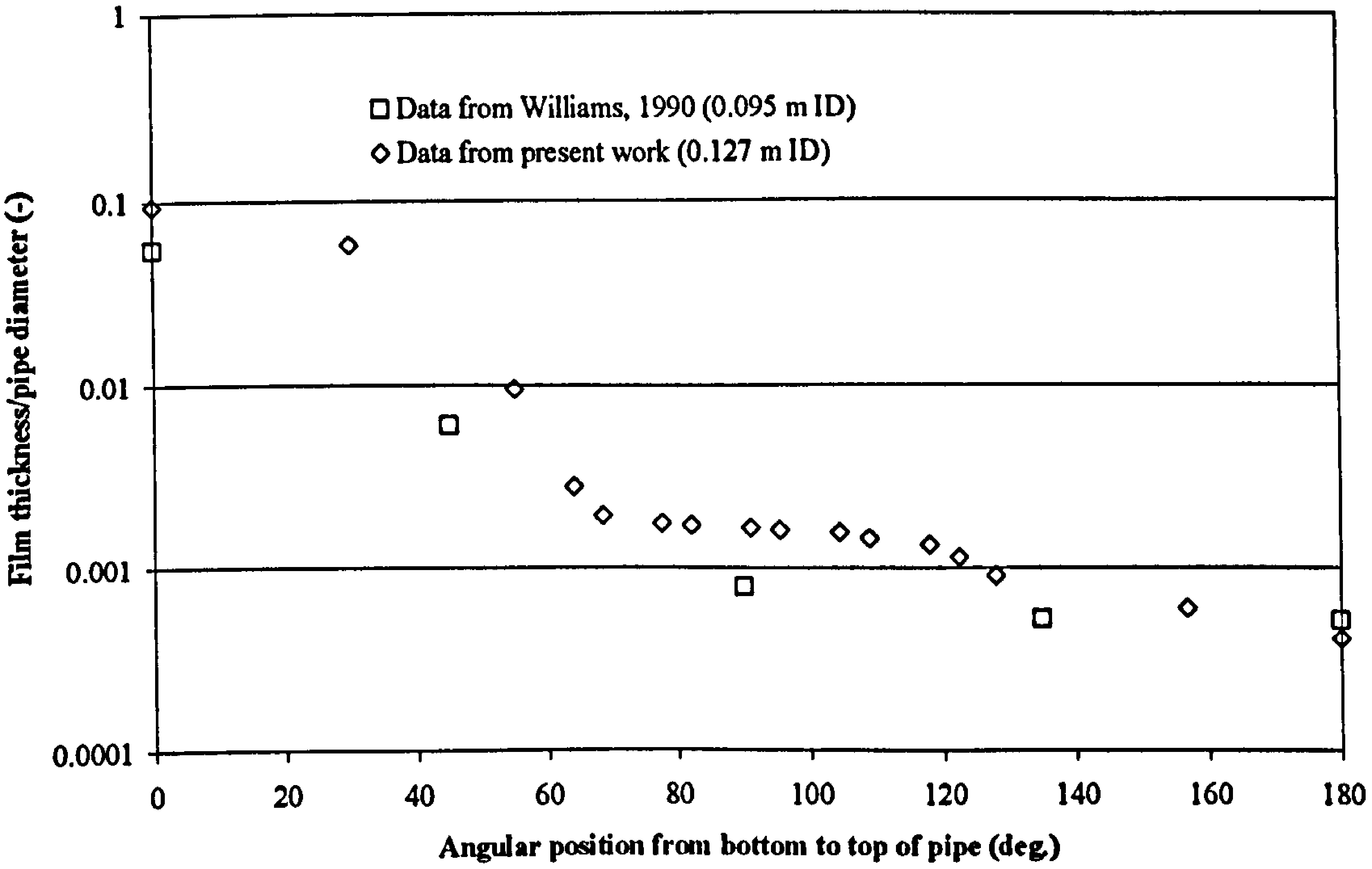

Figure III.2.29: *Film thickness distribution on a rectified plot showing comparison of case F (U_{gs}=28.1 m/s, U_{ls}=0.136 m/s, 0.127 m ID) against run 16 of the work of Williams, 1990 (U_{gs}=31.7 m/s, U_{ls}=0.123 m/s, 0.095 m ID). Ordinate axis is in logarithmic scale.*

III.2.9 Film thickness results within the T-junction.

In this section, the results obtained using the test section described in section III.2.6 will be presented. Because of the large number of wire probes, it was very difficult to fit flush mounted pin probes and allowance was made only for measurements at the bottom of the test section, where the film is thicker and the wire probes technique is employed. As in the previous set of experiments, measurements were taken for the six inlet conditions of Table 1, each for three splits.

Again, the most representative cases are presented. The full database can be found in appendix A. A map of the probes in the T-block is sketched in Figure III.2.30 showing the complexity of the database. Probes will be occasionally referred to on the basis of this convention.

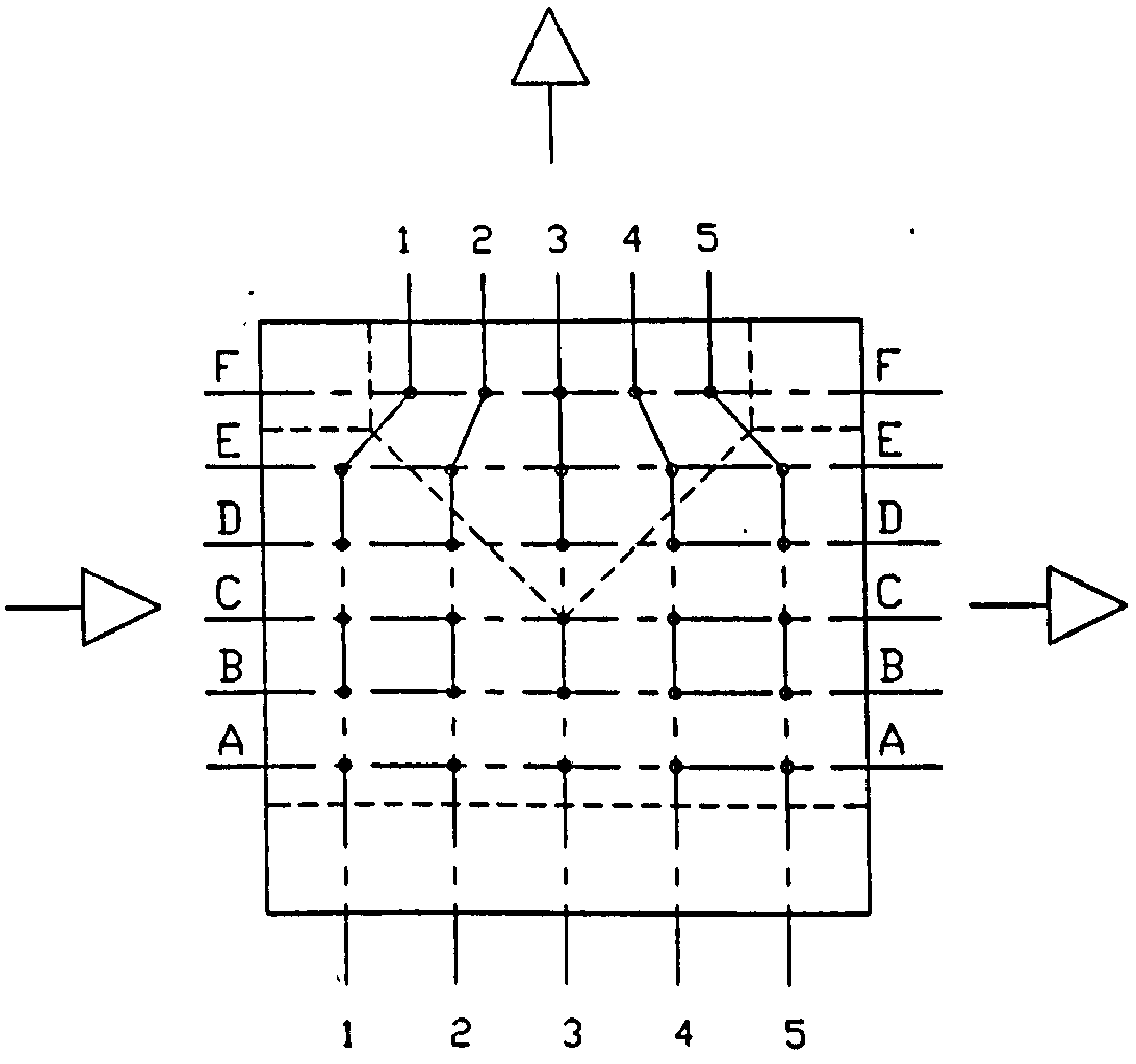

Figure III.2.30: *Top view of the T-block fitted with wire probes showing the location of probes. The distance between two consecutive rows of letters (A-F) is of 25 mm. The distance between two columns of numbers (1-5) is 36.75 mm except for the probes on row F which are spaced at 25 mm. The dotted lines show the contours of the T. Arrows indicate the direction of flow.*

Figure III.2.31 shows typical result from case c) (U_{gs}=24.5 m/s, U_{ls}=0.278 m/s, (G', L')=(0.54, 0.11)). The plot is a view of film distribution from the inlet to the T-junction. The five lines along which film thickness has been measured have been progressively named according to Figure III.2.30. Since the points F1, F2, F4 and F5 are not in line with the other points having the same second index they have not been represented in this Figure. Comparing inlet (row 1) against outlet (row 5) results and rows 2 and 4, it is possible to appreciate the effect of film climbing up the downstream corner again. A representation that allows a full view of the row F in the side arm is the one in Figure III.2.32, referring to run b) (U_{gs}=16.5 m/s, U_{ls}=0.278 m/s, (G', L')=(0.57, 0.08)). This is a view from the main pipe vertical axial plane, in direction of the side arm. The flow is from left to right and, for a clear representation, only rows C, D, E and F are plotted, for steps of 25 mm in the direction of the side arm.

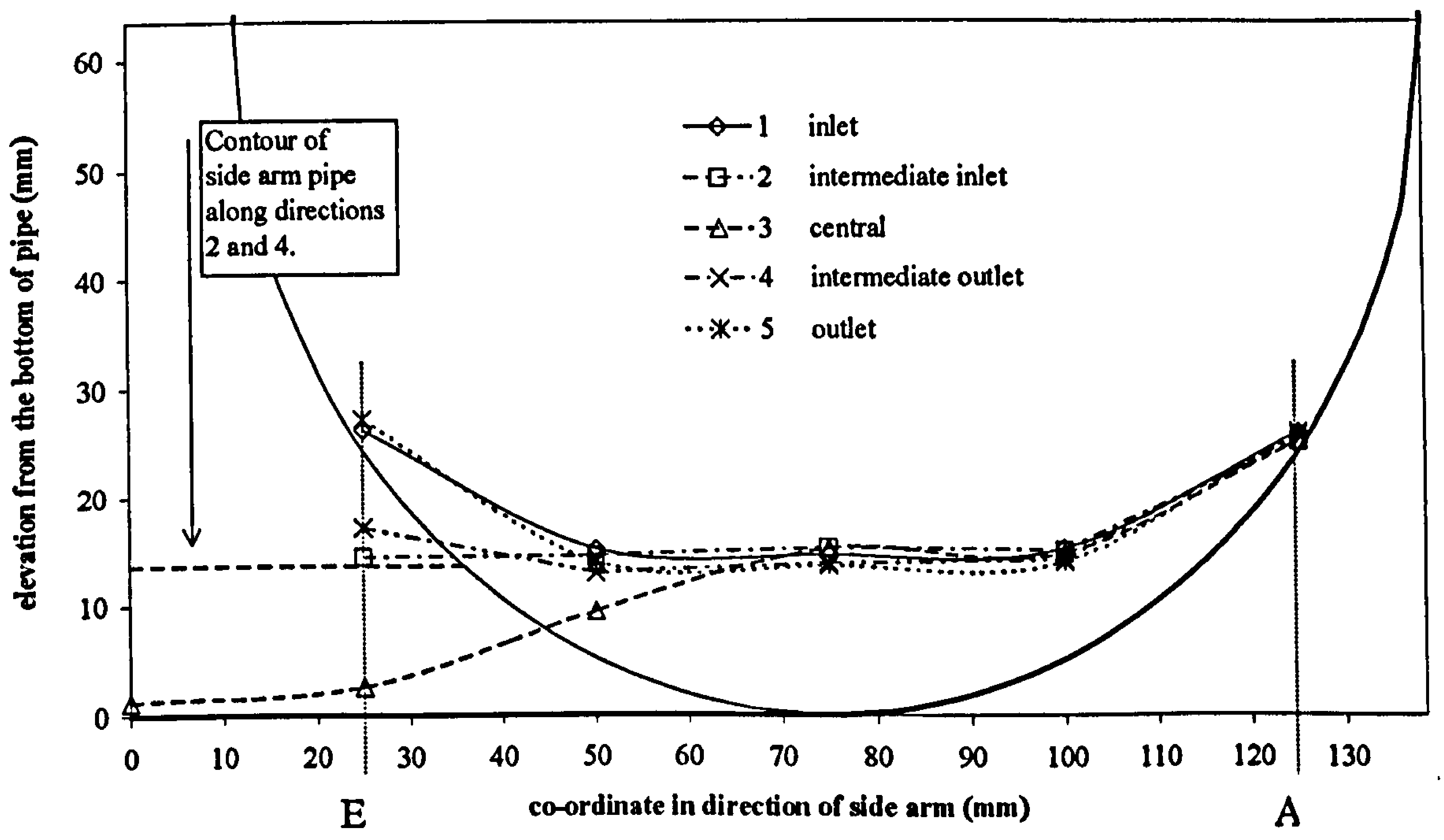

Figure III.2.31: *Film distribution results at the bottom from run c) (U_{gs}=24.5 m/s, U_{ls}=0.278 m/s). View from inlet section. Side arm on the left side of the plot, towards the origin. (G', L')=(0.54, 0.11).*

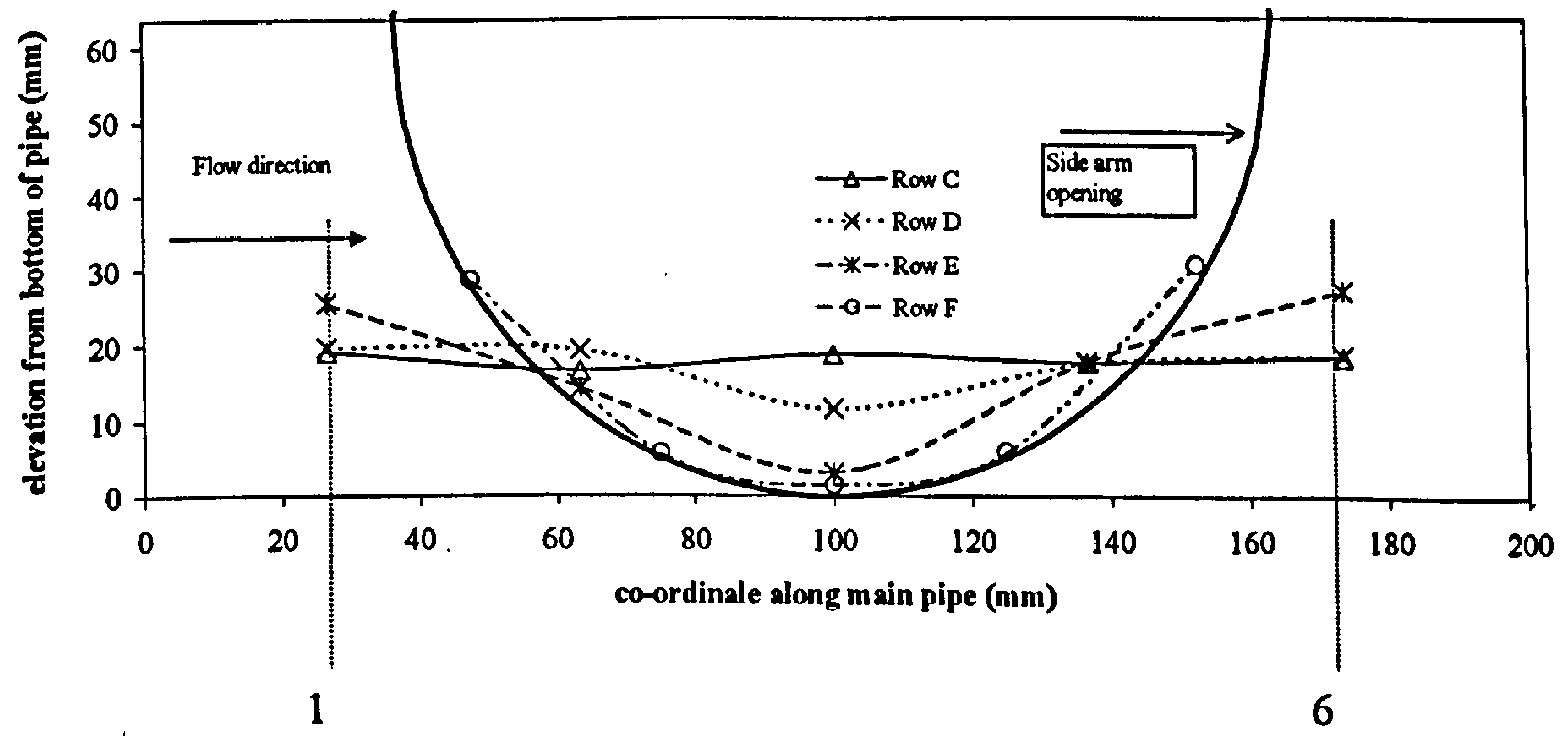

Figure III.2.32: *Film distribution results at the bottom from run b) (U_{gs}=16.5 m/s, U_{ls}=0.278 m/s). View from mean pipe axial vertical plane. (G', L')=(0.57, 0.08).*

From this representation, in all the database, it can be observed that the film thickness does not change significantly up to row C, going through the junction. For row C, slight variations corresponding to the centre of the T can cause either a peak or a trough. The liquid slowing down to turn in the side arm causes a thicker film. On the other hand, the film tends to become thinner because of its removal through the side arm. Row D remains unchanged up to few centimetres past the upstream corner and then bows down because of the physical absence of the main pipe wall. The liquid level increases again towards the run arm, usually to a slightly lower height. Similar behaviour is observed for row E. However, because of the film climbing on the downstream corner of the T, the liquid level after the junction is higher than upstream of it (points E2 and E4). Finally, row F presents the features discussed in the results from the 'harp' test section.

To appreciate the effect of different split conditions, it can be significant to plot for low, medium and high gas take off, the film contour along the side arm, Figure III.2.33 (row 3) and main direction, Figure III.2.34 (row C). Those Figures refer again to the inlet conditions of case c) and are fairly representative of all the database. The contour of the pipe has not been represented to allow the use of the different scale of abscissa and ordinate to magnify the small differences observed. In most cases, point C3 shows a relative maximum, in the plot along the side arm direction (Figure III.2.33). This is in fact the effect of the film slowing down in proximity of a dividing streamline for the liquid. Something similar can be often observed in a plot along the main direction (Figure III.2.34). Again, no clear trend can be seen from the results in dependence of phases split, probably due to the narrow range of take off examined.

In the specific case, from Figures III.2.33-34, no significant change or neat trend in film distribution is observed in the narrow range of diverted liquid fraction (0.08-0.15) where conductance measurements were performed. This restriction on the investigated range of diverted liquid fraction is due to the limited head provided by the centrifugal blower used to feed air to the system as already mentioned. This was not a problem for case d), e) and f), where it was possible to keep the inlet gas flow rate at a distance from the set-point (28.1 m/s) within the error allowed for the mass balance. This is possible because of the small liquid inlet. Within this section of the database, the most interesting trends were shown at the larger gas flow rates of runs e) (23 m/s) and f) (28.1 m/s).

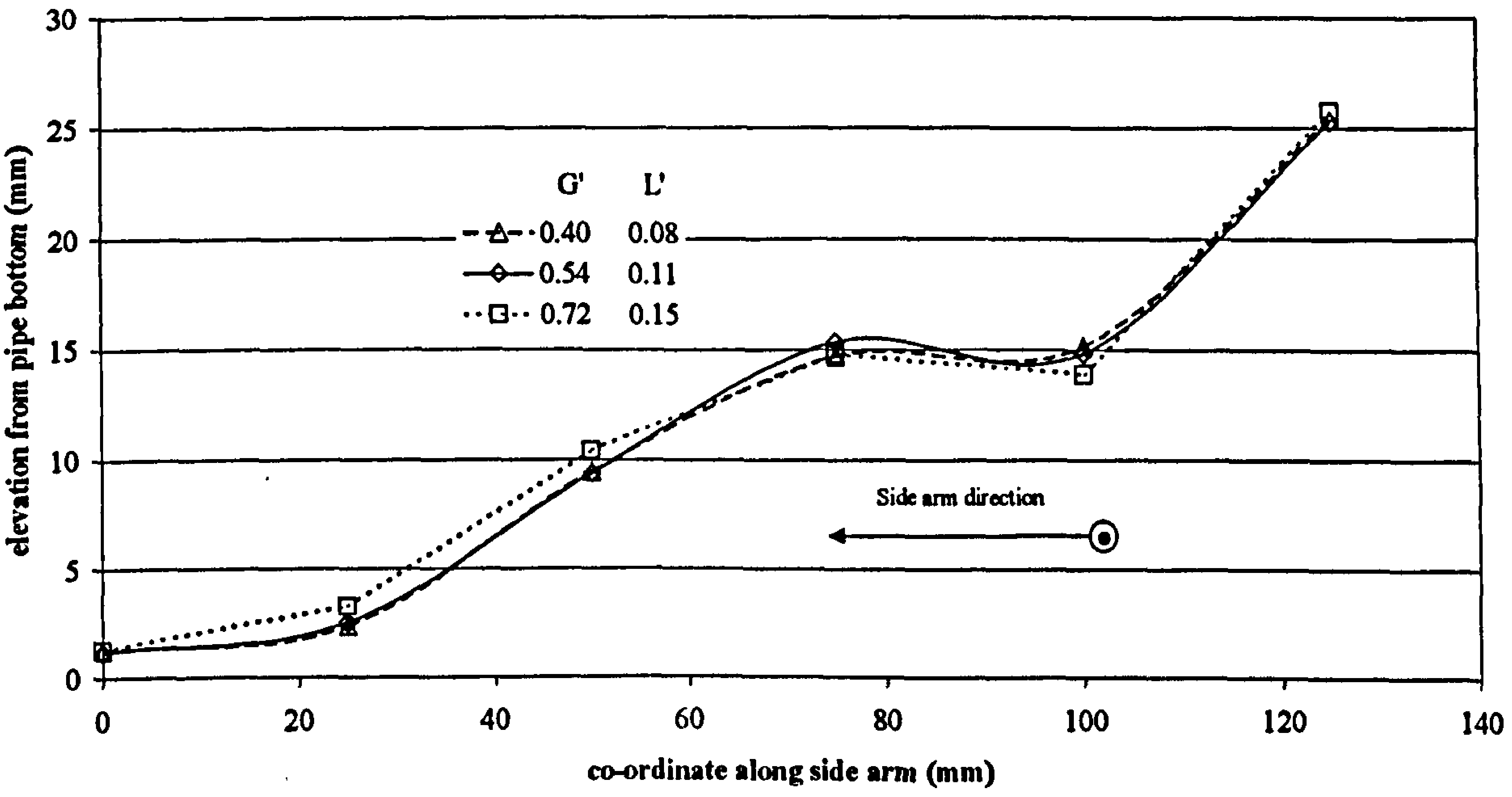

Figure III.2.33: *Film distribution along row 3, towards side arm, for the three split from run c) (U_{gs}=24.5 m/s, U_{ls}=0.278 m/s). The flow is entering the plane of the plot.*

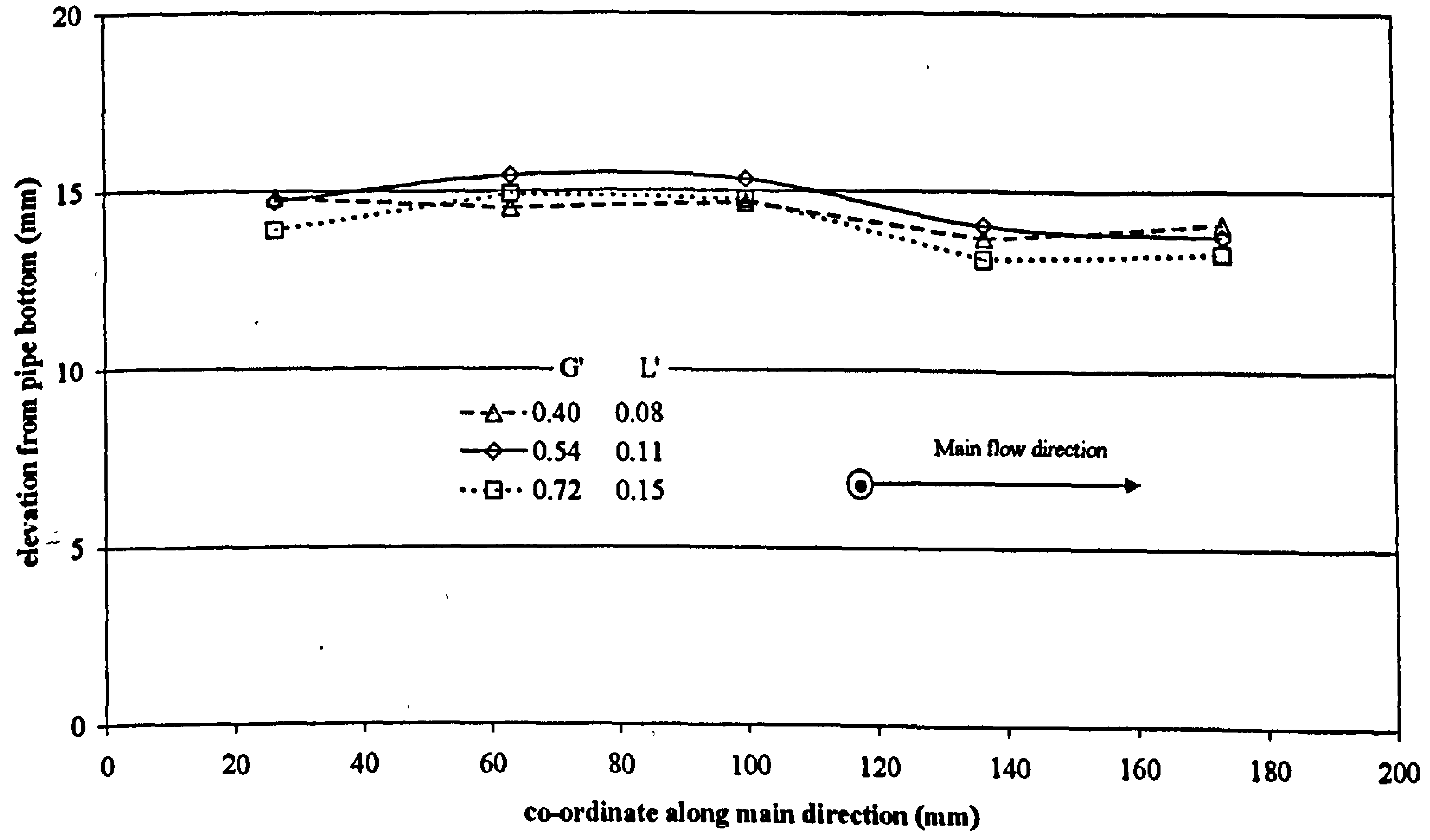

Figure III.2.34: *Film distribution along row C towards run outlet for the three split from case c) (U_{gs}=28.1 m/s, U_{ls}=0.136 m/s). The flow is entering the plane of the plot, towards the side arm. Main flow is from left to right.*

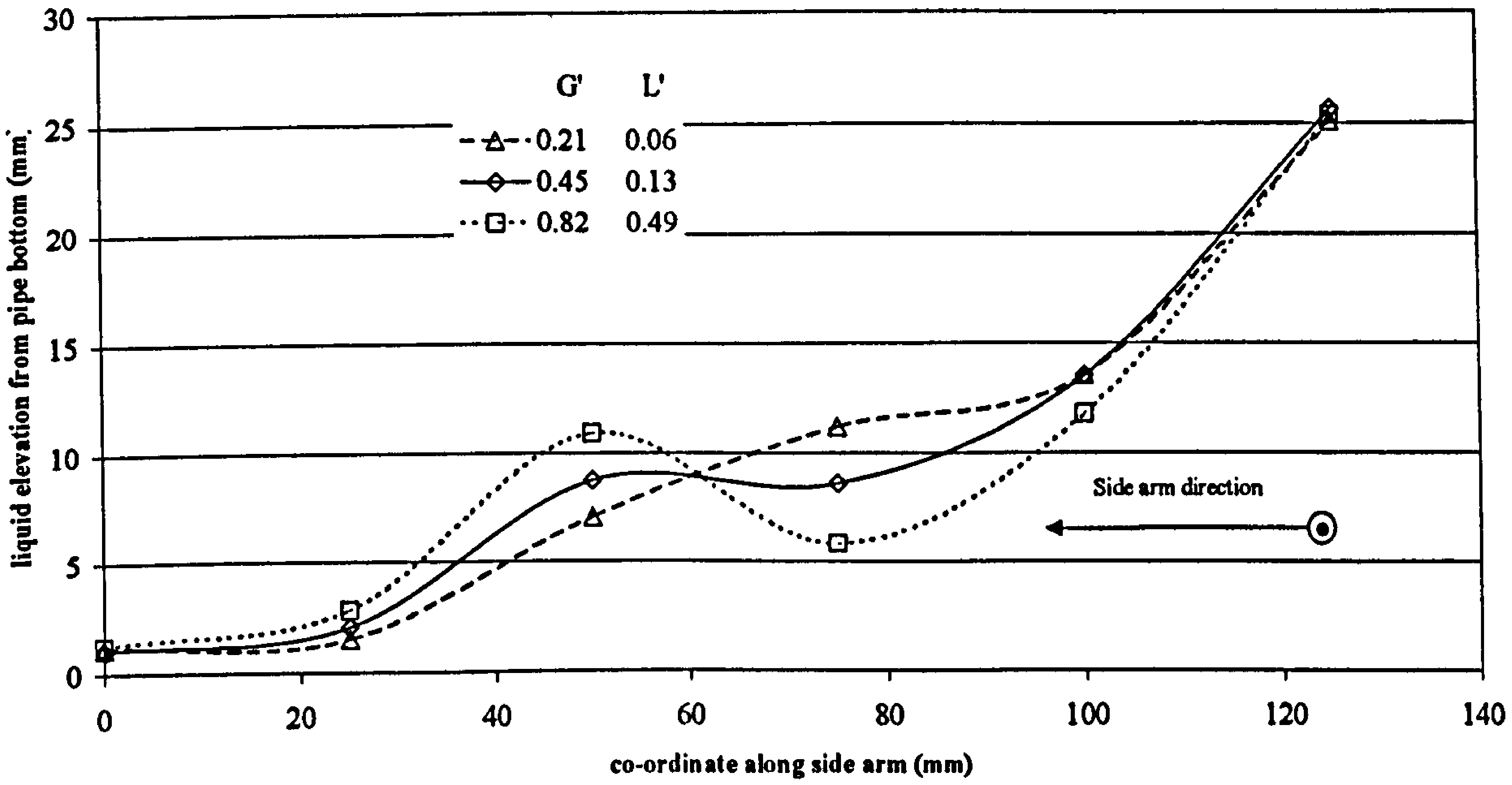

Figure III.2.35: *Film distribution along row 3, towards side arm, for the three splits from run f) (U_{gs}=28.1 m/s, U_{ls}=0.136 m/s). The flow is entering the plane of the plot.*

The most interesting behaviour is displayed by case f) where the fraction L', of liquid intake was varied between 0.06 and 0.49 (Figures III.2.35-36).

From the view of row 3 in Figure III.2.35, one can clearly see the film contour becoming less smooth as the fraction of diverted phases is increased to the extent that for the largest off-take, a relative maximum and minimum are shown. If one reasons in terms of a dividing streamline for the liquid, than the change of shape of the liquid contour could be explained by the fact that such dividing streamline would be moving from left to right as the split ratio is increased, affecting the liquid profile to a larger extent. Visually, the area below the three curves for the three splits seems unchanged but a larger proportion is contained on the left of the intersection of these three curves as the diverted fraction is increased. It is however interesting that from a simple smooth interpolation of data, the three curves intersect at the same point.

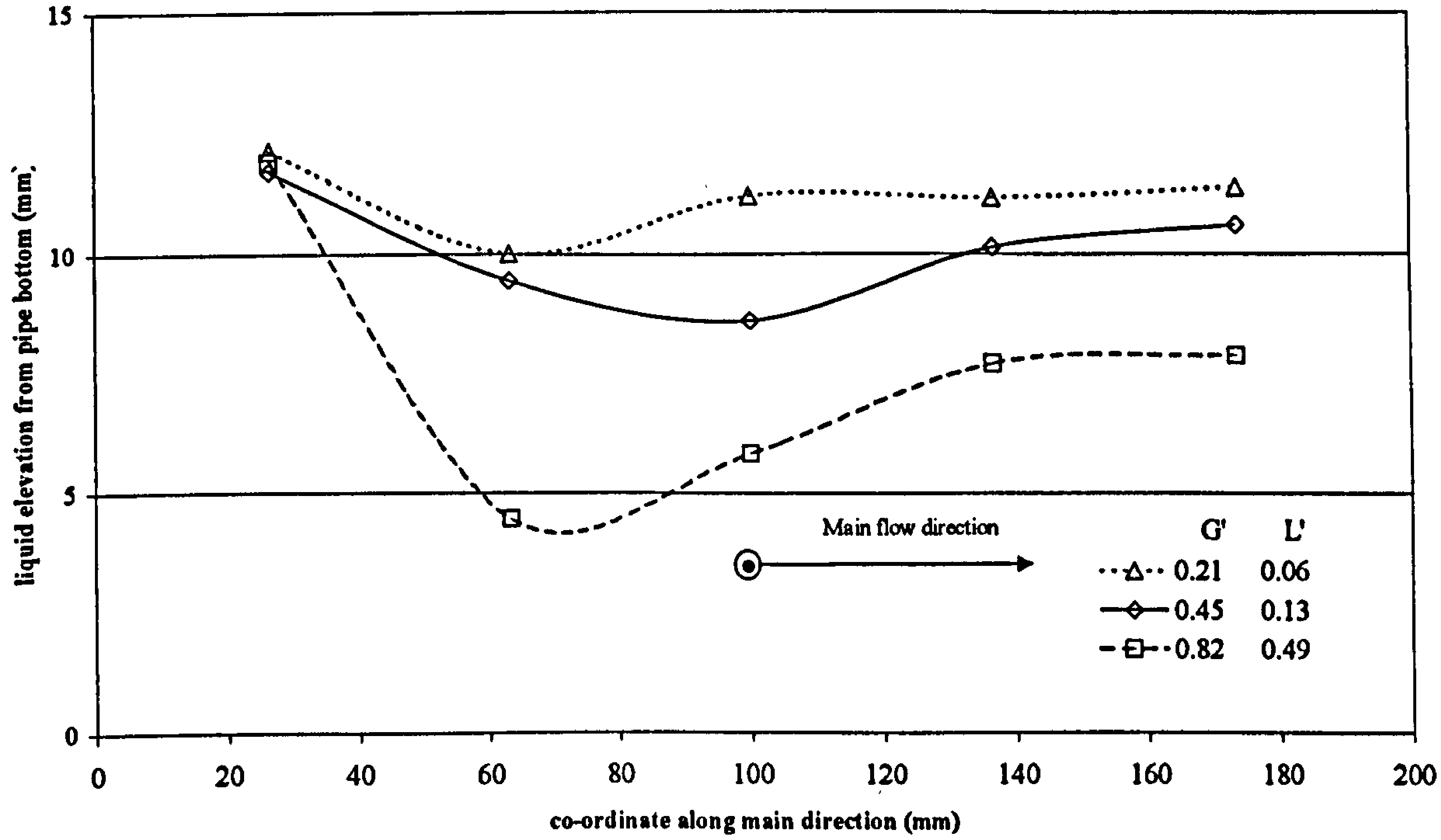

Figure III.2.36: *Film distribution along row C towards run outlet for the three split from case f) (U_{gs}=28.1 m/s, U_{ls}=0.136 m/s). The flow is entering the plane of the plot, towards the side arm. Main flow is from left to right.*

The view of row C, along the main direction shows again some interesting features. The film contour is strongly influenced towards the inlet to the junction and either probe C2 or C3 shows a marked minimum, before or level with the centre of the junction.

Case e), for the same liquid inlet of 0.136 m/s and a smaller gas inlet (23 m/s), shows less markedly the same features as case f) as far as the view along the side arm is concerned (Figure III.2.37). However, the range of split ratio investigated is narrower than that of case f). If the gas inlet is further decreased to 16.5 m/s (case d)), even for a larger range of split ratio, the features of the film contour along the side arm of the two cases previously illustrated are not observed (Figure III.2.38).

Regarding the film profile along the main direction, this is very similar for cases d) and e) in Figures III.2.39 and III.2.40 respectively. For these lower gas flow rate cases, point C3 shows a slight maximum. The liquid level decreases again towards the outlet to a lower value than that at the inlet section to the T (point C5 is lower than C1).

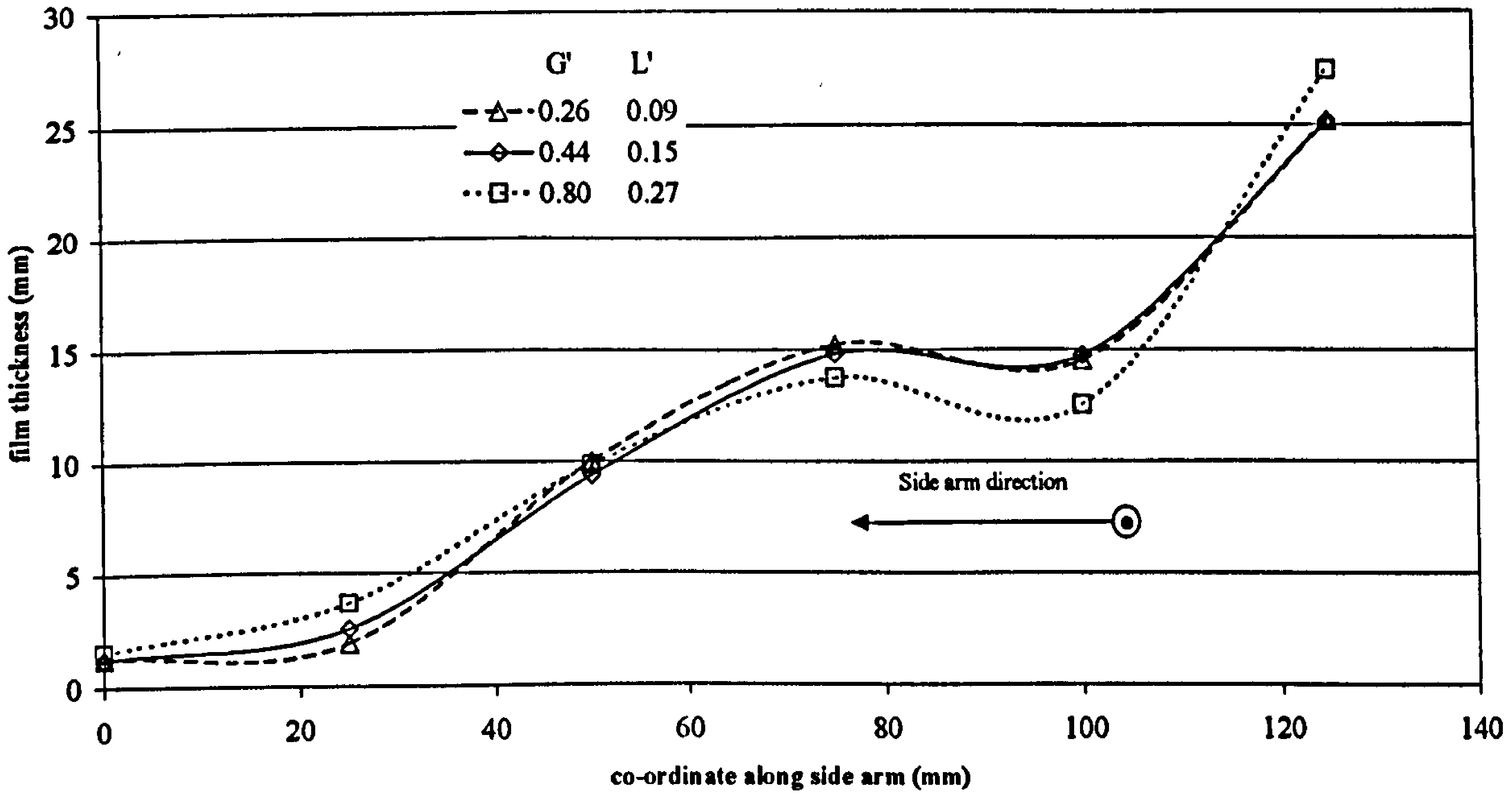

Figure III.2.37: *Film distribution along row 3, towards side arm, for the three splits from run e) (U_{gs}=23.0 m/s, U_{ls}=0.136 m/s). The flow is entering the plane of the plot.*

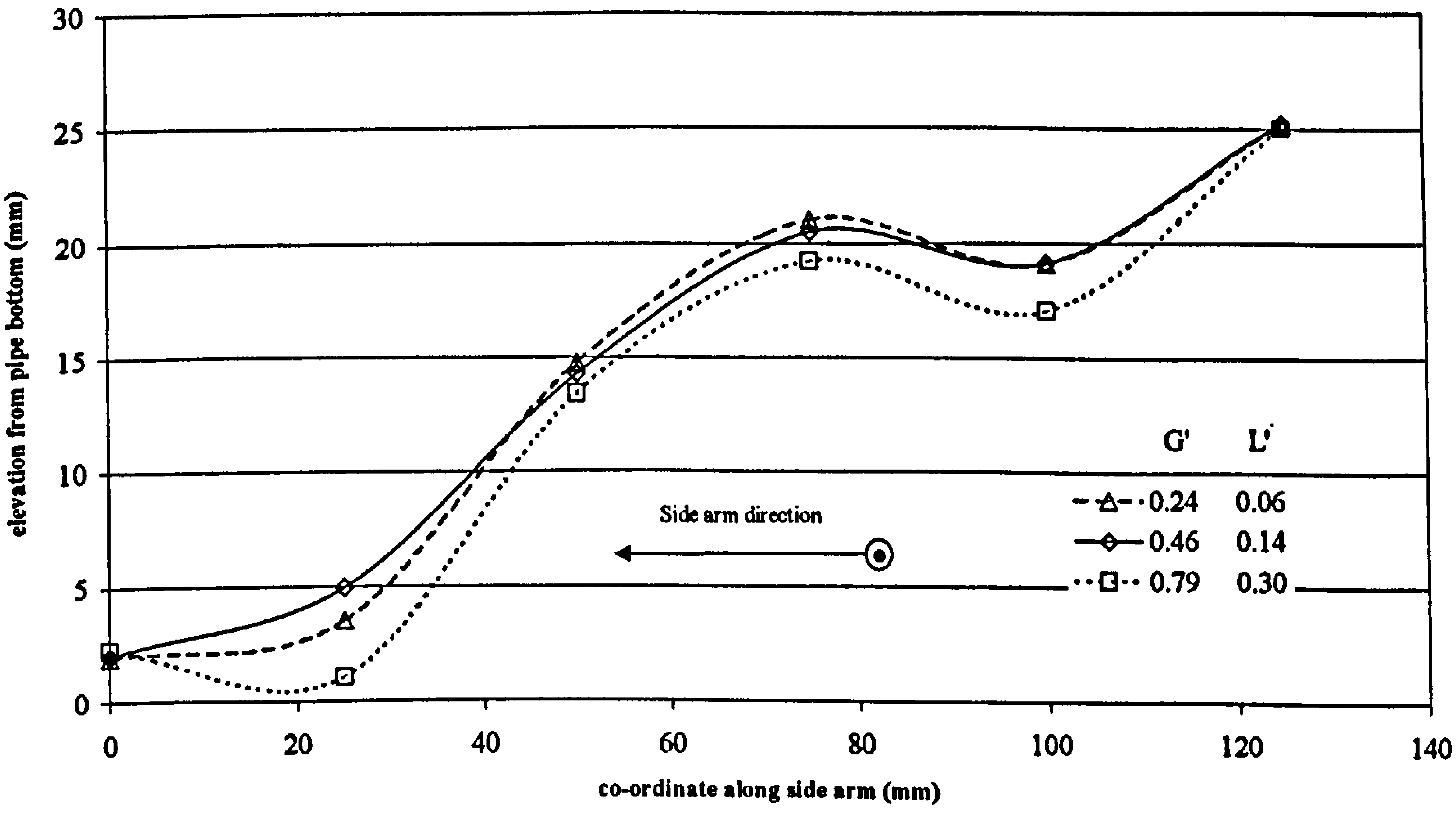

Figure III.2.38: *Film distribution along row 3, towards side arm, for the three splits from run d) (U_{gs}=16.5 m/s, U_{ls}=0.136 m/s). The flow is entering the plane of the plot.*

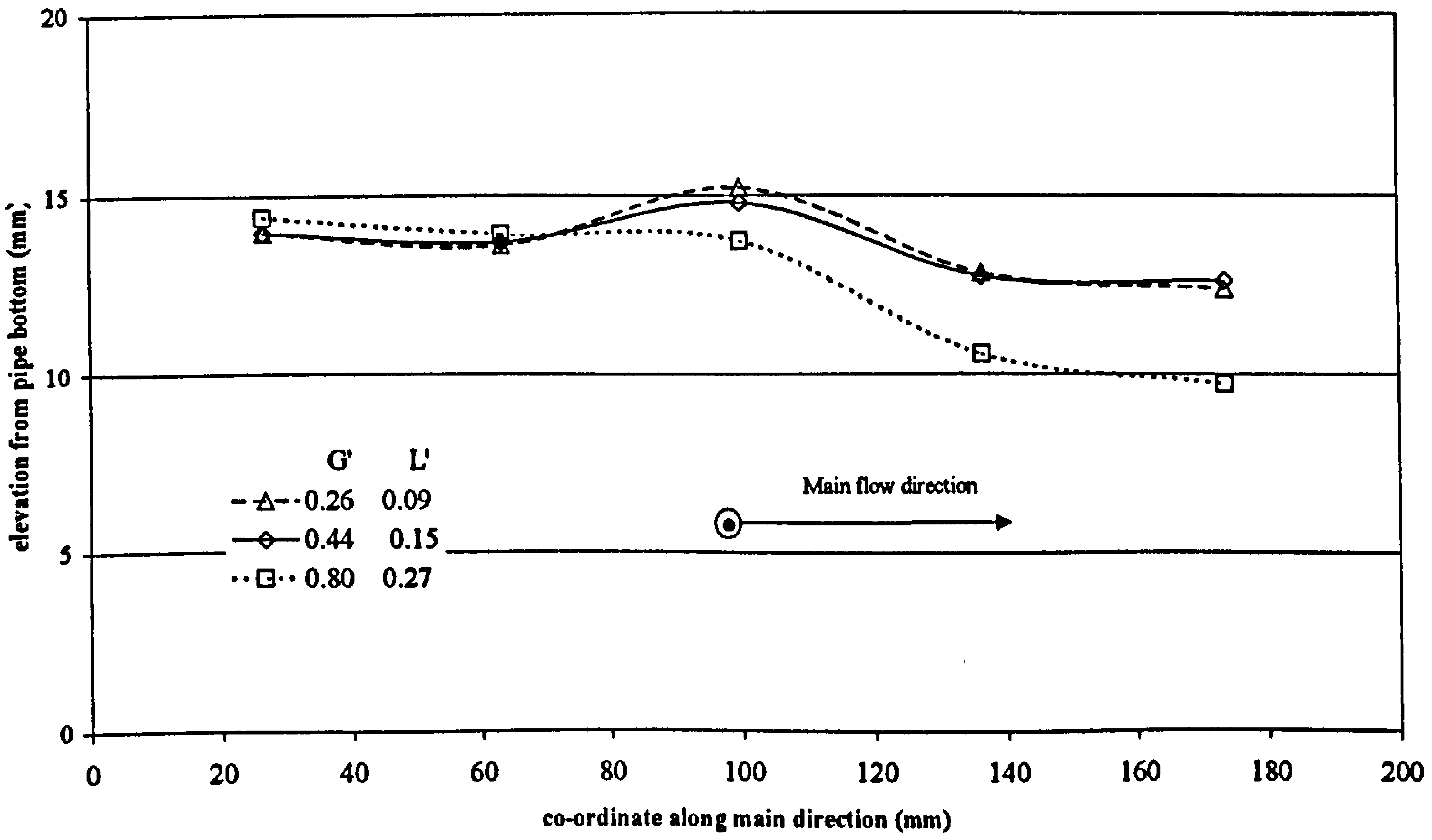

Figure III.3.39: *Film distribution along row C towards run outlet for the three splits from case e) (U_{gs}=23.0 m/s, U_{ls}=0.136 m/s). The flow is entering the plane of the plot, towards the side arm. Main flow is from left to right.*

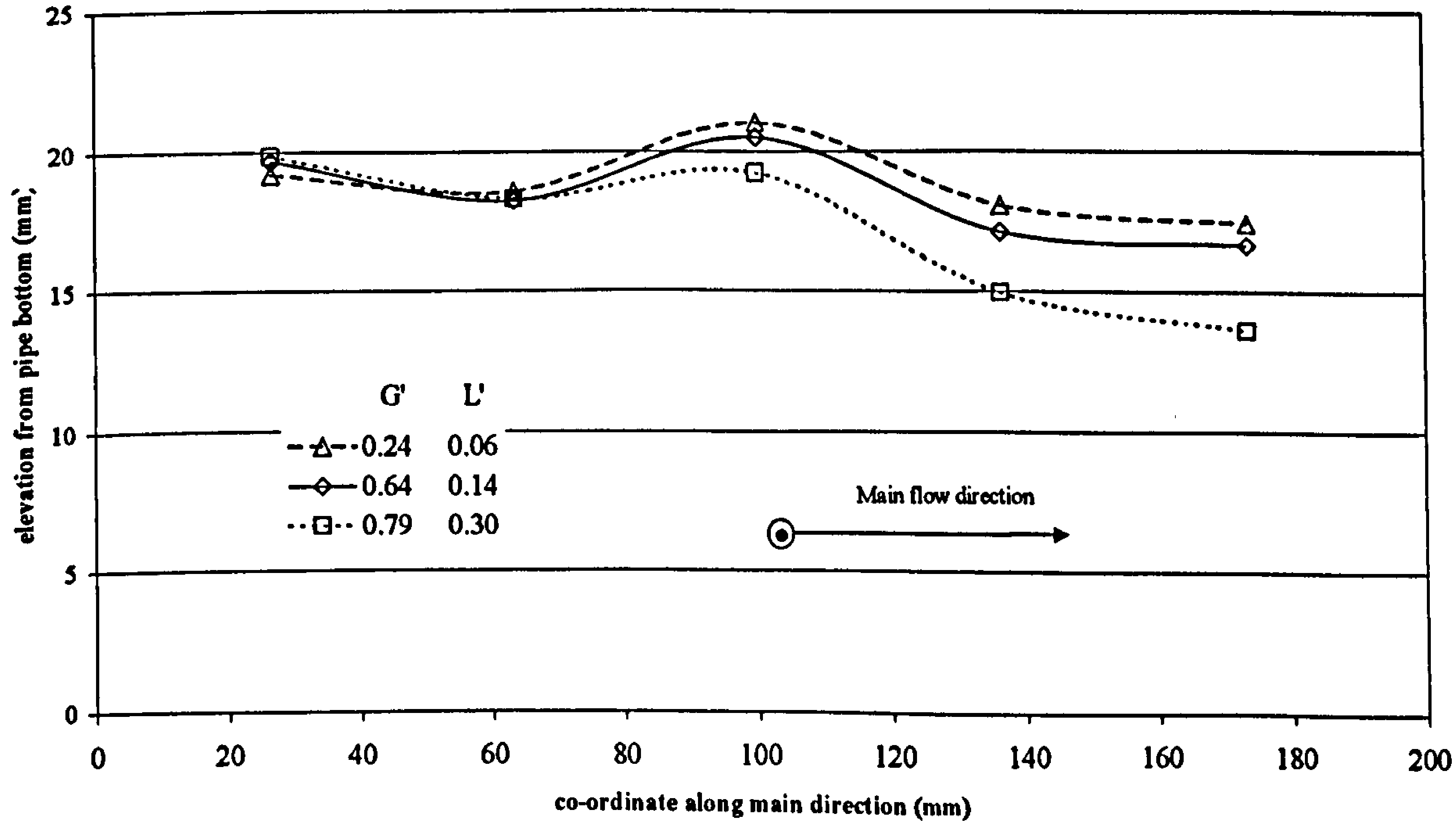

Figure III.2.40: *Film distribution along row C towards run outlet for the three split from case d) (U_{gs}=16.5 m/s, U_{ls}=0.136 m/s).*

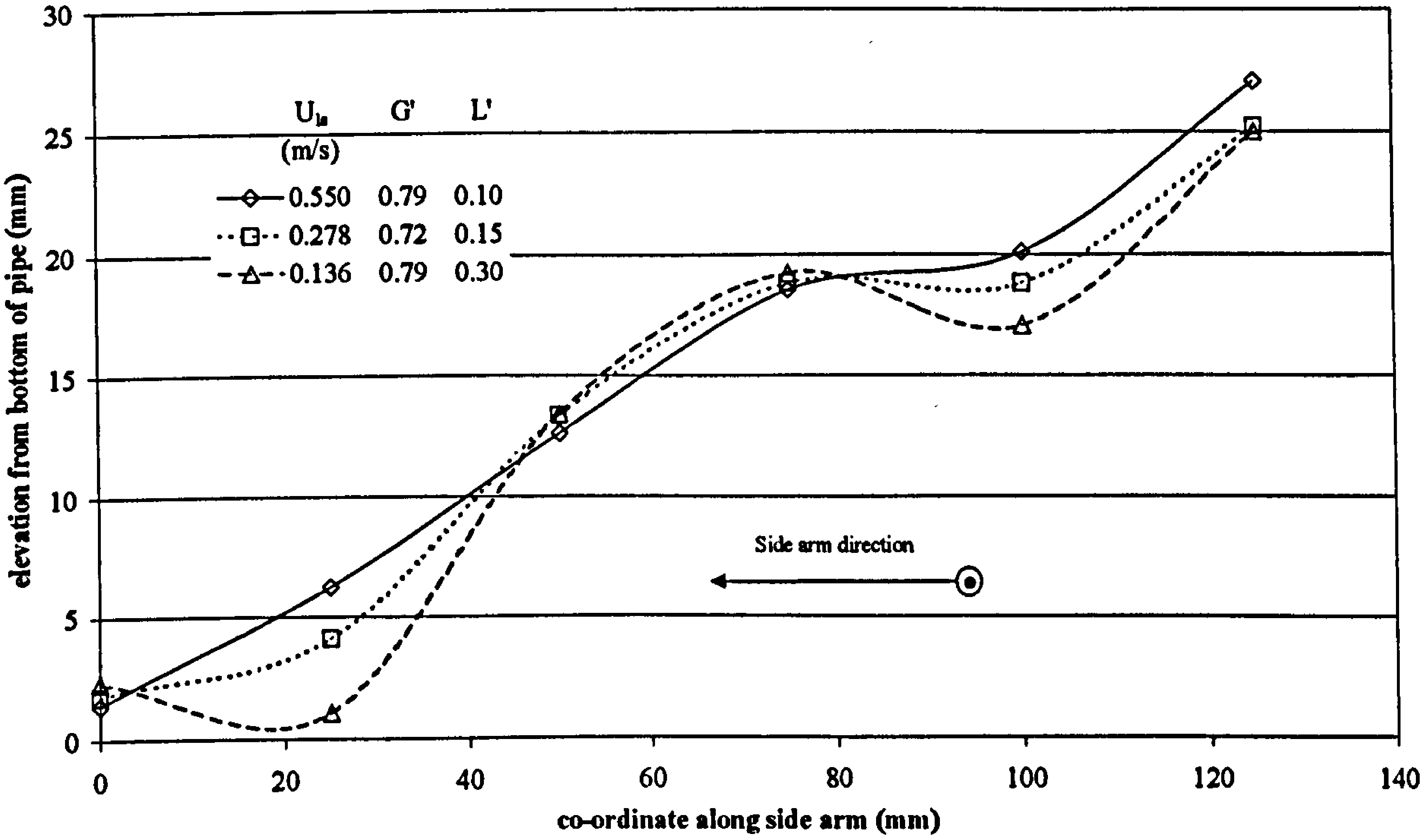

Figure III.2.41: *Film distribution along row 3, towards side arm, for a constant inlet gas velocity of 16.5 m/s. U_{ls}=0.550, 0.278, 0.136 m/s. Main flow is entering the plane of the plot.*

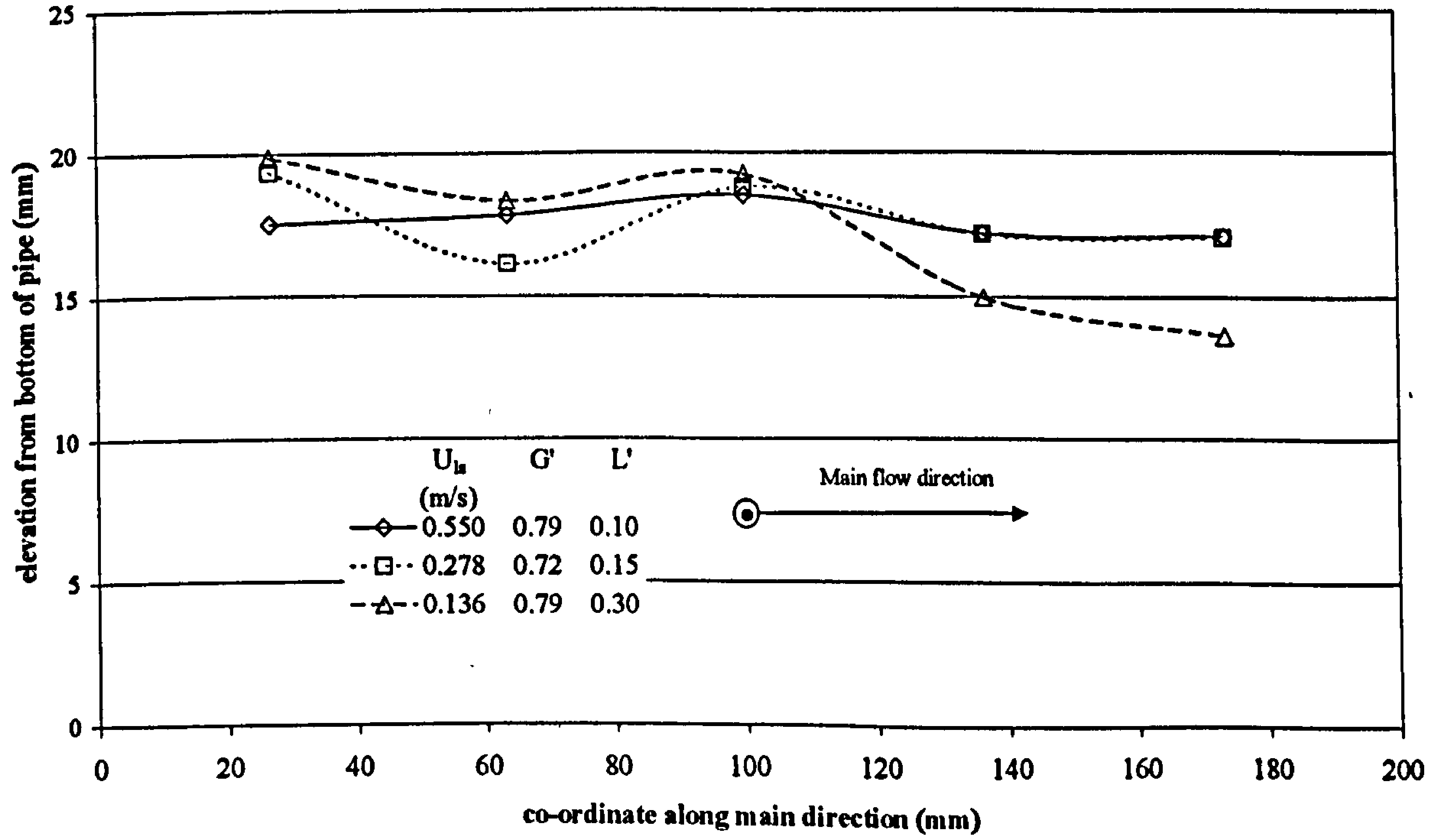

Figure III.2.42: *Film distribution along row C towards run outlet for a constant gas inlet of 16.5 m/s. U_{ls}=0.550, 0.278, 0.136 m/s.*

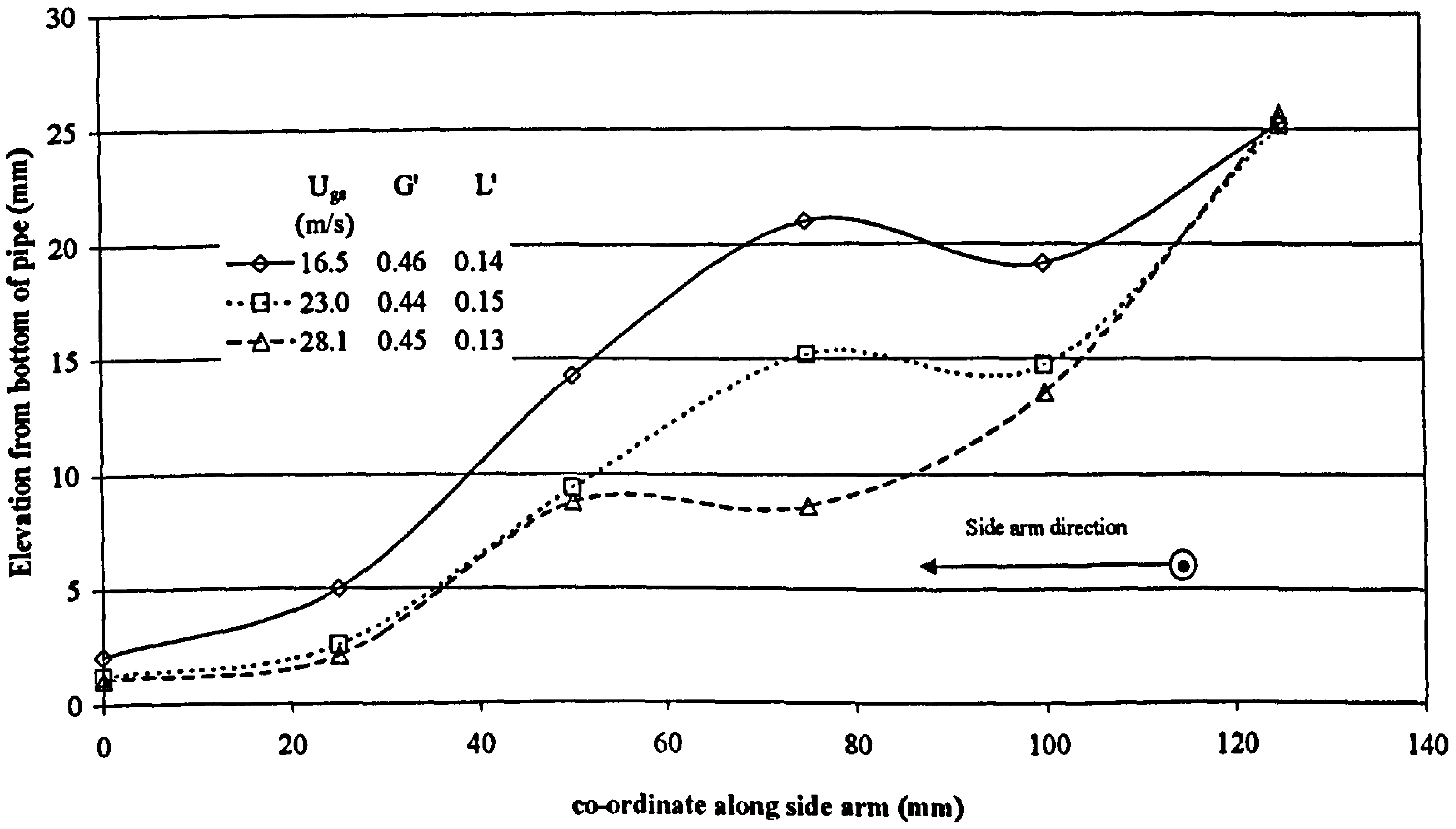

Figure III.2.43: *Film distribution along row 3 along side arm for a constant liquid velocity of 0.136 m/s. U_{gs}=16.5, 23.0, 28.1 m/s. The flow is, towards the side arm. Main flow is entering the plane of the plot.*

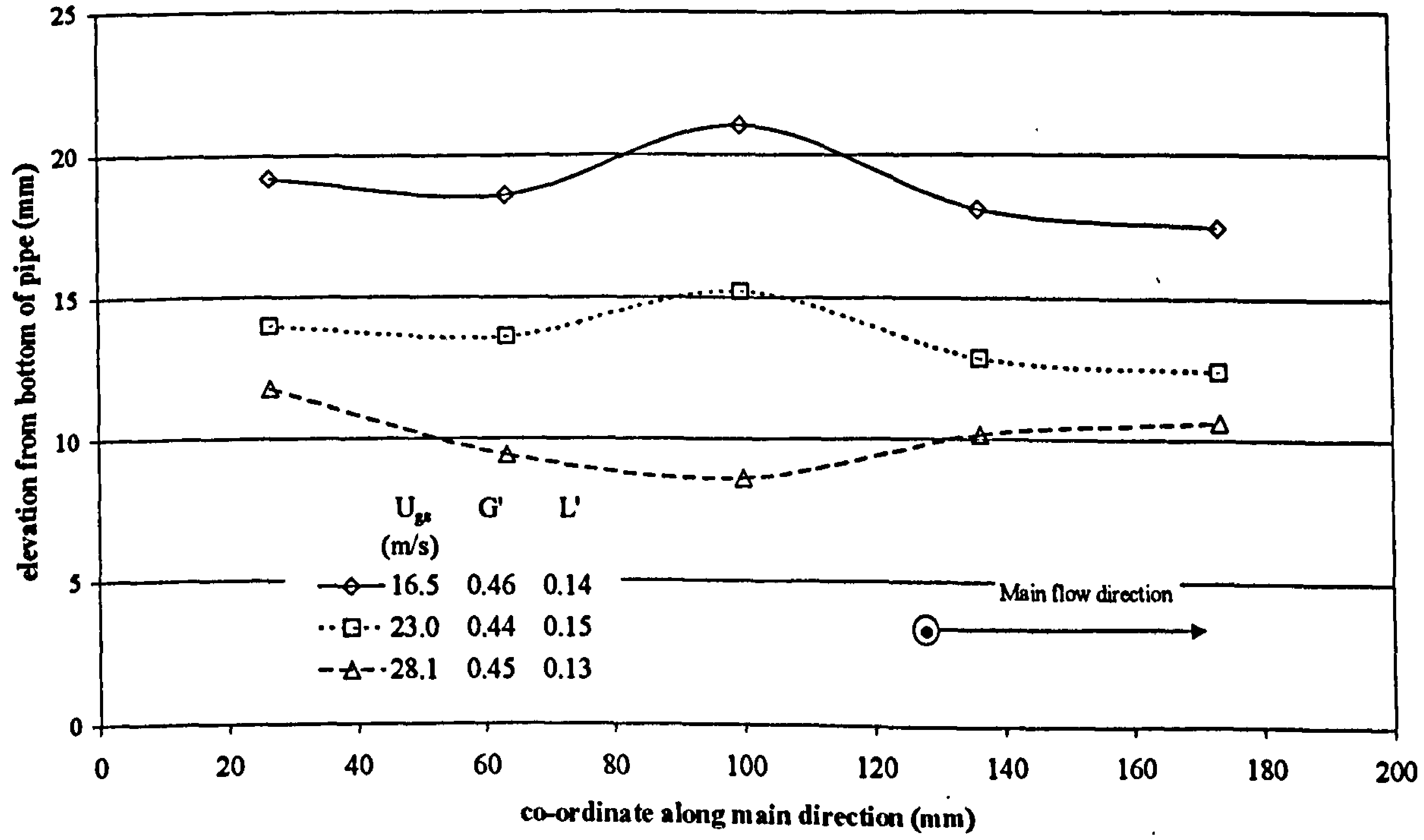

Figure III.2.44: *Film distribution along row C towards run outlet arm for a constant liquid velocity of 0.136 m/s. U_{gs}=16.5, 23.0, 28.1 m/s.*

Finally, similarly to what has been done for the results from other test sections, it is interesting to compare results obtained for similar split and for a constant gas or liquid superficial velocity, varying liquid and gas superficial velocity respectively. Figures III.2.41-42 show the results along side arm direction and main direction of cases a), b) and d) for a fraction of 72 to 79% gas being taken off. No general trend can be established and both for the plot along the run and side arm direction, variations are quite small. Case a), for the largest liquid flow rate, appears qualitatively different from the other two.

Cases d), e) and f), for $0.44<G'<0.46$ and $0.13<L'<0.15$ show a clear trend with a thinner film for increasing gas velocity (Figures III.2.43-44). This is in agreement with the findings of the conductance measurements at the inlet to the T (section III.2.8). In this case, it is the result from the run at the largest gas inlet (run f)) to show qualitatively different features.

III.2.10 Split data in the light of film thickness results.

Postponing further discussion of film thickness results till the next chapter, where comparison with physical models are made, it is useful at this stage to review the split data presented in section III.2 in the light of the features observed in the previous two paragraphs.

In agreement with the literature, it was found that the split of phases in horizontal annular flow, for the investigated range, is strongly gas dominated. Particularly, small and yet clear variations are observed with varying the inlet liquid superficial velocity in the direction of decreasing fraction of diverted liquid when liquid flow rate is increased (Figure III.1.4). Conversely, a uniform split characteristic is exhibited when only the inlet gas flow rate is varied (Figure III.1.5)

It is interesting to observe that this behaviour is reversed with regard to the film distribution around the pipe circumference, particularly with reference to the inlet contour. No significant variation of the film distribution is observed for a constant gas inlet of 16.5 m/s for the three liquid velocities investigated (0.55, 0.278, 0.136 m/s) in disagreement with previous findings (Rea, 1998; Paras *et al*, 1994) (Figure III.2.17). A trend was found when, for a liquid inlet of 0.136 m/s the gas superficial velocity was varied (16.5, 23.0, 28.1 m/s): more symmetrical flow for larger gas inlets with thinner film at the bottom and thicker at the top (Figure III.2.18). This is in agreement with the literature.

The fact that film thickness remains unchanged when liquid flow rate is increased could be explained by an increase of entrained fraction. Hence, because the liquid is only taken off from the film, less liquid will be diverted overall in the side arm in agreement with split data. However, a large increase of entrained fraction would be required and there is no proof of such a strong variation.

Less straightforward is the explanation of the behaviour observed for varying gas superficial velocity. The decrease in film thickness with larger gas flow rates is due to a larger entrained fraction and faster liquid due to the stronger shearing action of air on the gas liquid interface. Because entrained liquid can be reasonably assumed to travel past the junction, both occurrences are in the direction of a smaller fraction of liquid taken off with larger gas flow rate. Yet, for cases d), e) and f) no appreciable change in the distribution of gas and liquid between side and run arm is recorded. Figure III.2.19 shows the magnitude of larger symmetry and hence thicker film at the top recorded for increasing inlet of gas. This seems too weak an effect to justify the uniformity of behaviour in the three cases. Another effect that can be invoked is the higher pressure differential in the side arm. Because the gas inlet is larger, for the same fraction of gas taken off, more gas travels in the side arm. This increases the pressure drop and diversion of liquid in the side arm. Furthermore, the measurements within the T-junction show that for the same split of the phases, the way the film reacts to the presence of the side arm for the three gas velocities is rather different as shown in Figures III.2.43-44, especially for the largest gas flow rate.

However, the database explored is quite restricted and no extension of the above reasoning can be by any means generalised, not even to annular flow.

III.3 Observation of Hydraulic Jump in the run leg.

The hydraulic jump is a phenomenon widely studied in the hydraulics of open channels, occurring when a liquid film flow undergoes the transition from supercritical, momentum dominated (Fr>1) to sub-critical, gravity dominated (Fr<1). Here, the Froude number is calculated by using the liquid film velocity and height. It consists of a more or less gradual but significant thickening of the liquid film and, according to the upstream Froude number, hydraulic jumps have been classified in the categories shown in Figure III.3.1. An extensive review of models for hydraulic jumps can be found in Roberts (1994).

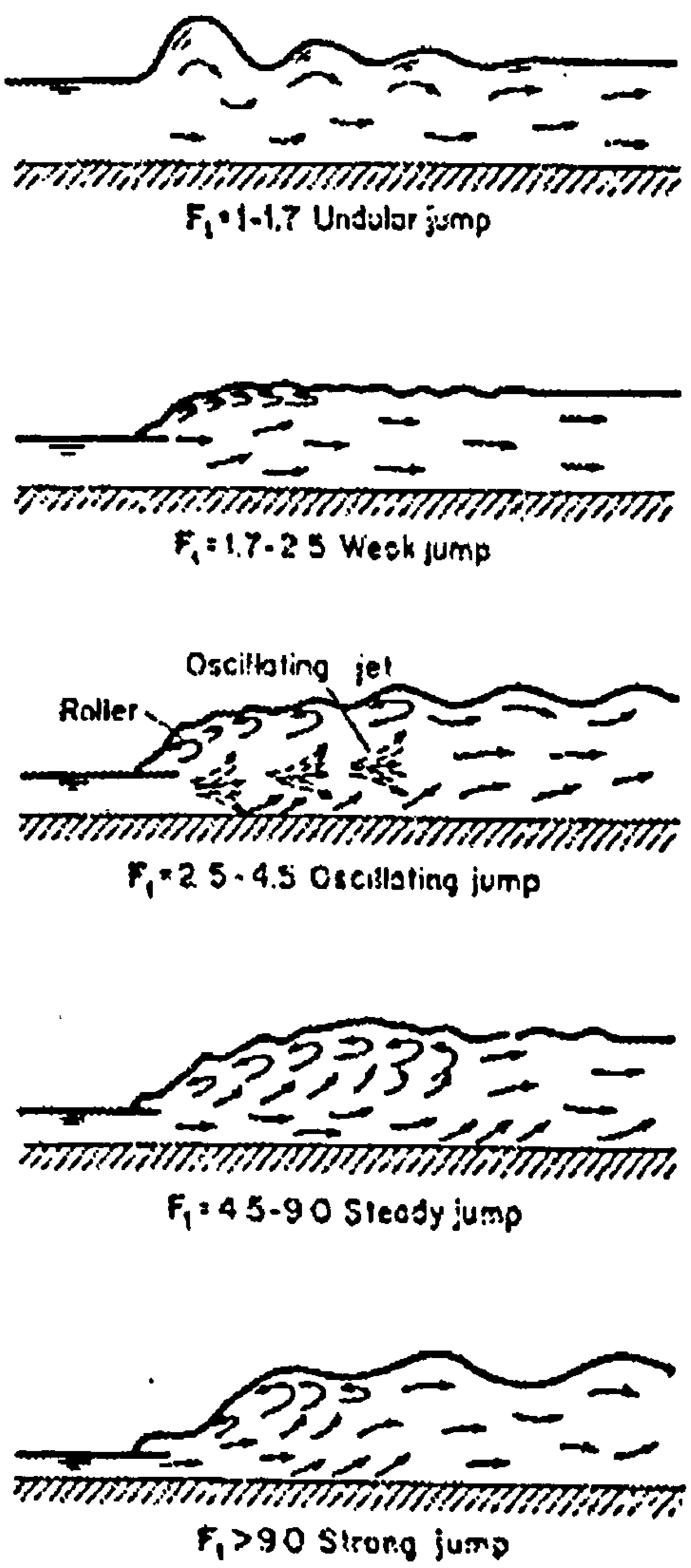

Figure III.3.1: *Classification of hydraulic jump from Chow (1959)*

The phenomenon of film stop is itself a formal hydraulic jump, where the film slows down by Bernoulli effect due to the loss of convective momentum through the side arm. Traditionally, hydraulic jumps in open channels are studied as they occur because of dissipation, for example below a regulating sluice. However, they are induced also by the presence of obstacles such as weirs. In the present case, the phenomenon of hydraulic jump in the run leg was caused by the interference of the momentum driven film, as it continued from the inlet pipe, with the gravity driven flow, occurring downstream of the butterfly valve, leading from the run leg outlet into the cyclone. As the butterfly valve was progressively shut, the length of extension of the gravity driven flow gradually moved towards the side arm opening, causing the secondary liquid take off mechanism into the side arm, when the hydraulic jump was close enough to the side arm.

The following (Figures III.3.2-13) illustrates the observations that were made by using a digital still camera, with 1/500 s exposure time. A side view (Figures III.3.3-7) and a top view (Figures III.3.8-13) of the hydraulic jump were produced when it occurred half way through the run leg.

For case a) (Figures III.3.2 and 6) of the present database, a heavy froth was observed at the transition zone extending for about 3 pipe diameters. Behind it, although it is not visible from the photos, there was a much smoother area were the bubbles formed at the jump collapsed travelling on the liquid surface. For case b) (Figures III.3.3 and 8), at a lower liquid flow rate, the jump appeared as belonging to the oscillating category ($2.5 < Fr < 4.5$) and from the side view it is possible to distinguish two oscillating jets. Behind the area of the jump, also called 'roller', a much thicker film appeared often bridging up to the top of the pipe and showing frequent slugging. Case c) is very similar to case b) but the slugging behind the roller is occasional. Cases d), e) and f) give place to hydraulic jumps close to the characteristics of undular jumps. Particularly, in case d) the undulation on the thick surface consisted of a secondary jump right behind the first. Case f) definitely shows a undular hydraulic jump and given the large gas flow rate, heavy liquid deposition on the pipe circumference is visible, after drops were generated at the T.

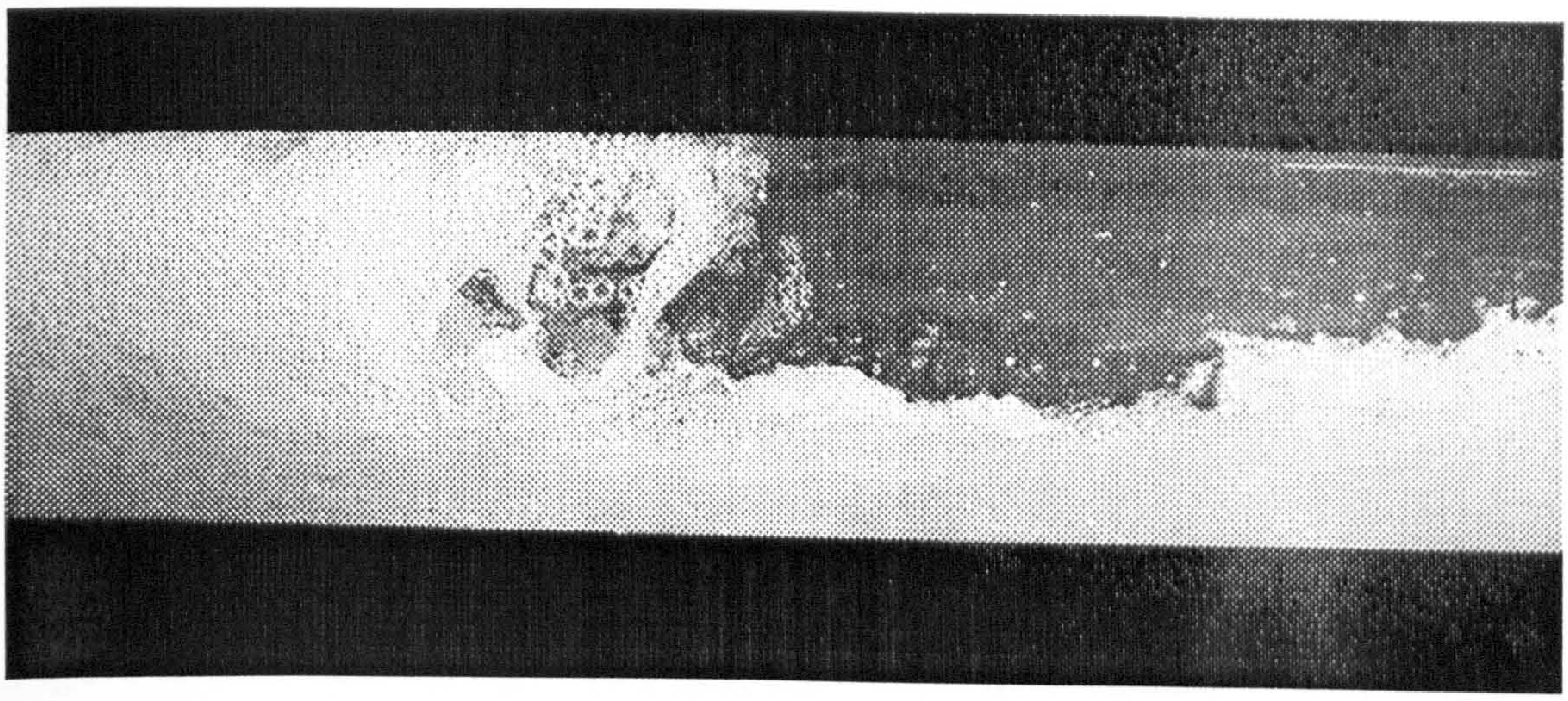

Figure III.3.2: Case a), U_{gs} = 16.5 m/s; U_{ls} = 0.55 m/s: (G',L') = (0.79,0.1). Side view of hydraulic jump, half way through the run leg.

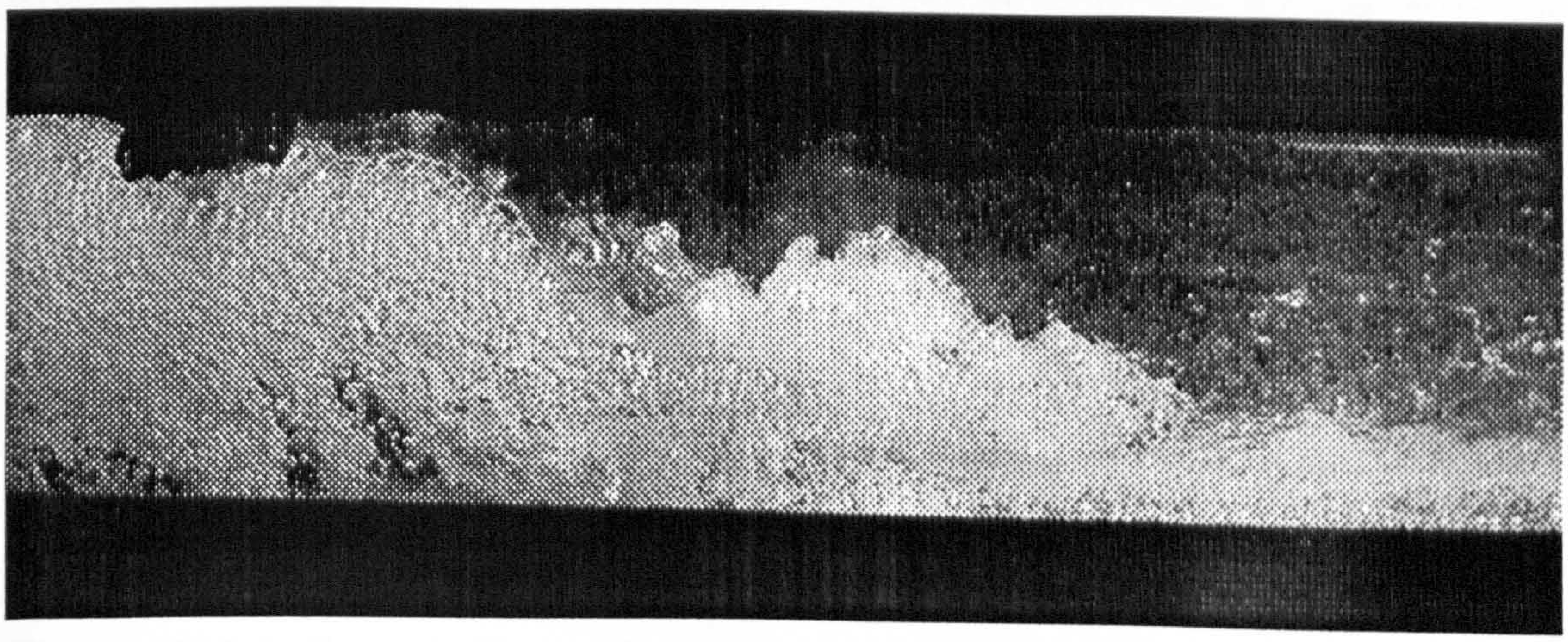

Figure III.3.3: Case b), U_{gs} = 16.5 m/s; U_{ls} = 0.278 m/s.: (G',L') = (0.65,0.12). Side view of hydraulic jump, half way through the run leg.

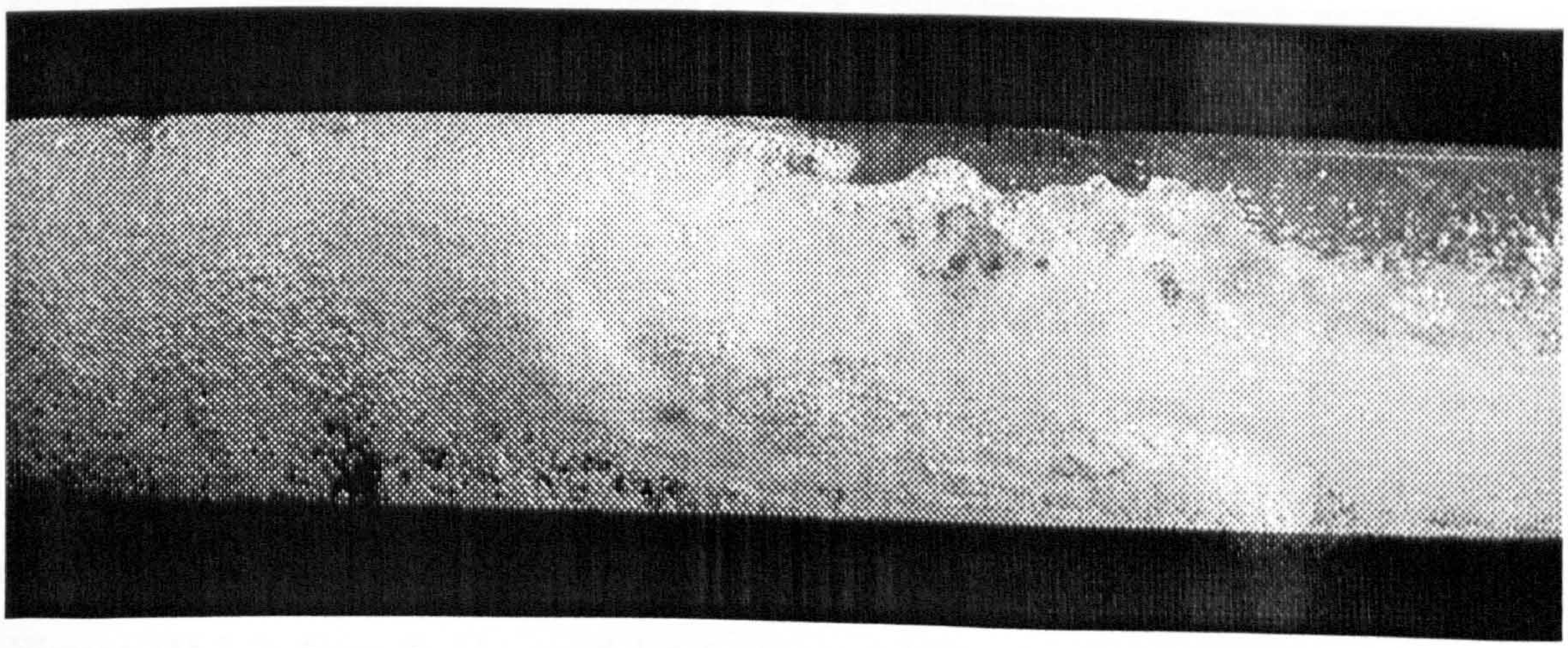

Figure III.3.4: Case c), U_{gs} = 24.5 m/s; U_{ls} = 0.278 m/s: (G',L') = (0.7,0.14). Side view of hydraulic jump, half way through the run leg.

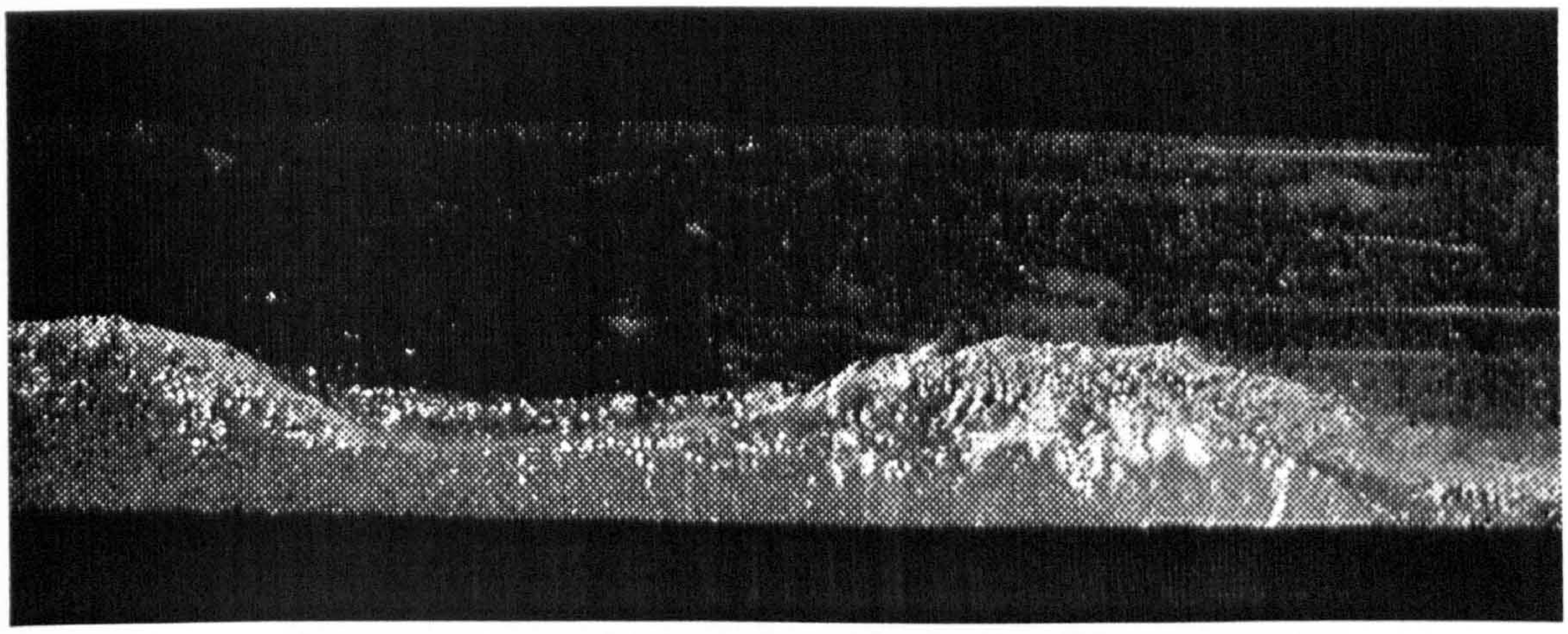

Figure III.3.5: Case d), U_{gs} = 16.5 m/s; U_{ls} = 0.136 m/s: (G',L') = (0.7,0.22). Side view of hydraulic jump, half way through the run leg.

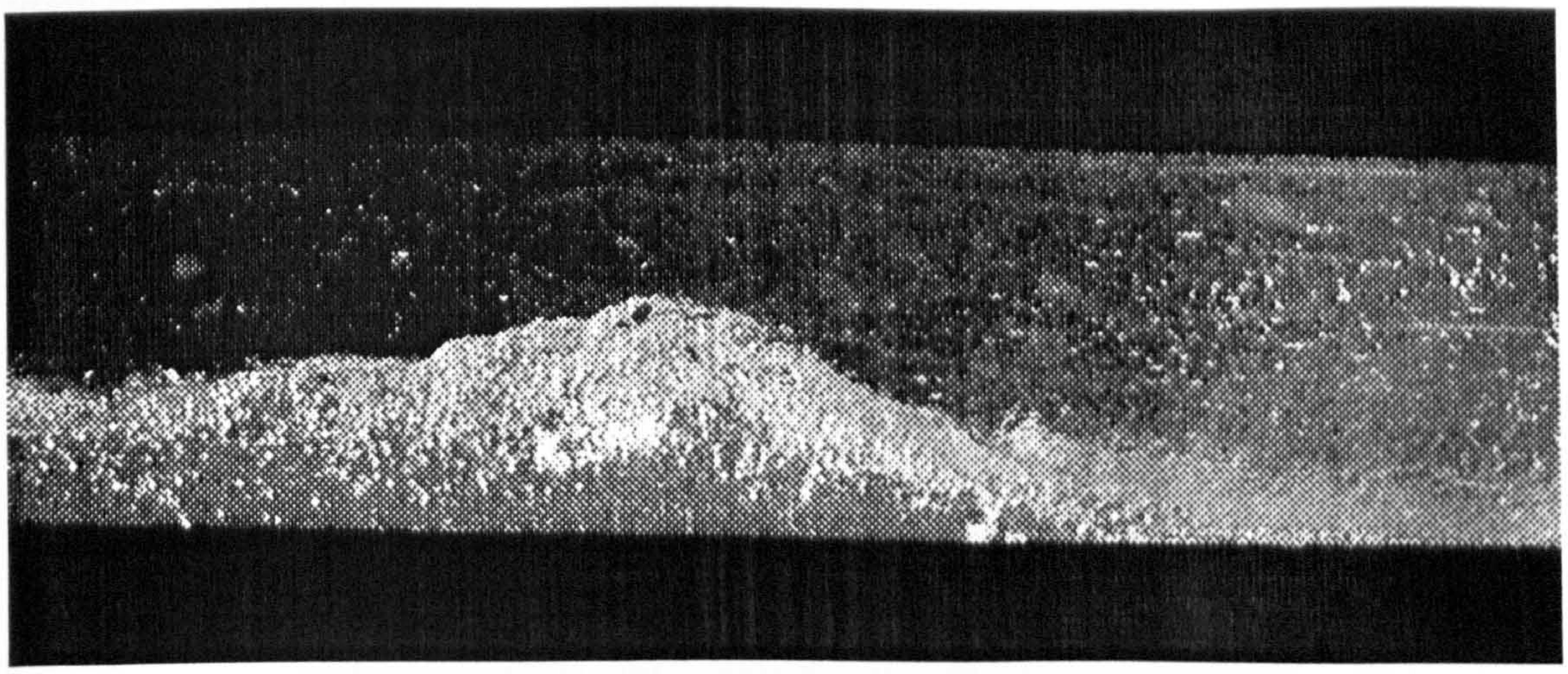

Figure III.3.6: Case e), U_{gs} = 23 m/s; U_{ls} = 0.127 m/s: (G',L') = (0.6,0.18). Side view of hydraulic jump, half way through the run leg.

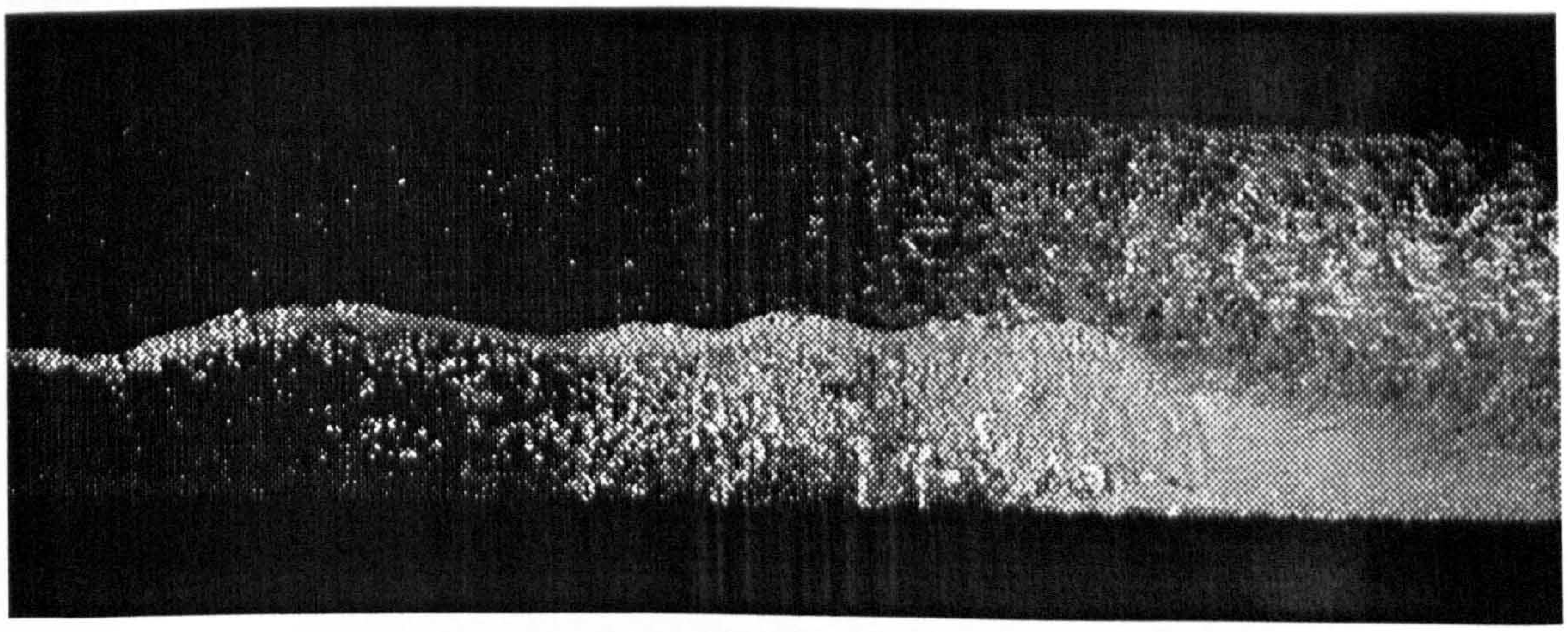

Figure III.3.7: Case f), U_{gs} = 28.1 m/s; U_{ls} = 0.136 m/s: (G',L') = (0.6,0.19). Side view of hydraulic jump, half way through the run leg.

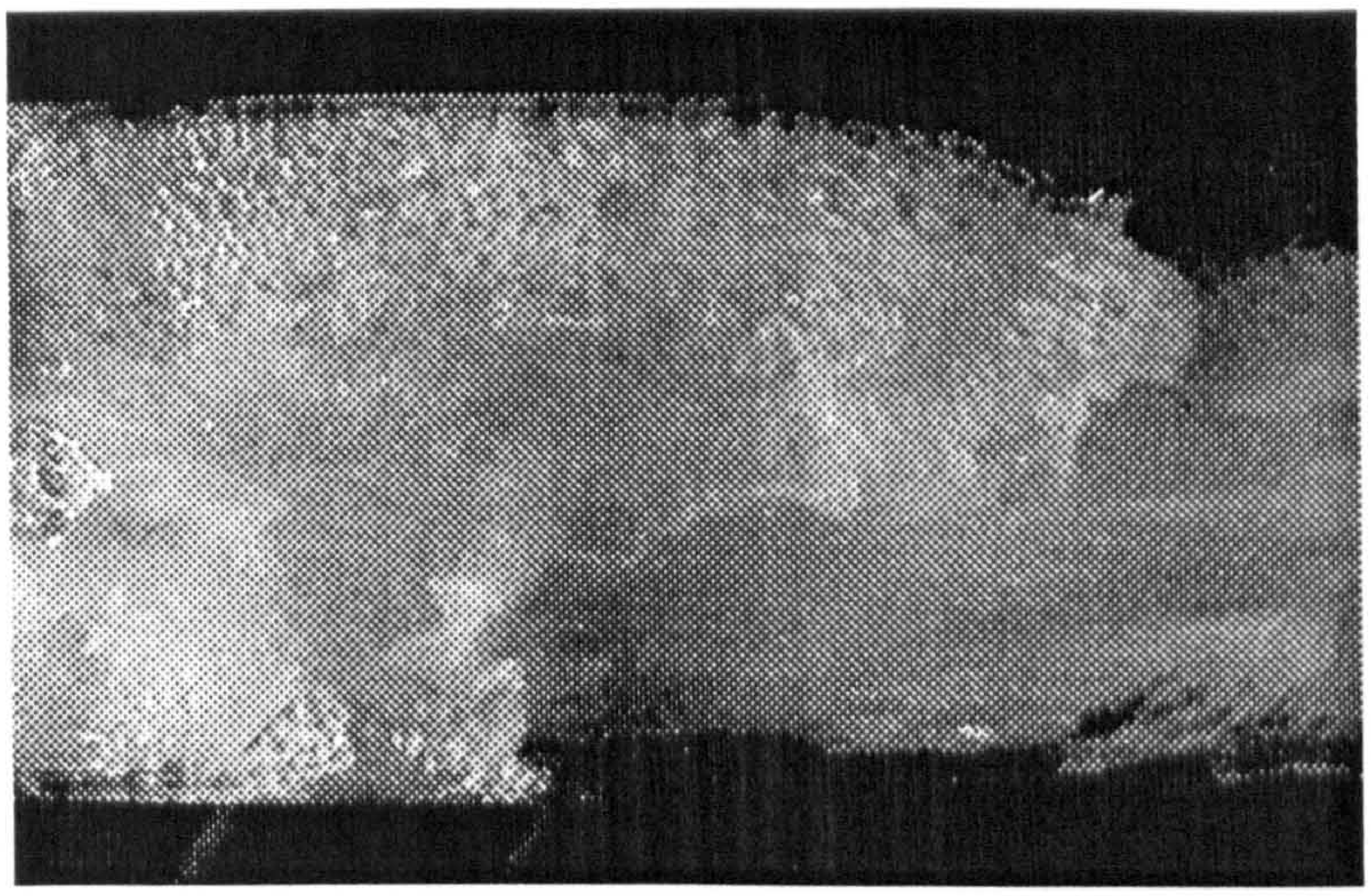

Figure III.3.8: Case a), U_{gs} = 16.5 m/s; U_{ls} = 0.55 m/s: (G',L') = (0.79,0.1). Top view of hydraulic jump, half way through the run leg.

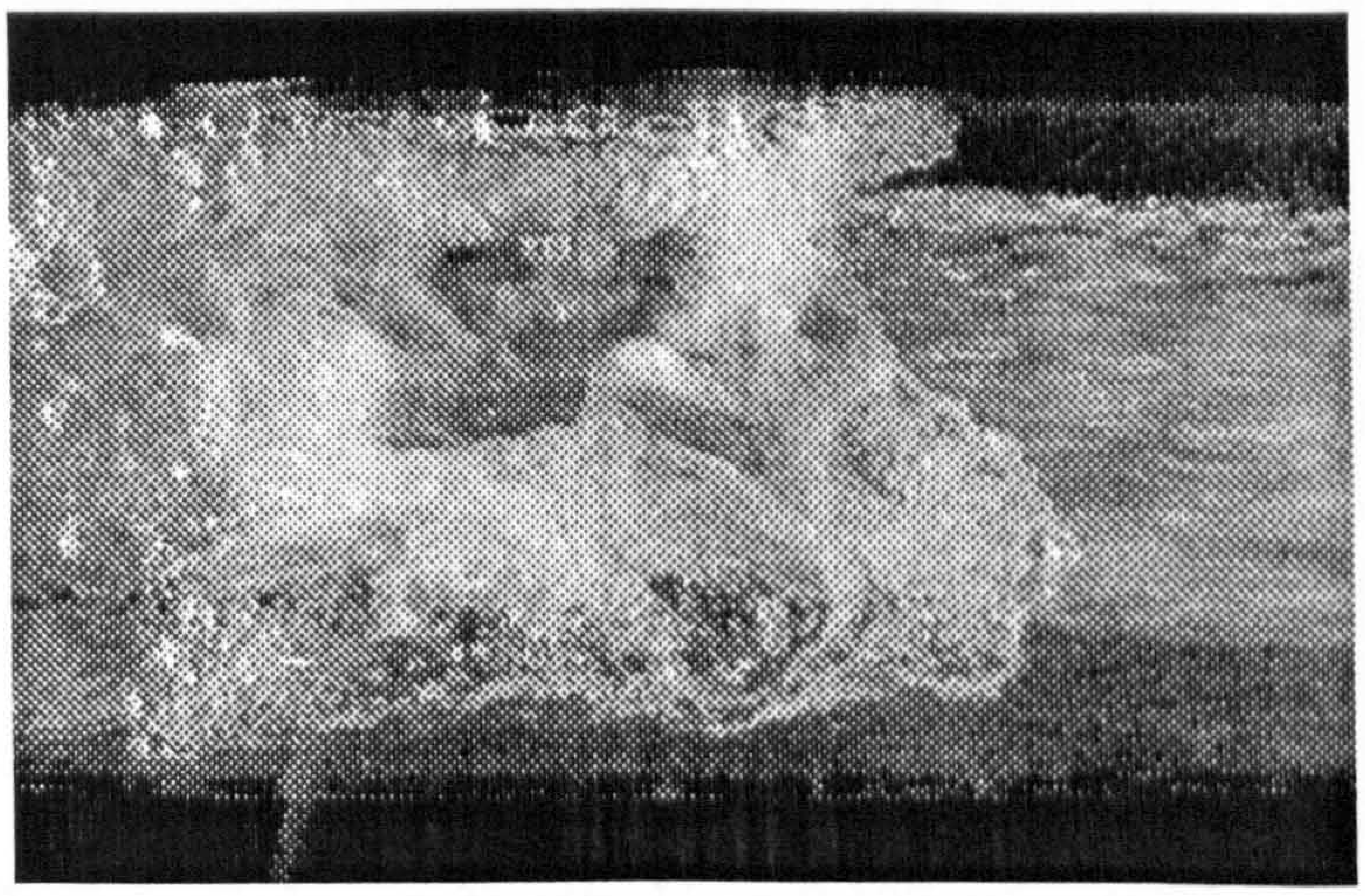

Figure III.3.9: Case b), U_{gs} = 16.5 m/s; U_{ls} = 0.278 m/s: (G',L') = (0.65,0.12). Top view of hydraulic jump, half way through the run leg.

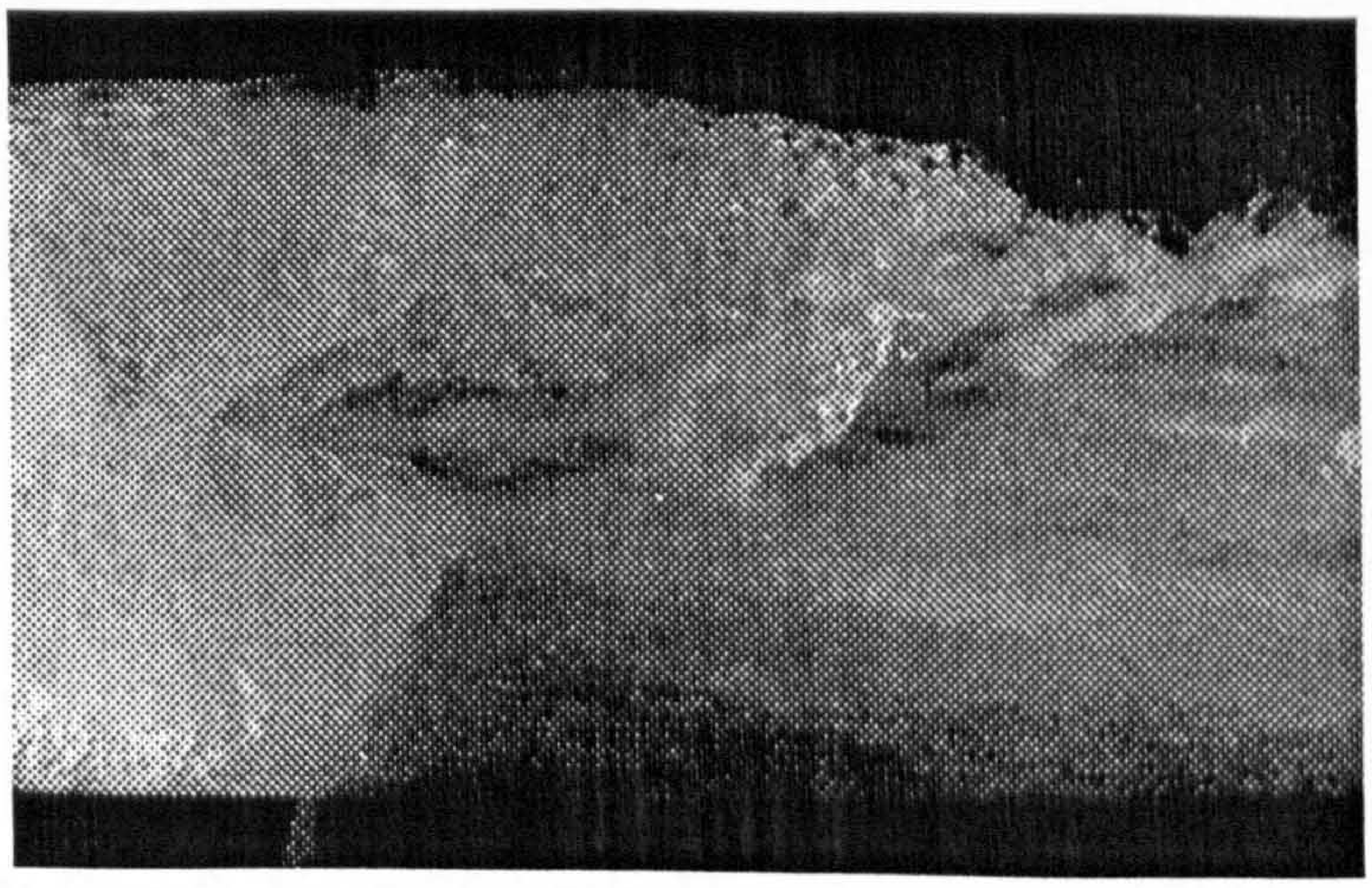

Figure III.3.10: Case c), U_{gs} = 24.5 m/s; U_{ls} = 0.278 m/s: (G',L') = (0.7,0.14). Top view of hydraulic jump, half way through the run leg.

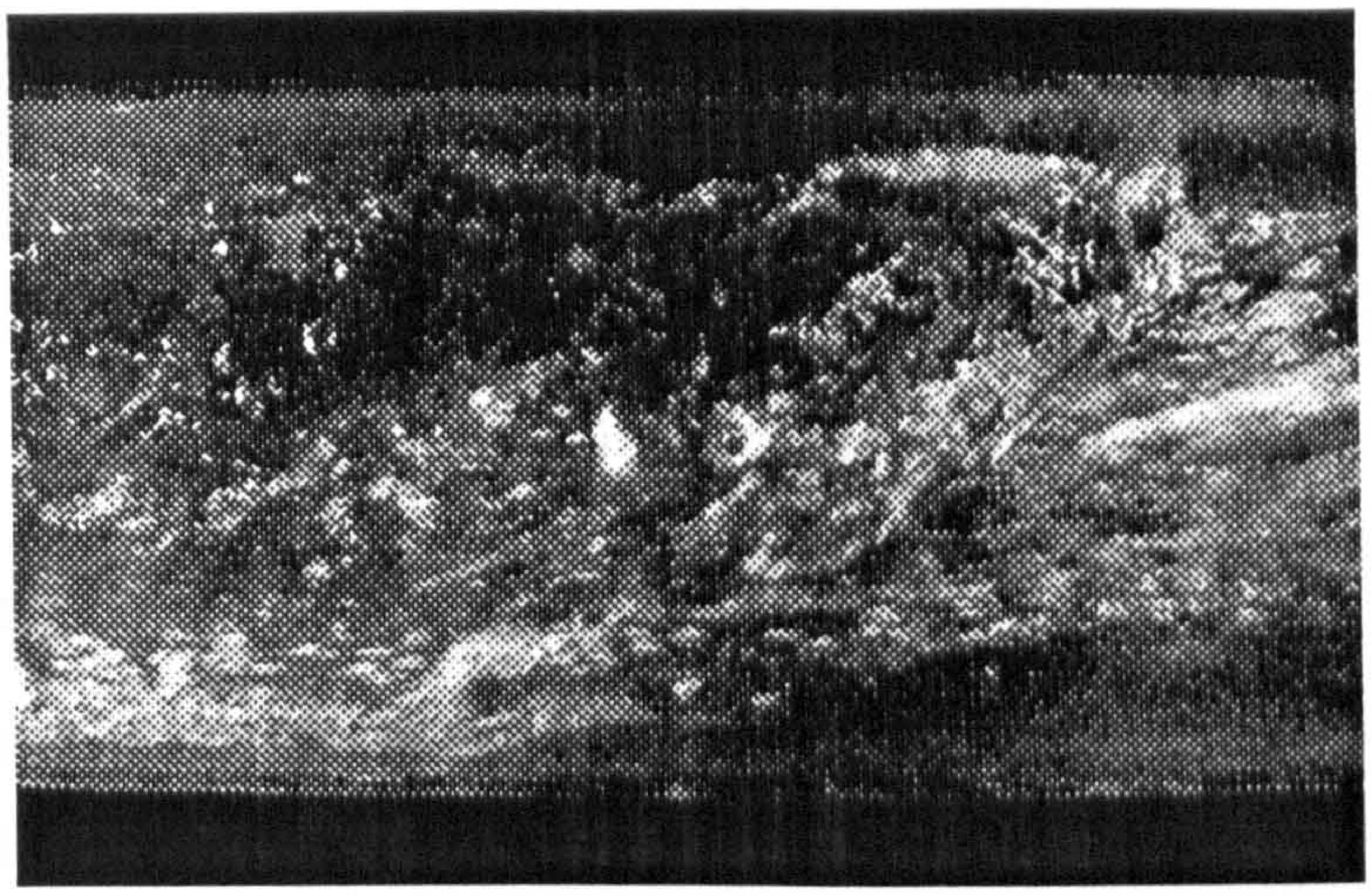

Figure III.3.11: Case d), U_{gs} = 16.5 m/s; U_{ls} = 0.136 m/s: (G',L') = (0.7,0.22). Top view of hydraulic jump, half way through the run leg.

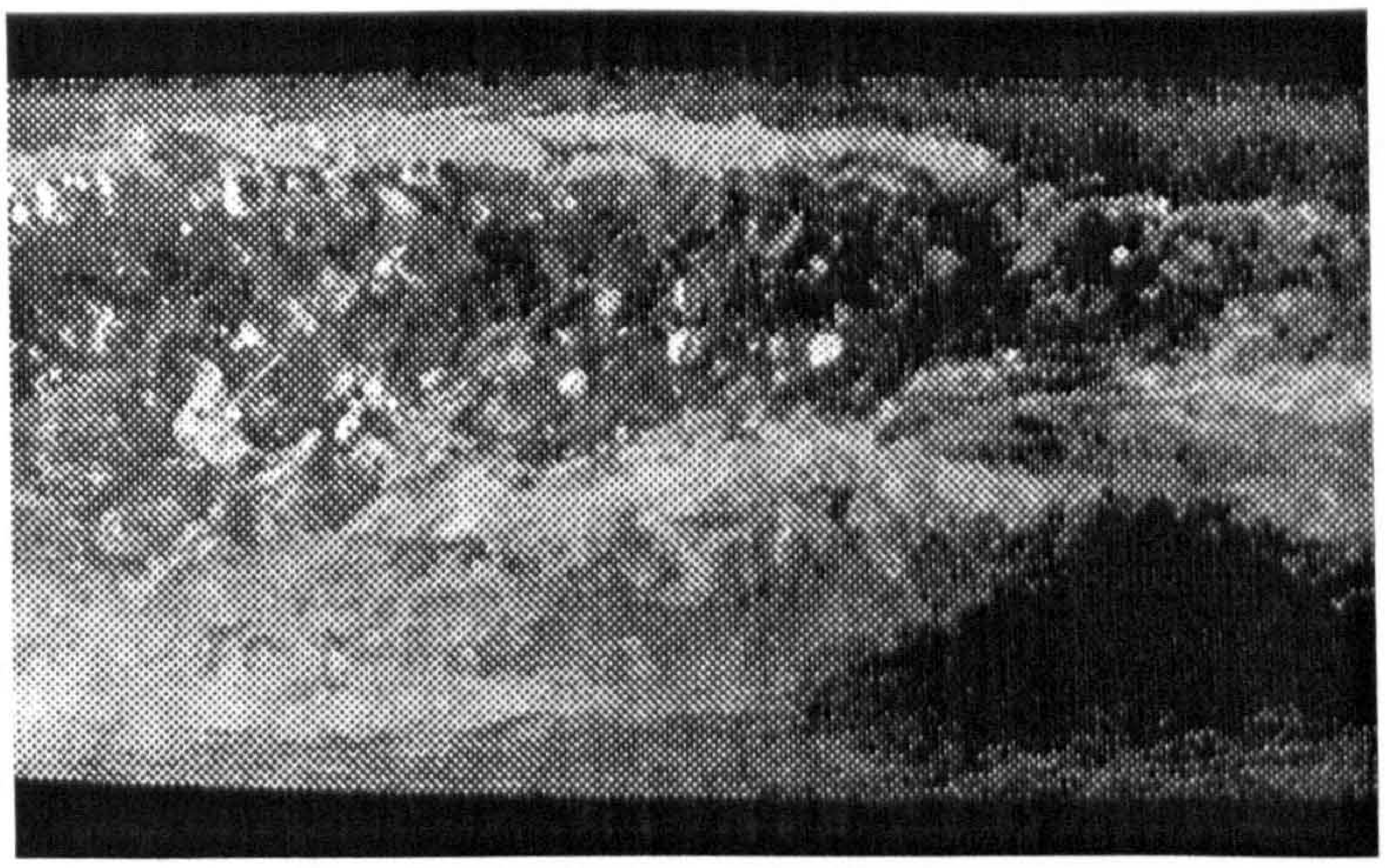

Figure III.3.12: Case e), U_{gs} = 23 m/s; U_{ls} = 0.127 m/s: (G',L') = (0.6,0.18). Top view of hydraulic jump, half way through the run leg.

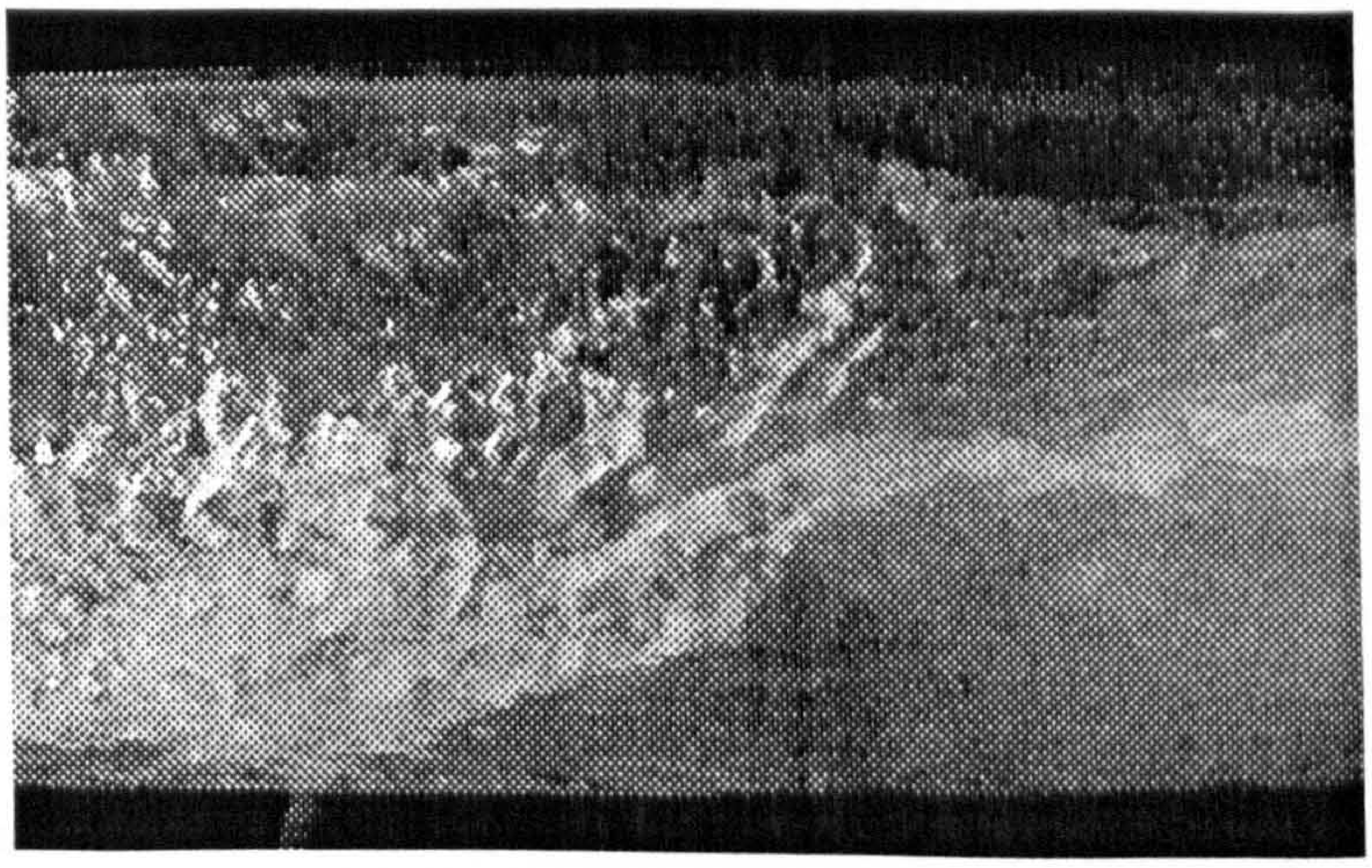

Figure III.3.13: Case f), U_{gs} = 28.1 m/s; U_{ls} = 0.136 m/s: (G',L') = (0.6,0.19). Top view of hydraulic jump, half way through the run leg.

Chapter IV

Comparison with available models

Introduction

This chapter presents the comparison of split data with two different models. In particular, the model developed by Adechy and Issa (1999) and Adechy (2000) is the most comprehensive simulation based on CFD and carried out in co-operation with the present experimental work. In addition, the model of Azzopardi and Whalley (1982) as developed by Roberts *et al* (1997) is used to predict the split of the phases. In applying this, the prediction by Hurlburt and Newell (2000) for the film thickness distribution is employed and compared to film thickness measurements at the inlet to the T-junction.

IV.1 Comparison with CFD model

The annular flow model developed by Adechy and Issa (1999) is based on a boundary layer assumption for the liquid film, so that the dominant gradients are in the direction normal to the main flow. Surface tension and inertial terms are neglected. The film is coupled to the core flow, which is simulated using a dispersed flow model. The droplets are assumed spherical and are tracked in a Lagrangian frame of reference. To account for the interaction between the two domains (film and core), mass and momentum transfer terms are modelled empirically. In particular, it is assumed that the droplets are created with a rate of entrainment given by the equation of Ueda (1979) as modified by Adechy & Issa (1999) with an ejection velocity as specified by Andreussi and Azzopardi (1983). Similarly, the rate of deposition is modelled by using the empirical correlation of James *et al* (1987). Because of the large relative velocity between the gas core and the liquid film, the momentum transfer is accounted for by assuming the liquid film as a standing wavy surface. Hence, a roughness coefficient k_s is obtained using the correlation of Wallis (1969) as a function of the film thickness h:

$$k_s = R\exp\left[-0.575\left(f_{smooth}\left(1-180\frac{h}{R}\right)\right)^{0.5}+2.001\right] \quad [IV.1.1]$$

where f_{smooth} is given by the formula of Blasius:

$$f_{smooth} = 0.079(Re_g)^{-0.25} \quad [IV.1.2]$$

The circumferential form drag is assumed to be of such entity to hold the waves against gravity and hence the author propose that this is proportional to the component in the circumferential direction of the gravity force:

$$\tau^2_{interface} = -C_0\rho_l g_c h \quad [IV.1.3]$$

where g_c is the circumferential component of the acceleration of gravity. and C_0 is a dimensionless, empirical coefficient depending on the Reynolds numbers of the two phases.

When this model was applied to a T-junction domain using the CFD software STAR-CD (Adechy, 2000), three main problems were encountered:

1) Care had to be taken to create the meshes at the corners to closely reproduce the sharp edged intersection of main and side arms.

2) The film thickness in the run outlet did not converge due to a feedback mechanism on the momentum equations from the hydrostatic pressure term, following the scheme in Figure IV.1.1.

3) Some phenomena observed during the experiments carried out in the present work suggested that the inertial term could not be neglected. For example, the liquid film climbing on the walls of side and run arm as described in III.3.8 are certainly dominated by the inertia of the impacting film

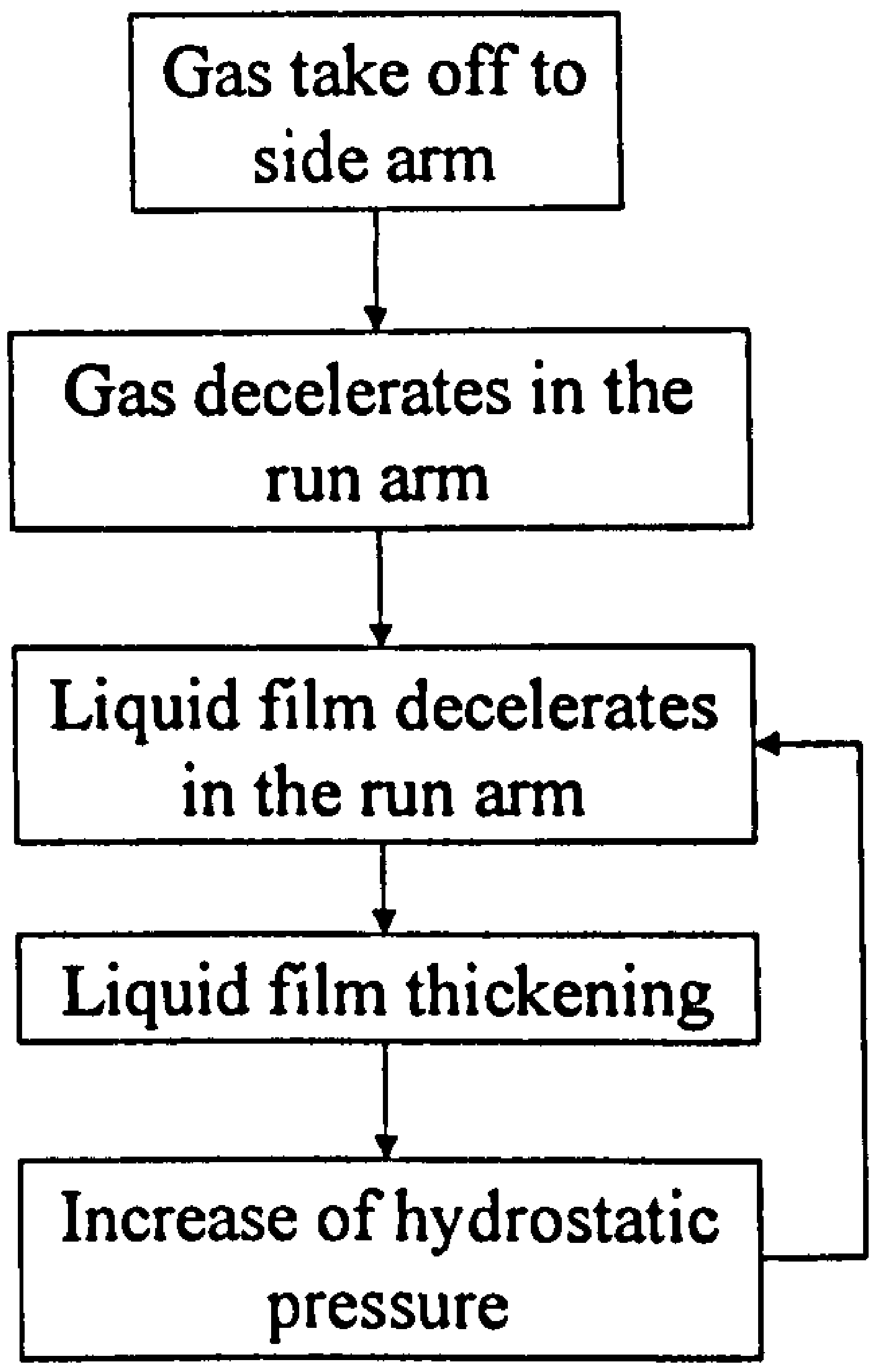

Figure IV.1.1: *Loop causing divergence in the boundary layer, film model (Adechy and Issa, 1999) when inertial term is neglected.*

For the above reasons, in the work of Adechy (2000) the model was revised by including inertial terms. Hence, the components of the momentum equation are:

$$\frac{\partial}{\partial z}(\rho ww)+\frac{\partial}{\partial x}(\rho uw)=-\frac{\partial P}{\partial z}+\frac{\partial}{\partial y}\left(\mu_{eff}\frac{\partial w}{\partial y}\right)+S_z \qquad \text{(axial)} \quad [IV.1.4]$$

$$\frac{\partial}{\partial z}(\rho uw)+\frac{\partial}{\partial x}(\rho uu)=-\frac{\partial P}{\partial x}+\rho g_x+\frac{\partial}{\partial y}\left(\mu_{eff}\frac{\partial u}{\partial y}\right)+S_x \quad \text{(circumferential)} \quad [IV.1.5]$$

$$0=-\frac{\partial P}{\partial y}+\rho g_y+S_y \qquad \text{(radial)}\ [IV.1.6]$$

where x,y,z are respectively the radial, circumferential and axial directions and u, v,w the relative velocity components.

The equations were integrated numerically by assuming a symmetrical film at the inlet and imposing the dimensions of the domain of integration exactly as those in the experimental apparatus employed in the present work and described in III.2.1. Particular attention was devoted to the generation of the mesh around the T-junction to closely simulate the sharp edged corners.

This is thought to be the first time that annular flow in a non-trivial geometry has been predicted in such a mechanistic way. The predictions were compared with data obtained in the present work for the same flow configuration and conditions. Particularly for case c) presented in chapter III (U_{gs} =24.5 m/s and U_{ls} = 0.278 m/s), the results in terms of film distribution in the three legs of the T and flow split are presented in Figures IV.1.2-5.

In terms of film thickness distribution, the model generally over-predicts the present findings (Figure IV.1.2). The transition to the thin film towards the top of the pipe is sharper than predicted. However, some interesting trends are reproduced. In Figure IV.1.3, the film distribution as predicted at the run outlet, shows the characteristic thicker film at the corner of the T, between 100-150°. The model also succeeds in predicting the double peak showed by the measurements in the side arm (Figure IV.1.4). Particularly, the first peak, between 100-150° is successfully located. However, the model shows some features that were not measured. The other peak, between 250-300^0 seems to correspond to the small peak as described also in section III.3.8 and Figure III.3.14. It is observed that the hypothesis of boundary layer at sharp bends is not valid and this is another possible reason why predictions in the side arm give place to unobserved features.

Finally, the split curve obtained by integration of the velocity profiles, shows good agreement with the measured characteristic for the specific case, although this gives place to very small variations of fraction of diverted liquid (L').

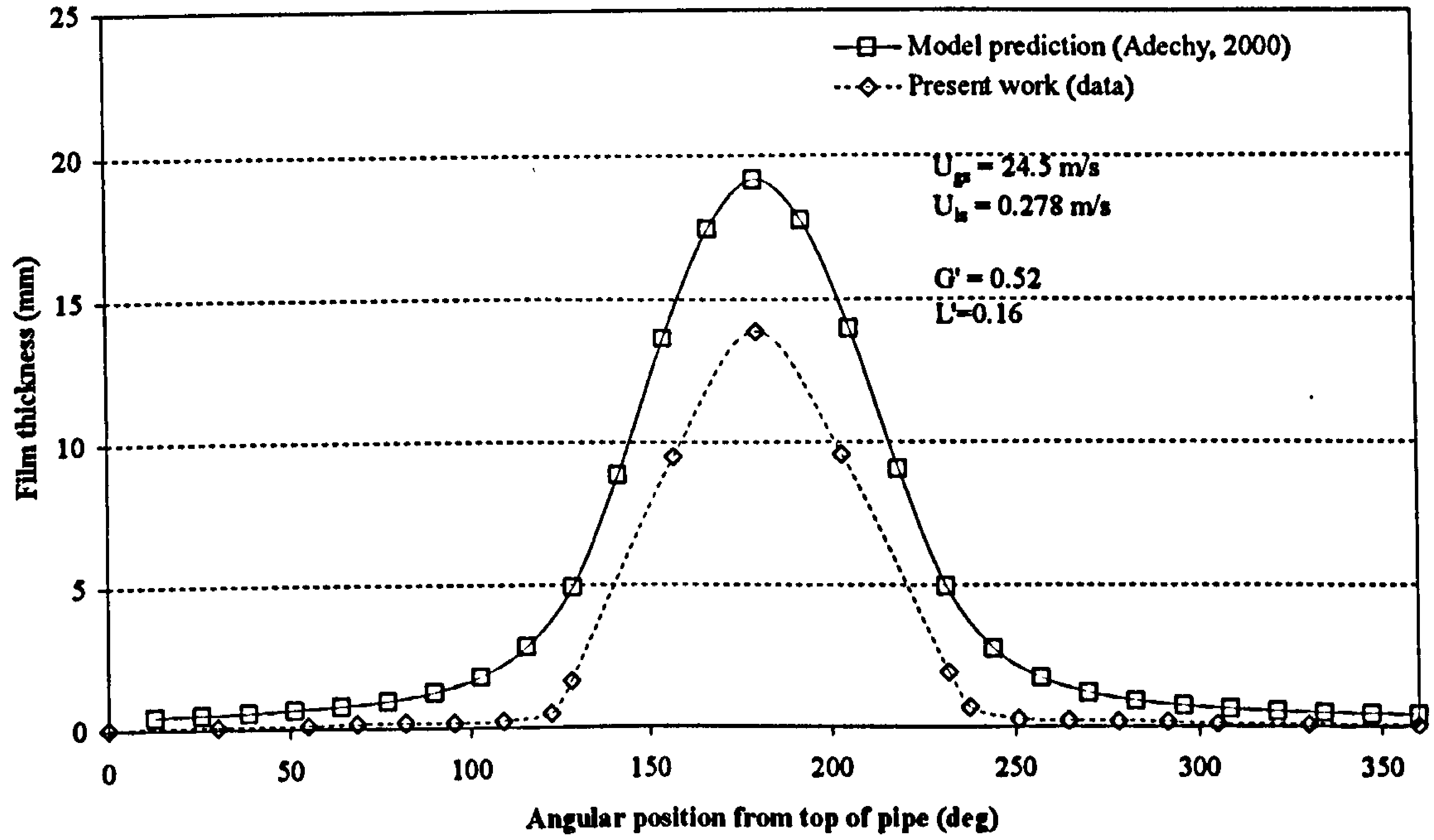

Figure IV.1.2: *Film distribution in the inlet leg. Comparison of model by Adechy (2000) and present work, for the inlet conditions of case c U_{gs} = 24.5 m/s, U_{ls} = 0.278 m/s and split conditions of (G',L')=(0.52,0.16).*

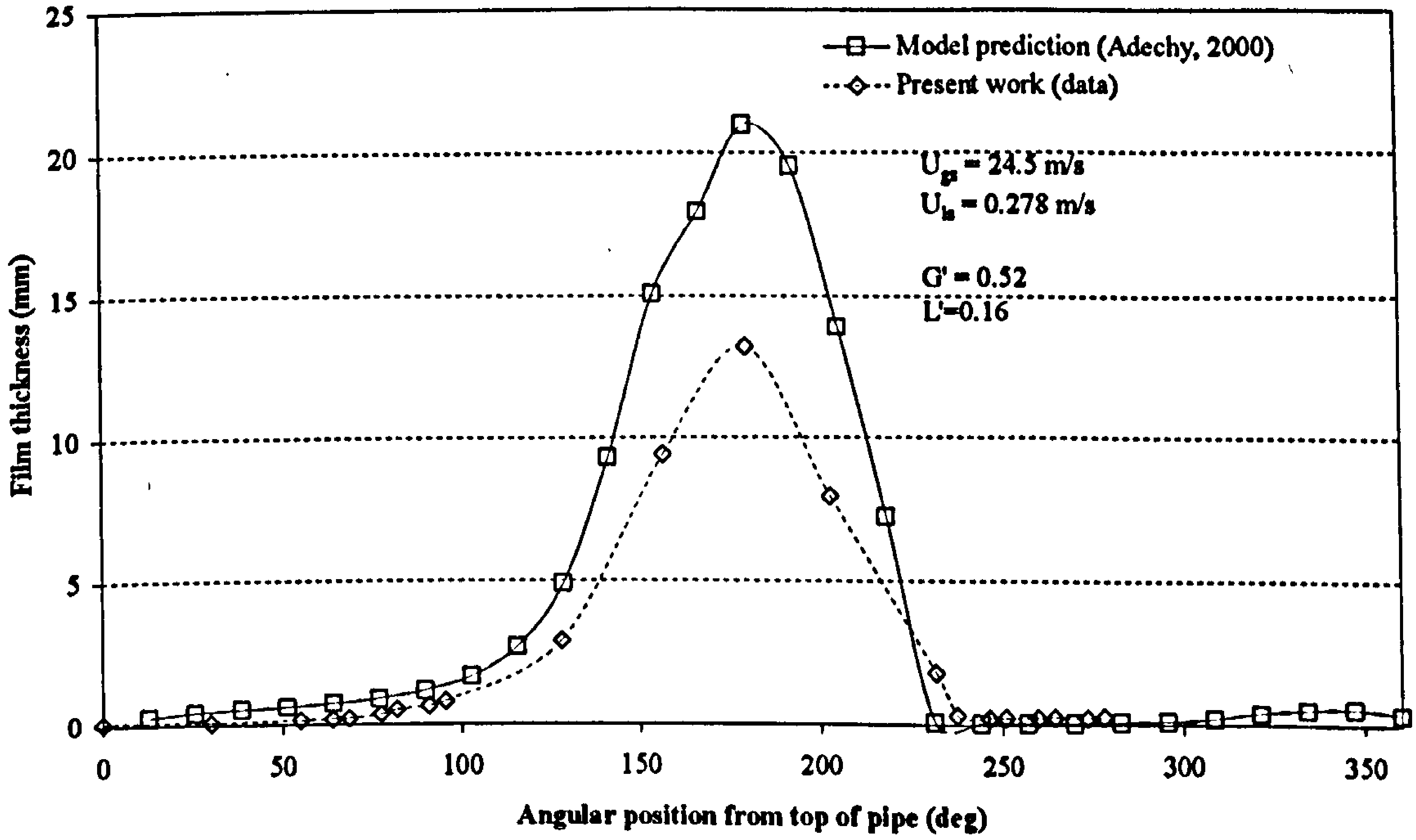

Figure IV.1.3: *Film distribution in the run arm. Comparison of model by Adechy (2000) and present work, for the inlet conditions of case c U_{gs} = 24.5 m/s, U_{ls} = 0.278 m/s and split conditions of (G',L')=(0.52,0.16).*

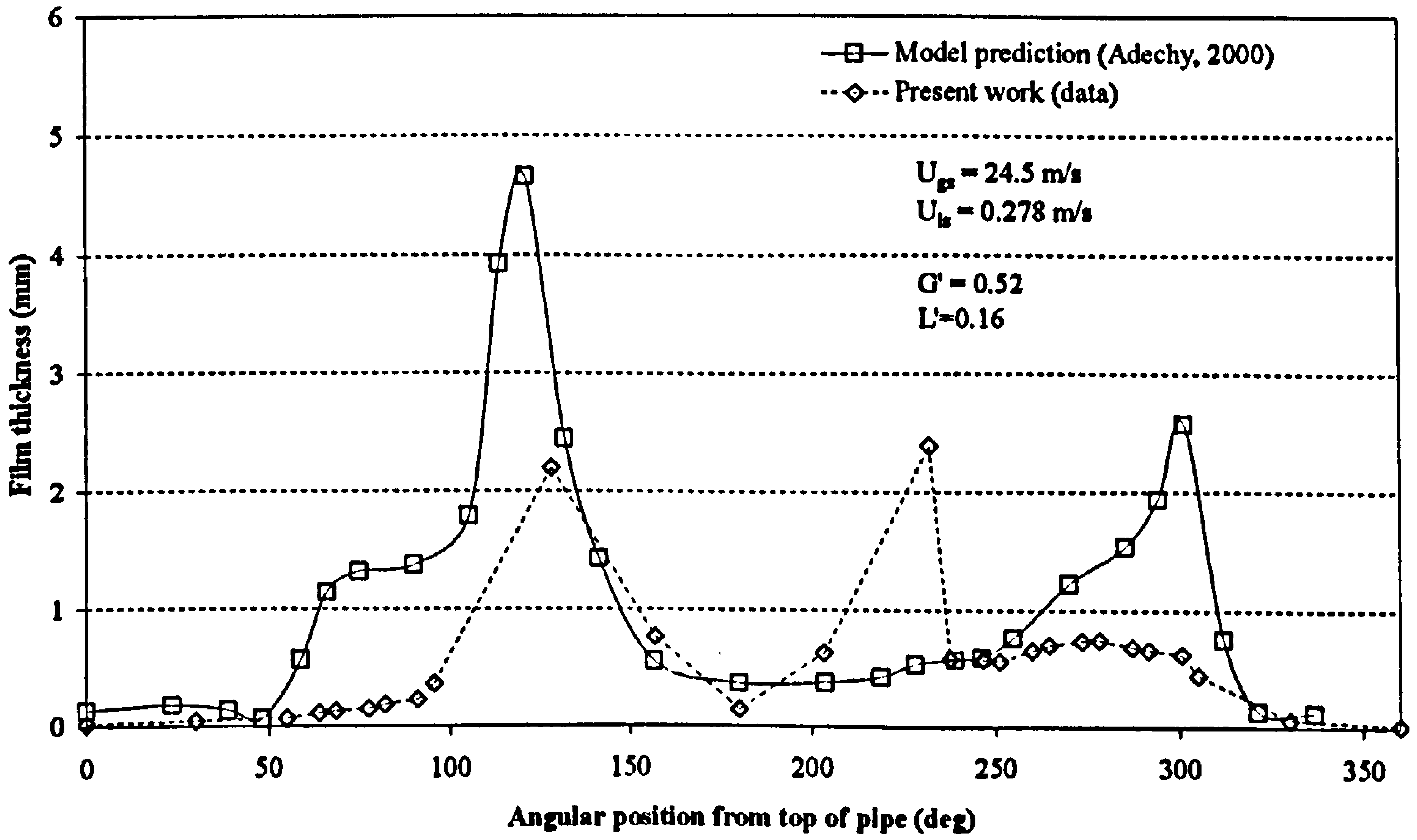

Figure IV.1.4: *Film distribution in the side arm. Comparison of model by Adechy (2000) and present work, for the inlet conditions of case c* $U_{gs} = 24.5$ *m/s,* $U_{ls} = 0.278$ *m/s and split conditions of (G',L')=(0.52,0.16).*

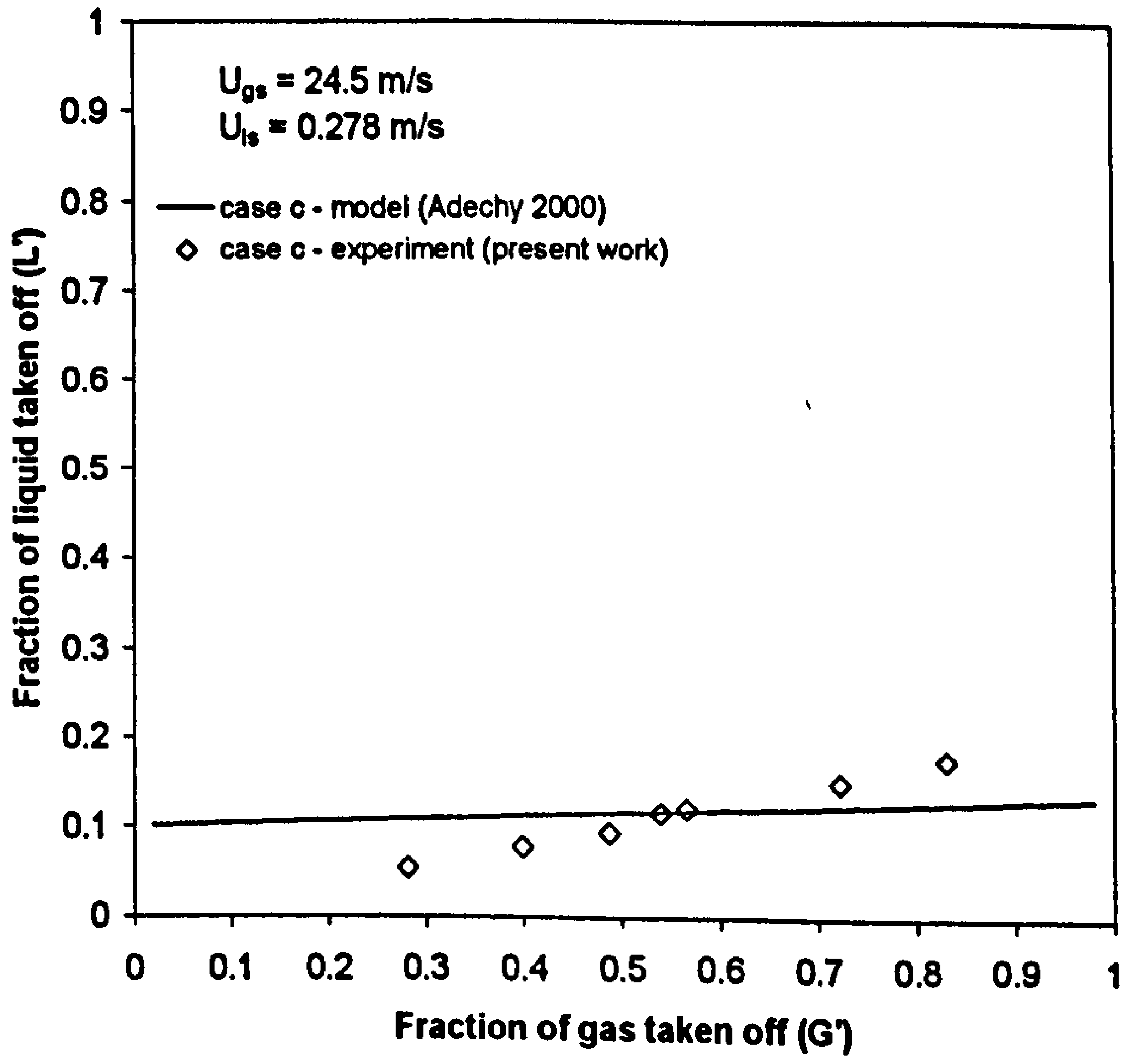

Figure IV.1.5: *Comparison of model by Adechy (2000) and present work, for the inlet conditions of case c* $U_{gs} = 24.5$ *m/s,* $U_{ls} = 0.278$ *m/s. Split data.*

IV.2 Comparison with the model by Hurlburt and Newell (2000).

The model developed by Hurlburt & Newell (2000) for the prediction of annular flow in a horizontal pipe is reported in section II.3.2. Briefly, it is a simplification of the model of Laurinat *et al* (1985) by neglecting the dispersion term against the axial shear, the effect of entrainment and deposition and the effect of hydrostatic pressure due to film thickness variation against the normal stress in the circumferential direction. The problem of circumferential film distribution is reduced to the solution of the differential equation, in dimensionless terms:

$$-\frac{\tau_{xx,max}}{18}\exp\left(-\frac{h^+-6}{18}\right)\frac{dh^+}{d\bar{x}}-\frac{1}{Fr}\sin\bar{x}=0 \qquad [IV.2.1]$$

h^+ is the film non-dimensional film thickness and $\bar{x}$ is the anticlockwise angle relative to the flow direction.

Equation IV.2.2 can be solved analytically for h^+ and the solution depends on the boundary condition given by the dimensionless film thickness at the pipe bottom h_o^+:

$$\frac{h^+-6}{h_o^+-6}=\frac{\ln[\alpha-\beta(\cos\bar{x}-1)]}{\ln\alpha} \qquad [IV.2.2]$$

where:

$$h^+=\frac{h}{\nu_l}\left(\frac{\tau_s}{\rho_l}\right)^{0.5} \qquad [IV.2.3]$$

$$\alpha=\exp\left(-\frac{h_o}{12}\right) \qquad [IV.2.4]$$

$$\beta=\frac{1}{\tau_{xx,max}Fr_{\tau_s}} \qquad [IV.2.5]$$

$$Fr_{\tau_s}=\frac{\tau_s}{\rho_l gR} \qquad [IV.2.6]$$

and τ_s is the shear for single phase flow of the gas in a smooth tube, used to render the equations non-dimensional:

$$\tau_s = 0.023 \mathrm{Re}_{gs}^{-0.2} \rho_g U_{gs}^2 \qquad [\mathrm{IV.2.7}]$$

The other equation needed is the mass balance for the liquid phase:

$$\dot{m}_{lf} = \dot{m}_l - \dot{m}_{lE} \qquad [\mathrm{IV.2.8}]$$

were the subscripts l, f and E refer respectively to liquid, film and entrained quantities and the entrained fraction is considered a known parameter. The local average liquid velocity is correlated and depending on the film thickness. Hence, its determination is coupled to the solution of equation IV.2.1.

Rather than by imposing the film thickness at the bottom, the problem is closed by implementing an empirical correlation for the symmetry parameter h_{avg}/h_o. This is correlated to the dimensionless number $(\dot{m}_g/\dot{m}_l)^{0.5}\mathrm{Fr}$. Here, h_{avg} is the average film thickness:

$$h_{avg} = \frac{1}{\pi}\int_0^{\pi} h(\bar{x})d\bar{x} \qquad [\mathrm{IV.2.9}]$$

and the empirical correlation proposed by Hurlburt and Newell (2000) is:

$$\frac{h_{avg}}{h_o} = \frac{4}{3\pi}\left(\frac{h_o}{D}\right)^{0.5} + 0.9\left[1 - \exp\left(-\frac{(\dot{m}_g/\dot{m}_l)^{0.5}\mathrm{Fr}}{90}\right)\right] \qquad [\mathrm{IV.2.10}]$$

Hence, once the inlet conditions are given, fixed a value for h_o, the value of h_{avg}/h_o is calculated through equation IV.2.8 and, because a theoretical expression of this ratio can be obtained from IV.2.9, depending on $\tau_{xx,max}$, the value of this constant can be found for any fixed h_o. The film distribution is finally given by IV.2.2, for the value of h_o that verifies the mass balance (equation IV.2.8), once the axial shear stress correlation and the average axial velocity correlation are implemented. Also, a model for the entrained fraction is needed to carry out the mass balance on the liquid and the correlation of Dallman was used in the specific case.

It must be pointed out that the model works for values of $h^+>6$, that is, when disturbance waves occur. For smaller values of h^+ it is not the normal Reynolds stress due to circumferential flow fluctuations (τ_{xx}) that is responsible for the presence of the film around the pipe against gravity, but the effect of entrainment and deposition. However, for simplicity, below $h^+ = 6$ integration was stopped and a constant, minimum value of h imposed for the remaining section of pipe circumference.

To discuss the results of this model, when compared to the data presented in Chapter III, we can refer to the same case c) of the previous section ($U_{gs} = 24.5$ m/s, $U_{ls} = 0.278$ m/s). When this model is tried for the inlet conditions of the present work, the presence of a 'cusp' at the bottom of the pipe, in the film thickness prediction is observed. The plot of Figure IV.2.1, on the pipe circumference shows this.

More precisely, the model gives inherently a zero derivative of $h(\bar{x})$ for $\bar{x}=0$ (pipe bottom). It is the second derivative at $\bar{x}=0$ that is negative and very large in its absolute value. Proper cusps are observed in mass transfer dominated models such as Fisher and Pearce (1978) and have been discussed by James *et al* (1987) and Roberts (1994). However, in the present case, the anomaly is caused by the hypothesis that the effect of static pressure in the liquid film, due to the film thickness variation, is negligible. Such a term appears in the momentum equation in the circumferential direction in the form:

$$-\frac{1}{a^+ Fr_{\tau_i}} \cos\bar{x} \frac{dh^+}{d\bar{x}} \qquad [IV.2.11]$$

and is indeed negligible when the film distribution is smooth, that is when $dh^+/d\bar{x}$ is small. In the case of the present work, all data were produced in the semi-annular flow regime. For such conditions, the sudden transition from the liquid pool at the bottom to the very thin film on the sides of the pipe circumference, gives place to values of $dh^+/d\bar{x}$ that are not negligible. Hence, the problem has been solved for the circumferential momentum balance:

$$-\frac{\tau_{xx,max}}{18}\exp\left(-\frac{h^{+}-6}{18}\right)\frac{dh^{+}}{d\bar{x}}-\frac{1}{Fr_{\tau_s}}\sin\bar{x}-\frac{1}{a^{+}Fr_{\tau_s}}\cos\bar{x}\frac{dh^{+}}{d\bar{x}}=0 \qquad [IV.2.12]$$

where the first term on the RHS is the normal stress, in the circumferential direction containing the model for τ_{xx} as proposed by Hurlburt & Newell (2000), the second term is due to the gravitational pull and the third is the new term due to static pressure variation. No analytical solution can be found for this problem and it was solved numerically giving place to the result shown in Figure IV.2.2 for case c). There, the prediction of the original model of Hurlburt & Newell (2000) is also plotted with the experimental data. It is evident that by introducing the above term, qualitative and quantitative prediction is much closer for this case, even showing the slight peak at the pipe bottom. Also, the progressive thinning of the film towards the top is well featured by the prediction.

In addition, the model of Azzopardi and Whalley (1982) as developed by Roberts *et al* (1997) is used for the prediction of phase split. This employs the concept whereby it is only the liquid from the film that is taken off into the side arm and that both phases are taken off from a common segment of the pipe area. The model is used including the possibility of the occurrence of film stop in the run arm. However, this never occurred for the conditions employed both from observation and modelling.

This approach was employed by Azzopardi and Rea (1999) to predict the split data of Roberts *et al* (1995, 1997) by using a previous version of the annular flow model presented above, Hurlburt (1997). Also, in that case, rather than using the symmetry correlation, an empirical correlation for the film thickness at the bottom of the pipe was used. However, this gave very unrealistic predictions for the present data.

Once the results of the annular flow model are fed to the split model of Roberts *et al* (1997) results for case c) appears as shown in Figure IV.2.3 where the prediction both with and without the component due to static pressure are plotted. The former gives better results also in terms of split of the phases and its quality is comparable to that of CFD predictions from Adechy (2000).

In Figures IV.2.4-5 are shown the results from the remaining five cases that were investigated, for the film thickness distribution and the effect of gas and liquid flow rates upon it. Comparison is not as good as for case c). In particular, the effect of liquid flow rate is predicted to be much stronger than measured. For case a), the thickness at the bottom is of 35 mm against the 16 mm measured and whilst comparison for case b) is reasonable, the results from case d) show an under prediction of the film thickness. The plot in Figure IV.2.5 shows the correct trend and magnitude for the effect of gas superficial velocity upon the film distribution. However, calculation suggests a smaller film thickness than measured, especially at the bottom. There are a number of reasons why the predictions could be incorrect:

1) The model assumes fully developed distribution and in the case of the experiments, for L/D~31 this is certainly not so.
2) The model is predicting a thickness at the bottom that is almost 30% of the pipe diameter. This is certainly not within the hypothesis of thin film.
3) The shear stress and average axial film velocity correlations employed are obtained for the case of vertical annular flow (Asali *et al*, 1985; Henstock and Hanratty, 1976) and so is the correlation of Dallman *et al* (1984) for the entrained fraction.
4) No mechanism of pumping action of the waves is considered. If this effect was accounted for, this would be expected to influence the film distribution in the sense of a more symmetrical film as the liquid flow rate increases and as is observed through cases d),b) and a)

With regard to the achievement of fully developed conditions, the way the inlet was designed is relevant. Although liquid at the inlet was introduced via a section of porous pipe wall in the attempt to create a uniform film around the pipe circumference, heavy splashing was observed at the inlet, especially for the largest liquid flow rates. For the lowest liquid flow rate liquid appeared more uniform around the pipe wall. In this respect, it is significant that case c), which gives the best comparison between data and predictions is also the case (Figure III.3.28) where the least degree of re-distribution of the liquid between the feed and the section before the T is measured. Probably, in all cases, steady state entrainment and deposition was not reached either.

With regard to the correlations used for the interfacial shear stress, it was observed from experiments that a very intense wave activity took place, especially at the pipe bottom. This suggests that τ_i could be larger than imposed in the model. However, the correlation of Andritsos and Hanratty (1987), produced for stratified flow in a 0.0953m ID pipe was also tested for this purpose without significant improvement in the prediction. Also, the film distribution depends on the correlation used for the average axial velocity in the film and the empirical fits of Henstock and Hanratty (1976) and Asali *et al* (1985) were produced for vertical pipes too.

It is interesting that the model is over-predicting the film thickness at large liquid flow rates and under-predicting at the lowest. This would suggest a much larger sensitivity of interfacial stress to inlet conditions.

With regard to the correlation for entrained fraction, it is significant that, even assuming zero entrainment, the model under-predicts the film thickness at the lowest liquid velocity (0.136 m/s). This reinforces the idea that the aspect to be corrected is that related to interfacial shear/average axial velocity. Certainly, the entrainment and interfacial shear are coupled as a larger interfacial shear enhances the phenomenon of entrainment. Not so in the model, where the entrained fraction of Dallman *et al* (1984) is only a function of inlet flow rates. Table IV.1 resumes inlet conditions and the entrained fraction as predicted by Dallman *et al* (1984) and implemented in the model.

Table IV.1: *Inlet superficial velocities and entrained fraction according to Dallman et al (1984)*

Case	U_{gs} (m/s)	U_{ls} (m/s)	E (Dallman *et al*)
a)	16.5	0.550	0.088
b)	16.5	0.278	0.087
c)	24.5	0.278	0.36
d)	16.5	0.136	0.083
e)	23.0	0.136	0.29
f)	28.1	0.136	0.49

Finally, both measurements and modelling are affected by the implicit assumption that the liquid film does not entrain gas. The entrainment of gas in the liquid film was experimentally observed by Hewitt *et al* (1990) and it could well be

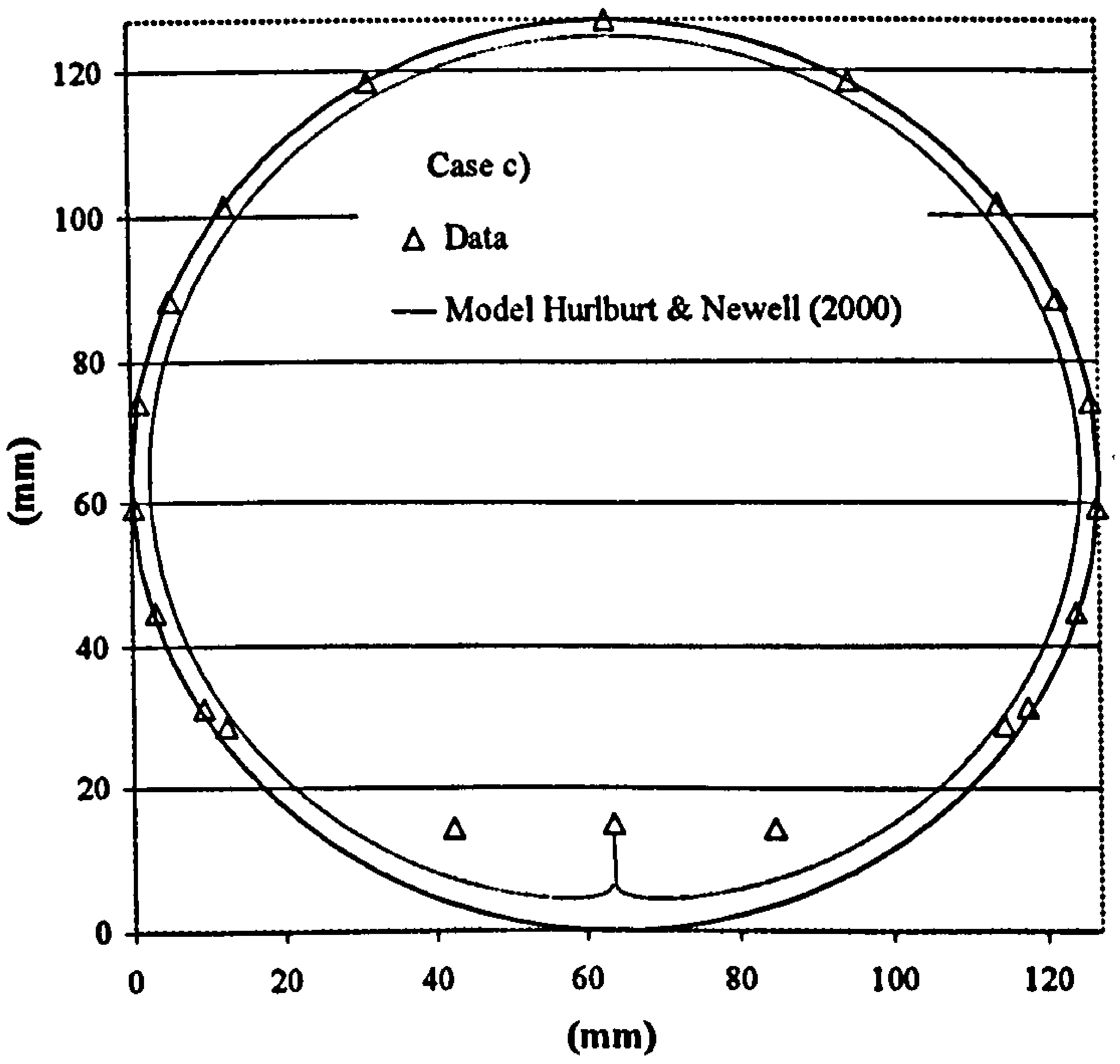

Figure IV.2.1: *Film distribution in the inlet leg. Comparison of present data with the prediction of the model by Hurlburt & Newell (2000), for the inlet conditions of case c* U_{gs} *= 24.5 m/s,* U_{ls} *= 0.278 m/s.*

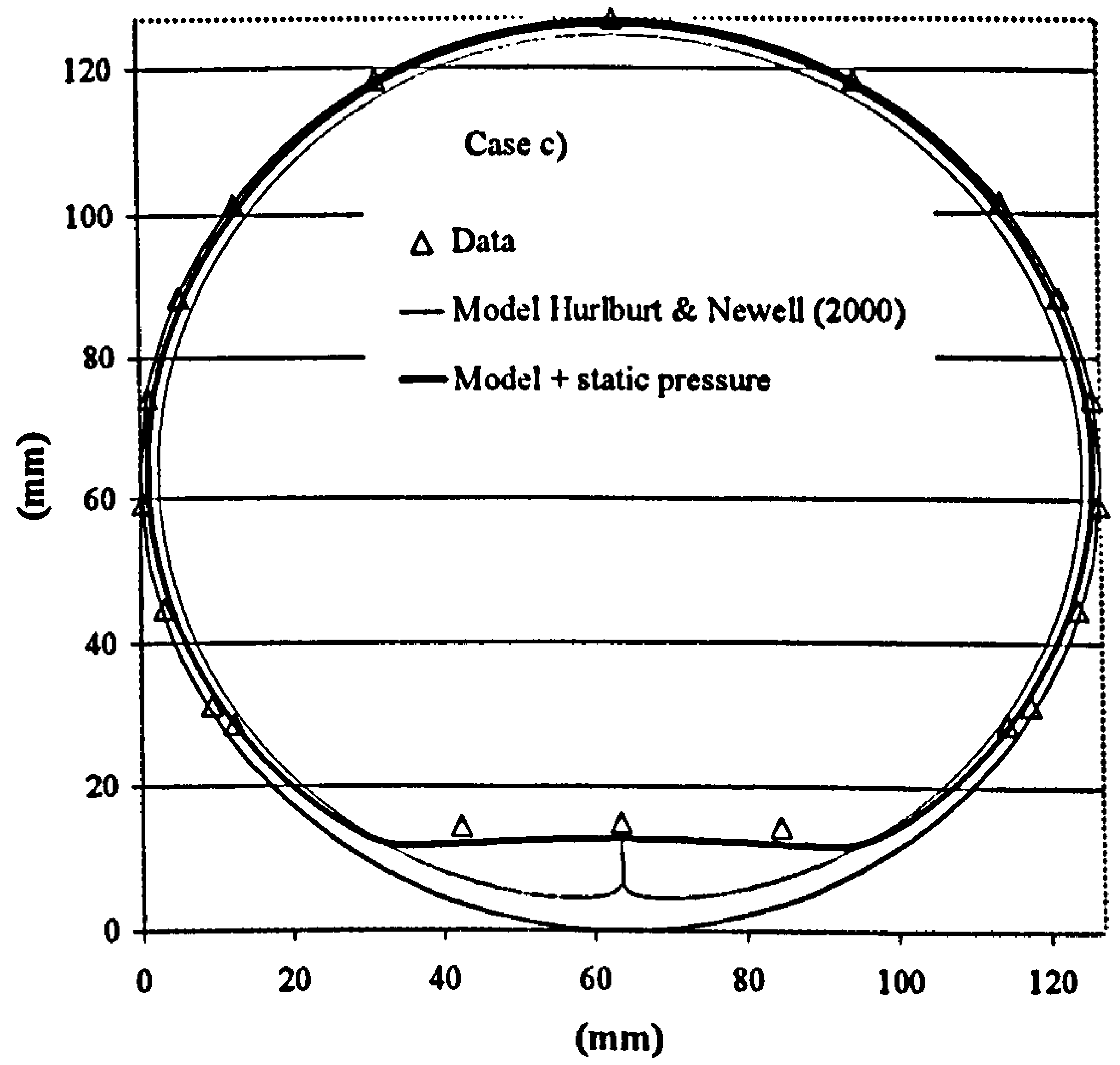

Figure IV.2.2: *Film distribution in the inlet leg. Comparison of present data with the prediction of the model by Hurlburt & Newell (2000) enhanced by the presence of static pressure term, for the inlet conditions of case c* U_{gs} *= 24.5 m/s,* U_{ls} *= 0.278 m/s.*

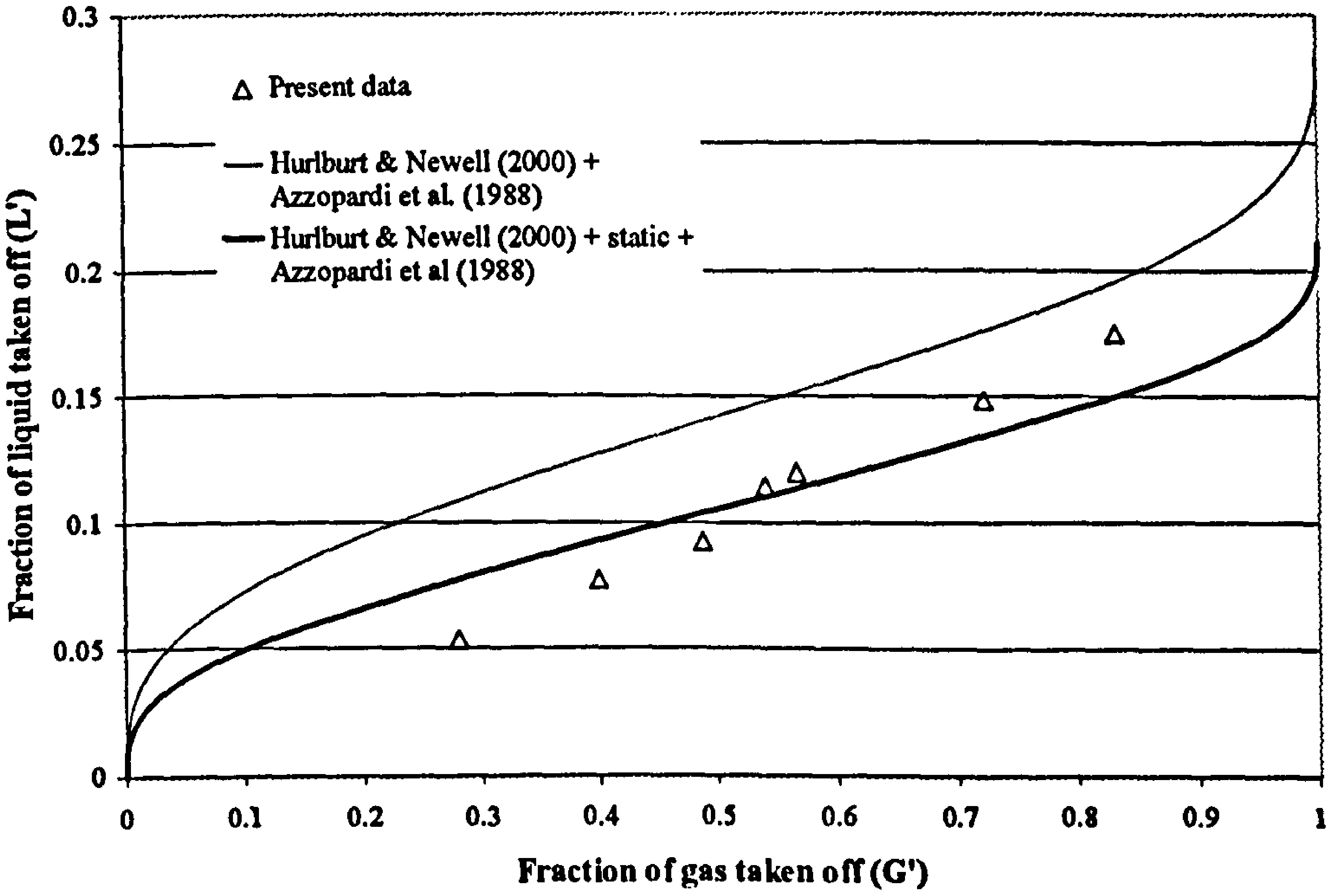

Figure IV.2.3: *Split diagram. Comparison of present data with the model by Roberts et al (1997) when annular flow of Hurlburt and Newell (2000) with or without static pressure term and the entrained fraction of Dallman et al (1984) are imposed. Case c):* U_{gs} *= 16.5 m/s;* U_{ls} *= 0.278 m/s.*

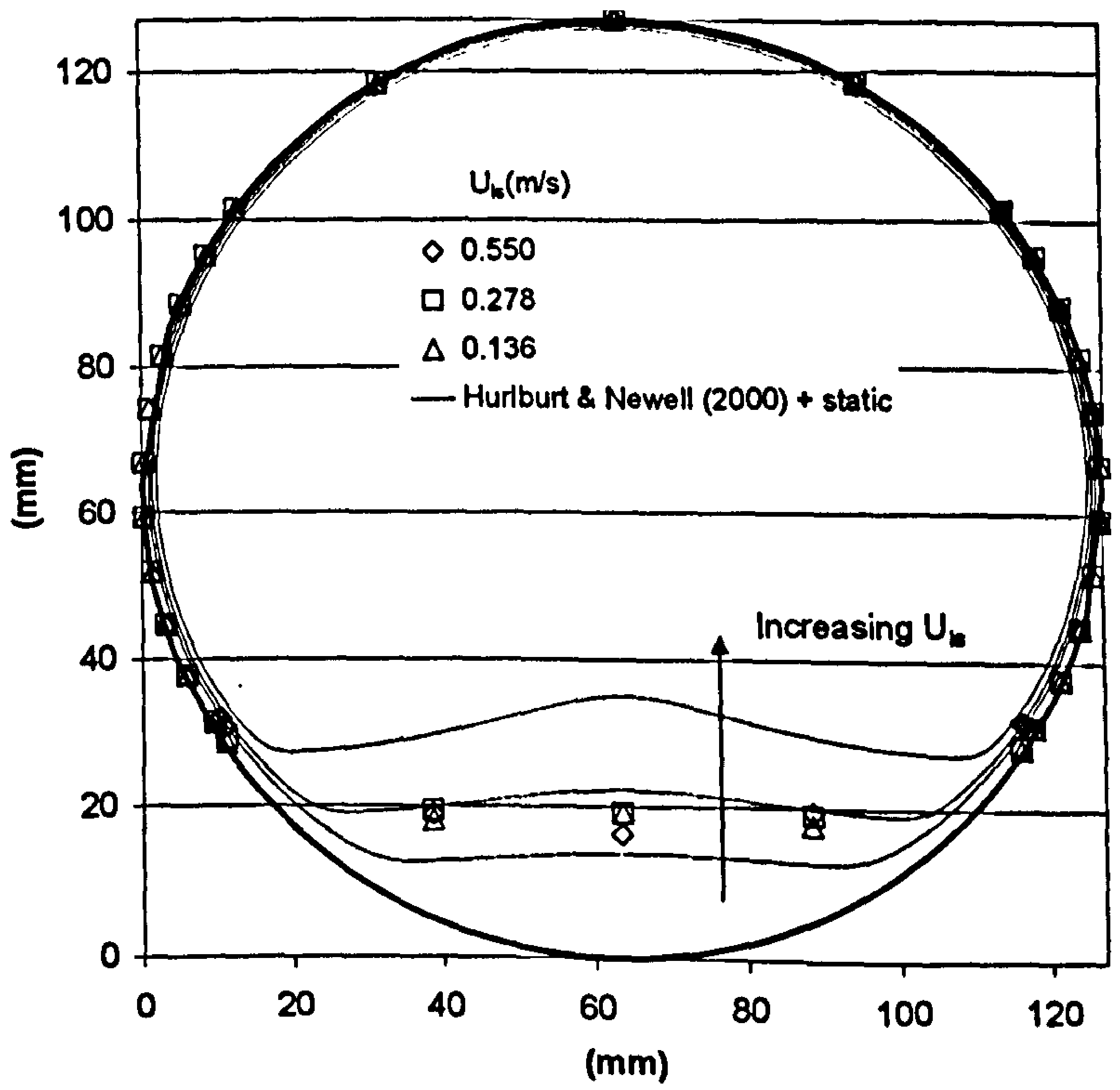

Figure IV.2.4: *Film distribution in the inlet leg. Comparison of present data with the model by Hurlburt and Newell (2000) including static pressure term for varying* U_{ls}*. Cases a), b) and d).* U_{gs} *= 16.5 m/s,* U_{ls} *= 0.55, 0.278, 0.136 m/s.*

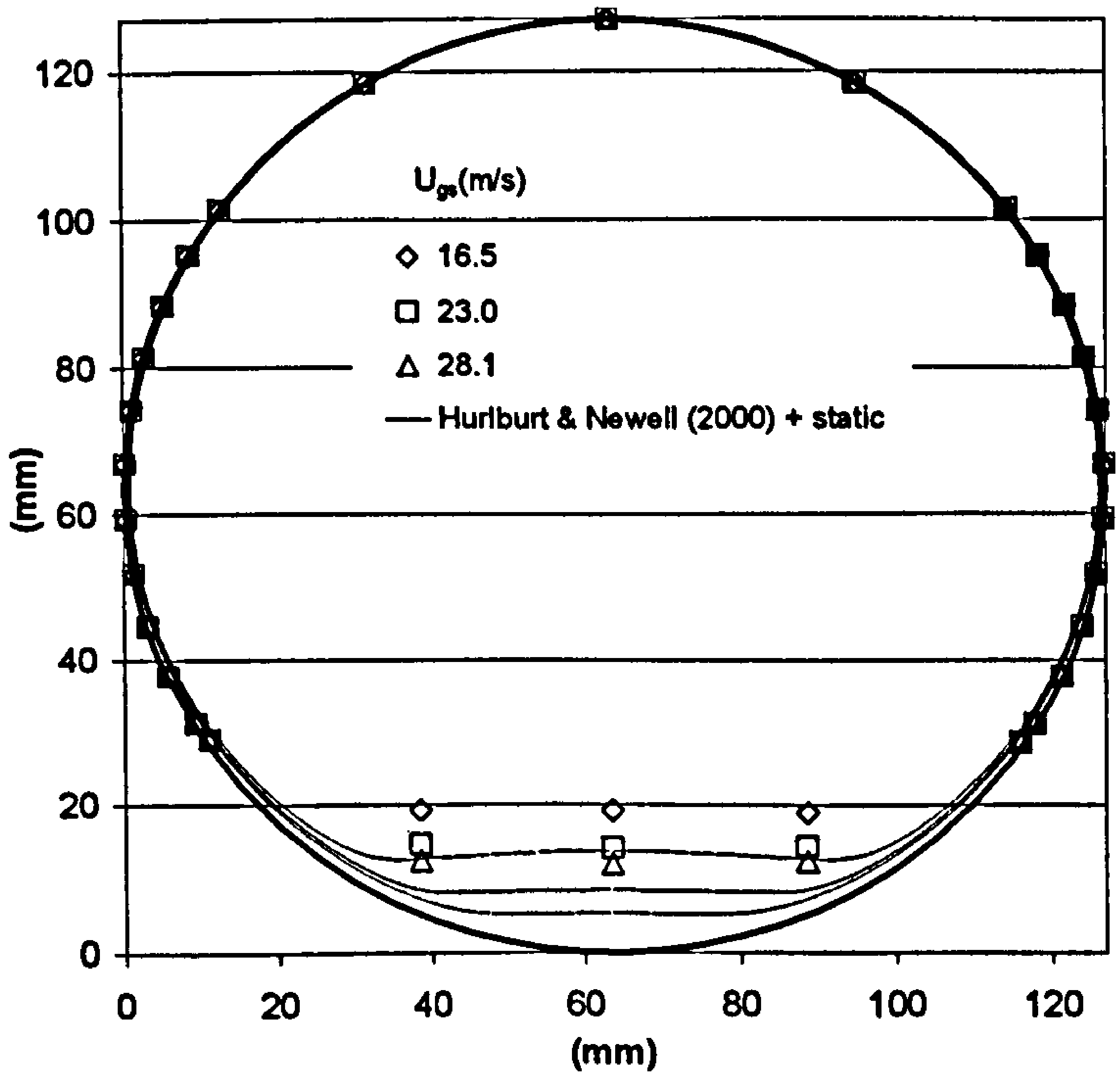

Figure IV.2.5: *Film distribution in the inlet leg. Comparison of present data with the model by Hurlburt and Newell (2000) including static pressure term for varying* U_{ls}*. Cases a), b) and d).* $U_{ls} = 0.136$ *m/s,* $U_{gs} = 16.5, 23.5, 28.1$ *m/s.*

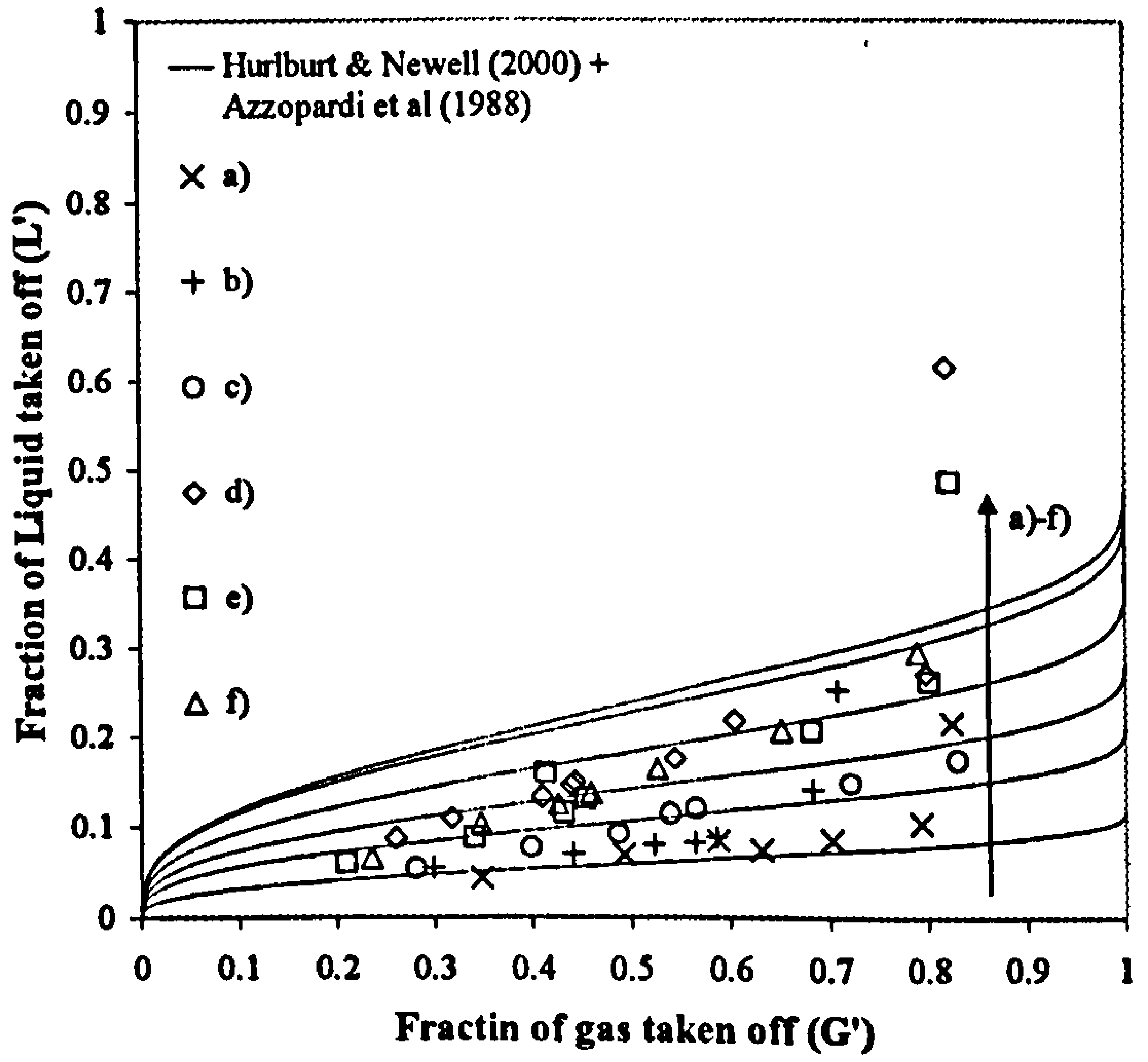

Figure IV.2.6: *Split diagram. Comparison of present data with the model by Roberts et al (1997) when annular flow of Hurlburt and Newell (2000) and the entrained fraction of Dallman et al (1984) are imposed.*

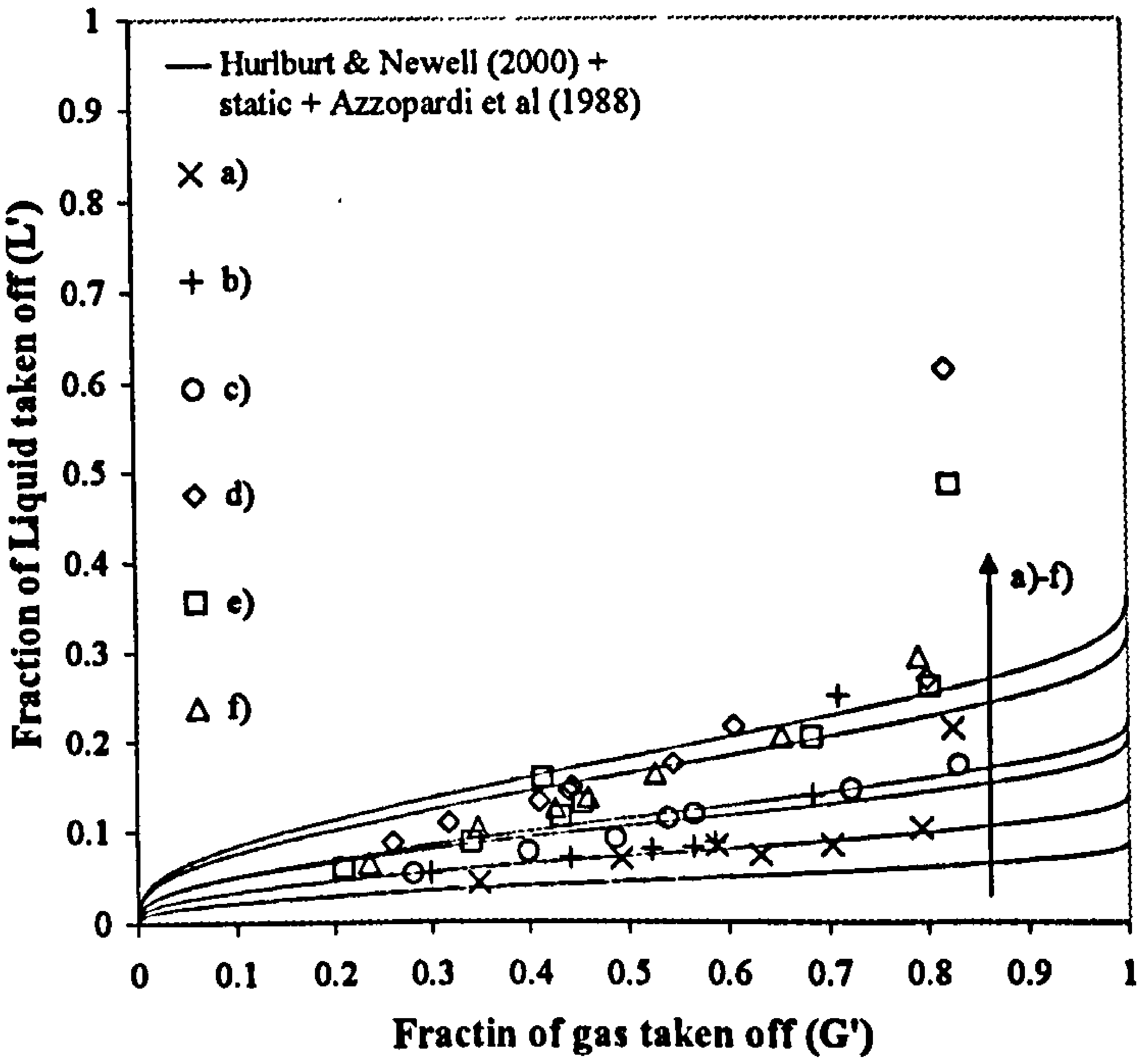

Figure IV.2.7: *Split diagram. Comparison of present data with the model by Roberts et al (1997) when annular flow of Hurlburt and Newell (2000) with static pressure term and the entrained fraction of Dallman et al (1984) are imposed.*

significant in the present case, given the extent of wave activity at the interface. In fact, it was observed in most cases, especially for large liquid flow rate.

Figures IV.2.6 and 7 show the improvement brought about by including the static pressure term in the annular flow model, when the split prediction using Roberts *et al* (1997) is compared to the present database. The predictions of Figure IV.2.7, including static pressure, better cover the split data, although not all features are correct. Particularly, at large gas take off, the data move very steeply towards total diversion to the side arm (point (1,1)). Observation proved that this phenomenon is due to secondary liquid take off occurring when a hydraulic jump, formed in the run leg, approaches the T-junction and liquid is entrained from it and extracted to the side arm. This is in some ways analogous to the secondary take off that will be largely discussed in chapter V.

Chapter V

Slug/Churn flow splitting at a vertical T-junction

Introduction

This chapter presents the results of experiments carried out in a vertical regular T-junction with horizontal side arm. All pipes were 0.076 m ID. For this geometry, split experiments were performed in the slug/churn flow regime, for two lengths of the run leg (1.9 and 0.7 m).

As already mentioned in section II.6, unlike in the case of annular (Azzopardi and Whalley, 1982) and bubbly flow (Issa and Oliveira, 1994), little effort has been devoted to propose an explanation for the split of gas/liquid mixtures at T-junctions when slug flow travels in the inlet pipe. Likewise, churn flow has been treated as a special case of annular flow (Lahey *et al.*, 1985) resulting in coarse predictions in the low take off region. For this reason, in addition to the experimental data, both for the case of slug and annular flow, an explanation of observed phenomena and semi-empirical correlations are produced to fit the present database.

Section V.1, contains a description of the apparatus and the results of experimental tests. Section V.2 is dedicated to the discussion of results and analysis of data including a correlation for the prediction of the split characteristic in slug flow.

V.1 Two-phase flow split

V.1.1 Experimental apparatus and procedure

The experiments described in this chapter were carried out on a facility which has parts in common with that described in section III.2.1 and very similar to it (Figure V.1.1). The system was constructed of acrylic pipes of 0.076 m ID with a wall thickness of 0.003 m. These are connected to the T-piece, which is machined out of an acrylic resin cube. The corners of the T where the side arm joins the main tube, are square edged (zero radius of curvature).

The arrangement for the feed and mixing of the phases is sketched in Figure V.1.2. Air was fed axially to the inlet pipe from the laboratory main (6 bar) and metered with calibrated orifice plates (0.0254 - 0.0127 m orifice diameter) coupled to a DP cell and a chart recorder. The gas flow passed through a cap with multiple holes through which air was fed to mix with the liquid.

By switching valves around the inlet to the horizontal rig, water was diverted to the bottom of the main pipe of the vertical T-junction rig. The water was delivered by the same set of pumps used in the horizontal apparatus. The liquid entered the mixing section through a lateral inlet and flowed through the annular gap between the inner surface of the inlet pipe and the cap. The devices described in section III.2.1 were used for metering liquid at the inlet. These are a bank of rotameters when the small pump was employed and a magnetic flowmeter for the larger flow rates delivered by the large pump.

Given the high pressure on the air side, the risk of liquid feed back to the air line was envisaged only in the shut down phase provided that the gas was fed first, in the start up procedure. A drain at the bottom of the mixing section ensures that minimum spillage of liquid into the air feed occurs at shut down. Gas flow rate was regulated by a gate valve, just before the mixing section in the high-pressure air line. The centre of the junction is 6 m (79D) downstream of the mixing section. The divided streams flow in the side arm for 1.1 m and in the run for 1.9 m before butterfly valves that control the resistances. A number of runs were also done with a reduced length of the vertical run arm of 0.7 m. Phase separators are placed at the extremities of the outlet branches. These were simple cylindrical vessels, 0.33 m diameter and 1 m tall. From the bottom of each separator, the liquid could either be returned to the storage tank or fed to a weigh tank mounted on a load cell for flow rate measurement via timed weighing. Air is discharged to the atmosphere after metering by calibrated orifice plates (0.0106, 0.0184 and 0.0318 orifice diameter).

The experimental procedure was the same as used for the horizontal T-junction and described in section III.2.2. Because the air was fed from the high-pressure line of the laboratory, it was possible to keep the set-point flow rate for all inlet conditions and the split characteristic could also be obtained for points close to

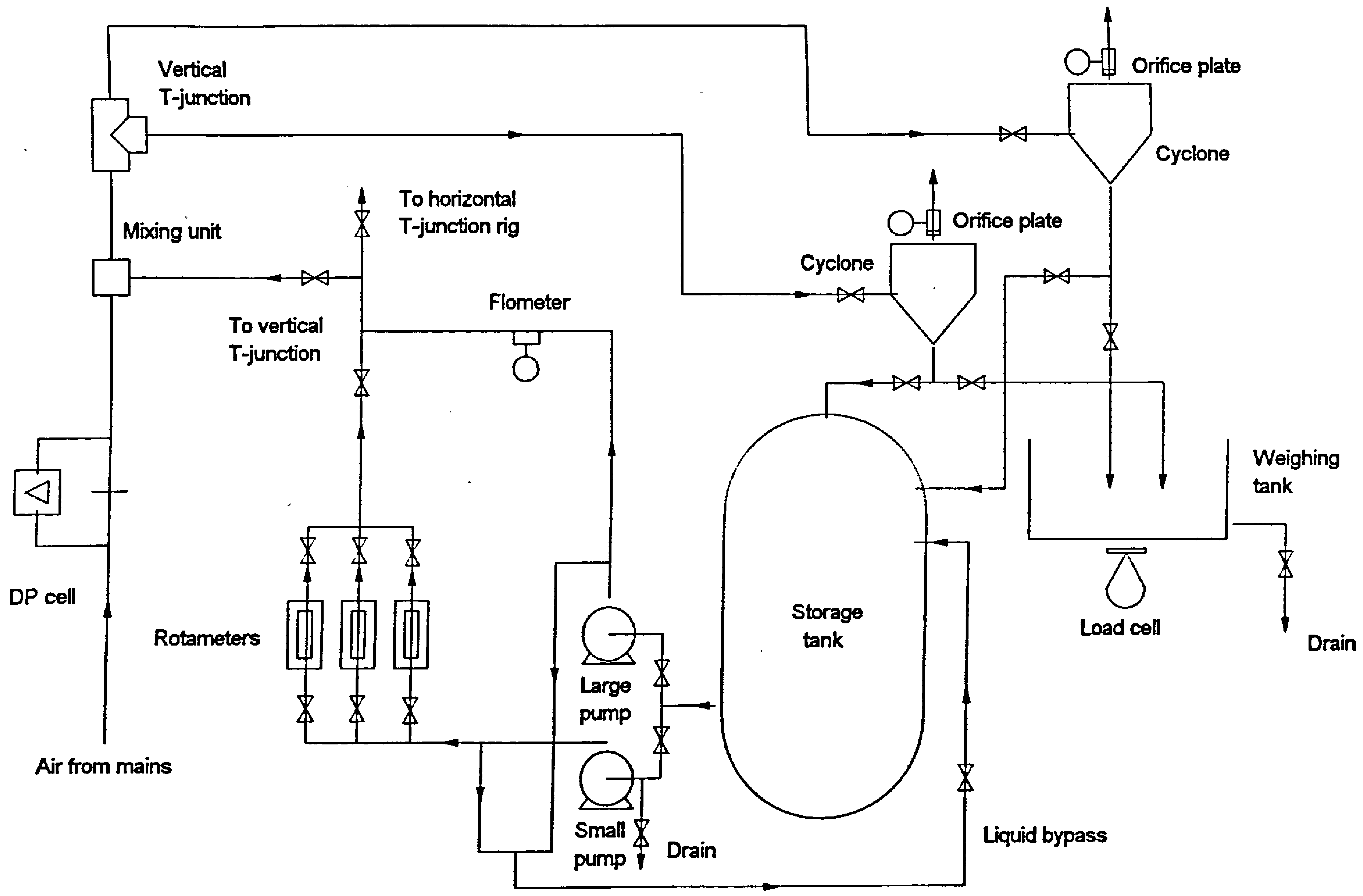

Figure V.1.1: *Sketch of the experimental apparatus for the vertical T-junction rig.*

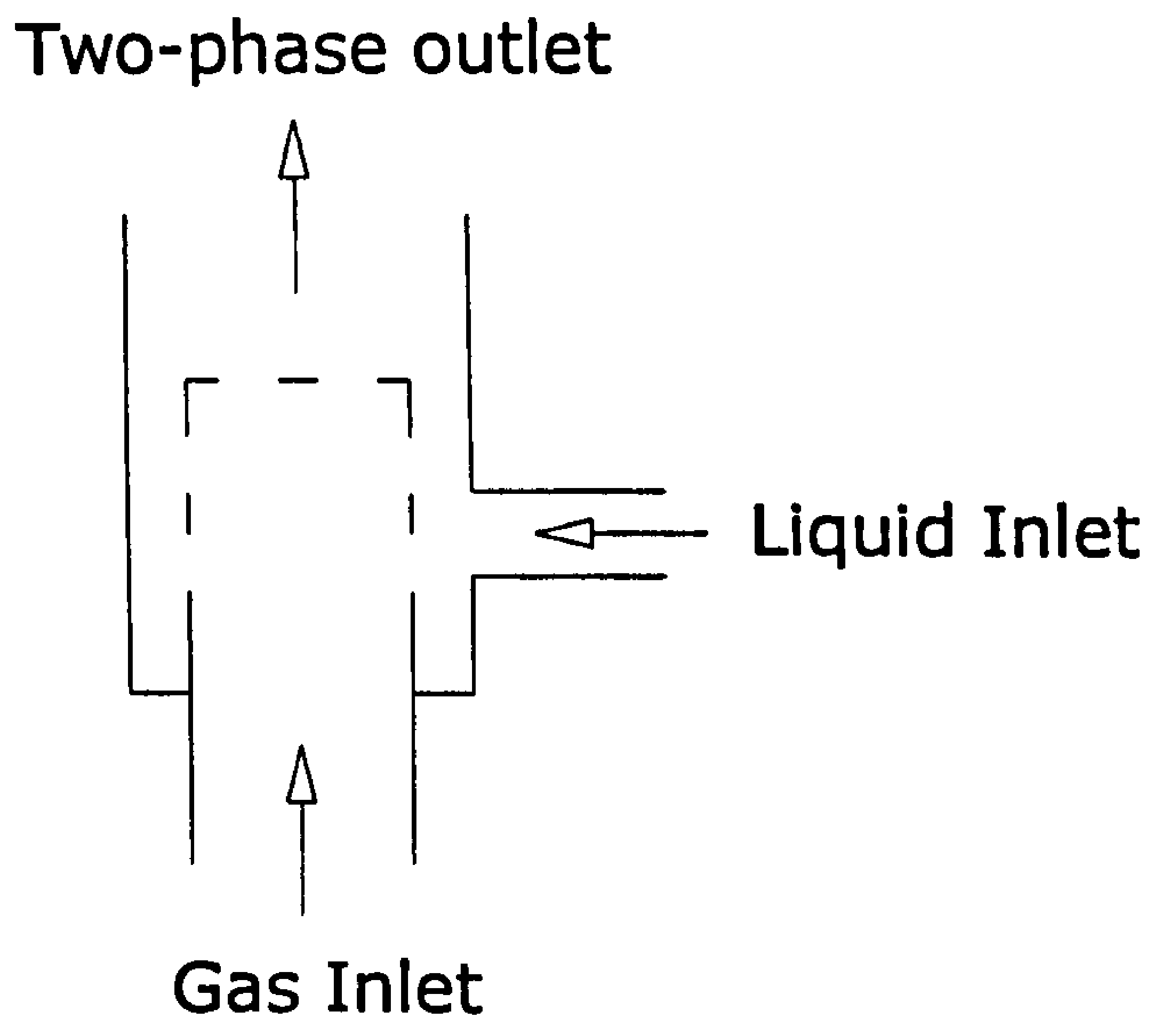

Figure V.1.2: *Sketch of the mixing section at the inlet to the main pipe.*

the extremes (0,0), (1,1). A measurement was considered satisfactory when the mass balance between the inlet and the two outlets was within 8% for the gas and 5% for the liquid phase with most data falling within 3% for the liquid and 6% for the gas.

V.1.2 Flow split results

A flow pattern map showing where data were taken is presented in Figure V.1.3, where the boundaries between flow patterns are those predicted by the model of Taitel *et al* (1980). The data shown in Figure V.1.3 are the result of an experimental programme carried out at the University of Nottingham since 1993 and still continuing. The data of series B and D have been produced in the present work. However, for a better understanding, data from series A and C will be presented in this section since physical interpretation and modelling are part of the present work and are presented in the remaining sections of this chapter.

Series A are the data reported by Azzopardi *et al* (1994) in the slug flow regime. A view of the observed trends is given in Figures V.1.4 a) and b). In all the database of series A, flow split is liquid dominated. Figure V.1.4 a), shows that there is no influence of the gas flow rate on the split of the phases for a liquid inlet flow rate

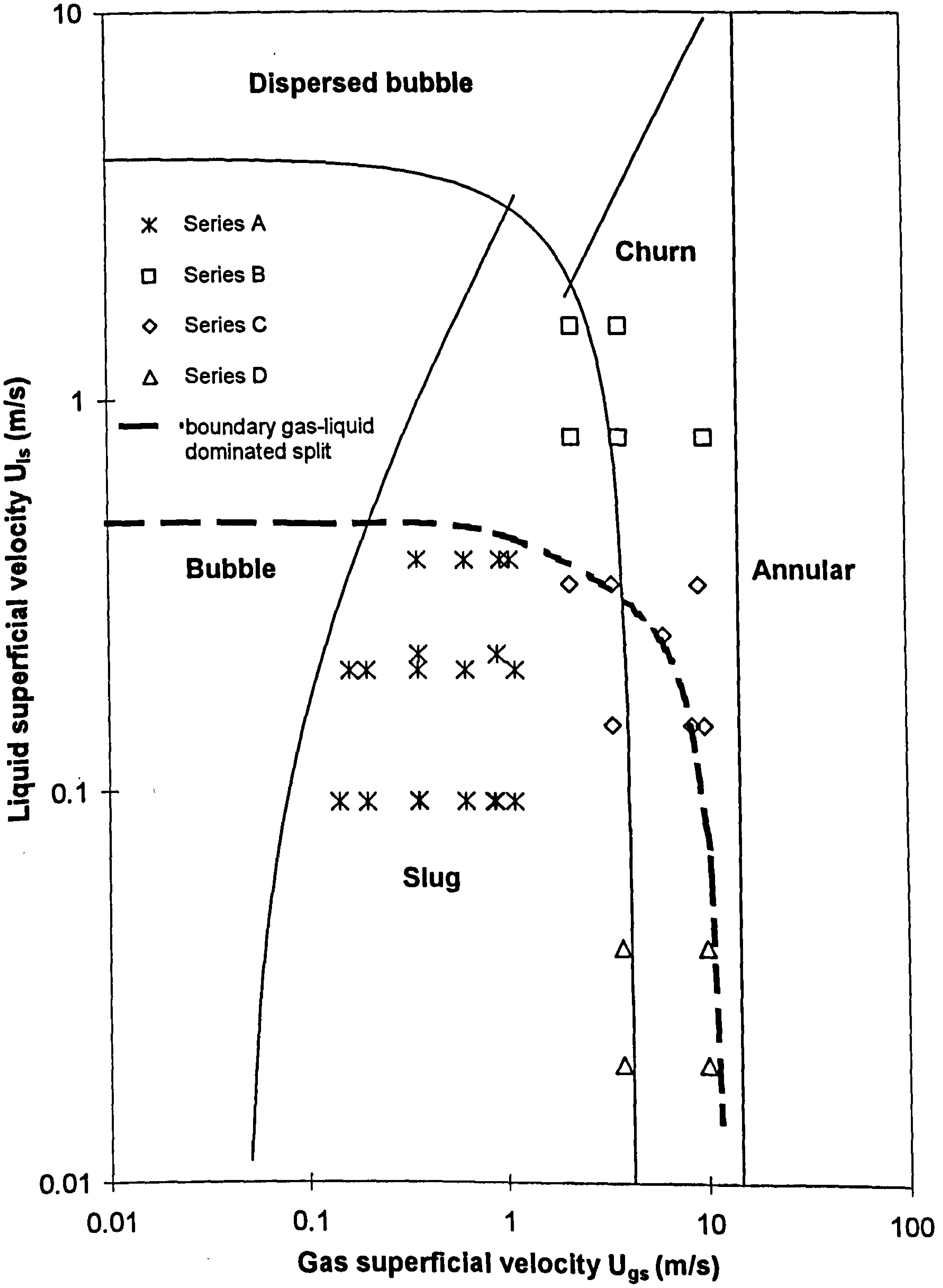

Figure V.1.3: *Flow pattern map as predicted by the model of Taitel et al.(1980) for a 0.076 m ID vertical pipe and atmospheric pressure (air/water). Series A and C are the work previously reported by Azzopardi et al (1994) and Azzopardi et al (1996) respectively.*

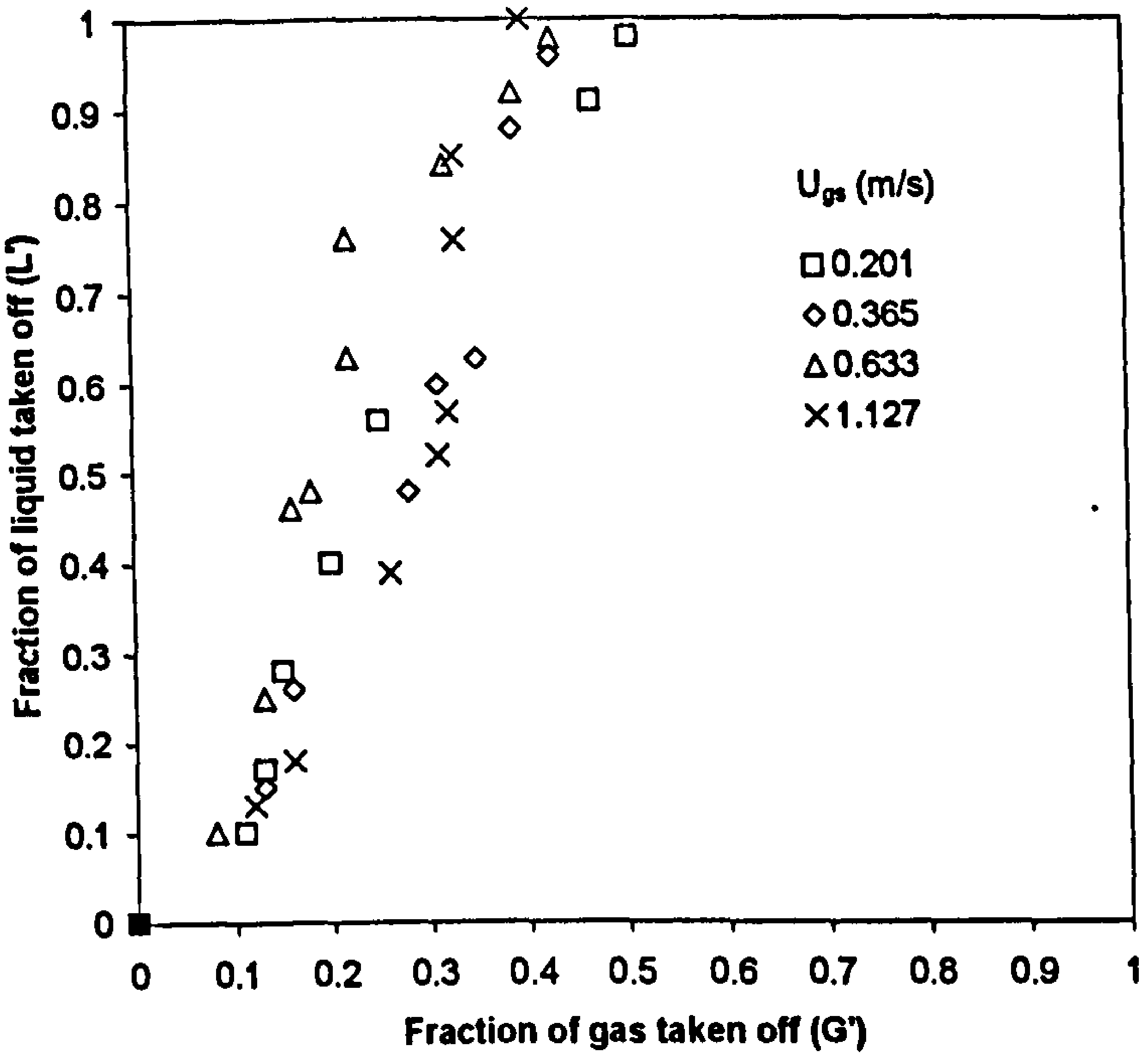

a) $U_{ls} = 0.2$ m/s

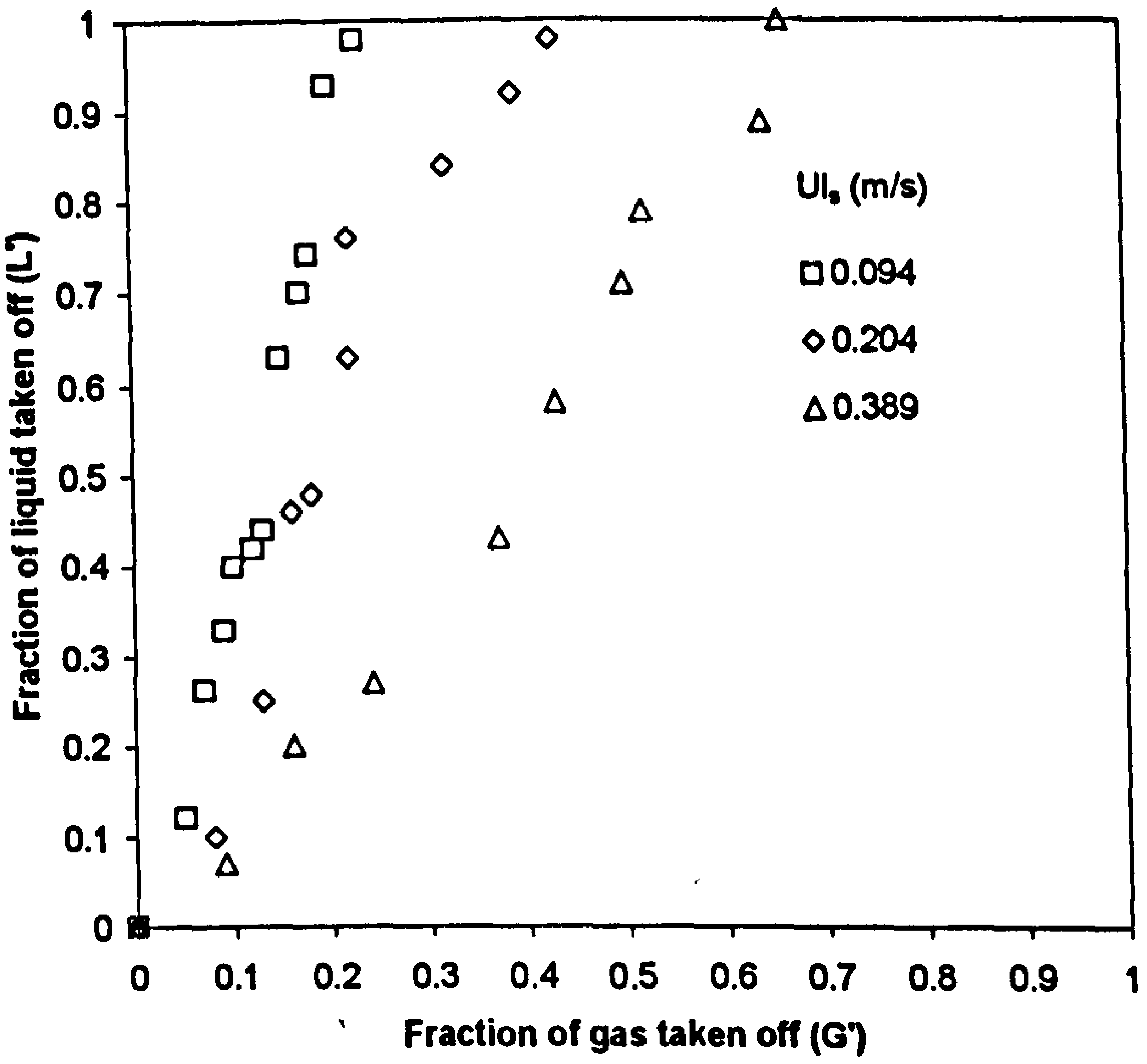

b) $U_{gs} = 0.63$ m/s

Figure V.1.4: *Flow split characteristic from data in slug flow (series A) as obtained by Azzopardi et al (1994) showing: a) the effect of gas superficial velocity for a constant* $U_{ls} = 0.2$ *m/s; b) the effect of liquid superficial velocity for a constant* $U_{gs} = 0.63$ *m/s.*

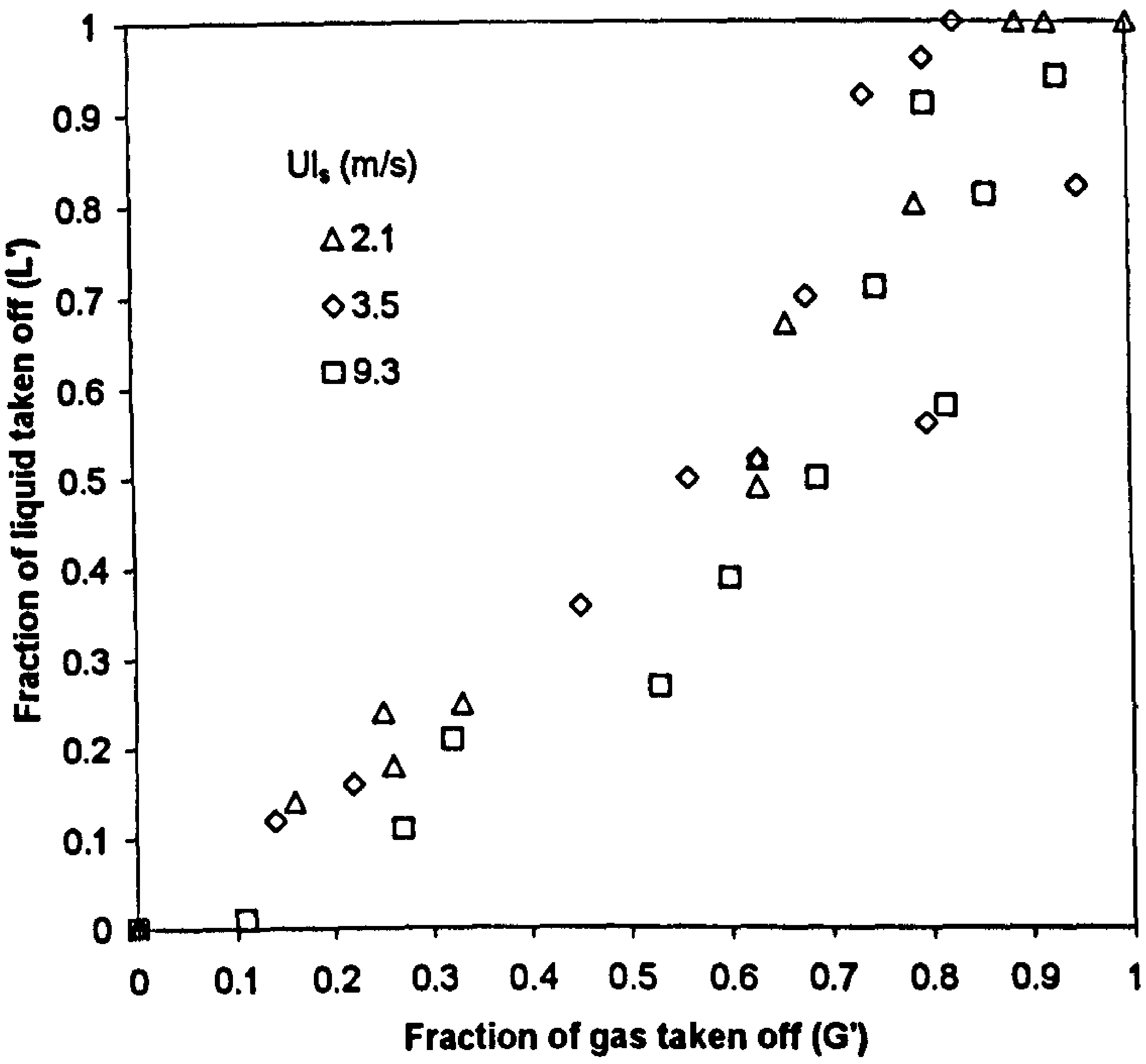

a) $U_{ls} = 0.35$ m/s

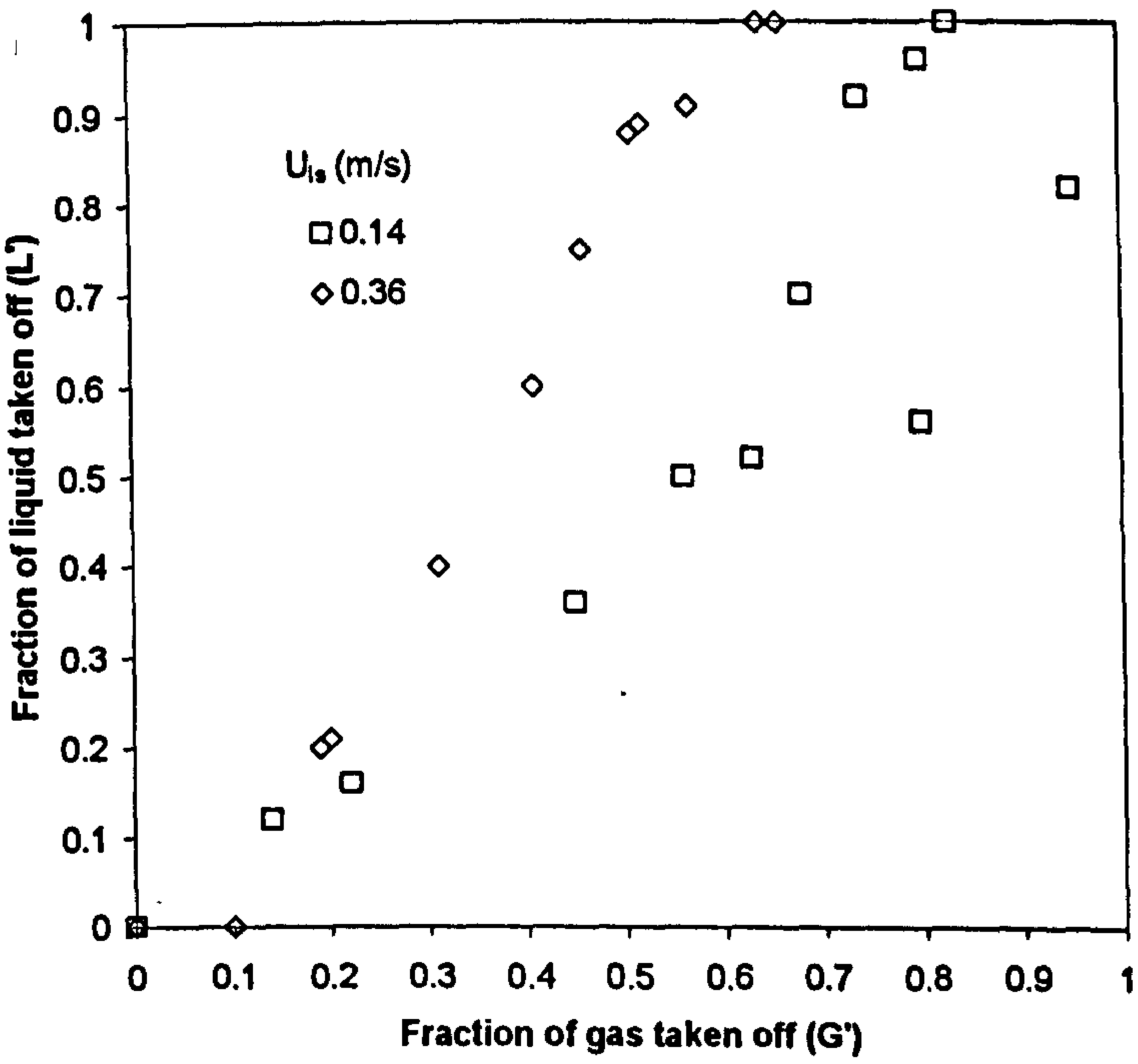

b) $U_{gs} = 3.5$ m/s

Figure V.1.5: *Flow split characteristic from data on slug/churn boundary (series C) as obtained by Azzopardi et al. (1996) showing: a) the effect of gas superficial velocity for a constant U_{ls} = 0.35 m/s; b) the effect of liquid superficial velocity for a constant U_{gs} = 3.5 m/s.*

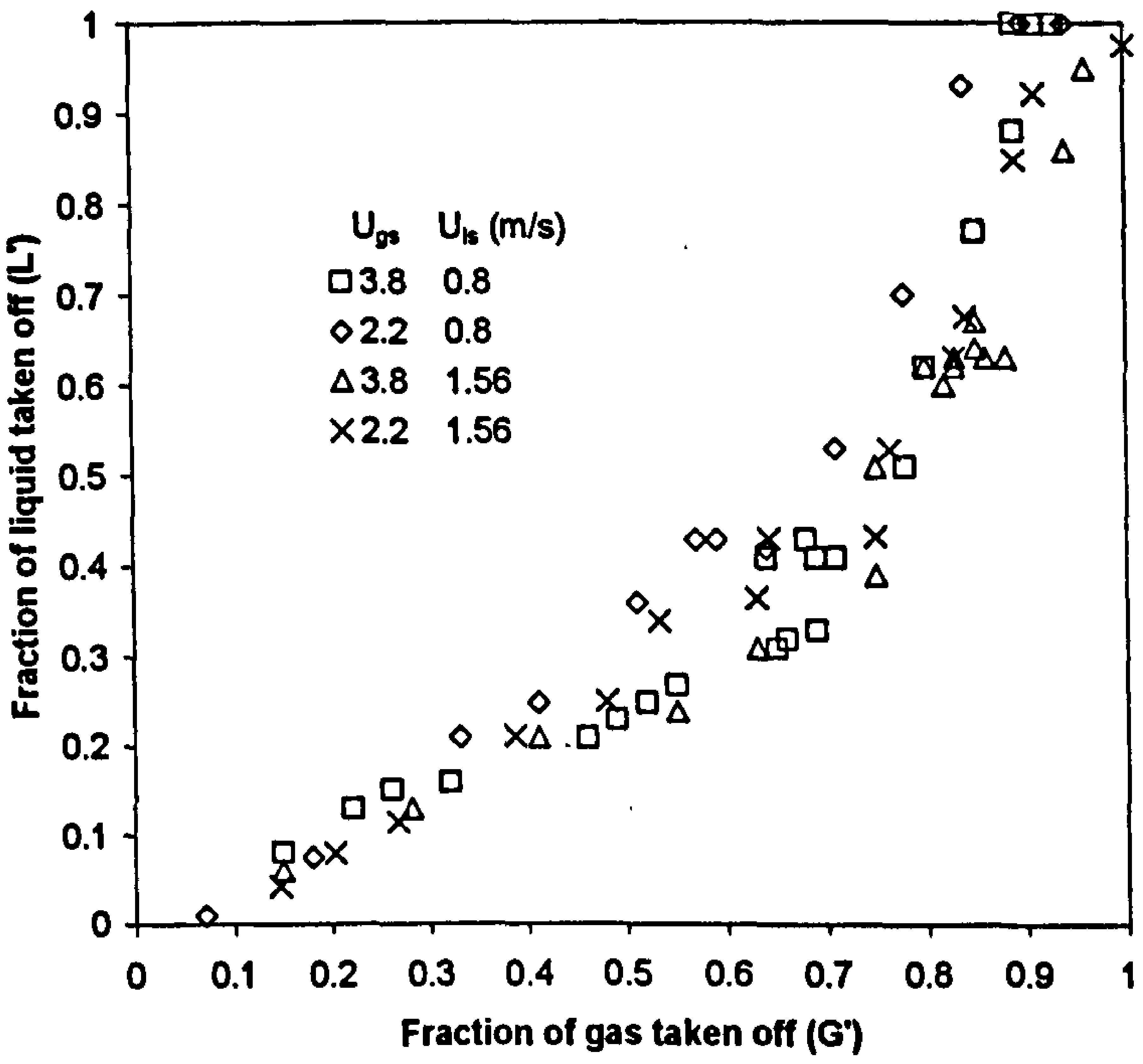

Figure V.1.6: *Flow split characteristic from data on slug/churn boundary and large liquid inlet (from series B) showing gas dominated split at the junction and small variations in the split characteristic*

of 0.2 m/s when gas inlet is varied between 0.201 and 1.127 m/s. Changing liquid inlet flow rate between 0.094 and 0.389 m/s for a constant U_{gs} = 0.63 m/s, causes the liquid take off to decrease. However, the split remains liquid dominated as displayed in Figure V.1.4 b). Azzopardi *et al* (1994) did not give an explanation for this behaviour but observed the mechanism of split of a Taylor bubble by using high-speed videos (1000 fps). This will be recalled in section V.2 where a semi-empirical approach is attempted to model this behaviour.

However, it is known that split behaviour in the high quality churn and annular flow patterns is often gas dominated. The data points of series C, across the slug to churn boundary, were produced in the attempt to establish a preliminary transition boundary between gas and liquid dominated split behaviour. This is shown in Figure V.1.5 a), together with the effect of gas flow rate on the split of the phases. Similarly to series A, no simple trend or significant variation is observed. Again (Figure V.1.5 b)), the effect of liquid flow rate is more significant but this time, increasing liquid flow rate causes a larger intake of liquid in the side arm, as opposed to what is described above for the case of series A. This might be due to the larger gas flow rate

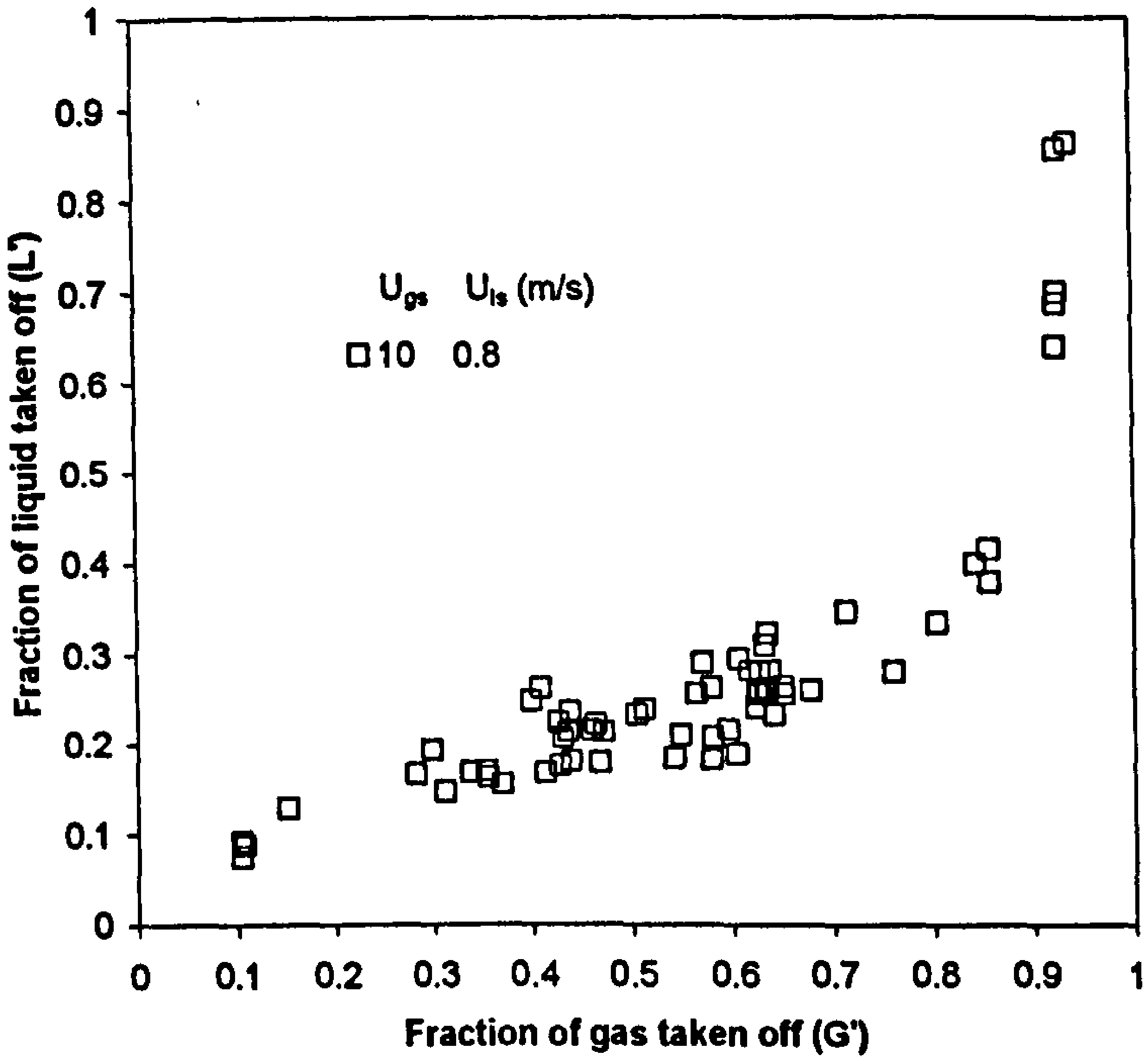

Figure V.1.7: *Flow split characteristic from data in the churn flow regime for U_{gs} = 10 m/s and U_{ls} = 0.8 m/s (from series B). Shows gas dominated split and the scatter of data between 30% and 70% of gas take off.*

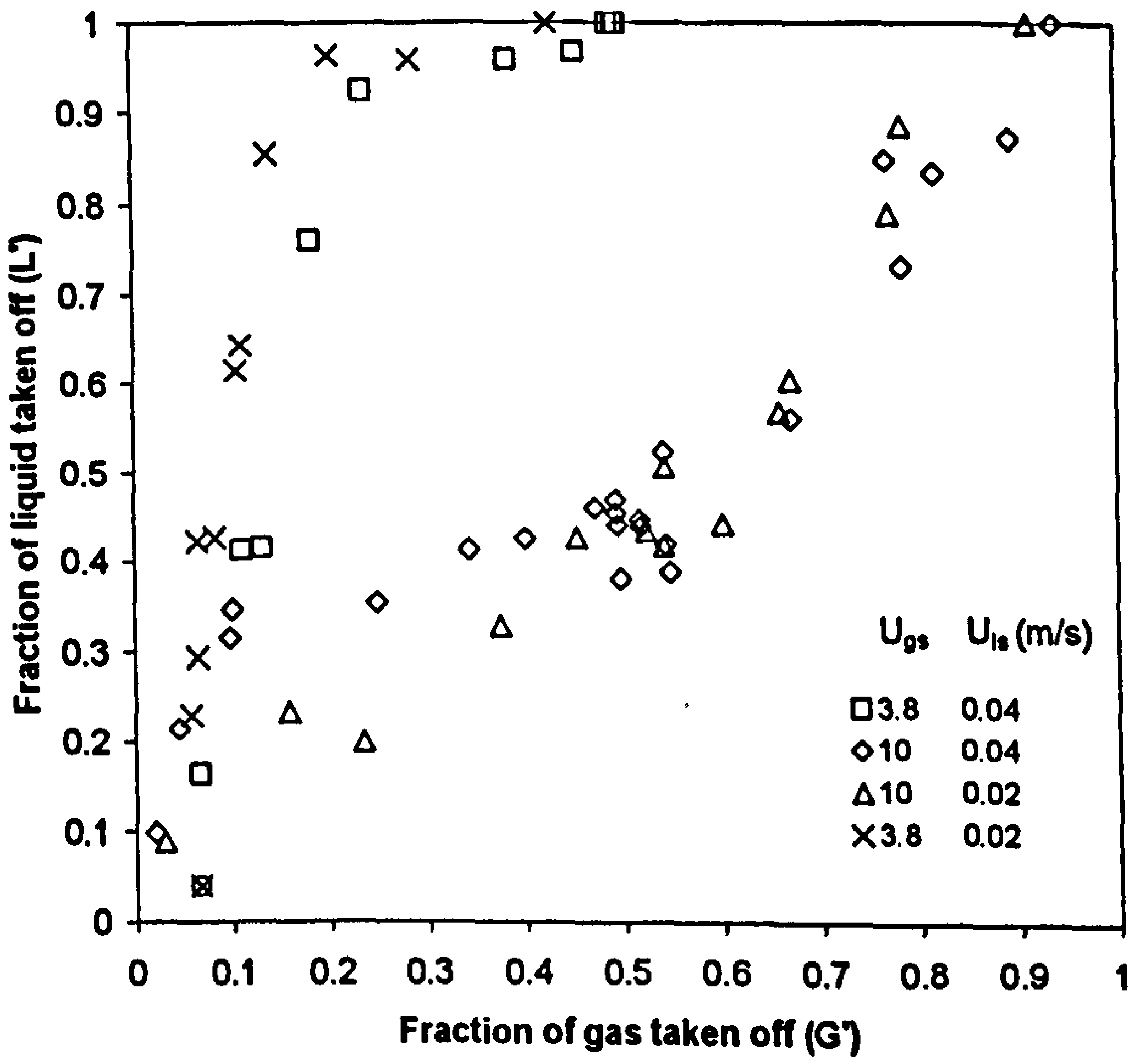

Figure V.1.8: *Flow split characteristic from series D in the low liquid churn flow. Shows liquid dominated split for U_{gs} = 3.8 m/s and even split for U_{gs} = 10 m/s. Liquid superficial velocity is U_{ls} = 0.02 m/s and 0.04 m/s.*

and to the fact that the two inlet conditions are right along the slug/churn transition boundary on a flow pattern map (Figure V.1.5 b)). The empirical boundary between liquid and gas dominated behaviour represented by data set C is the line of equation:

$$U_{ls} = 0.49 - 0.041U_{gs} \quad [V.1.1]$$

also represented in Figure V.1.3. It is worth pointing out that this does not coincide with either a theoretical or an experimentally observed flow pattern transition boundary.

The data of series B were obtained across the slug/churn transition for a lower quality than series C. Accordingly with its location relative to the split regime boundary, the characteristic is gas dominated as shown in Figure V.1.6 containing four of the five inlet conditions of series B. The characteristic for the fifth inlet condition, for high gas churn flow, is represented in Figure V.1.7. There, the behaviour is even more markedly gas dominated and similar to annular flow. However, a very scattered characteristic was found between 30% and 70% of gas take off. This will be considered in more detail in section V.2.

Finally series D data are considered. These relate to the slug to churn boundary transition and in the churn flow regime, for low liquid superficial velocity (0.02 and 0.04 m/s), Figure V.1.8. The two cases for U_{gs} = 10 m/s fall near the line of even separation obtained from data set C. The characteristic confirms the validity of this boundary also for much lower liquid flow rate. For U_{gs} = 3.8 m/s, behaviour is liquid dominated again, as in the slug flow data of series A.

V.2 Interpretation of results for vertical main flow. Data analysis and modelling

In the light of current understanding and of experimental data produced by other authors, it is possible to analyse further and discuss the data presented in the previous section in an attempt to explain features and to propose predictive methods. In particular we will suggest a transition boundary between gas and liquid dominated behaviour, applicable to a larger database, including several pipe diameters and operating pressures. Also, on the basis of series B results, the occurrence of *flooding* will be taken into consideration in the interpretation of trends and finally, a predictive semi-empirical equation will be presented for data series A, in the slug flow regime.

V.2.1 Development of a criterion for the gas to liquid dominated split transition.

From series C data, Azzopardi *et al* (1996) proposed an empirical transition boundary between gas (above the boundary) and liquid (below the boundary) dominated behaviours. One would expect this transition to occur when some two-phase flow parameter assumes a particular value, indicating a qualitative change in the preference of extraction of one phase or the other. Reasoning in terms of momentum of the phases, an inversion of its ratio around a certain value would be a physically plausible criterion. However, because of the negative slope of the transition boundary, this can not be. In fact, for increasing gas superficial velocity, the liquid velocity for the transition to occur decreases and the ratio of momenta (varying with the square of velocities), either based on superficial velocity or on the real velocity of the phases, can not be constant. However, for the five points on the transition boundary, although gas and liquid superficial velocities change by a factor of two and five respectively, the sum of the superficial momentum fluxes keeps constant around a value of 120 kg/ms^2, within 9% (Table V.2.1). If we define a split index as the average of the displacement of L' from the even split value (i.e. L'=G') for the N points of the experimental curve this can be written as:

$$\psi = \frac{\sum_{i=1}^{N} L'_i - G'_i}{N} \qquad [V.1.2]$$

this parameter will assume positive values for liquid dominated and negative values for gas dominated split behaviour. Even split characteristics will give place to values of ψ close to zero.

In particular if the points were taken at regular intervals of G', this parameter would vary between –0.5 and 0.5 respectively for the curves of total gas separation (abscissa) and of total liquid separation (ordinate). Also, it would represent a discrete approximation of the area between the split characteristic and the line of even separation.

From Table V.2.2, one can see that for the 5 points on the transition boundary (C.2, C.3, C4, C.5 and C.7), $|\psi| < 0.13$. If one assumes this limit on ψ as a criterion

Table V.2.1: *Values calculated for the parameter ψ from the split curves and the sum of superficial momenta of the phases.*

Series data	U_{gs} (m/s)	U_{ls} (m/s)	ψ (-)	$\rho_g U_{gs}^2+\rho_l U_{ls}^2$ (kg/ms^2)
series A.1	0.201	0.2	0.18157	40.0485
series A.2	0.365	0.2	0.24237	40.1599
series A.3	0.633	0.2	0.32634	40.4808
series A.4	1.127	0.2	0.20886	41.5242
series A.5	0.633	0.094	0.37167	9.31683
series A.6	0.365	0.389	0.225	151.481
series A.7	0.145	0.094	0.12667	8.86123
series A.8	0.201	0.094	0.36	8.88448
series A.9	0.365	0.094	0.32	8.99587
series A.10	0.896	0.091	0.41	9.24438
series A.11	1.11	0.094	0.36	10.3145
series A.12	0.164	0.2	0.021	40.0323
series A.13	0.633	0.389	0.13	151.802
series A.14	0.94	0.389	0.23	152.381
series A.15	0.37	0.223	0.16	49.8933
series A.16	0.88	0.095	0.74	9.95428
series A.17	0.37	0.095	0.29	9.18928
series A.18	0.11	0.223	0.17	49.7435
series A19	1.07	0.39	0.105	153.474
series A20	0.96	0.39	0.099	153.206
series B.1	3.8	0.78	-0.16	625.728
series B.2	3.8	1.56	-0.20	2450.93
series B.3	2.2	0.78	-0.087	614.208
series B.4	2.2	1.56	-0.19	2439.41
series B.5	10	0.8	-0.29	760
series C.1	9.3	0.35	-0.08	226.288

Table V.2.1: *(Continued) Underlined data are the five relevant points of series C.*

Series data	U_{gs} (m/s)	U_{ls} (m/s)	ψ (-)	$\rho_g U_{gs}^2+\rho_l U_{ls}^2$ (kg/ms^2)
series C.2	3.5	0.35	0.005	137.2
series C.3	2.1	0.35	-0.019	127.792
series C.4	9.85	0.148	0.098	138.331
series C.5	8.55	0.148	0.13	109.627
series C.6	3.5	0.148	0.19	36.604
series C.7	6.18	0.25	-0.03	108.331
series D.1	3.8	0.04	0.38	18.928
series D.2	10	0.04	0.007	121.6
series D.3	10	0.02	-0.04	120.4
series D.4	3.8	0.02	0.49	17.728

to label a split characteristic as being even, the result can be seen Figure V.2.1. There, the sum of superficial momenta is plotted vs. the gas superficial velocity and the points giving place to split characteristics with values of ψ outside of the interval [-0.13,0.13] are considered gas or liquid dominated accordingly to the sign of ψ.

The criterion works reasonably well in the present database. The two empty diamonds of Figure V.2.1 just above the transition line refer to series A (runs 6 and 14) and are liquid dominated although the sum of superficial momenta exceeds 120 kgm/s. The asterisk belonging to series B (run B.3) has a value of sum of the momenta of 614 kgm/s^2 and yet, the value of ψ is in the range for even split. However, from Figure V.2.2, it can be seen that the split is gas dominated for run B.3. The small value of ψ is due to the contributions to the sum of ψ of opposite sign due to the fact that the system swaps from gas to liquid dominated behaviour around G'=0.8. The parameter ψ can not account for this. An attempt is now made to produce a criterion for split data obtained for different pipe diameters and operating pressures. For this purposes, the data from Azzopardi & Purvis (1987; D = 0.0318 m,

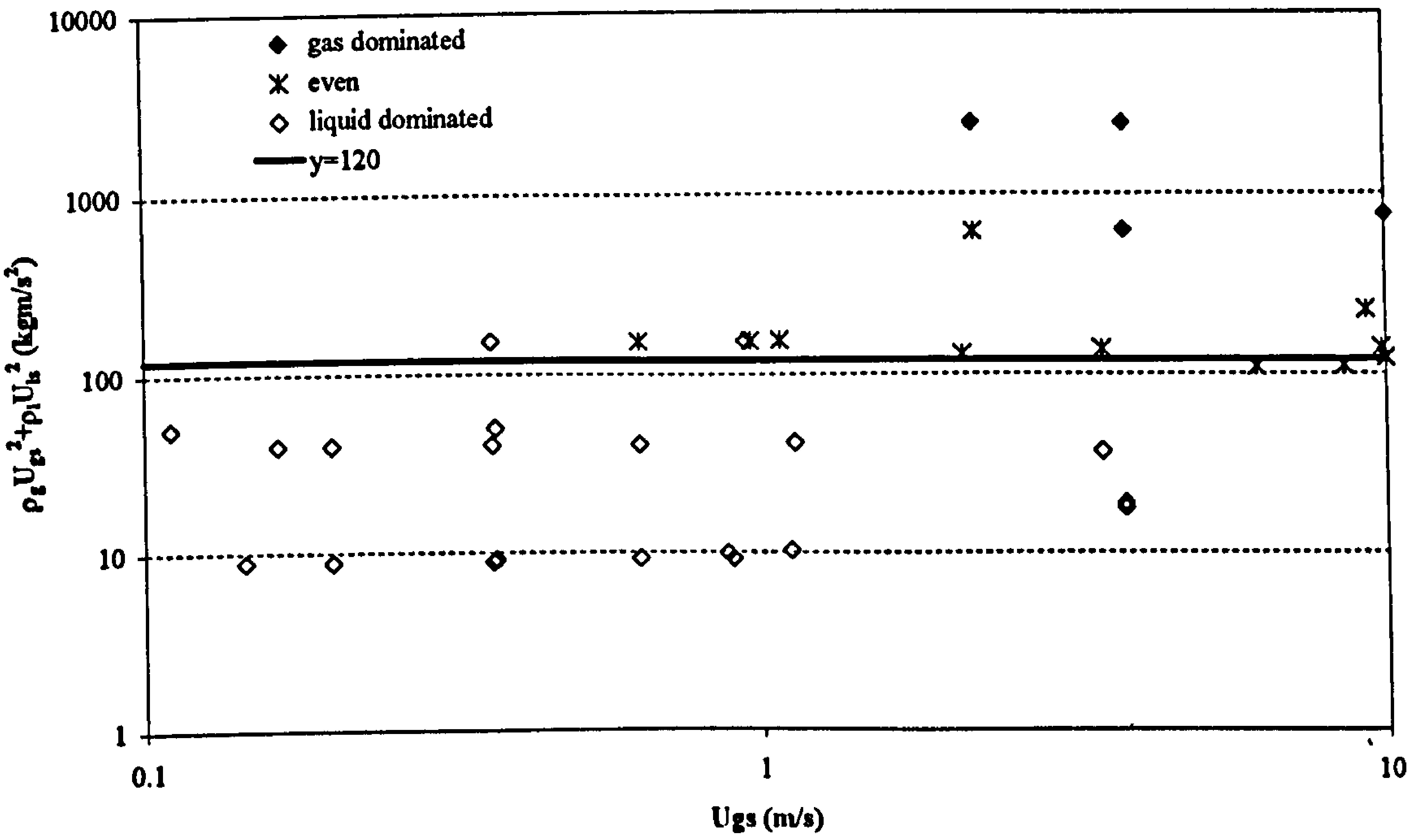

Figure V.2.1: *Plot showing the criterion of the sum of the superficial momenta. The points labelled 'even' (dash) are those with* $-0.13<\psi<0.13$*, all clustering around the horizontal line of* $y=120$ *kg/ms*^{2}.

P= 1.5 bar) Hewitt *et al* (1990; D= 0.0318 m, P = 3 bar) Suu (1992; D = 0.021 m, P = 2.4 bar) and Azzopardi (1994; 0.125 ID, P= 1bar) will be added to the database of the present work. These data are all for air/water and vertical up-flow and cover all flow patterns.

Rea (1998) found that, for horizontal stratified flow, plotting the Reynolds number of the two phases calculated using the model by Taitel and Dukler (1976), led to a boundary for strongly gas dominated separation. In that work, the aim was to investigate the possibility of using a T-junction as a partial phase separator. For this reason, the condition imposed was to consider a split curve to be gas dominated when for 80% of the incoming gas taken off in the side arm, the fraction of diverted liquid is smaller than 20%.

In the present case, the use of the parameter ψ was difficult because in the annular flow database, inversions around the even split line (x=y) occur frequently (as in the case of Figure V.2.2). For this reason, a different and more local condition is now imposed to label a split characteristic as being gas or liquid dominated. One can refer to the fraction of liquid diverted when 50% of the gas is taken off in the side arm in the following manner:

- $(L'-G')_{G'=0.5} < -0.15$ Gas dominated split
- $-0.15 < (L'-G')_{G'=0.5} < 0.15$ Even split
- $(L'-G')_{G'=0.5} > 0.15$ Liquid dominated split

By using these definitions it was found that the sum of the superficial momenta multiplied by the square of the pipe diameter, remains reasonably constant for even splits occurring at a ratio of liquid to gas superficial velocity in the range 0.002 - 0.36. For lower or higher ratios, a higher value of the combination used of the two superficial momenta is needed. Figure V.2.3.shows a plot of $(\rho_g U_{gs}^2+\rho_l U_{ls}^2)D^2$ vs. U_{ls}/U_{gs} with the proposed transition boundary. The points below the transition boundary give place to liquid dominated and those above to gas dominated split, at G' = 0.5.

If the actual velocities based on the slip ratio by Chisholm are used, no qualitative change of the diagram in Figure V.2.3 is observed. This is so also if the two Reynolds numbers of gas and liquid are plotted. Figure V.2.4 shows the

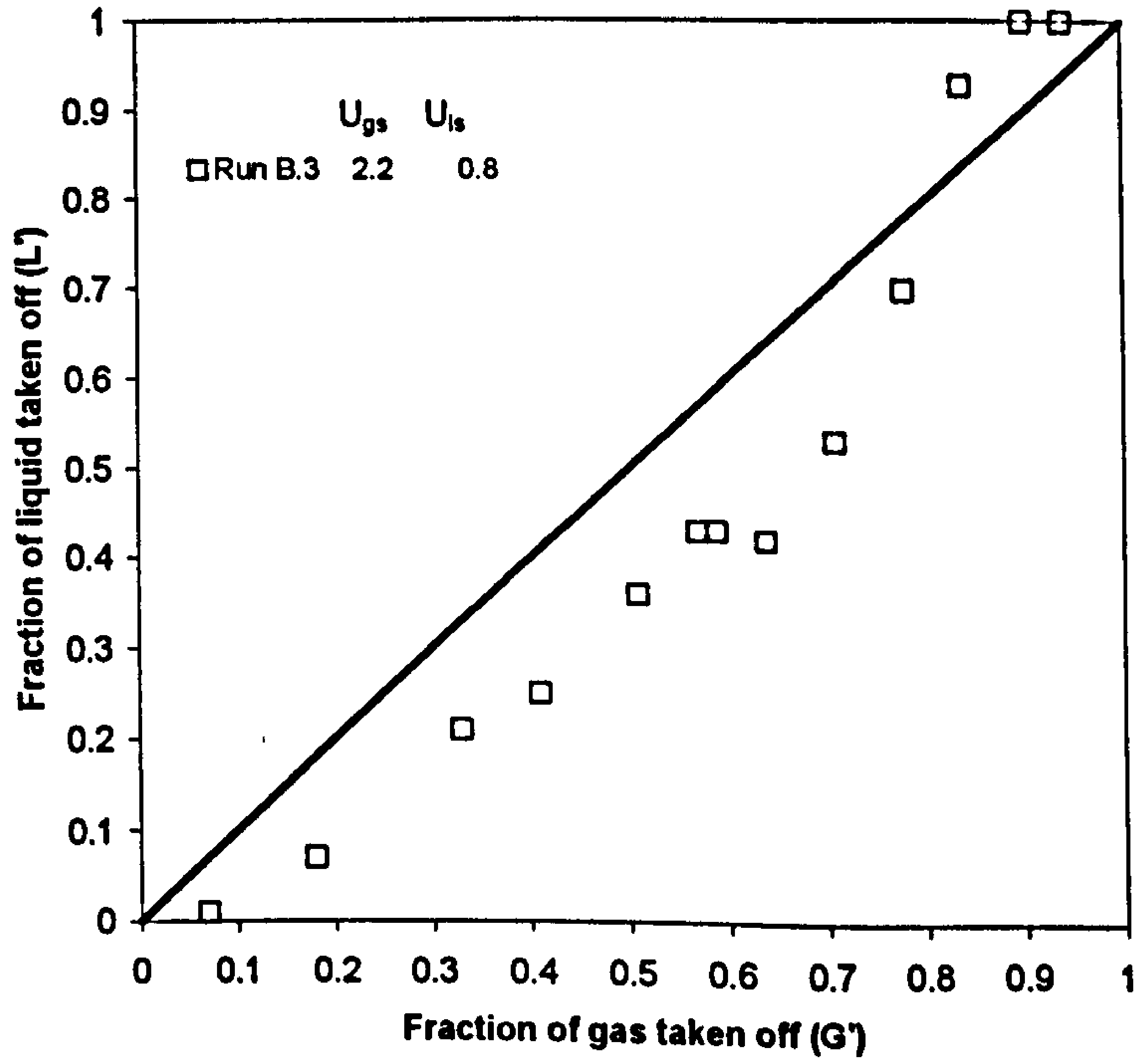

Figure V.2.2: *Split data from series B Separation is gas dominated for most of the curve. $\psi = -0.087$ because of the inversion occurring around G' = 0.8.*

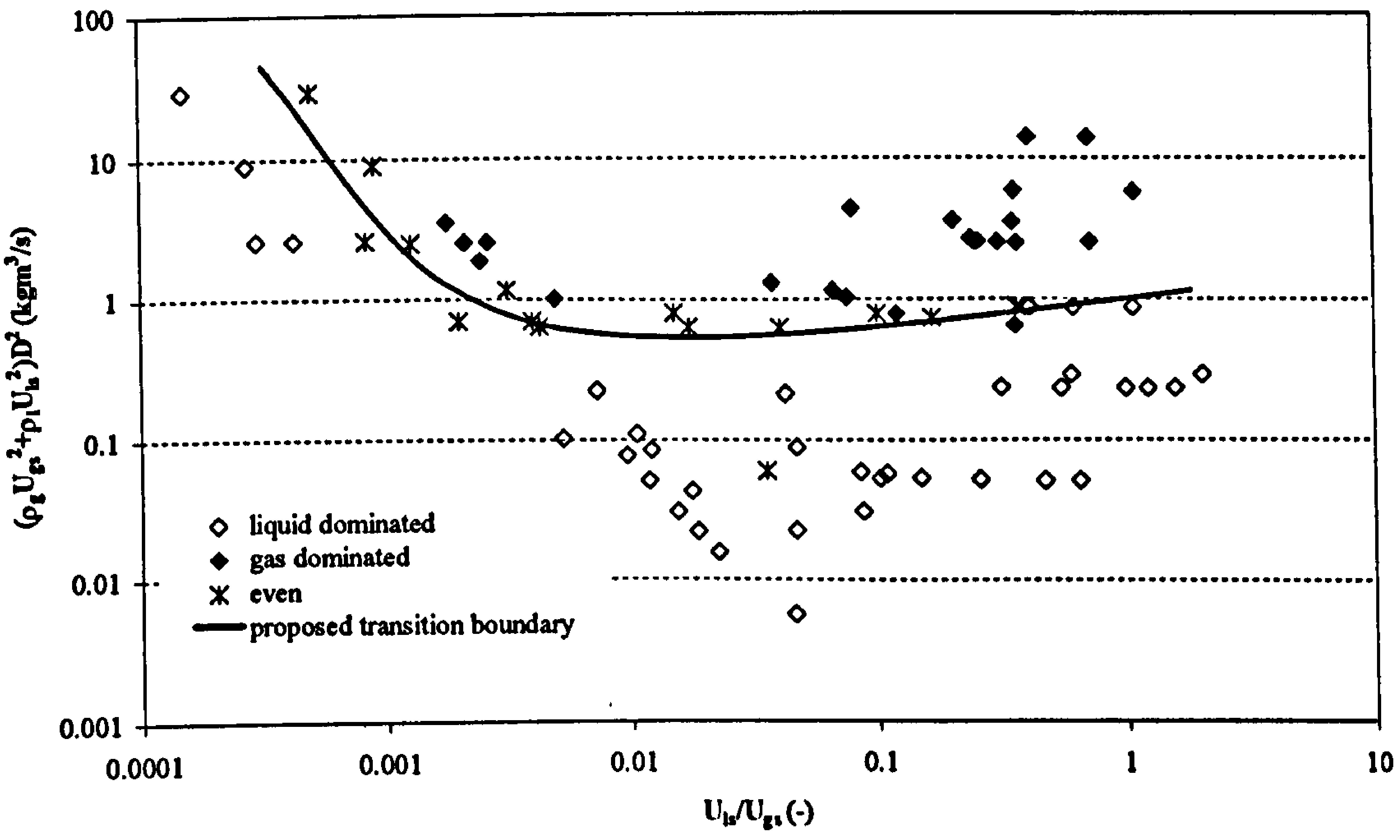

Figure V.2.3: *Gas to liquid dominated transition boundary based on the split at G'=0.5. Sum of momenta by diameter to the power of two, vs. the ratio of superficial velocities. Enlarged air/water database.*

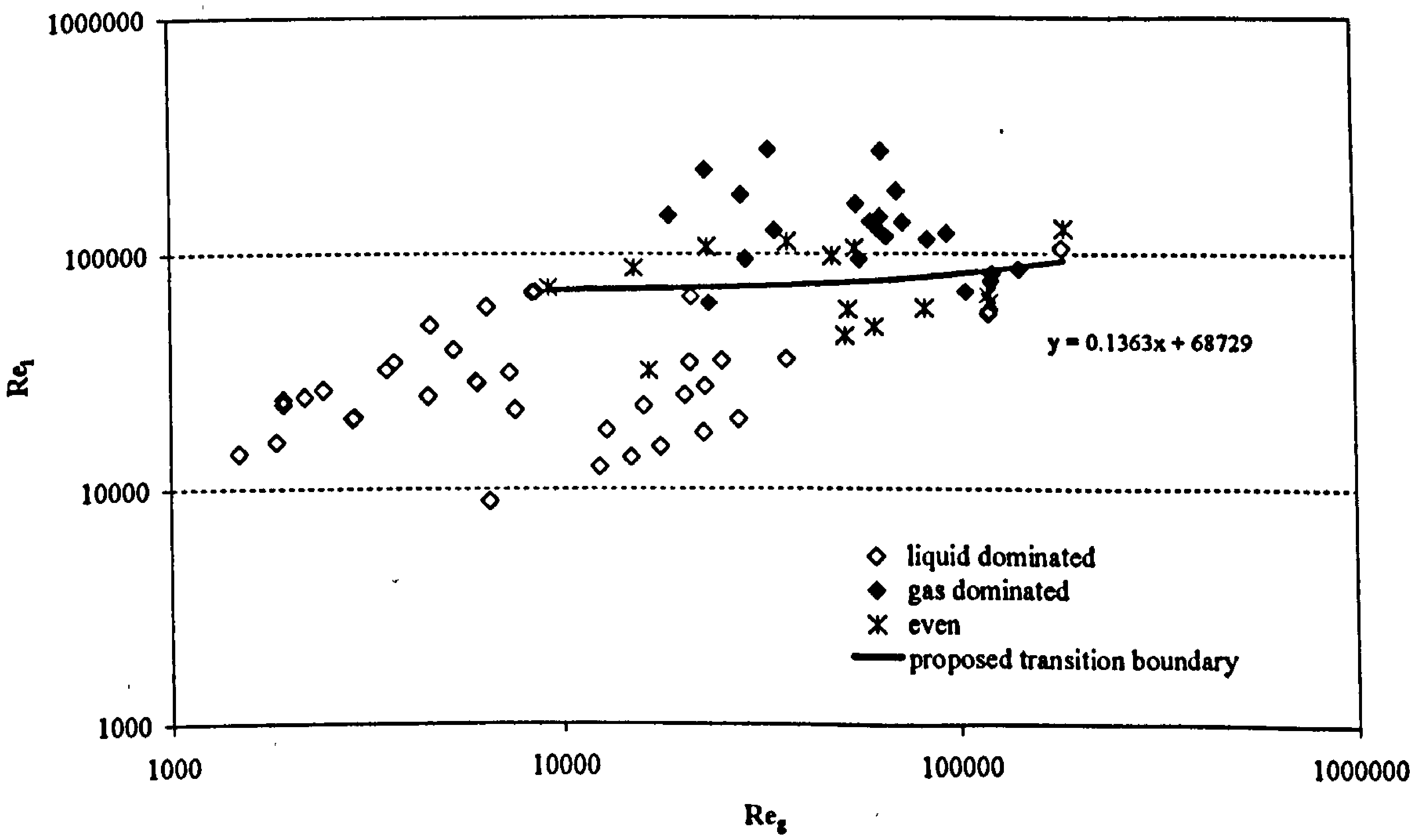

Figure V.2.4: *Gas to liquid dominated transition boundary (linear fit) based on the split at G'=0.5 on the plane of Reynolds numbers. Re_g and Re_l are based on phase velocities obtained with a slip ratio from model of Chisholm (1972).*

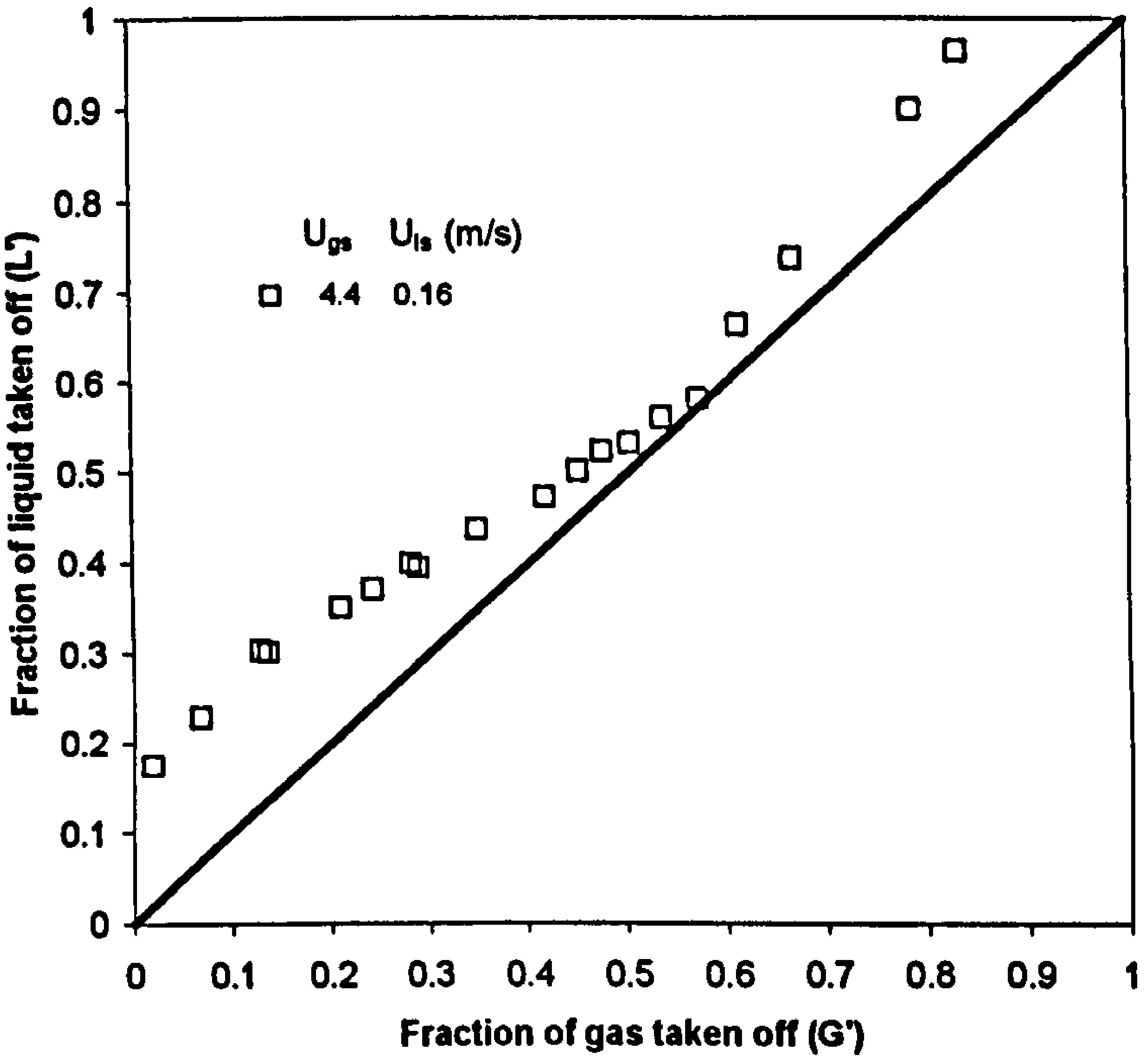

Figure V.2.5: *Plot showing a value of* $(L'-G')_{G'=0.5}$ *close to zero, although overall split characteristic is liquid dominated. Data from Azzopardi and Purvis (1987).*

transition boundary on the plane of the two Reynolds numbers calculated with the slip ratio formula of Chisholm, in the style of Rea (1998). An exception occurs for one point well in the liquid dominated region which shows even split for G'=0.5 (U_{gs} = 4.4 m/s; U_{ls} = 0.16 m/s). This is due to having used a local condition to define gas or liquid dominated split. As shown in Figure V.2.5, the split characteristic for this point, which is obtained from the database of Azzopardi and Purvis, shows overall liquid dominated features, approaching the curve of even split only around G' = 0.5.

V.2.2 Gas dominated separation in churn flow, flooding and an occurrence of Hysteresis. Series B Data.

The inlet flow rates utilised in the series B data were selected so that these data would be compared with those of Hewitt *et al* (1990) who took data at 3 bar in a 0.0318 m ID, regular T-junction. Of particular interest for our investigation, are the data produced for U_{gs} = 2.2 m/s and U_{ls} = 0.79 m/s and 1.59 m/s. Because of the different pressures employed in the two experiments, in the present work data were produced both for the same gas superficial velocity and for the gas velocity corresponding to the same gas superficial momentum (U_{gs} = 3.8 m/s). This was to investigate whether the superficial velocity or the momentum of the phases is more significant in determining the split of the phases. However, Figures V.2.6 a) and b) show that the split characteristic produced in the present work (0.076 m ID and 1 bar) is fairly close to the results of Hewitt *et al.* (1990) for both equal superficial velocity and momentum based on the superficial velocity. It can be noted that the data produced for the same gas momentum are slightly closer to the data at 3 bar, especially for large gas take off. However differences are very small and no general conclusion can be drawn to assess which case best reproduces results obtained for different pipe diameters and operating pressures.

A common feature of all data of series B, is the change of slope in the split characteristic occurring between 60-80% gas take off. Until the liquid take off increases steeply, the slope of the split characteristic is ~0.5 and then steeply increases towards the point (1,1) of total take off. Azzopardi and Baker (1981) obtained a similar result and proposed a probabilistic model to predict the split of the phases. This was then developed in a more general form by Lahey *et al.* (1987), as presented in section II.4. The authors assumed that there is a probability for the liquid to be taken off with the gas in the side arm, which depends on the local ratio of liquid and gas kinetic energies. By restricting to the segment of pipe subtended by the side arm, the authors obtain a linear model for G'=f(L'), independent of the inlet conditions based on the following assumptions:

- Slip ratio $U_r = U_{gs}/U_{ls} = 2$
- Gas and liquid velocity profiles are flat
- No other quantity depends on the spatial co-ordinates (e.g. void fraction)

The model is then adjusted through an empirical parameter to fit data and the slope of 0.55 in a L' vs. G' diagram is obtained, as observed experimentally.

The model works well for low take off and predicts a slope in the G' vs. L' diagram of 0.55, in agreement with the present database. However, this simple model cannot predict the change of slope. This is not surprising since the probabilistic approach of Azzopardi and Baker (1981) is based on the morphology of the flow in a straight pipe (its flow pattern) and does not consider the effect of the T-junction geometry. More specifically, it cannot account for indirect mechanisms of liquid take off such as the occurrence of flooding in the run leg of the T.

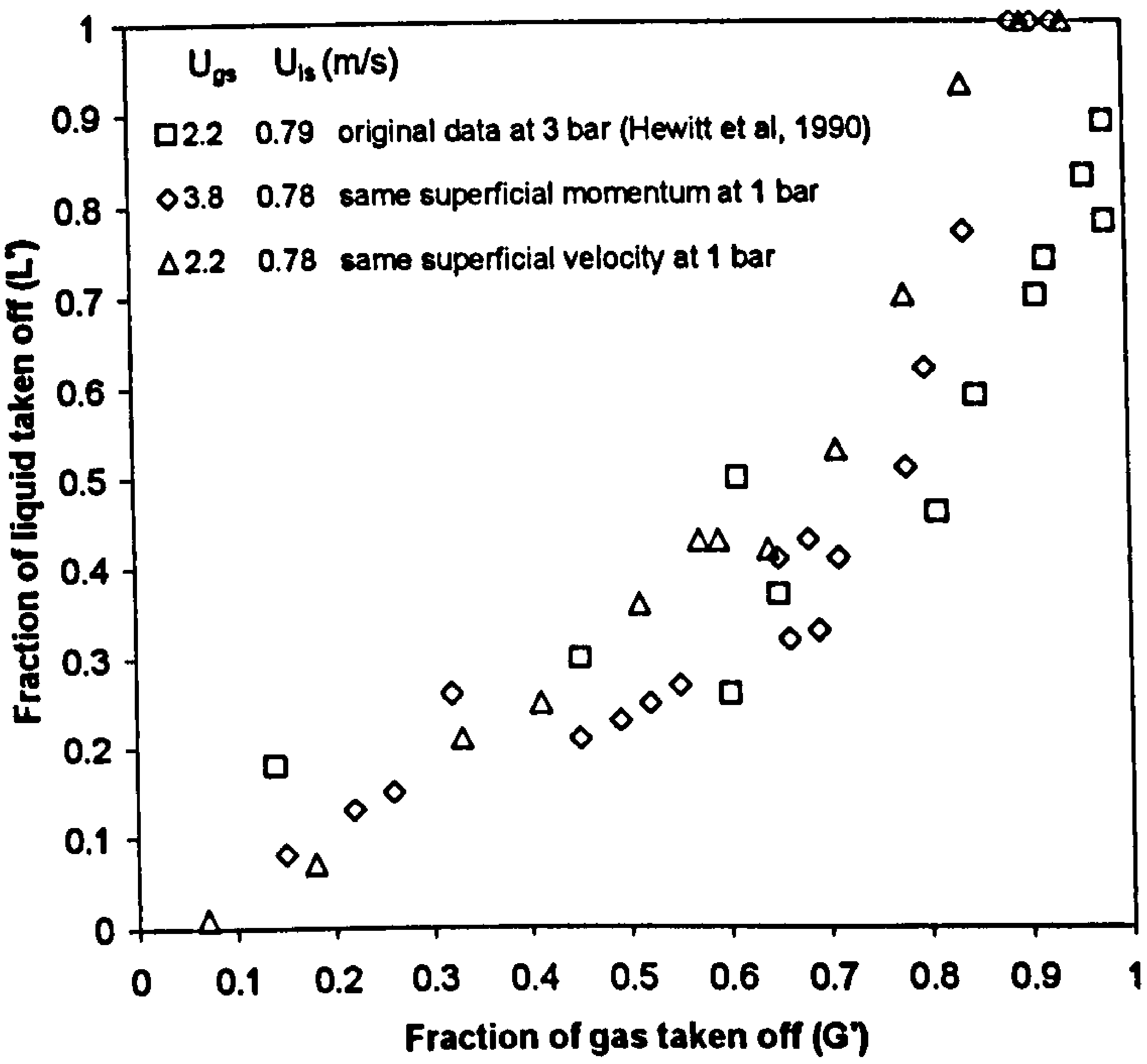

a)

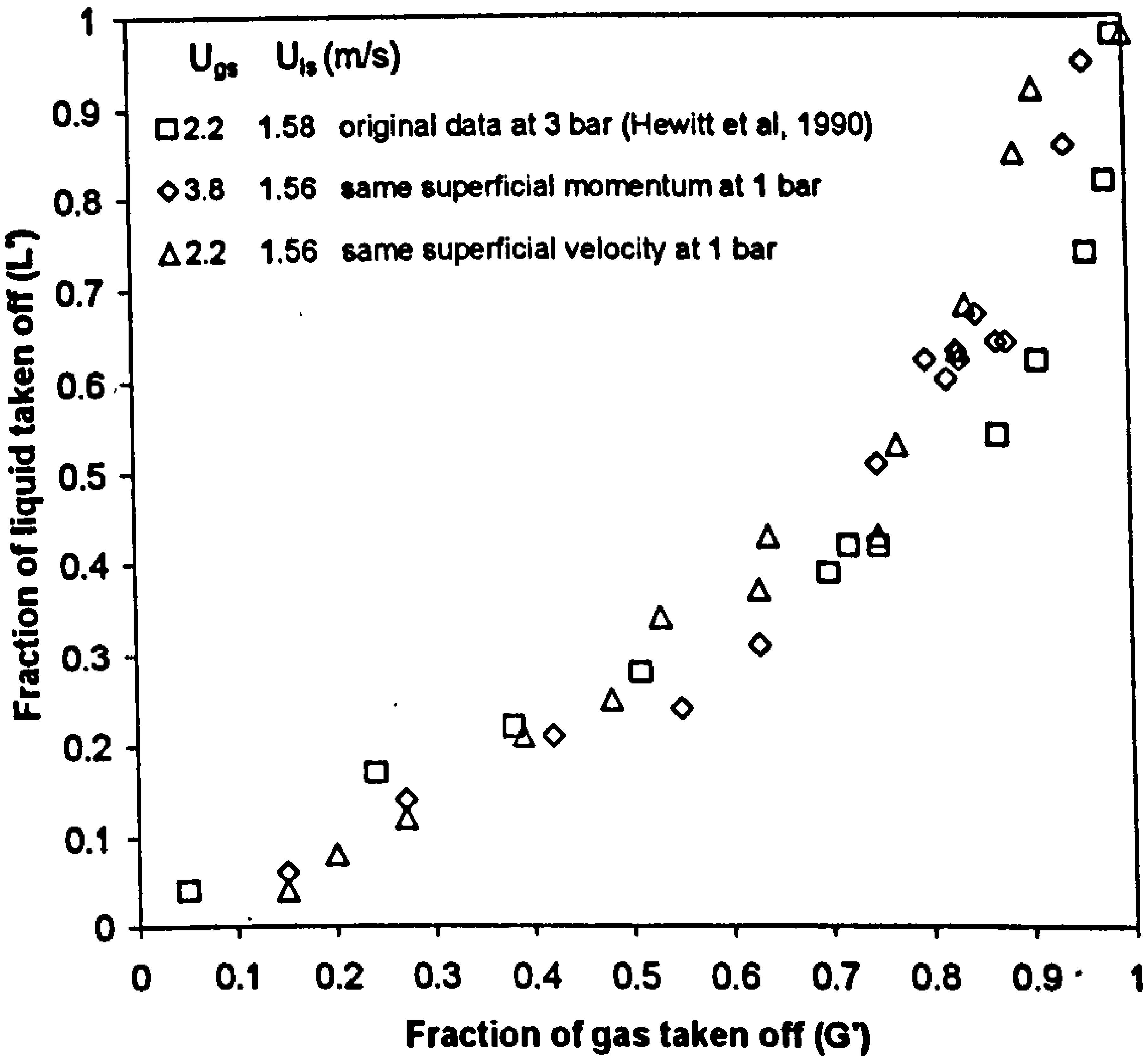

b)

Figure V.2.6: *Comparison between present data in a 0.076 m vertical T at 1 bar with those produced by Hewitt et al. (1990) in a 0.032 m vertical T at 3 bar for the same superficial velocity and momentum based on the superficial velocity of the phases.*

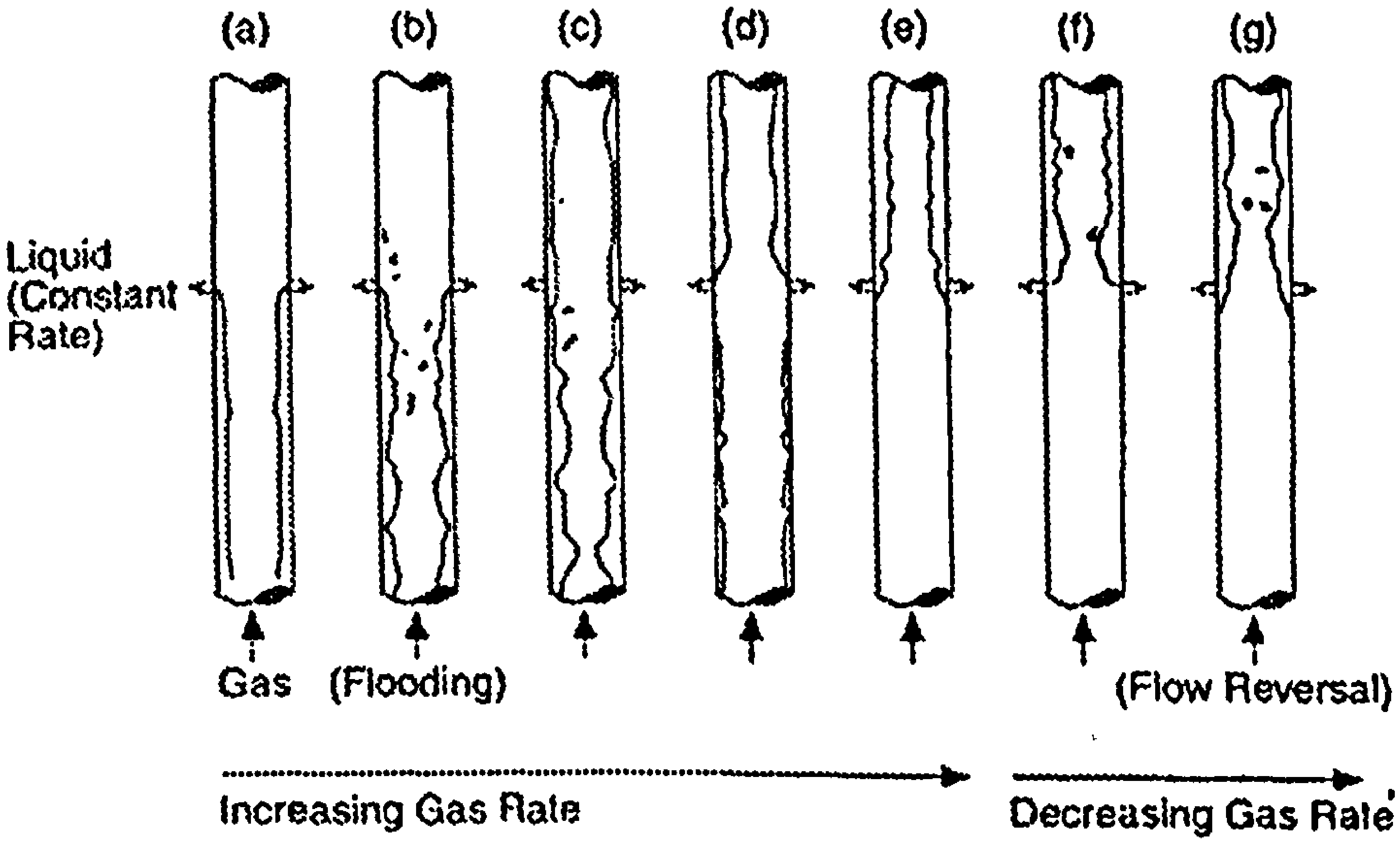

Figure V.2.7: *Flooding and flow reversal in vertical flow.*

Flooding is a well known concept that can be understood with reference to Figure V.2.7. For a constant liquid flow rate, as gas flow rate is increased, flooding occurs when liquid is observed above the liquid inlet. The inverse phenomenon is called flow reversal. For each liquid flow rate, there is a flooding velocity of the gas, which can be predicted by semi-empirical equations. The most common fitting equations are of the general form proposed by Wallis (1961):

$$\sqrt{U^*_{gs}} + m\sqrt{U^*_{ls}} = C \qquad [V.2.1]$$

where the dimensionless velocity:

$$U^*_{is} = U_{is}\left[\frac{\rho_i}{gD(\rho_l - \rho_g)}\right]^{\frac{1}{2}} \quad i = g, l \qquad [V.2.2]$$

and m and C are adjustable parameters. A detailed review of predictive equations can be found in McQuillan and Whalley (1984).

Below flooding, all of the liquid falls down. Above flooding, a certain amount of liquid will fall down and the rest is carried up until, for large enough gas flow rates, the liquid is completely carried up the pipe, above the point of liquid inlet.

In the run arm of a T-junction, it is very likely that conditions are below flooding when a large fraction of gas is taken off. However, because of their larger momentum in the inlet pipe and of flow restriction due to eddy circulation, some liquid will travel past the junction and will start to slow down as the phases relax after the T. One can argue that the amount of liquid that will fall down, back to the side arm, depends on the length of the run arm. The balance of the momentum of the up-flowing liquid and gas drag against gravity and frictional losses would establish whether the liquid can reach the top of the run arm and be diverted into the horizontal leg and thence into the separator before it starts falling down, back to the junction.

To better understand the above, the data of series B will be analysed in the following manner:

- Using m=1 and C=1 in equation V.2.1, the correlation by Wallis (1961) is employed to draw a boundary for the occurrence of flooding in the run arm. Above this curve, in the diagram of G' vs. L', the phases in the run are below the flooding conditions

- A balance between gravity and momentum of the phases based on the homogeneous model ($U_g=U_l$) is used to predict the effect of run arm length on the secondary mechanism of liquid take off.

Although it is known that flooding depends on pipe length, no flooding correlation takes this into account. The plots including flooding boundary on the basis of the equation of Wallis (1961) are reported below.

From Figure V.2.8 it can be seen that for the low liquid velocity cases of series B, the split characteristic follows the direct take off line predicted by Azzopardi and Baker (1981). After this initial trend, the split curve grows steeply towards total liquid take off. This occurs when the direct take off would fall in the area above the dotted line, below flooding. Also, the experimental trend of detachment from the direct take-off curve occurring at lower values of G' for the smaller gas flow rate is reflected by the intersection of the equation of Wallis (1961) with the direct take off line from Azzopardi and Baker (1981), for the two cases.

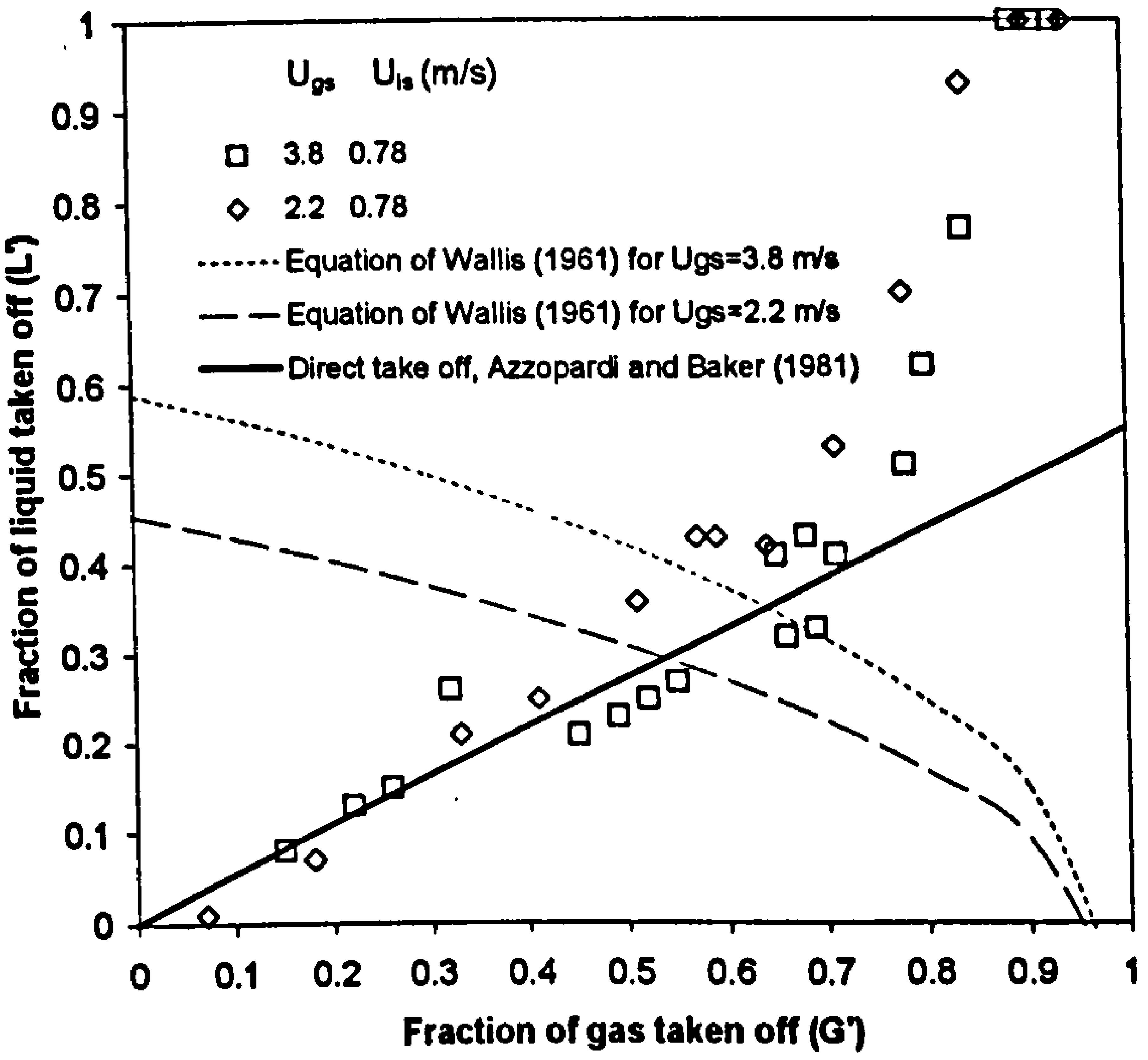

Figure V.2.8: *Plot showing detachment of split characteristic from the direct take off predicted by Azzopardi and Baker (1981). Detachment occurs when run arm conditions of gas and liquid velocity are below flooding, above the dotted lines.* $U_{ls}=0.78$ *m/s*

Figures V.2.9 and V.2.10, show respectively the results for U_{gs} =2.2 - 3.8m/s U_{ls}= 1.56 m/s and U_{gs} = 10 m/s, U_{ls} = 0.78 m/s. In the former, the curves obtained using the model by Wallis (1981), intersect the line of direct take off for a value of G' larger than measured when the split curve detaches from direct take off. However, the final portion of the split curve is below flooding. This is not surprising given the limited accuracy of flooding correlations. Furthermore, it must be considered that a certain portion of liquid would fall down even above flooding, as long as total carry over does not occur (see Figure V.2.7). Since the cases of Figure V.2.9 are obtained for a larger inlet liquid flow rate than V.2.8, there might be a more significant portion of liquid that can fall down back to the junction before the conditions in the run arm fall below flooding. The case in Figure V.2.10, where U_{ls} = 0.78 m/s and U_{gs} = 10 m/s, again gives a reasonable point of intersection between direct take off and flooding conditions in comparison to the area of detachment of the split curve.

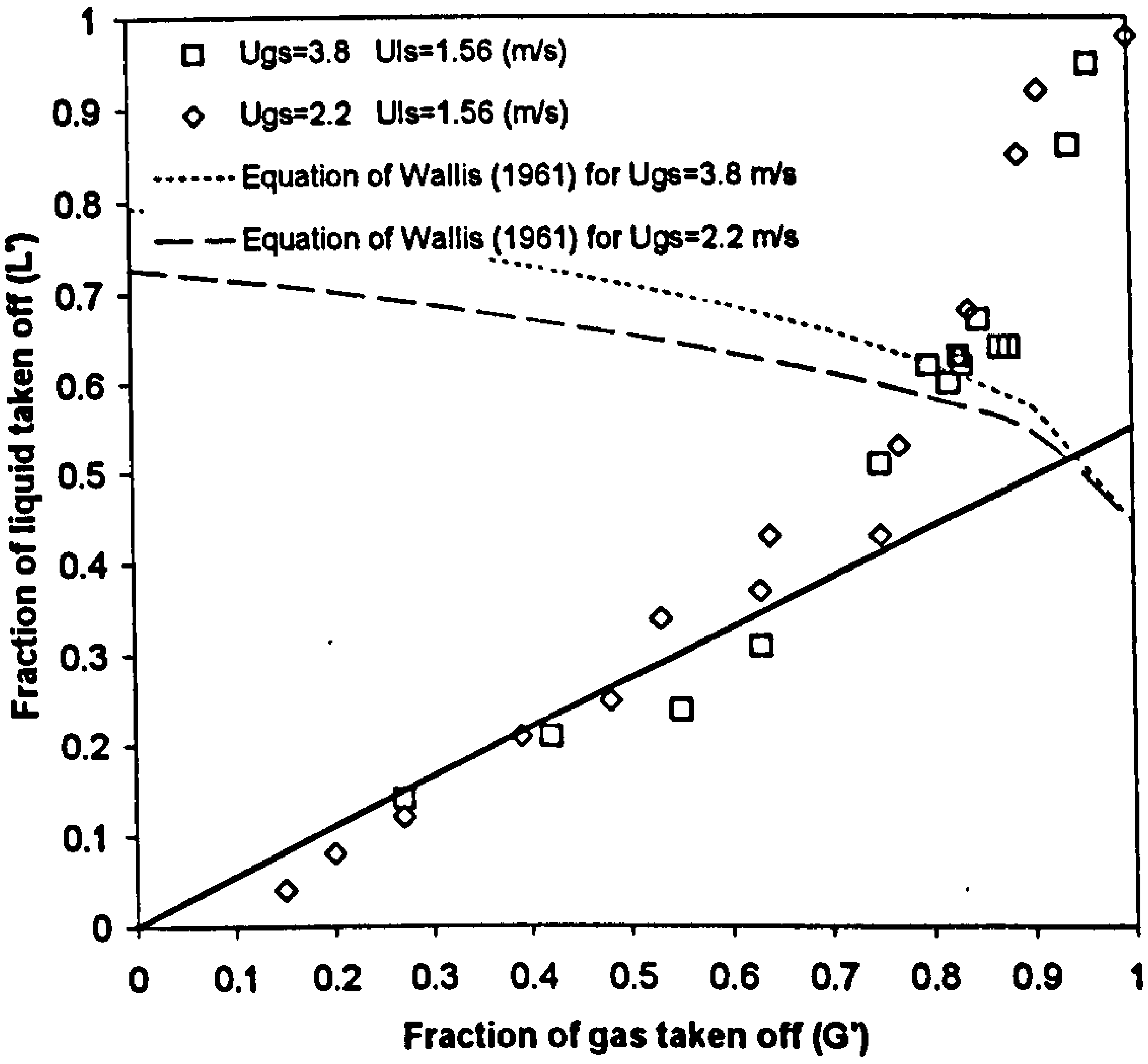

Figure V.2.9: *Plot showing detachment of split characteristic from the direct take off predicted by Azzopardi and Baker (1981). Detachment occurs before flooding in the run arm.* U_{ls}*=1.56 m/s*

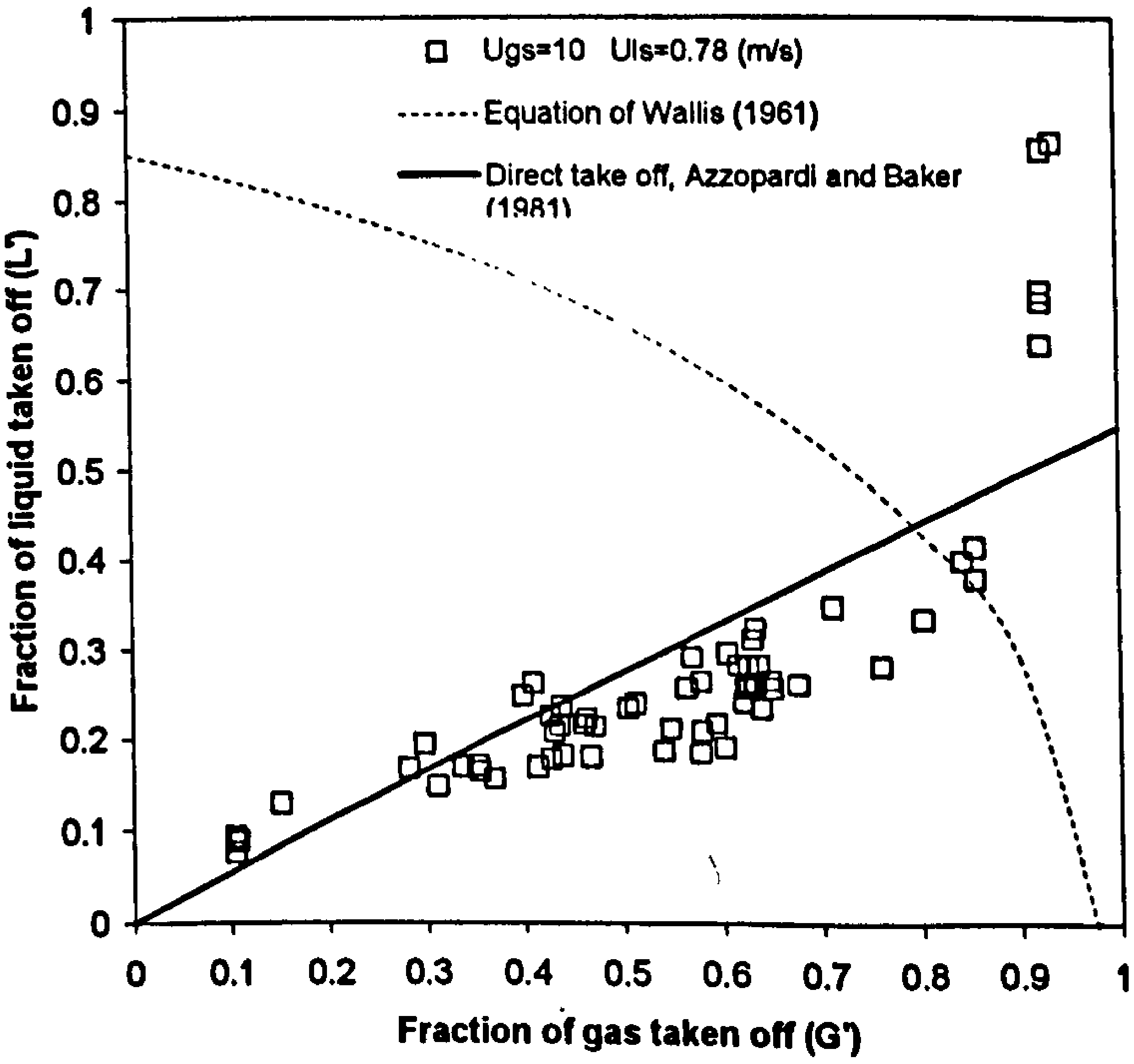

Figure V.2.10: *Plot showing detachment of split characteristic from the direct take off predicted by Azzopardi and Baker (1981).* U_{gs} *= 10 m/s;* U_{ls} *= 0.78 m/s.*

As mentioned above, a condition of flooding does not imply that only below it liquid will fall back, hence the result of Figure V.2.9. To account for this, one must consider that the factor determining whether or not the liquid will fall back depends on the balance between momentum and drag of the gas phase against gravity and frictional losses. If the momentum of the mixture is large enough, a certain portion of it will reach the top of the run branch still with enough momentum to be captured into the run outlet.

If frictional losses and drag forces are neglected, it is possible to write a balance between the momentum of the mixture and its gravitational pull. This would give, on a plot of G' vs. L', the couples for which the average momentum of the mixture is just large enough for it to reach the top of the run pipe. Above this line increasing fractions of liquid will fall back and detachment from the line of direct take off is expected. The gravitational component of the balance will contain also the length H of the run leg and its effect can be understood. The balance is:

$$\rho_g \varepsilon A U_g^2 + \rho_l (1-\varepsilon) A U_l^2 = AH\left[\rho_g \varepsilon + \rho_l (1-\varepsilon)\right]g \qquad [V.2.3]$$

[mixture momentum at run inlet] = [weight of mixture in the run]

(A is the cross sectional area, U_i is the velocity of phase i at the run inlet, and ε is the void fraction in the run. By definition:

$$\varepsilon = \frac{1}{1 + U_r \dfrac{(1-L')U_{ls}}{(1-G')U_{gs}}} \qquad [V.2.4]$$

U_{is} is the superficial velocity of phase i in the inlet pipe and $U_r = U_g/U_l$ is the slip ratio. For homogeneous model, this is given by $U_r = 1$.)

Looking at equation V.2.3, it could be argued that no pressure difference has been accounted for in the balance. This would be valid if the gas could be considered as a stagnant phase and the liquid driven only by its momentum in a gas continuum. Because the flow is in the churn regime and because the split is gas dominated, this is true to an extent. Another way of looking at it is to assume that the difference of pressure between the T outlet to the run leg and the top of the run, is just enough to compensate for frictional losses, in which case they would appear but have opposite sign in the balance V.2.3. Bearing in mind the above, equation V.2.3 can be developed to obtain an explicit solution for the homogeneous model as follows:

$$L' = \frac{U_{ls} - \sqrt{Hg} + (1 - G')U_{gs}}{U_{ls}} \qquad [V.2.5]$$

For the inlet flow rates investigated, the model gives rise to negative values of L'. Although physically unacceptable as a result, this circumstance suggests that the mixture momentum would never be large enough to bring any liquid to the top of the run arm. In the reality, the momentum of the mixture is larger than calculated with a homogeneous or slip model based on the quality at the inlet of the run leg. The momentum of the mixture will be in fact larger for two reasons:

1) The mixture is carrying straight from the inlet pipe where momentum is larger due to larger flow rates.
2) The mixture is accelerated by the restriction caused by eddy circulation at the wall opposite to the side arm opening, immediately downstream of the T.

Also, the portion of pipe occupied by the downstream eddy reduces the effective length of the run arm significantly. To account for these factors, because it is very difficult to predict their influence, an empirical adjustable parameter has been introduced in to the gravitational component instead. More precisely, a reducing factor has been imposed on the length of the side arm so that equation V.2.3 becomes

$$\rho_g \varepsilon A U_g^2 + \rho_l (1 - \varepsilon) A U_l^2 = A \kappa H [\rho_g \varepsilon + \rho_l (1 - \varepsilon)] g \qquad [V.2.6]$$

where the constant κ (<1) ultimately contains unknown effects such as those of the length of downstream eddy, inter-phase drag, friction losses and the extra momentum at the inlet to the run due to the reasons discussed above. Best fit with the observed change of slope on the G' vs. L' diagram has been obtained for κ = 0.158.

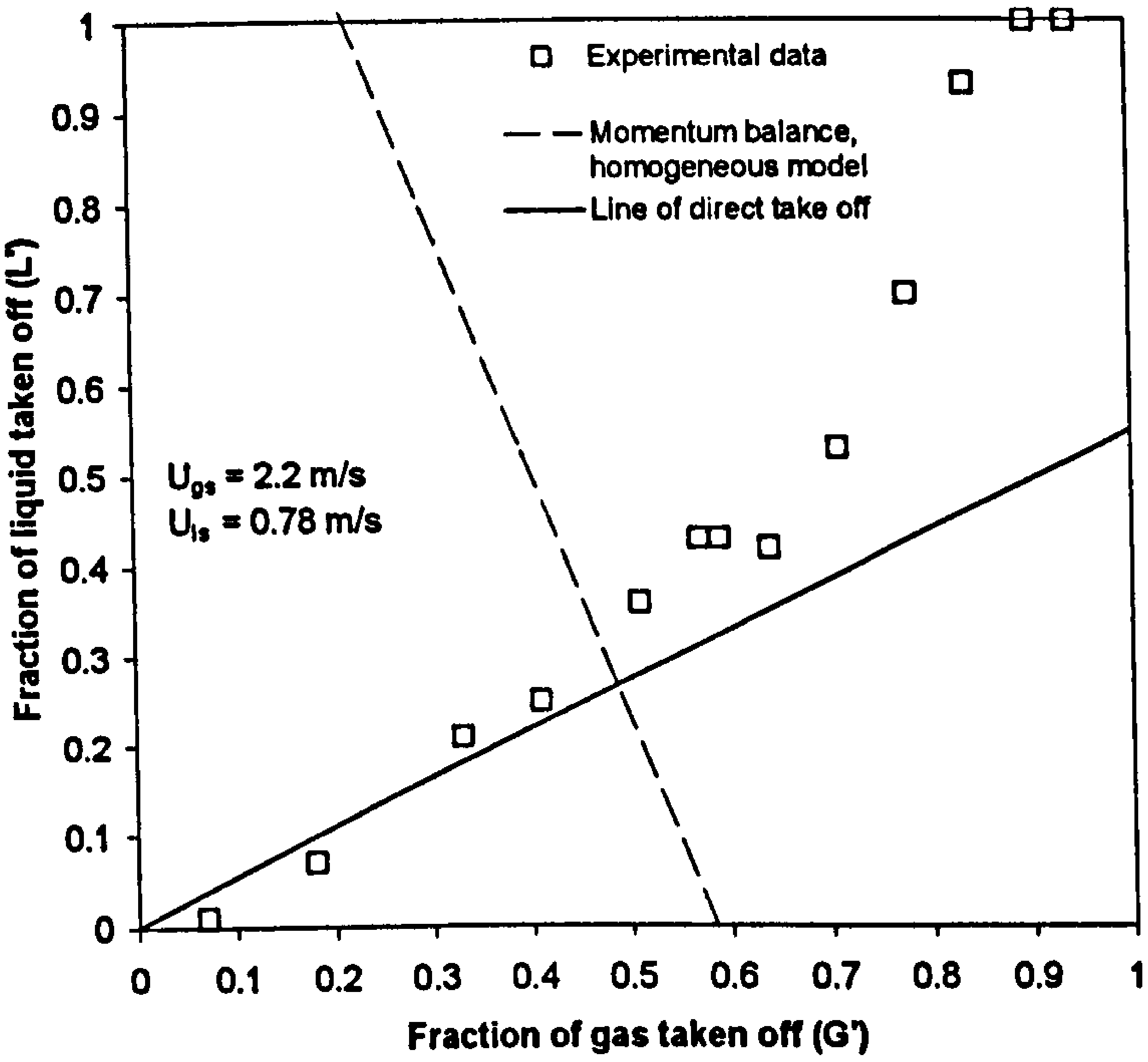

Figure V.2.11: *Series B. Prediction of secondary liquid take off initiation using a homogeneous mode for* $\kappa = 0.158$*.* $U_{gs} = 2.2$ *m/s;* $U_{ls} = 0.78$ *m/s.*

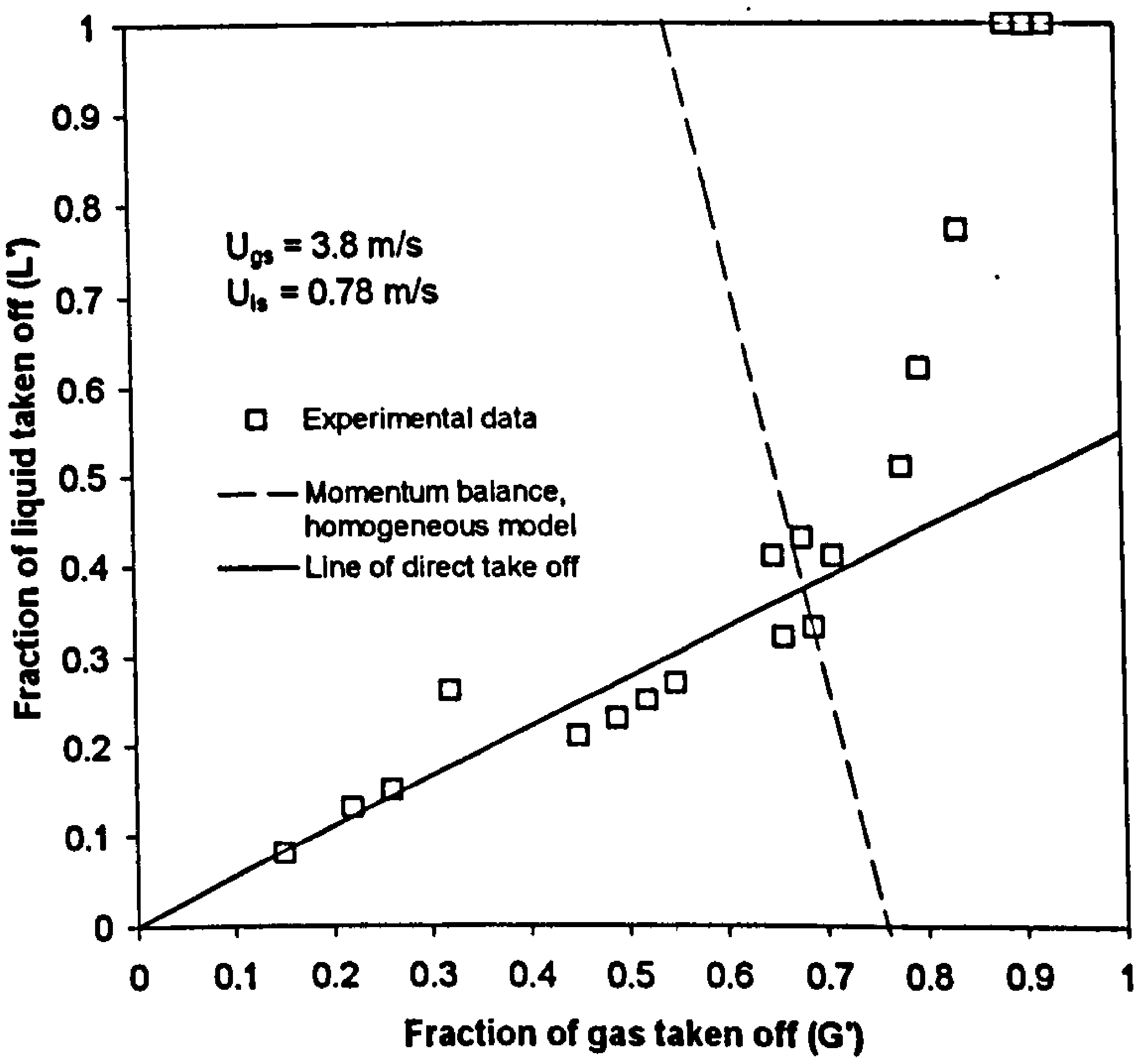

Figure V.2.12: *Series B. Prediction of secondary liquid take off initiation using a homogeneous model for* $\kappa = 0.158$*.* $U_{gs} = 3.8$ *m/s;* $U_{ls} = 0.78$ *m/s.*

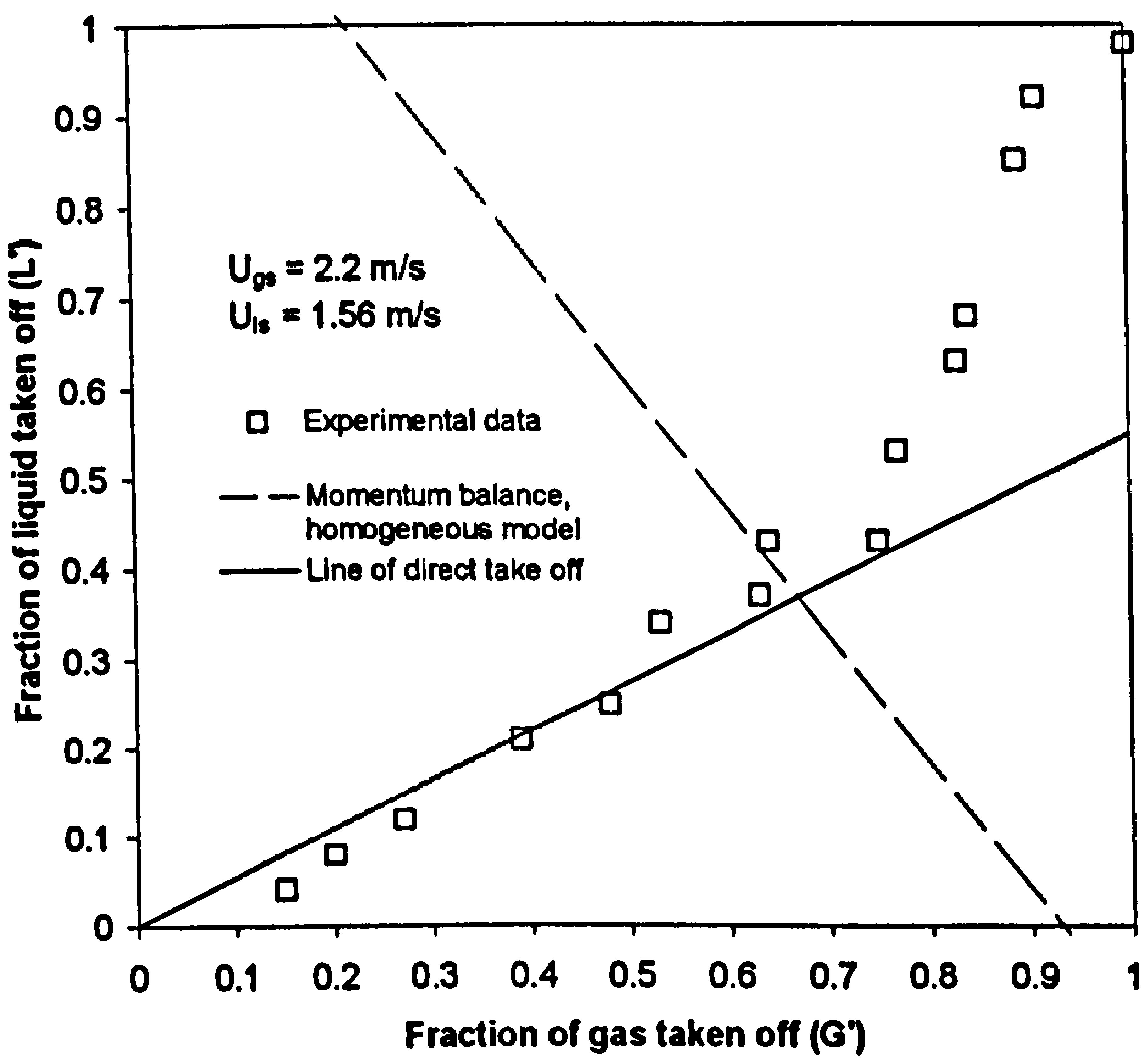

Figure V.2.13: *Series B. Prediction of secondary liquid take off initiation using a homogeneous model for $\kappa = 0.158$. $U_{gs} = 2.2$ m/s; $U_{ls} = 1.56$ m/s.*

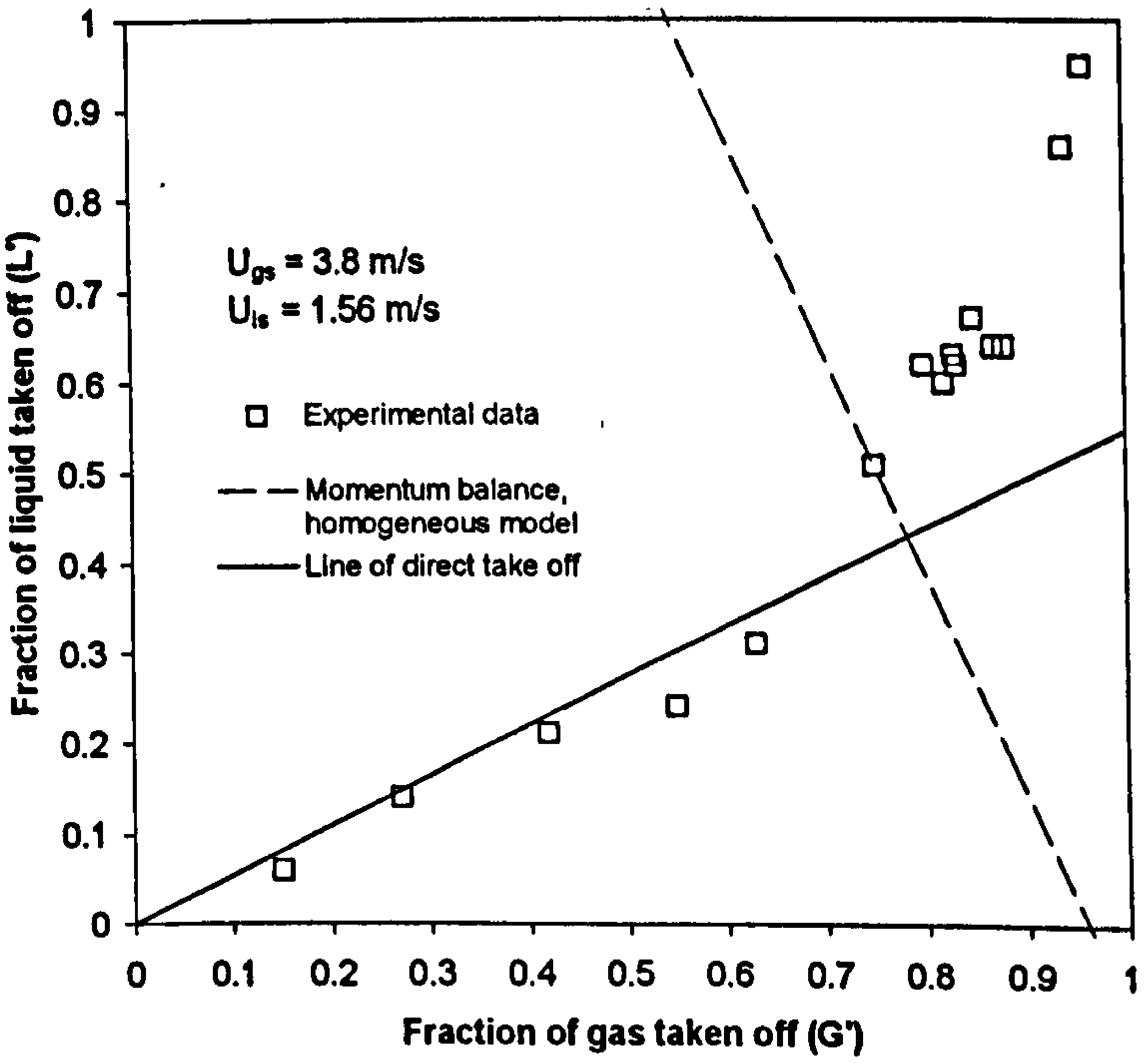

Figure V.2.14: *Series B. Prediction of secondary liquid take off initiation using a homogeneous model for $\kappa = 0.158$. $U_{gs} = 3.8$ m/s; $U_{ls} = 1.56$ m/s.*

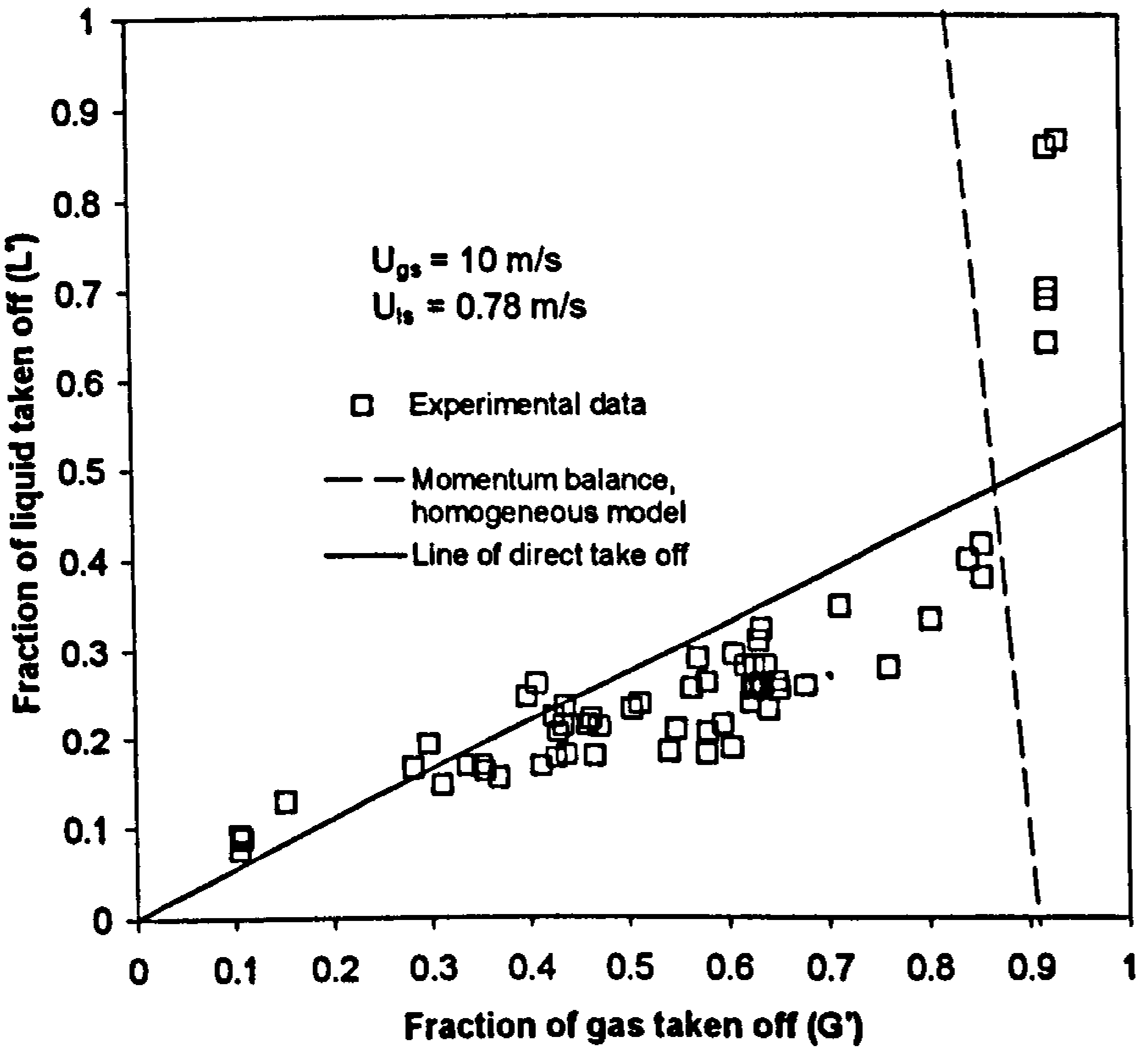

Figure V.2.15: *Series B. Prediction of secondary liquid take off initiation using a homogeneous model for $\kappa = 0.158$. $U_{gs} = 10$ m/s; $U_{ls} = 0.78$ m/s.*

Figure V.2.11-15 present the results of this model for the five inlet conditions of series B with the experimental curve as obtained with a run arm length of 1.9 m.

Although an empirical value for κ had to be assumed, which is unlikely to be independent of inlet conditions, the use of a momentum balance gives a better picture of the trends than the flooding correlation does. For example, in Figures V.2.13 and 14, an intersection is found with the line of direct take off also for the cases at large liquid superficial velocity (U_{ls} = 1.56 m/s) where the flooding correlation over predicted the area of detachment from direct take off (see Figure V.2.9).

In Figures V.2.16-19, the effect of run arm length is investigated from the experimental results and the prediction of secondary take off initiation still assuming $\kappa = 0.158$ for all the inlets except for $U_{gs} = 2.2$ and $U_{ls} = 1.56$. Experiments were made with a reduced run arm length of 0.7 m and comparison of measured and predicted trends reinforces the above ideas above. For a shorter run it is expected that a smaller momentum is needed for the mixture to reach the top of the run outlet hence secondary take off initiation would start for larger values of G'. This is confirmed by data and by the displacement of the line representing the momentum balance, based

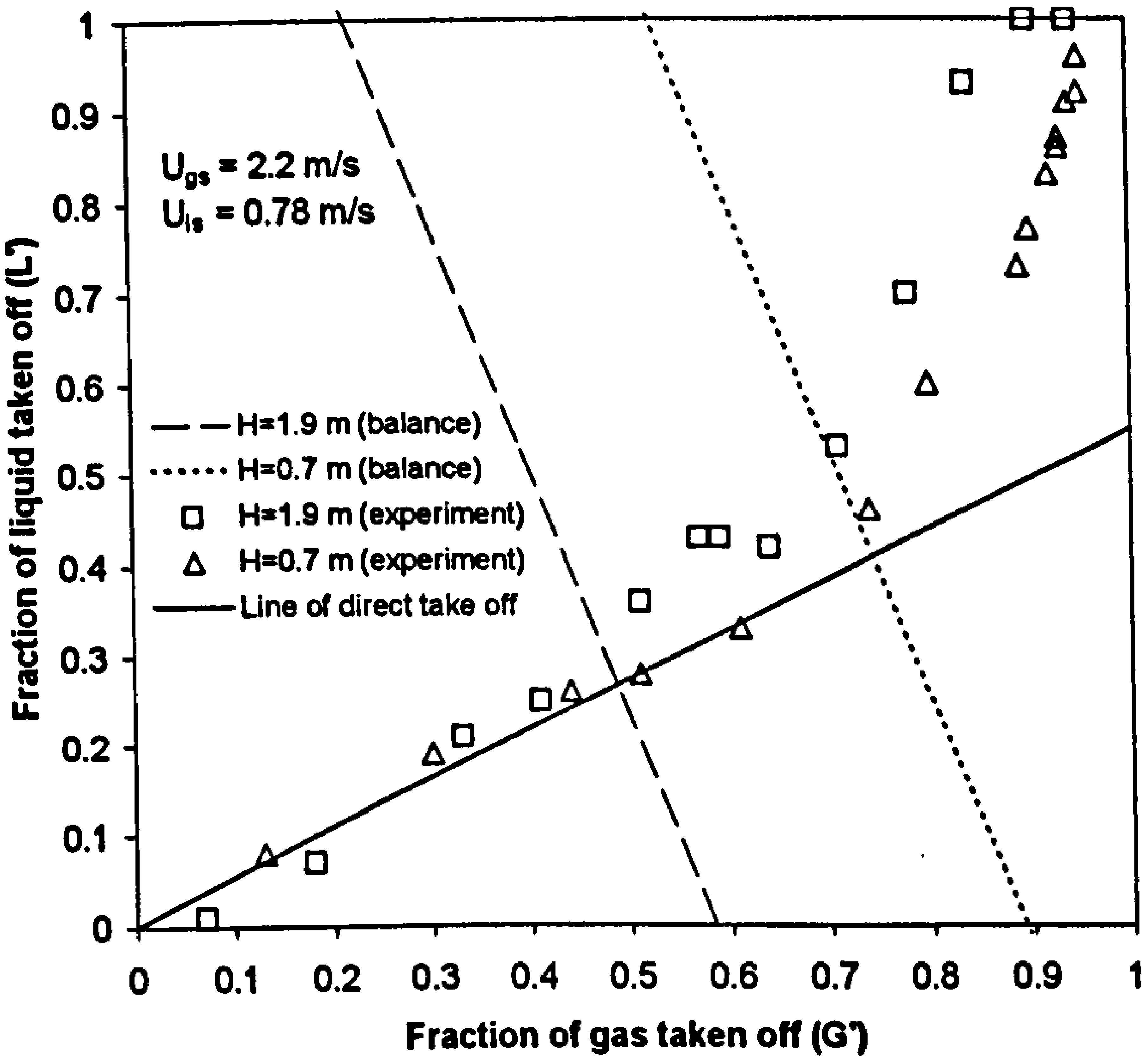

Figure V.2.16: *The effect of run arm length. Experimental data and prediction of secondary take off initiation by momentum balance.* U_{gs} *= 2.2 m/s;* U_{ls} *=0.78 m/s for* κ*= 0.158*

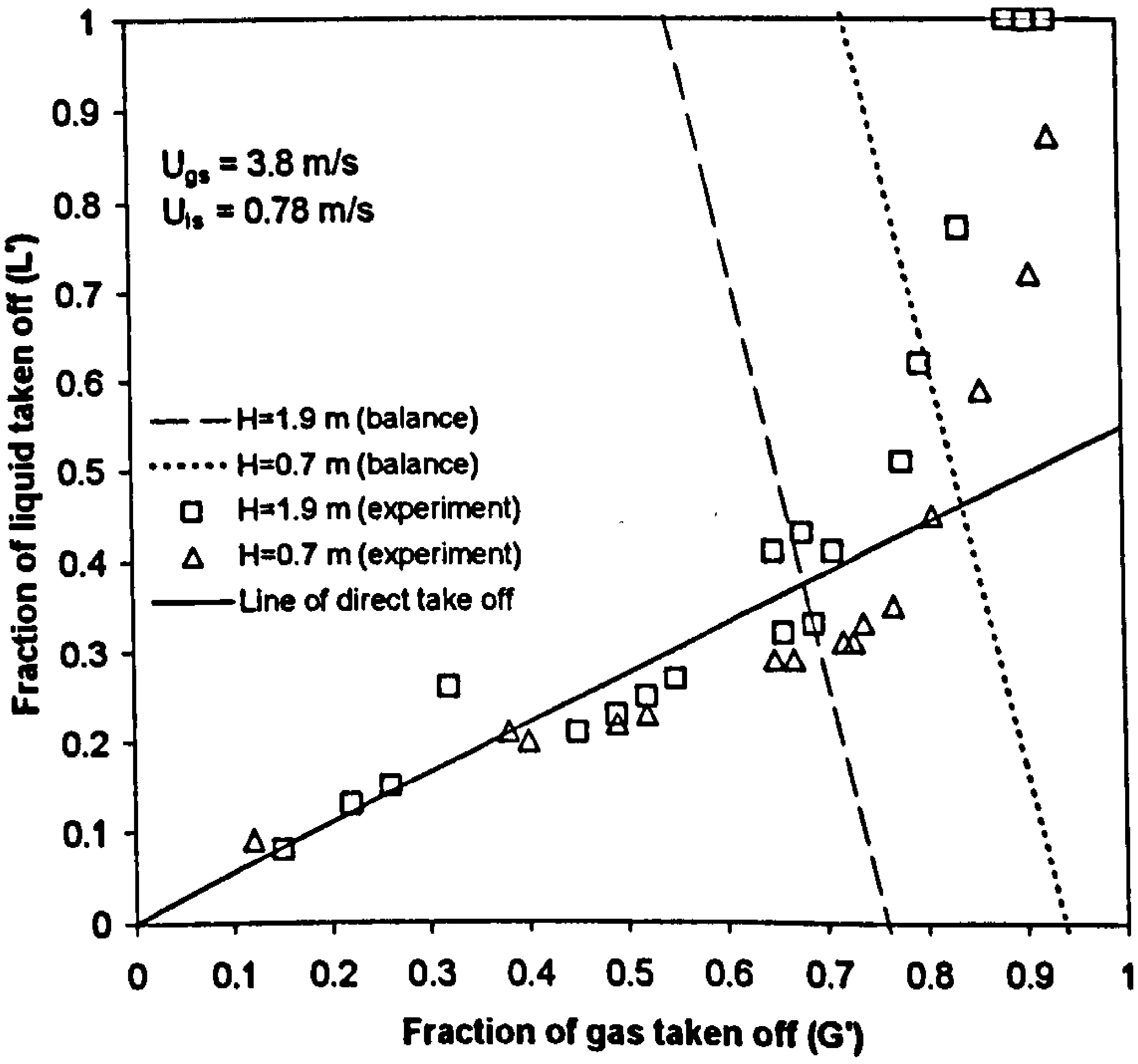

Figure V.2.17: *The effect of run arm length. Experimental data and prediction of secondary take off initiation by momentum balance.* U_{gs} *= 3.8 m/s;* U_{ls} *=0.78 m/s for* κ*= 0.158*

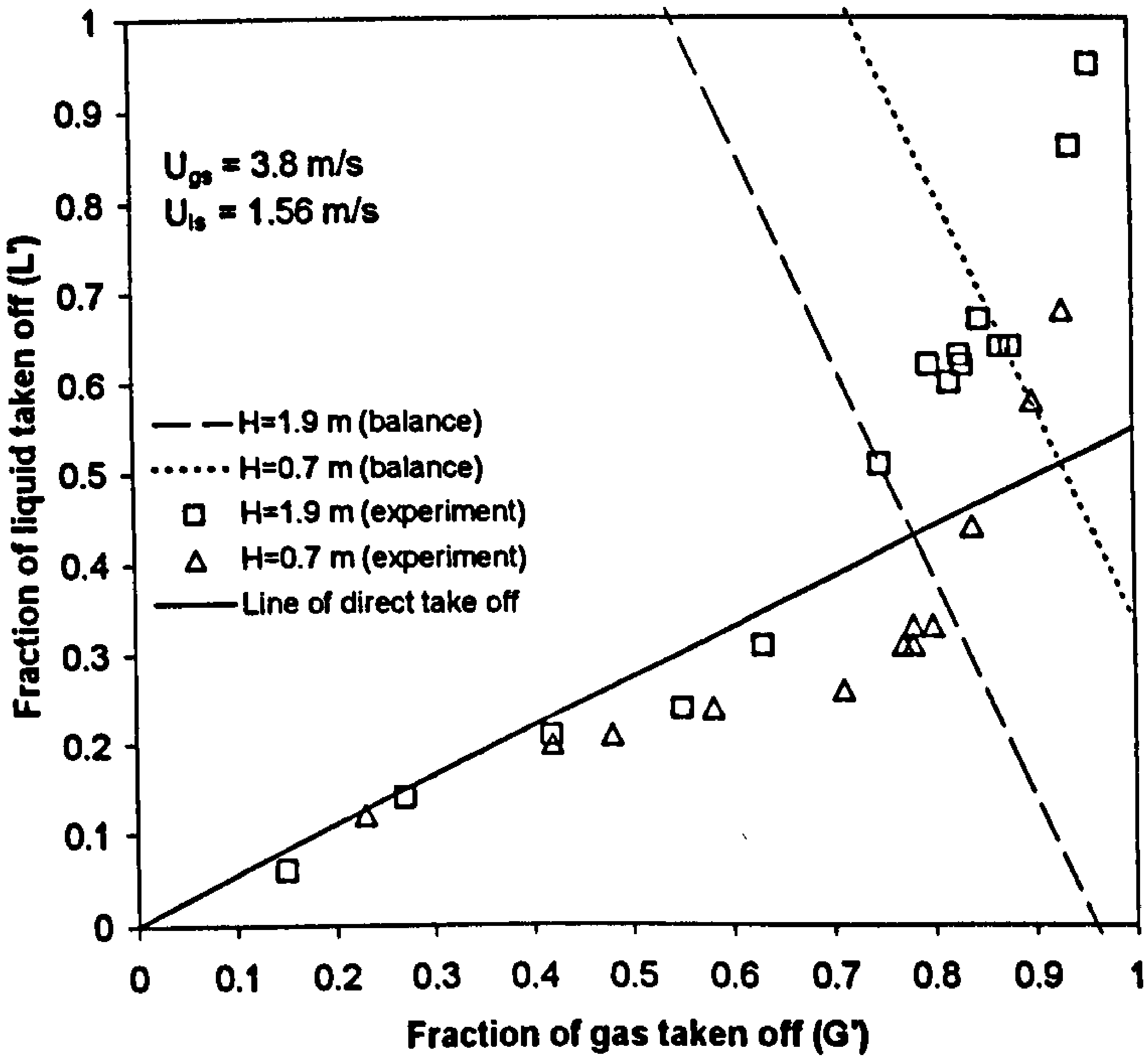

Figure V.2.18: *The effect of run arm length. Experimental data and prediction of secondary take off initiation by momentum balance.* U_{gs} *= 3.8 m/s;* U_{ls} *=1.56 m/s for* κ *= 0.158*

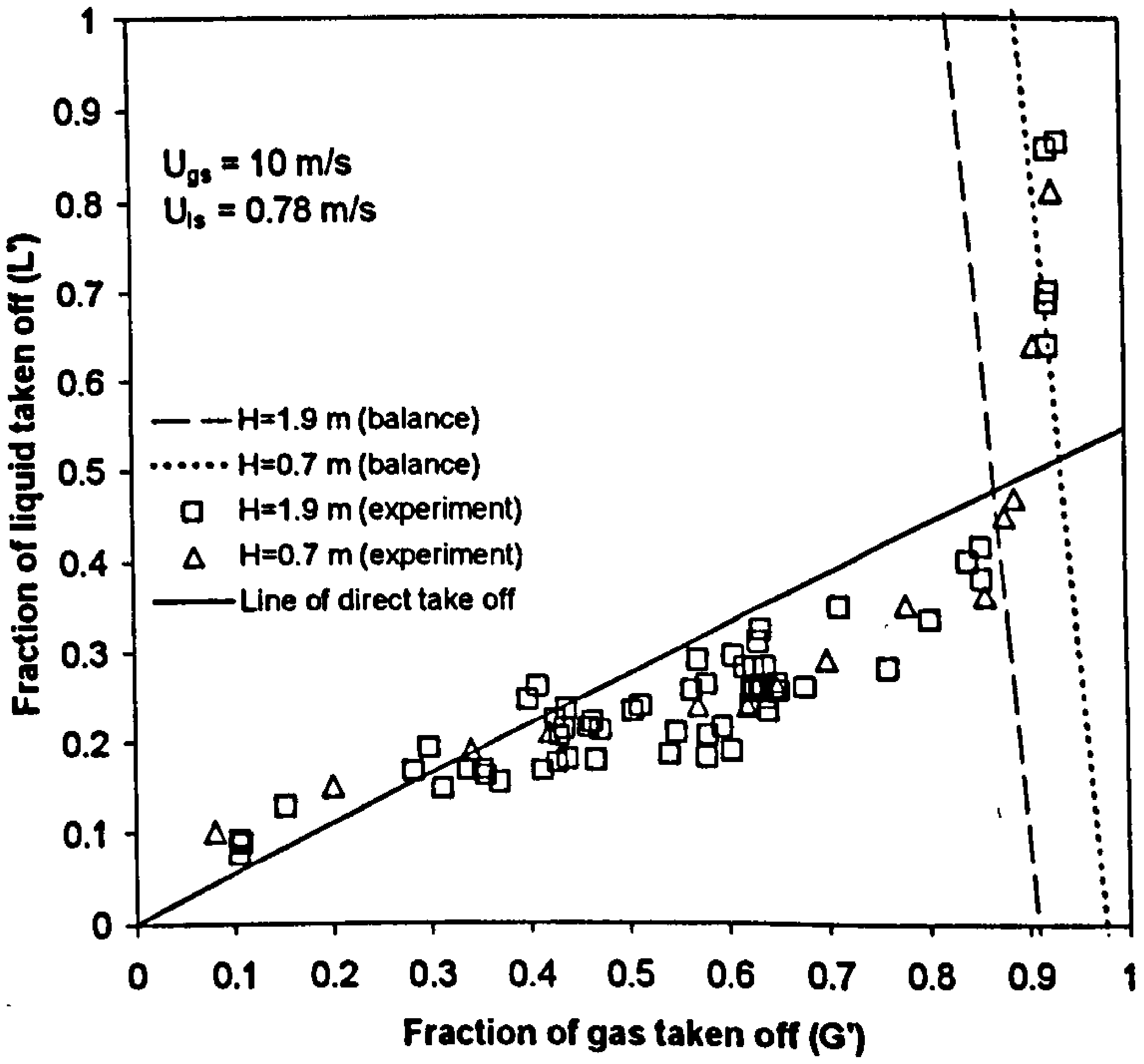

Figure V.2.19: *The effect of run arm length. Experimental data and prediction of secondary take off initiation by momentum balance.* U_{gs} *= 10 m/s;* U_{ls} *=0.78 m/s for* κ *= 0.158*

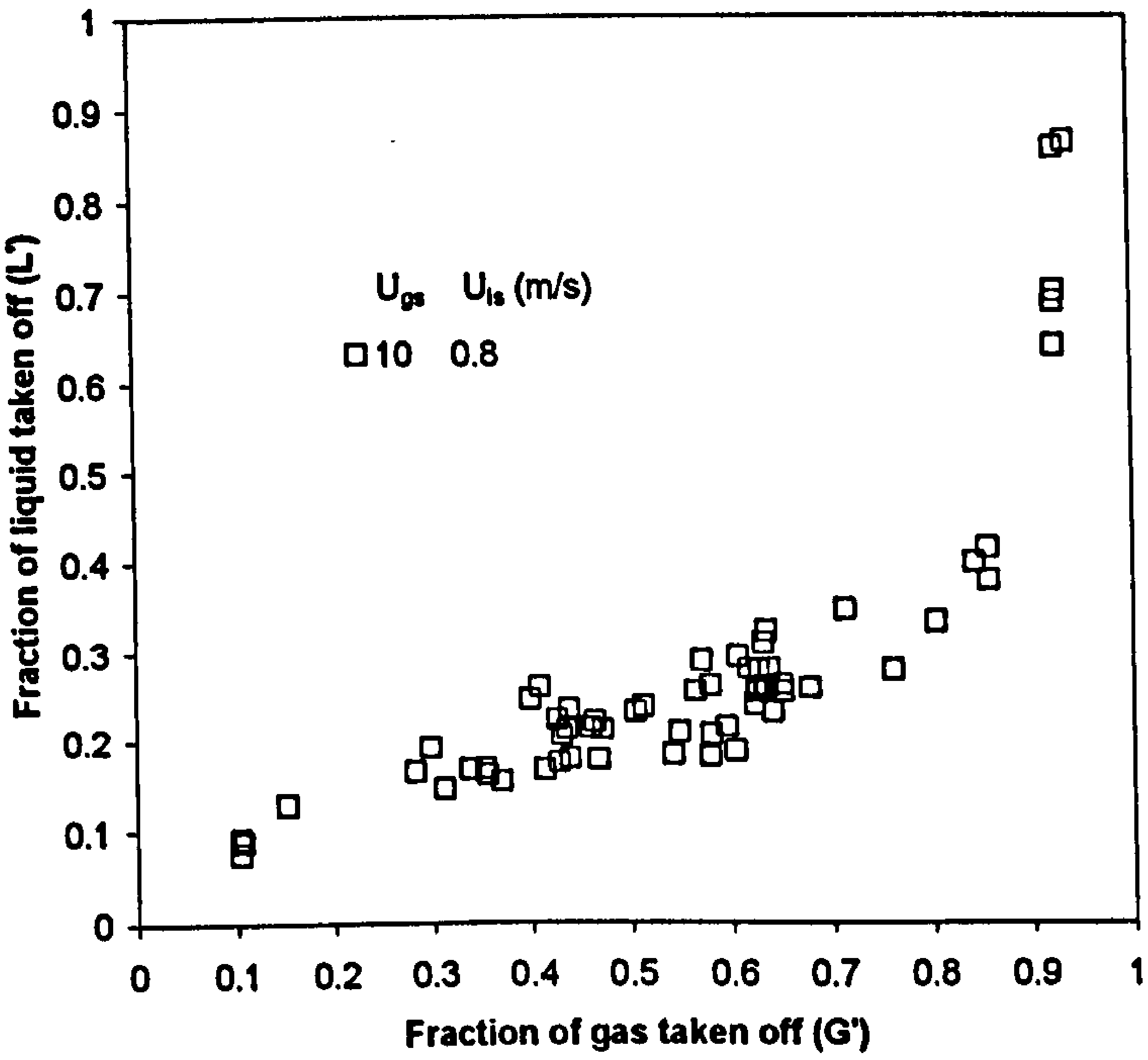

Figure V.2.20: *Scatter in the split characteristic in the range G' = 0.3-0.7 from series B* $U_{gs} = 10$ *m/s,* $U_{ls} = 0.78$ *m/s.*

on a homogeneous model, towards larger values of G'. However, in some cases the experiments give place to an initial take off below the prediction of Azzopardi & Baker (1981) and for those cases although trends are correct, the initiation of secondary take off is slightly over predicted. In particular, the case of $U_{gs} = 10$ m/s and $U_{ls} = 0.78$ m/s does not show any appreciable change in the split characteristic for the two cases and the model predicts only a small displacement of the balance equation line (Figure V.2.19). For this last set of data, another interesting feature was observed and is reported below.

From Figure V.2.20 it is possible to see that there was a visible scatter in the central part of the split graph, between G'= 0.3-0.8. This was initially thought to be due to inaccuracy in measurements. However, all the points of Figure V.2.20 were obtained within the error on gas and liquid mass balance as specified at the beginning of this chapter and even with a more restrictive condition, an area of scatter was still observed in the database.

Data were analysed by eliminating those points with excessive errors on the mass balance, particularly for the gas phase. When the error on mass balance is

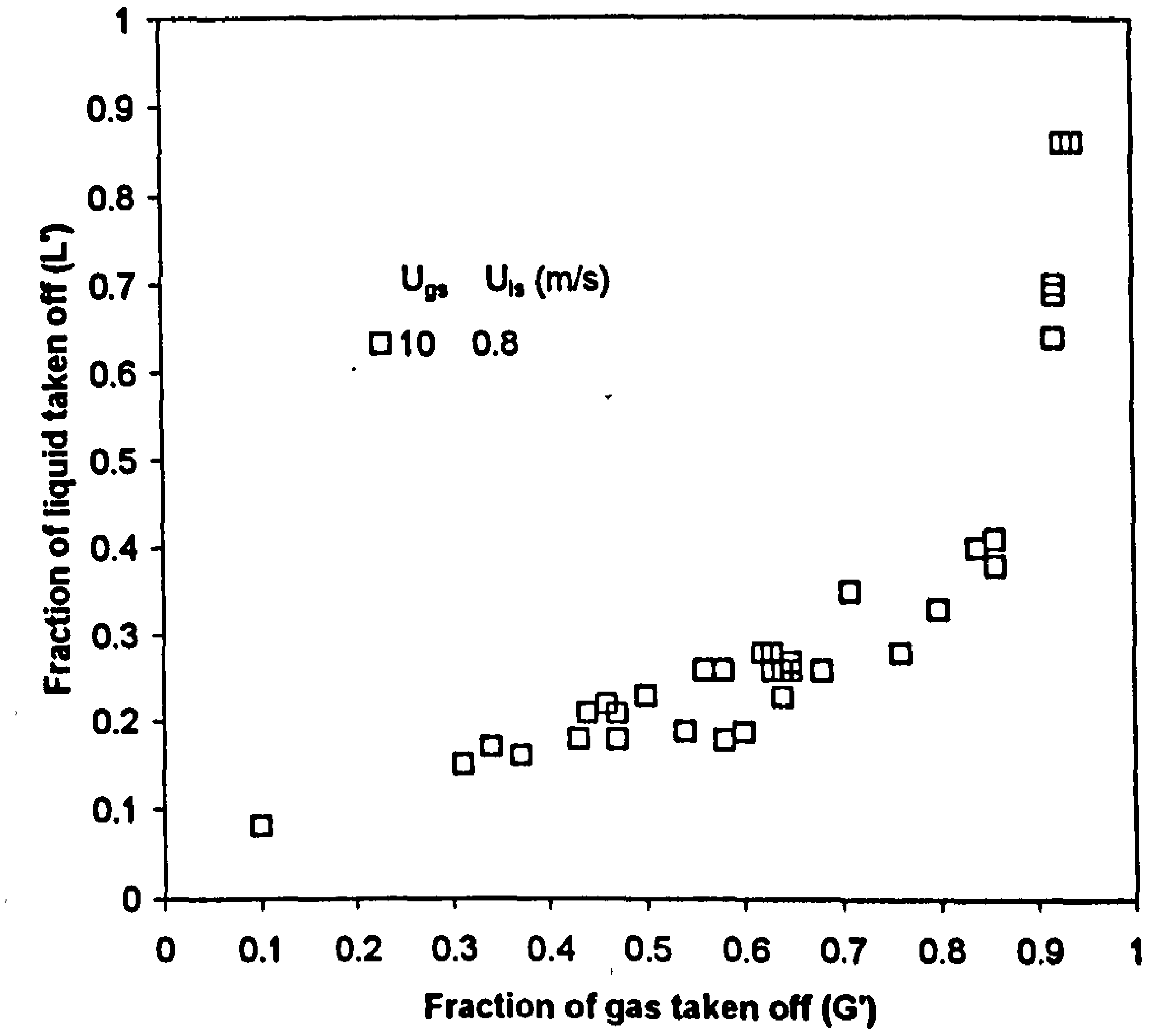

Figure V.2.21: *Series B, $U_{gs} = 10$ m/s, $U_{ls} = 0.78$ m/s. Data for error on mass balance below 6%. The scatter is resolved in two branches in the range G' = 0.45-0.65.*

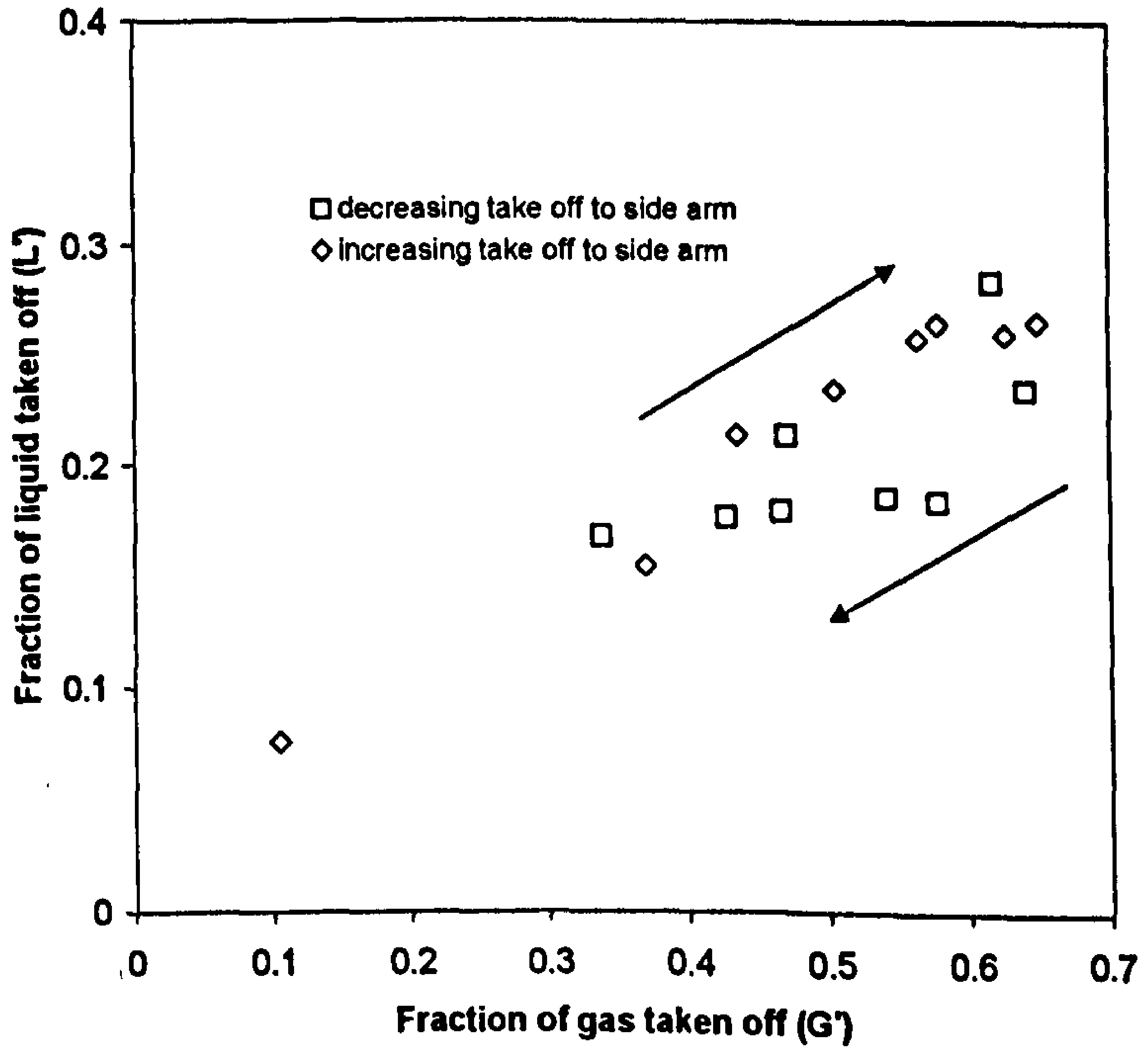

Figure V.2.22: *Series B, $U_{gs} = 10$ m/s, $U_{ls} = 0.78$ m/s. Result of split experiment by systematically moving from small towards large take off and vice-versa.*

restricted to values below 6%, the split characteristic looks as shown in Figure V.2.21. The wide zone of scatter is reduced to a smaller area in the range of G' = 0.45-0.65, where two branches are observed giving place to a larger or smaller liquid take off for the same value of G'. This gave place to the idea that the scatter might be due to the existence of two regimes depending on the evolution of the couples (G',L'). In other words, the occurrence of a hysteresis loop was hypothesised. For this reason, experiments have been carried out by producing the split characteristic systematically entering the central zone coming from large (point (1,1)) or small (point (0,0)) fractions of mixture diverted in the side arm. The results of this experiment are presented in Figure V.2.22 showing that the lower branch was obtained when coming from the point (1,1) and the upper one when coming from (0,0). The observations above and the fact that the change of slope occurs just after the hysteresis, would imply that the way the phase split depends, among the others, on whether the secondary take off is being approached (from low take off) or has been just suppressed (from large take off). However, no further studies were carried out on this phenomenon.

V.2.3 Series A data. Empirical correlation for the split characteristic in slug flow – The mechanism of split of a Taylor bubble.

Data in the slug flow regime, were taken in the conditions of series A as previously reported by Azzopardi *et al* (1994). Separation is very liquid dominated. Figures V.1.4a-b, illustrate the trend of phase split as the superficial velocity of one of the phases is changed, keeping the other constant. It is shown that the fraction of incoming gas taken off increases with liquid superficial velocity (Figure V.1.4b). Overall, there is not a strong effect of gas superficial velocity variations on the split of the phases (Figure V.1.4a). The dominance of the liquid phase upon the phase split can be explained in terms of the mechanism of gas take off from the Taylor bubbles. The observations of Azzopardi *et al* (1994) using high-speed videos indicate that these bubbles deform around the junction in a peculiar fashion. The top of a bubble is partly pulled towards the side arm as the lateral pull affects it. The liquid film on the wall is seen to fall from the run arm and to split the gas bubble isolating a part of it, which is taken off in the side arm. Part of this falling film itself is captured in the side arm. Since this phenomenon affects a variable part of the top of the Taylor bubble, the fraction of gas that is taken off in the side arm is very small. Hence, separation is liquid dominated to the extent that, in most cases, before 50% of the gas is taken off, all of incoming liquid travels into the side arm.

To understand the effect of inlet gas and liquid superficial velocity on the phase split, it can be argued that the dominating phenomenon in the gas take off is local, in the sense that it affects only the top of the bubble. Hence, regardless of the length of the bubble, the amount that is taken off is fixed when all the other conditions are kept constant. Therefore, the bigger the bubble, the smaller is the value G' of the gas fraction taken off. Another parameter to be considered is the bubble velocity. Although the phenomenon of bubble deformation is local, the zone of the bubble split by the falling film will depend on the bubble velocity. The assumption can be made that the falling film cutting the bubble is mainly driven by gravity. This is reasonable for the magnitude of gas velocities involved in the slug flow regime. On the basis of this hypothesis, when the bubble is faster, the length travelled by the penetrating film through the Taylor bubble is deeper and the diverted fraction in the side arm is larger. Thence, increasing the bubble velocity causes an increase in the value of factional gas take off.

To understand in better detail the trends observed in Figure V.1.4, it is useful to look at the problem in terms of a simplified slug flow model. In general, slug flow is made up of liquid slugs and gas bubbles of variable length and void fraction depending on fluid properties, pipe diameter and inlet flow rates. Also, there is a slip velocity between the two phases and Nicklin and Davidson (1962) expressed the velocity of a bubble raising in a flowing liquid as:

$$U_b = 1.2 * \left(U_{gs} + U_{ls}\right) + 0.35\sqrt{gD} \qquad [V.2.7]$$

In first approximation one can assume that the slug flow is made of alternating gas and liquid pockets where no liquid is entrained in the bubble and vice-versa. Also, because the slip ratio calculated on the basis of equation V.2.7 in the database of Azzopardi *et al* (1994) varies between 2 and 6 with most values in the region of 3, a slip of 1 (homogeneous model) will be employed. Finally, there is evidence that the length of a slug is a weak function of inlet flow rates and strongly depends on pipe diameter. Slug length is seen to vary between 7D and 15D (e.g., Griffith and Wallis,1961; Costigan and Whalley, 1996) and here will be assumed to be constant.

On the basis of the above approximations and of the considerations made over the effect of bubble length and velocity on the split of gas, it can be argued that:

1) If inlet quality is increased by increasing the gas flow rate whilst liquid inlet is kept constant, the bubble will grow in length (which would reduce the gas fractional take off). By closure of the mass balance on the liquid phase, the overall velocity of the two phases must increase. Hence, the gas bubble's velocity increases leading to a higher fraction of gas taken off. The two effects eventually cancel out, explaining the small sensitivity of the split characteristic to inlet gas superficial velocity as shown in Figure V.1.4a.
2) If inlet quality is increased by decreasing the liquid flow rate whilst keeping a constant gas inlet flow rate, the liquid slug velocity must decrease because of its fixed length. Therefore, the bubble's velocity decreases (hence, smaller gas fractional take off). By closure of the mass balance on the gas phase, the bubble must be longer (the fraction of gas taken off decreases). In this case, the two effects are additive, hence the reduction of the fraction of gas in the side arm. This could explain the data plotted in Figure V.1.4b.

If the mechanism above is taken into consideration, a model based on the physical interaction between the falling film and the rising bubble could be used to predict the trends in the split equations as observed in series A data. In the following, the development of an empirical correlation based on this reasoning is presented.

The time τ necessary for the liquid film to sweep the side arm opening can be calculated on the hypothesis of a gravity driven mechanism:

$$\tau = \frac{-v_0 + \sqrt{v_0^2 + 2gD}}{g} \qquad [V.2.8]$$

where v_0 is the initial falling velocity of the liquid. Here it is assumed that this initial velocity depends on the head of liquid above the splitting bubble. Such head is the length of the liquid slug after part of it has been diverted into the side arm and, if β is the factor by which the slug length scales on the pipe diameter:

$$v_0 = \sqrt{2g\beta D(1-L')} \quad [V.2.9]$$

and substituting in the previous equation:

$$\tau = \frac{\sqrt{2gD}\left(\sqrt{1+\beta(1-L')} - \sqrt{\beta(1-L')}\right)}{g} \quad [V.2.10]$$

In the hypotheses of homogeneous flow, slug and bubble move at the same velocity $U_g = U_l = U_{gs} + U_{ls}$. Hence, the frequency f of slug and bubbles transit through a section of pipe is equal and in the approximation of no entrainment of one phase in the other is given by:

$$f = \frac{U_{ls}}{\beta D} = \frac{U_{gs}}{\lambda} \quad [V.2.11]$$

where λ is the length of the bubble and:

$$\lambda = \frac{U_{gs}}{U_{ls}}\beta D \quad [V.2.12]$$

and finally, the residence time of the bubble across the side arm opening is:

$$t = \frac{\lambda}{U_g} = \frac{U_{gs}}{U_{ls}(U_{gs}+U_{ls})}\beta D \quad [V.2.13]$$

From previous considerations, it would be expected that the amount of gas $\dot{M}_{g3}$ diverted into the side arm increases with the ratio τ/t up to a limit defined by the amount $\dot{M}_{g1}$ of gas at the inlet.

An example of such a function is found in the kinetics of enzymatic reactions. Without going in the details, there is a limiting velocity of reaction defined by the concentration of enzyme, and although velocity increases with the concentration of substrate, it will never exceed a certain value V_{max}. This is described by the equation of Michaelis & Menten (1913):

$$\frac{V}{V_{max}} = \frac{[S]}{K_s + [S]} \quad [V.2.14]$$

where [S] is the molar concentration of substrate and K_s is a physical constant representing the concentration of substrate that would give place to half of the maximum velocity.

In the present case, the analogue of the concentration is the ratio τ/t and if $\dot{M}_3$ is the analogue of V and $\dot{M}_1$ the analogue of V_{max}, then the equation for the present case is:

$$\frac{\dot{M}_{g3}}{\dot{M}_{g1}} = G' = \frac{\tau/t}{\theta + \tau/t} \quad [V.2.15]$$

Another condition that should be satisfied by equation V.2.15 is that:

$$\lim_{L'\to 0} G' = 0 \quad [V.2.16]$$

Given that, once the inlet flow rates are specified, t is a constant and τ has a finite limit for L'≠0, the only way to satisfy condition V.2.16 is to assume that:

$$\lim_{L'\to 0} \theta = \infty \quad [V.2.17]$$

A mathematical form of θ that satisfies the above condition is:

$$\theta = \frac{\chi}{(L')^{\alpha}} \quad \alpha > 0 \quad [V.2.18]$$

From V.2.10 and V.2.13:

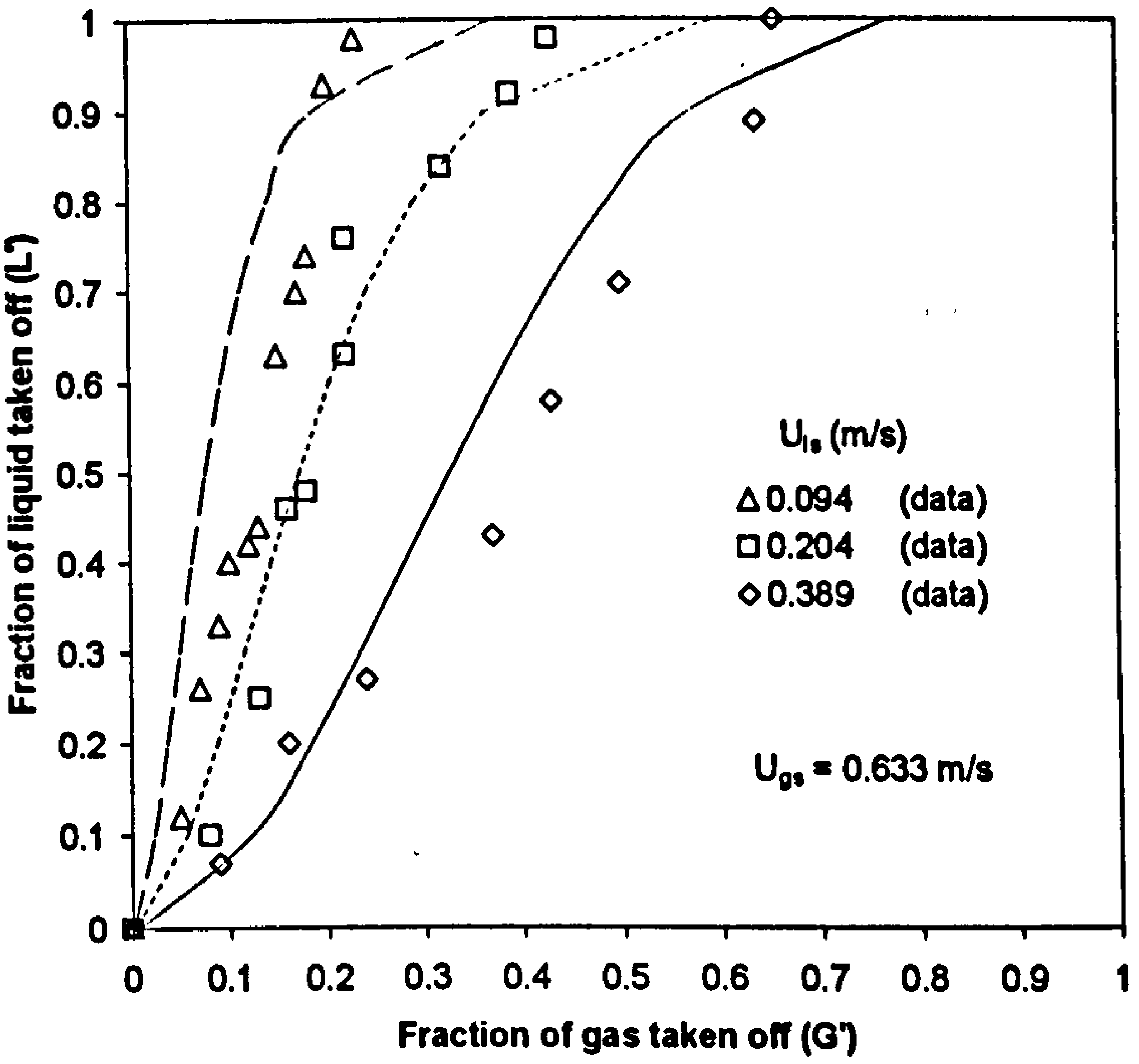

Figure V.2.23: *Series A. Comparison of split results with equation V.2.15 by assuming $\alpha = 0.6$, $\beta = 10$ and $\chi = 0.03$. Sensitivity to liquid inlet flow rate.*

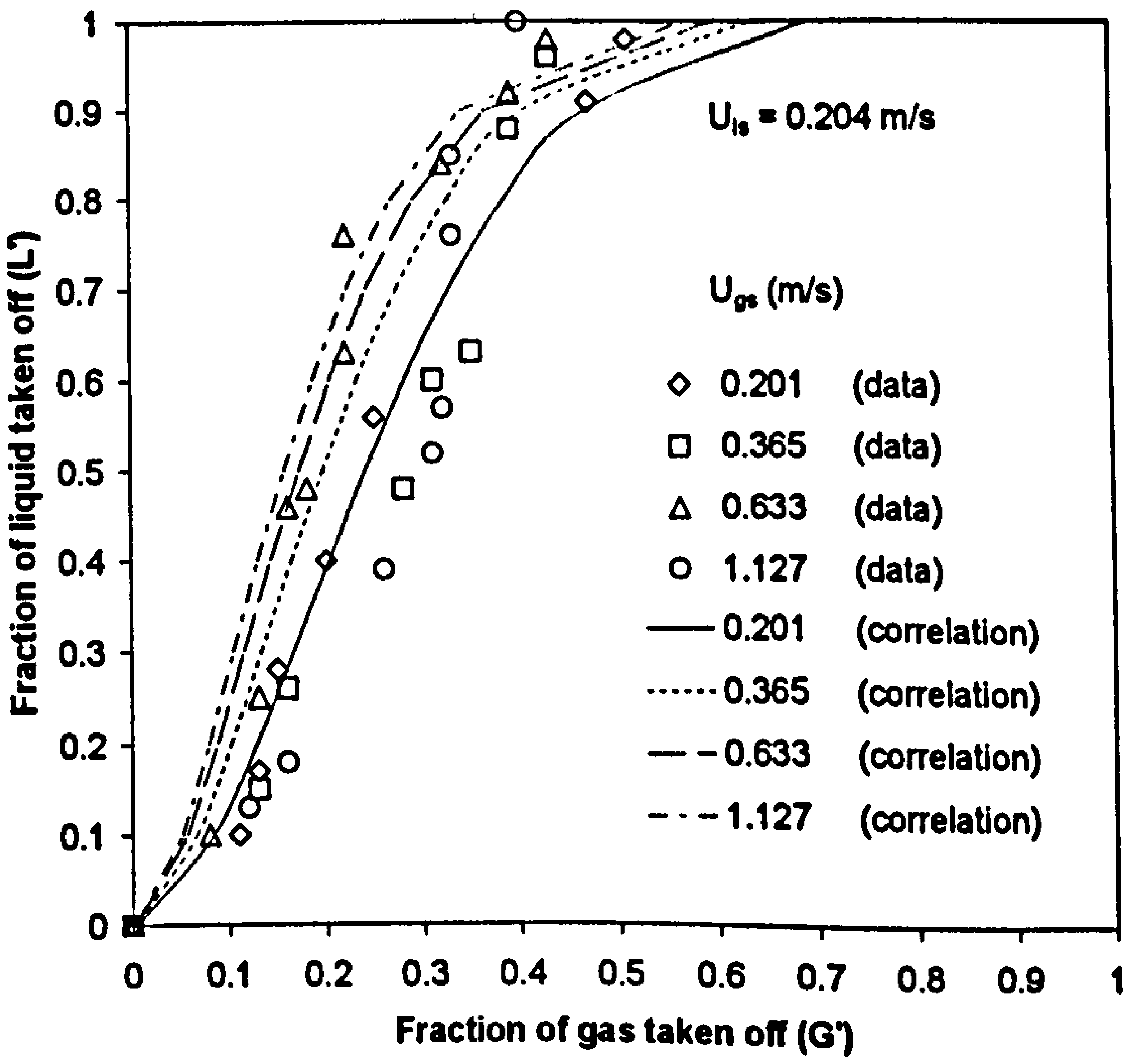

Figure V.2.24: *Series A. Comparison of split results with equation V.2.15 by assuming $\alpha = 0.6$, $\beta = 10$ and $\chi = 0.03$. Sensitivity to gas inlet flow rate.*

$$\frac{\tau}{t}=\frac{U_{ls}\left(U_{ls}+U_{gs}\right)\sqrt{2gD}\left[\sqrt{1+\beta\left(1-L'\right)}-\sqrt{\beta\left(1-L'\right)}\right]}{\beta DgU_{gs}} \qquad [V.2.19]$$

and the proposed correlation is equation V.2.15 where τ/t and θ are functions of L' given respectively by equations V.2.19 and V.2.18. β is now assumed constant and equal to 10, as suggested by previous experiments (Griffith and Wallis, 1961; Costigan and Whalley, 1996) and a good fit of data was obtained for α=0.6 and χ=0.03 as shown in Figures V.2.23-24. Although not all the trends are picked up accurately, Figure V.2.23 shows the sensitivity to the liquid flow rate comparing experimental points to the proposed correlation. For this case and the case of Figure V.3.24, where gas flow rate is varied, the correlation predicts the correct trends. Comparisons with all the database of series A is presented in Appendix B.

Chapter VI

Conclusions and further work

VI.1 Final considerations and conclusions

In the present work, knowledge of the split of gas/liquid flow at T-junctions has been improved in several areas.

Annular and bubbly vertical flows, where the boundaries between the phases are of simple representation, have been modelled in the past in a number of manners and with successful outcome. We have concentrated in the more complex slug and churn flow regimes where the mechanism of split is less clear. By introducing a mechanism for the onset of secondary take off in churn flow and by using the mechanism of split of a Taylor bubble in slug flow, semi-empirical correlations have been developed to predict the experimental trends and to validate the ideas developed to understand the phenomena of split.

The case of horizontal annular flow is less straightforward than the vertical case and is still a cause of debate. Hence, we have concentrated on detailed measurement of the annular film and a large database has been produced to compare with predictive techniques. Particularly, the T-junction has been used as a relatively simple geometry to validate CFD simulations of Adechy (2000). Original data, showing the film distribution within the T-junction, have also been produced. The model of Hurlburt and Newell (2000) is a simple model that, by including the effect of static pressure variations, results in good predictions, especially when fed to the split model of Roberts *et al* (1997).

An analogy can be drawn between the findings in horizontal and vertical geometry, particularly with regard to the steep change in the slope of the split curve observed in horizontal annular flow and in vertical churn flow. The former is caused by the hydraulic jump occurring downstream of the T and the latter occurs because of flooding, when the momentum of the liquid is not large enough to reach the top of the run leg. Although conceptually different in the physics, the findings could be transferred from one area to the other.

We can list the following conclusions:

i) Air/water split experiments have been carried out in a horizontal T-junction (0.127 m ID) in the annular and semi-annular flow regimes, showing the expected gas dominated split behaviour

ii) Wire probes and flush mounted pin probes have been used to implement a conductance technique to measure film thickness distribution in the three legs of the T. It was found that the effect of gas flowrate is strong and caused the liquid film to become thinner as this was increased. The effect of liquid flowrate is barely appreciable for the investigated database. Appropriate test sections have been designed.

iii) A T-block test section was designed and fitted with wire probes for the investigation of liquid film distribution within the T-junction

iv) From the film thickness results, trends in the split data have been interpreted (section III.3.10). Particularly, the small variation of liquid film thickness with increasing liquid flowrate leaves the entrained fraction as only possible explanation for the observed trend of split data. A suggestion has been made to explain the rather uniform split behaviour for varying gas flowrate. This is based on the contrasting action of liquid entrained fraction in the gas core and pressure differential in the side arm.

v) The hydraulic jump occurring downstream of the T-junction, for large enough fraction of diverted mixture, has been observed and recognised as a cause for the steep increase in the slope of the split characteristic. Still pictures have been taken and the jumps have been classified.

vi) Comparison has been carried out between the film thickness measurements at the inlet pipe and the model of Hurlburt and Newell (2000). This has been shown to give place to a sharp peak in the film distribution at the bottom of the pipe, never observed in the experiments.

vii) Introduction of the static pressure term, due to the variation of film thickness, has been introduced in the model of Hurlburt and Newell (2000) and resolved numerically to give place to improved predictions, without the sharp peak discussed in vi). However, predictions do not agree with data at low gas superficial velocity.

viii) The film distribution obtained from vi) and vii) were fed to the split model of Roberts *et al* (1997). Again, the introduction of the static pressure term gives place to improved results, even in terms of split prediction.

ix) Air/water split experiments have been carried out in the high and low velocity churn flow regimes, for the case of a 0.076 m ID vertical T-junction. In addition, the database produced by Azzopardi *et al.* (1994 and 1996) has been interpreted.

x) A criterion has been established to predict gas or liquid dominated behaviour when 50% of the incoming gas is taken off in the side arm. This is based on experimental observation and incorporates data for several pipe diameters and pressures.

xi) The flooding correlation of Wallis (1961) has been used to show the importance of this phenomenon to the onset of secondary take off of liquid in the churn flow regime. A simple method based on a balance between momentum flux and gravity, successfully predicts the point of detachment from the direct take off line (Azzopardi & Baker, 1981; Lahey *et al.*, 1985) of the split curve.

xii) Evidence has been gathered showing the occurrence of a hysteresis phenomenon in the split of large gas velocity, churn flow.

xiii) A semi-empirical correlation based on the analogy with saturation kinetics reactions has been developed to explain the liquid dominated split behaviour measured by Azzopardi *et al* (1994) and to predict trends. This is based on the observed mechanism of split of a Taylor bubble.

VI.2 Further work

With regard to the work developed in this thesis, the following recommendations for future work are made:

i) For the horizontal annular flow, little attention has been paid in the experimental campaign to the liquid phase as droplets. Not only in terms of entrained fractions but also in microscopic terms. It is suggested that experiments should be carried out to characterise drop size and velocity distributions in the cross sectional area. More than in terms of split predictions, this would be useful for the validation of predictive methods such as CFD.

ii) Pressure drop measurement should be carried out to complement the present data. These would be of interest for a more accurate estimate of the interfacial shear stress to be implemented in the predictive models and to clarify the reason of disagreement between experiments and models.

iii) Further investigations should be carried out to better understand the hysteresis phenomenon observed for high quality churn flow. It is known that simple devices involving two dynamic entities (in the present case the two phases) can give place to memory effects.

iv) The occurrence of interference between the hydraulic jump occurring in horizontal flow and the side arm opening could be studied in a similar manner to what has been done for the flooding phenomenon in vertical flow, to predict the onset of secondary take off in horizontal annular flow.

References.

Adechy, D (2000), PhD Thesis, Imperial College of Science, Technology and Medicine, London (in preparation).

Adechy, D and Issa RI (1999), Numerical modelling of horizontal annular flows, *2nd Int. Symp on Two-phase Flow Modelling and Experimentation, Pisa (Italy), 23-26 May, 1607-1615.*

Alves, GE (1954), Co-current liquid-gas flow in a pipeline contactor, *Chemical and Process Engineering*, **50**, 449-456.

Andreussi, P & Azzopardi, BJ (1983)3, Droplet deposition and interchange in annular two-phase flow, *International Journal of Multiphase Flow*, **9**, 681-695.

Andritsos, N & Hanratty, TJ (1987), Influence of interfacial waves in stratified gas-liquid flows, *AIChE Journal*, **33**, 444-453.

Anner, L (1968), Investigation of flow losses in mine ventilation, *Freiberger Forschunghefte*, VEB, Leipzig.

Arirachakaran, S (1990), Two-phase flow splitting phenomenon at a regular horizontal side-arm tee, PhD Thesis, University of Tulsa.

Asali, JC (1984), Entrainment in vertical gas liquid flows, PhD Thesis, University of Illinois, Urbana.

Asali, JC, Hanratty TJ and Andreussi, P (1985), Interfacial drag and film height for vertical annular flow, *AICHEJ*, **31**, 895-902.

Azzopardi, BJ (1984), The effect of side arm diameter on two-phase split at a T-junction, *International Journal of Multiphase Flow*, **10**, 509-512.

Azzopardi, BJ (1988), Measurements and observations of the split of annular flow at a vertical T-junction, *International Journal of Multiphase Flow*, **14**, 701-710.

Azzopardi, BJ (1989), The split of annular-mist flows at vertical and horizontal Ts, *Proceedings of the 8th International Conference on Offshore Mechanics and Arctic Engineering*, The Hague, The Netherlands, ASME, New York.

Azzopardi, BJ (1994), The split of vertical annular flow at a large diameter T-junction, *International Journal of Multiphase Flow*, **20**, 1071-1083.

Azzopardi, BJ (1999), Phase split at T-junctions, *Multiphase Science and Technology*, **11**, 223-329.

Azzopardi, BJ & Baker, SR (1981), Two-phase flow in a T-junction. The effect of flow pattern in vertical upflow, *Report* AERE-R10174.

Azzopardi, BJ, Erlebach, CB and Roberts, PA (1994), Dividing churn/slug flow at a vertical T-junction, *10^{th} International Heat Transfer Conference, Brighton, August.*

Azzopardi, BJ & Freeman-Bell, G (1981), The effect of side arm diameter on the two-phase flow split at a T-junction, *Report* AERE-M3290.

Azzopardi, BJ, Nixon, AM and Rea, S (1996), The split of vertical churn flow at a T-junction, *European Two-Phase Flow Group Meeting*, Grenoble (France), 2-5 June.

Azzopardi, BJ and Memory, SB (1989), The split of two-phase flow at a horizontal T – annular and stratified flow, *4^{th} Int. Conf. on Multi-Phase Flow*, Nice, France, 19-12 June (Pub BHRA)

Azzopardi, BJ & Purvis, A (1987), Measurements of the split of a two-phase flow at a vertical T-junction, *UKAEA Report*, AERE R12441.

Azzopardi BJ & Smith, PA (1992), Flow split at a T-junction: effect of side arm orientation and downstream geometry, *International Journal of Multiphase Flow*, 18, 861-875.

Azzopardi, BJ and Teixeira JCF (1994), Detailed measurements of vertical annular two-phase flow – Part I: drop velocities and sizes, *Trans. ASME, J. Fluids Eng.*, 116, 792-795.

Azzopardi, BJ & Whalley, PB (1982), The effect of flow pattern on two phase flow in a T-junction, *International Journal of Multiphase Flow*, 8, 491-507.

Azzopardi, BJ and Rea, S (1999), Modelling the split of horizontal annular flow at a T-junction, *Trans. IchemE*, 77, part A, 713-720.

Azzopardi BJ and Zaidi, SH (1998), Drop sizes and velocities in annular two-phase flow, *Proc. ILASS '98*, 153-158.

Ballyk, JD, Shoukry, M and Chan, AMC (1988), Steam-water annular flow in a horizontal dividing T-junction, *International Journal of Multiphase Flow*, 14, 265-285.

Ballyk JD and Shoukry, M (1990), On the development of a model for predicting phase separation phenomena in dividing two-phase flow, *Nuclear Engineering and Design*, 123, 67-75.

Banerjee, S, Rhodes, E and Scott, DS (1961), Film inversion in co-current two-phase flow in helical coils, *AIChemE J.*, 13, 189-.

Barnea, D, Shoham, O and Taitel, Y (1980), Flow pattern characterization in two phase flow by electrical conductance probe, *International Journal of Multiphase Flow*, 6, 387-397.

Biesheuvel, A & van Wijngaarden, L (1984), Two phase flow equations for a diluite dispersion of gas bubbles in liquid, *Journal of Fluid Mechanics*, 168, 301-318.

Buell, JR, Soliman, HM and Sims, GE (1994, Two-phase pressure drop and phase distribution at a horizontal tee junction, *International Journal of Multiphase Flow*, 20, 819-836.

Butterworth, D (1972), Air-water annular flow in a horizontal tube, *AERE-R 7575.*

Butterworth, D (1974), Analysis of film flow and its application to condensation in a horiziontal tube, *International Journal of Multiphase Flow*, 1, 671-682.

Chadwick, MA (1965), 100MW(e) prototype steam generating heavy water reactor refuelling machine test rig, *The British Ship Research Association,* Marine Engineering Contract Report N. W. 37

Charron, Y and Whalley, PB (1995), Gas –liquid annular flow at a vertical T-junction – part I. Flow separation, *International Journal of Multiphase Flow*, 21, 569-589.

Chisholm, D (1967), Pressure loss in bends and tees during steam/water flow, *NEL Report* N° 318.

Chisholm, D (1972), An equation for velocity ratio in two phse flow, *N.E.L. Report* N. 535.

Chisholm, D (1973), Pressure gradients due to friction during the flow of evaporating two-phase mixtures in smooth tubes and channels, *International Journal of Heat and Mass transfer,* 16, 354-360.

Chow, VT (1959), Open-channel Hydraulics, *McGraw-Hill*

Cohen, SL and Hanratty, TJ (1968), Effect of waves at a gas-liquid interface on a turbulent air flow, *J. Fluid Mech*, 31, 467-469.

Collier, JG (1976), Single phase and two-phase flow behaviour in primary circuit components, *International Symposium on Two-phase flow and Heat transfer in water-cooled* NATO Advanced Study, *Inst. on Two-phase Flows and Heat transfer*, Istanbul, Turkey.

Costigan, G & Whalley, PB (1997), Slug flow regime identification from dynamic void fraction measurements in vertical air-water flows, *International Journal of Multiphase Flow*, 23, 263-282.

Dallman, JC (1978), Investigation of separated flow model in annular gas-liquid two-phase flows, PhD Thesis, University of Illinois, Urbana.

Davis,MR and Fungtamasan, B (1990), Two phase flow through pipe junctions, *International Journal of Multiphase Flow*, 16, 799-817.

Drew, DA & Lahey, RT Jr. (1987), The virtual mass and lift force on a sphere in rotating and straining flow, *International Journal of Multiphase Flow*, 13, 113-121.

Fairhurst, CP (1986), Two-phase flow distribution in branching systems, *BHRA* Report, Cranfield, UK.

Fisher SA and Pearce, DL (1978), A theoretical model for describing horizontal annular flows, *Int. Seminar on Momentum, Heat and Mass Transfer in Two-Phase Energy and Chemical Systems*, Dubrivnik, Yugoslavia, (Ed. F Durst, GV Tsiklauri, NH Afgan), McGraw-Hill, 327-337.

Fukano, T and Ousaka, A (1989), Prediction of the circumferential distribution of film thickness in horizontal and near-horizontal gas-liquid annular flow, *International Journal of Multiphase Flow*, 15, 403-419.

Gardel, A (1957), Les pertes de charge dans les écoulements au travers de branchements en té, *Bulletin Technique de la Suisse Romande*, 9, 122-130 and 10, 143-148.

Gardel, A & G Rechsteiner (1970), Les pertes de charge dans les branchements en té de conduites de section circulaire, *Bulletin Technique de la Suisse Romande*, 29, 363-391.

Gosman, AD, Issa, RI, Lekakou, C, Looney, MK and Politis, S (1992), Multi-dimensional modelling of turbulent two-phase flows in stirred vessels, *AIChE Journal*, 38, 1853.

Griffith, P & Wallis, GB (1961), Two-phase slug flow, *J. Heat Transfer*, 83, 307-.

Hamersma, PJ & Hart, J (1987), A pressure drop correlation for gas/liquid pipe flow with a small liquid holdup, *Chemical Engineering Science*, 42, 1187-1196.

Hart, J, Hamersma, PJ and Fortuin, JMH (1989), Correlations predicting frictional pressure drop and liquid holdup during horizontal gas-liquid pipe flow with a small liquid holdup, *International Journal of Multiphase flow*, 15, 947-964.

Hart, J, Hamersma, PJ and Fortuin, JMH (1991), Phase distribution during gas-liquid flow through horizontal dividing T-junctions, *Nuclear Engineering and Design*, 126, 293-312.

Henstock, WH & Hanratty, TJ (1976), The interfacial drag and height of the wall layer in annular flows, *AIChEJ*, 22, 990-1000.

Henry, JAR (1981), Dividing annular flow in a horizontal Tee, *International Journal of Multiphase Flow*, 7, 343-355.

Hewitt GF, Gill LE, Roberts DN amd Azzopardi BJ (1990), The split of low inlet quality gas/liquid flow at a vertical T – Experimental data, *UKAEA Report* AERE M3801

Hewitt, GF and Govan, AH (1990), Phenomenological modelling of non –equilibrium flows with phase change, *Int. J. Heat and Mass Transfer*,33, 229-242.

Hewitt, GF & Hall-Taylor, NS (1978), Annular two-phase flow, Pergamon Press Ltd., Oxford.

Hong, KC (1978), Two-phase flow splitting at a pipe tee, *J. Pet. Technol.*, 270-296.

Hurlburt, ET and Newell TA (2000), Prediction of the circumferential film thickness distribution in horizontal annular gas-liquid flow, *ASME Journal of Fluids Engineering*, 122, 1-7.

Hutchinson, P, Butterworth, D and Owen, RG (1974), Development of a model for horizontal annular flow, AERE-R7789, *Atomic Energy Research Establishment*, Harwell, UK.

Hurlburt, ET and Newell, TA (2000) "Prediction of the circumferential film thickness distribution in horizontal annular gas-liquid flow." *ASME Journal of Fluids Engineering*, 122: 1-7.

Hwang, ST, Soliman, HM and Lahey, RT Jr (1988), Phase separation in dividing two-phase flows, *International Journal of Multiphase Flow*, 14, 439-458.

Hwang, ST (1986), A study on phase separation in branching conduits, *PhD Thesis*, Rensselaer Polytechnic Institute, Troy, N. Y.

Honan, TJ & Lahey, RT (1980), The measurement of phase separation in wyes and tees, *Nuclear Engineering and Design*, 64, 93-102.

Issa, RI & Olivera, PJ (1994), Numerical prediction of phase separation in two-phase flow through T-junctions, *Computer Fluids*, 23, 347-372.

Jayanti, S, Wilkws, NS, Clarke, DS and Hewitt, GF (1990), The prediction of turbulent flows over roughened surfaces and its application to interpretation of mechanisms of horizontal annular flow, *Proc. Roy. Soc.*, A431, 71-88.

James, PW, Wilkes, NS, Conkie, W and Burns, A (1987), Developments in the modelling of horizontal annular two-phase flow, *International Journal of Multiphase Flow*, 13, 173-198.

Johansen, SE (1979), Experimental study of gas-liquid flow in a pipe tee, M.S. Thesis, University of Tulsa.

Katsaounis, A, Papanikas, DG, Fertis, DK and Margaris, DP (1997), Dynamic T-junction separator for multiphase transport lines, *Proc. 4th World Conf. on Experimental Heat Transfer, Fluid Mechanics and Thermodynamics*, Brussels (Belgium), *(Ed. M Giot, F Mayinger and G.P. Celata)*, Pub Edizione ETS, 1045-1052.

Lahey, RT (1987), Data set N. 9, dividing flow in a Tee junction, *Multiphase Science & Technology*, 3, Hemisphere press.

Lahey, RT (1988), Dividing flow in a Tee-junction, *Multiphase Science & Technology*, 3, 316.

Lahey RT (1990), The analysis of phase separation and phase distribution phenomena using two-fluid models, *Nuclear Engineering and Design*, 122, 17-40.

Lahey, RT, Azzopardi, BJ and Cox, M (1985), Modelling two phase flow division at T-junctions, *2nd. Int. Conf. Multi-Phase Flow, London, U.K., 19-21 June, pub., BHRA.*

Launder BE, Reece, GJ and Rodi, W (1975), Progress in the development of a Reynolds-stress turbulence closure, *Journal of Fluid Mechanics*, 68, 537-566.

Laurinat, JE (1982), Studies of the effects of pipe size on horizontal annular two-phase flow, PhD Thesis, University of Illinois, Urbana.

Laurinat, JE, Hanratty, TJ and Jepson, WP (1985), Film thickness distribution for gas-liquid annular flow in a horizontal pipe, *PhysicoChemical Hydrodynamics*, 6, 179-195.

Lemonnier, H and Hervieu, E (1991), Theoretical modelling and experimental investigation of single-phase and two-phase division at a T-junction, *Nucl. Eng. and Design*, 125, 201-213.

Lin, TF, Jones, OC, Lahey, RT Jr, Block, RC Jr and Murase, M (1985), Film thickness measurements and modelling in horizontal annular flow, PHC *PhysicoChemical Hydrodynamics*, 6, 197-206.

Lockart, RW & Martinelli, RC (1949), Proposed correlations for isothermal two-phase flow in pipes, *Chemical Engineering Progress*, 45, 39-48.

Ma, YP, Pei, BS Lin, WK and Hsu, YY (1990), Analysis of a fluid-mechanic model of a horizontal Tee-junction, *Heat Transfer and Fluid Flow*, 92, 134-140.

Marti, S & Shoham, O (1997) A unified model for stratified-wavy two-phase flow splitting at a reduced T-junction with an inclined branch arm, *International Journal of Multiphase Flow*, 4, 725-748.

McCreery, GE(1984), A correlation for phase separation in a tee, *Multi-phase Flow and Heat Transfer III. Part B*: Applications, pub. Elsevier Science Pub. B.V., Amsterdam (Ed. TN Veziroglu and AE Bergles) 165- 178.

McCreery, GE and Banerjee, S (1990), Phase separation of dispersed annular (rivulet or thin film) flow in a Tee – Part I: Experiments, *International Journal of Multiphase Flow*, 16, 429-445.

McCreery, GE and Banerjee, S (1991), Phase separation of dispersed annular (rivulet or thin film) flow in a Tee – Part II: Analysis, *International Journal of Multiphase Flow*, 17, 309-325.

McNown, JS (1954), Mechanics of manifold flow, *ASCE Trans.*, 119, 11.3-1142.

McQuillan, KW and Whalley, PB (1984), A comparison between flooding correlations and experimental flooding data for gas-liquid flow in vertical circular tubes, *Chem., Eng. Sci.*, 40, 1425-1440.

Michaelis,L & Menten, M (1913), Die kinetik der intertinwerkung, *Biochem Z* , 49, 333-369.

Miller, DS (1971), Internal flow. A guide to losses in pipe and duct systems, *British Hydromechanics Research Assoc.*, U.K.

Mudde, RF, Groen, JS and van den Akker, HEA (1993), Two-phase flow redistribution phenomena in a large T-junction, *International Journal of Multiphase Flow*, 19, 563-573.

Muller, U and Reimann, J (1991) Redistribution of two-phase flow in branching conduits: a survey, *Proc. Int. Conf. Multiphase Flows '91*, Tsukuba, September 24-27 1991, Tsukuba, Japan.

Nicklin, DJ & Davidson, JF (1962), The onset of instability in two phase slug flow, *Inst. Mech. Engrs. Symp Two Phase Flow*, London (U.K.)

Nigmatulin, RI (1979), Spatial averaging in the mechanics of heterogeneous and dispersed systems, *International Journal of Multiphase Flow*, 353.

Oranje, L (1973), Condensate behaviour in gas pipelines is predictable, *Oil and Gas J.*, 71, 39-44.

Paras SV, Vlachos, NA and Karabelas, AJ (1994), Liquid layer characteristics in stratified-atomisation flow, *International Journal of Multiphase Flow*, 20, 939-.

Peng, F (1994), A study of dividing two-phase flow in horizontal inlet T-junctions, PhD thesis, McMaster University, Hamilton, ON

Peng, F, Shoukri, M and Chan, AMC (1996), Effect of branch orientation on annular two-phase flow in T-junctions, *ASME Journal of Fluid Engineering*, 108, 166-171.

Peng, F & Shoukri, M (1997), Modelling of phase redistribution of horizontal annular flow divided in T-junctions, *The Canadian Journal of Chemical Engineering*, 75, 264-271.

Penmatcha, VR, Ashton, PJ, Shoham, O (1996), Two-phase stratified flow splitting at a T-junction with an inclined branch arm, *International Journal of Multiphase Flow*, 22, 1105-1122.

Popp, M & Sallet, DW (1983), Experimental investigation of one- and two-phase flowthrough a tee-junction. Presented at the *International Conference on Physical Modelling in Multiphase Flow*, Coventry, England.

Rea, S (1998), Stratified flow at T-junctions, PhD Thesis, Nottingham University.

Rea, S & Azzopardi, BJ (2000), The split of horizontal stratified flow at a large diameter T-junction, In preparation.

Reimann, J, Brinkmann, HJ and Domansky, R (1988), Gas-liquid flow in dividing T-junctions with horizontal inlet and different branch orientations and diameters, *Kernforschungszentrum Karlsruhr, Institute fur Reactorbauelemente*, Report KfK 4399.

Roberts, PA (1994), Two-phase flow at T-junctions, PhD Thesis, Nottingham University.

Roberts, PA, Azzopardi, BJ & Hibberd, S (1995), The split of horizontal semi-annular flow at a large diameter T-junction, *International Journal of Multiphase Flow*, 21, 455-466.

Roberts, PA, Azzopardi, BJ and Hibberd, S (1997), The split of horizontal annular flow at a T-junction, *Chemical Engineering Science*, 52, 3441-3453.

Rouhani, Z (1969), Modified correlations for void fraction and two-phase pressure drop and, *AE-RTV*-8841.

Rubel, MT, Soliman, HM and Sims, GE (1988), Phase distribution during Steam-water flow in a horizontal T-junction, *International Journal of Multiphase Flow*, 14, 425-438.

Rubel MT, Timmerman, H, Soliman, HM, Sims, GE and Ebadian, MA (1994), Phase distribution of high-pressure steam-water flow at large diameter T-junctions, *Trans. ASME, J. Fluids Eng.*, 116, 592-598.

Saba, N & Lahey, RT (1982), Phase separation phenomena in branching conduits, *NUREG* CR – 2590.

Saba, N & Lahey, RT Jr (1984), The analysis of phase separation phenomena in branching conduits, *International Journal of Multiphase Flow*, 1, 1-20.

Seeger, W, Riemann, J and Muller, U (1986), Two-phase flow in a T-junction with a horizontal inlet – Part I: Phase separation, *International Journal of Multiphase Flow*, 12, 575-585.

Sekoguchi, K, Ousaka, A, Fukano, T and Moritomo, T (1982), Air water annular two phase flow in a horizontal tube (1st report, circumferential thicknesses), *Bullettin of the JSME*, 25, 1559-

Shoham, O, Brill, JP and Taitel, Y (1987), Two-phase flow splitting in a T-junction - Experiment and modelling, *International Journal of Multiphase Flow*, 42, 2667-2676.

Srichai, S (1994), High pressure two-phase separated flow, PhD Thesis, Imperial College of Science, Technology and Medicine, London.

Stacey T, Azzopardi BJ and Conte, G (2000), The split of Annular two phase flow at a small diameter T-junction, *International Journal of Multiphase Flow*, 26, 845-856.

✓ Suu, T (1992), Air-water two-phase flow through a pipe junction (effect of the Reynolds number on the local void fraction distribution), *JSME Int. J. Ser. II*, 35, 76-81.

Taitel_Y, Bornea, D and Dukler, AE (1980), Modelling flow pattern transitions for steady upward gas-liquid flow in vertical tubes, *AIChE Journal*, 26, 345-354.

Taitel, Y & Dukler, AE (1976), A model for predicting flow regime transitions in horizontal and near horizontal gas-liquid flow, *AIChE Journal*, 22, 47-55.

Ueda, T (1979), Entrainment rate and size of entrained droplets in annular two-phase flow, *Bullettin of the JSME*, 22, 1258-1265.

Verbeek, PJH, Miesen, R and Schellenkens, CJ (1992), Liquid entrainment in annular dispersed upflow, *8th Annual Eur. Conf. on Liquid Atomisation and Spray Systems*, Amsterdam, Sept. 30 – Oct. 2.

Wallis, GB (1961), Flooding velocities for air and water in vertical tubes, *UKAEA Report*. AEEW-R123.

Wallis, GB (1969), One dimensional two-phase flow, McGraw-Hill.

Walters, LC, Soliman, HM and Sims, GE (1998), Two-phase pressure drop and phase distribution at reduced T-junctions, *International Journal of Multiphase Flow*, 24, 775-792.

Whalley, PB (1980), Air-water two phase flow in helically coiled tube, *International Journal of Multiphase Flow*, 6, 345-

Williams, LR (1986), Entrainment measurements in a 4-inch horizontal pipe, MSc Thesis, University of Illinois, Urbana-Champaign, USA.

Williams, LR (1990), Efect of pipe diameter on horizontal annular two phase flow, PhD Thesis, University of Illinois at Urbana-Champaign.

Wren, EMK, Azzopardi BJ and Rea S (1999), Geometric effects on phse split in a large diameter T-junction, *2nd Int. Symp. on Two-Phase Modelling and Experimentation*, Pisa, Italy, 23-26 May.

✓ Zetzmann, K (1984), Phase separation of an air-water flow in a verical T-junction, *German Chemical Engineering*, 7, 305-312.

Zuber, N (1964), On the dispersed two phase flow in the laminar flow regime, *Chemical Engineering Science*, 19, 897.

Nomenclature

Roman Symbols	Descriptions	Dimensions
$\dot{M}$	Mass flow rate	kg/s
$\bar{x}$	Anticlockwise angle from pipe bottom	-
$\bar{w}$	mean local axial velocity of the film	m/s
$\dot{m}$	mass flux	kg/m^2s
A	Cross sectional area	m^2
a	Radius	m
C_D	Drag coefficient	-
D	Pipe diameter	m
E	Entrained fraction	-
F	Force	N
f	Friction factor	-
Fr	Froude number	-
g	Acceleration of gravity	m/s^2
G'	Fraction of incoming gas taken off	-
h	film thickness	m
H	Length of run arm	m
K	Constant of Azzopardi (1988)	-
L'	Fraction of incoming liquid taken off	-
M	Force	N
Q	Volumetric flow rate	m^3/s
R	Pipe radius	m
r	rate	kg/m^2s
Re	Reynolds number	-
t	Characteristic time	-
U	Velocity	m/s
We	Weber number	-
x	gas mass quality	-
X_c	Capacitive reactance	Ω
Δp	Pressure drop	Pa/m

Greek Symbols	Descriptions	Dimensions
Γ	Circumferential film flowrate	kg/ms
β	Angle between inlet and side arm direction	-
δ	Film thickness	m
ε	Void fraction, Energy dissipation rate	-, m^2/s^3
ϕ	Angle between horizontal and side arm direction	-
κ	von Karman constand, parameter in equationV.2.6	-
μ	Viscosity	Pas
ν	Kinematic viscosity, turbulent diffusivity	m^2/s, Pas
θ	Angle between vertical and main pipe direction, angle subtended by segment, parameter in equation V.2.15, Anticlockwise angle from pipe top.	-
ρ	Density	kg/m^3
τ	Stress	Pa
ψ	Split index	-

Subscripts

g	Gas
l	Liquid
F	Film
s	Superficial
J	Junction
D	Deposition
A	Atomisation
w	Wall
avg	Average
o	Bottom
max	Maximum
eff	effective
b	Bubble
1	Inlet pipe
2	Run pipe
3	Side arm

Appendix A

Table A.1: *Split data: the runs employed also for film thickness measurements are numbered: 1 = Average G', 2 = Large G', 3 = Small G'.*

U_{gs} (m/s)	U_{ls} (m/s)	Case	Run	G'	L'
16.5	0.55	A	A.1	0.63	0.07
				0.70	0.09
			A.2	0.79	0.10
				0.83	0.22
				0.59	0.09
				0.49	0.07
			A.3	0.35	0.04
16.5	0.278	B	B.1	0.57	0.08
				0.59	0.09
				0.68	0.14
			B.2	0.83	0.25
				0.52	0.08
				0.44	0.07
			B.3	0.30	0.05
24.5	0.278	C	C.1	0.54	0.11
				0.57	0.12
			C.2	0.72	0.15
				0.83	0.18
				0.49	0.09
			C.3	0.40	0.08
				0.28	0.05
16.5	0.136	D	D.3	0.26	0.09
				0.32	0.11
				0.41	0.13
			D.1	0.44	0.15
				0.44	0.15
				0.55	0.18
				0.61	0.22
			D.2	0.80	0.27
				0.82	0.61
23	0.136	E	E.1	0.45	0.13
				0.43	0.12
				0.34	0.09
			E.3	0.21	0.06
			E.2	0.82	0.49
				0.80	0.26
				0.68	0.21
				0.41	0.16
28.1	0.136	F	F.1	0.46	0.14
				0.53	0.17
				0.65	0.21
			F.2	0.79	0.30
			F.3	0.24	0.06
				0.35	0.10
				0.43	0.12

Table A.2: Film thickness measurements (mm) at the three sections before and after the T junction, 0.125 m from the centre of the T.

θ	a).m.1	a).m.2	a).m.3	a).s.1	a).s.2	a).s.3	a).r.1	a).r.2	a).r.3
0.00	0.04	0.04	0.03	0.34	0.53	0.25	0.08	0.27	0.04
30.00	0.06	0.02	0.03	0.08	0.20	0.06	0.24	0.46	0.10
53.25	0.10	0.09	0.09	0.07	0.15	0.09	0.38	0.32	0.41
60.00	n/a	n/a	n/a	0.10	0.22	0.13	0.41	0.46	0.40
66.75	0.13	0.12	0.13	0.11	0.18	0.12	0.41	0.50	0.43
73.50	n/a	n/a	n/a	0.11	0.17	0.13	0.42	0.51	0.43
80.25	0.17	0.16	0.16	0.16	0.17	0.16	0.43	0.57	0.41
87.00	n/a	n/a	n/a	0.22	0.16	0.14	0.45	n/a	0.41
93.75	0.20	0.19	0.19	0.29	0.36	0.19	0.48	0.64	0.43
100.50	n/a	n/a	n/a	n/a	n/a	0.76	n/a	n/a	1.77
107.25	0.51	0.56	0.57	n/a	0.38	0.36	0.57	0.75	0.48
114.00	n/a	n/a	n/a	n/a	n/a	0.47	n/a	n/a	n/a
120.75	1.67	1.72	1.73	n/a	0.70	n/a	n/a	n/a	n/a
124.23	4.29	4.74	4.32	2.98	3.02	1.57	2.42	3.19	2.33
156.82	14.34	15.53	15.02	0.74	1.02	1.05	13.81	13.45	15.15
180.00	16.33	17.82	17.31	1.52	1.87	0.74	17.12	17.01	18.05
203.19	13.74	14.99	15.20	1.61	1.71	1.86	14.96	16.22	15.00
235.77	2.96	4.66	4.03	2.56	3.27	2.08	3.85	3.46	3.44
239.25	1.64	1.86	1.93	0.73	0.91	0.65	2.03	1.58	1.80
246.00	n/a	n/a	n/a	0.68	0.90	0.60	0.99	0.76	0.81
252.75	0.46	0.51	0.54	0.70	0.88	0.56	0.45	0.41	0.36
259.50	n/a	n/a	n/a	0.71	n/a	0.61	0.23	0.28	0.17
266.25	0.22	0.22	0.22	0.73	0.94	0.59	0.22	0.29	0.17
273.00	n/a	n/a	n/a	0.75	n/a	0.62	0.21	0.25	0.13
279.75	0.17	0.16	0.16	0.75	1.02	0.63	0.20	0.28	0.17
286.50	n/a	n/a	n/a	0.76	n/a	0.66	0.19	0.25	0.14
293.25	0.15	0.14	0.14	0.77	0.96	0.65	0.17	0.26	0.15
300.00	n/a	n/a	n/a	0.79	0.96	0.66	0.15	0.26	0.14
306.75	0.09	0.08	0.08	0.82	1.03	0.67	0.12	0.22	0.11
330.00	0.07	0.06	0.06	n/a	0.87	n/a	0.08	0.20	0.06
360.00	0.04	0.04	0.03	0.34	0.53	0.25	0.08	0.27	0.04

Legend:
θ = angle in degrees measured from top of pipe, anticlockwise in the direction of flow
i) = case i)
m = main leg (inlet)
s = side arm
r = run arm
1 = average G'
2 = large G'
3 = small G'

Table A.2: *Continued*

θ	b).m.1	b).m.2	b).m.3	b).s.1	b).s.2	b).s.3	b).r.1	b).r.2	b).r.3
0.00	0.02	0.03	0.03	dry	0.06	dry	0.09	0.07	0.01
30.00	0.06	0.02	0.02	dry	0.02	dry	0.06	0.05	0.00
53.25	0.09	0.09	0.08	0.05	0.07	dry	0.13	0.28	0.07
60.00	0.12	0.12	0.12	0.07	0.11	dry	0.27	n/a	0.12
66.75	0.12	0.12	0.12	0.07	0.10	dry	0.42	0.56	0.21
73.50	0.13	0.11	0.11	0.10	0.09	dry	n/a	n/a	0.36
80.25	0.14	0.13	0.13	0.11	0.09	dry	0.70	0.73	0.55
87.00	0.14	0.06	0.07	0.12	0.08	dry	n/a	n/a	n/a
93.75	0.14	0.13	0.13	0.17	0.12	dry	0.85	1.00	0.72
100.50	0.16	0.15	0.15	0.26	0.19	dry	n/a	n/a	n/a
107.25	0.19	0.21	0.21	0.48	0.37	dry	1.19	n/a	1.02
114.00	0.28	0.28	0.29	n/a	n/a	0.13	n/a	n/a	n/a
120.75	0.58	0.59	0.60	n/a	n/a	0.19	n/a	n/a	n/a
124.23	1.09	1.12	1.16	1.96	3.03	0.64	3.06	4.19	2.37
156.82	14.63	14.99	14.91	0.71	0.97	2.19	13.65	13.96	13.61
180.00	18.98	19.24	19.20	0.54	0.22	1.25	18.36	16.83	18.68
203.19	14.18	14.66	14.52	0.83	0.96	0.79	14.37	12.04	15.32
235.77	1.37	1.42	1.44	2.03	2.61	1.55	1.36	1.17	1.59
239.25	0.74	0.79	0.81	0.71	0.83	0.53	0.60	0.36	0.90
246.00	0.34	0.34	0.37	0.70	0.83	0.51	0.24	0.21	0.32
252.75	0.24	0.24	0.24	0.68	0.86	0.51	0.19	0.22	0.19
259.50	0.20	0.16	0.17	0.74	n/a	0.56	0.19	0.18	0.10
266.25	0.17	0.17	0.17	0.76	0.96	0.55	0.19	0.22	0.12
273.00	0.15	0.12	0.12	0.84	n/a	0.61	0.18	0.18	0.09
279.75	0.14	0.14	0.14	0.83	1.04	0.63	0.17	0.21	0.11
286.50	0.14	0.15	0.11	0.84	n/a	0.66	0.15	0.18	0.09
293.25	0.14	0.13	0.13	0.79	0.95	0.63	0.14	0.20	0.11
300.00	0.11	0.11	0.11	0.79	0.93	0.64	0.07	0.18	0.10
306.75	0.08	0.08	0.08	0.71	0.85	0.55	0.07	0.15	0.07
330.00	0.05	0.04	0.04	0.15	0.37	0.12	0.05	0.10	0.03
360.00	0.02	0.03	0.03	dry	0.06	dry	0.09	0.07	0.01

Legend:

θ = angle in degrees measured from top of pipe, anticlockwise in the direction of flow
i) = case i)
m = main leg (inlet)
s = side arm
r = run arm
1 = average G'
2 = large G'
3 = small G'

Table A.2: *Continued*

θ	c).m.1	c).m.2	c).m.3	c).s.1	c).s.2	c).s.3	c).r.1	c).r.2	c).r.3
0.00	0.04	0.04	0.04	0.02	0.03	0.02	0.04	0.07	0.02
30.00	0.05	0.03	0.03	0.01	0.01	dry	0.04	0.07	0.02
53.25	0.11	0.11	0.11	0.07	0.06	dry	0.13	0.15	0.10
60.00	n/a	n/a	n/a	0.11	0.09	0.09	0.17	0.19	0.15
66.75	0.15	0.15	0.16	0.13	0.09	0.10	0.17	0.22	0.15
73.50	n/a	n/a	n/a	0.15	0.08	0.12	0.25	0.35	0.18
80.25	0.18	0.18	0.19	0.18	0.09	0.13	0.42	0.52	0.26
87.00	n/a	n/a	n/a	0.23	0.10	0.13	0.64	0.66	0.44
93.75	0.17	0.17	0.18	0.36	0.18	0.20	0.72	0.81	0.61
100.50	n/a	n/a	n/a	n/a	n/a	0.94	n/a	n/a	n/a
107.25	0.22	0.22	0.22	n/a	n/a	0.49	n/a	n/a	0.88
114.00	n/a	n/a	n/a	n/a	n/a	n/a	n/a	n/a	n/a
120.75	0.44	0.47	0.44	n/a	0.87	n/a	n/a	n/a	n/a
124.23	1.59	1.60	1.63	3.19	3.44	3.07	2.83	2.88	2.87
156.82	9.88	9.49	9.88	0.76	0.59	0.93	8.92	9.42	8.80
180.00	14.85	13.88	14.81	0.14	0.07	0.35	13.67	13.21	14.06
203.19	9.94	9.57	9.94	0.63	0.77	0.64	8.94	7.96	9.79
235.77	1.83	1.92	1.83	3.46	3.70	3.34	1.43	1.79	1.78
239.25	0.65	0.67	0.69	0.58	0.70	0.49	0.43	0.30	0.57
246.00	n/a	n/a	n/a	0.57	0.74	0.46	0.22	0.22	0.25
252.75	0.25	0.25	0.26	0.56	0.75	0.47	0.18	0.24	0.18
259.50	n/a	n/a	n/a	0.65	0.81	0.51	0.12	0.23	0.12
266.25	0.20	0.20	0.20	0.70	0.85	0.55	0.15	0.26	0.13
273.00	n/a	n/a	n/a	0.73	0.87	0.59	0.12	0.22	0.10
279.75	0.18	0.18	0.18	0.74	0.83	0.61	0.19	0.25	0.13
286.50	n/a	n/a	n/a	0.68	0.76	0.63	0.17	0.20	0.11
293.25	0.17	0.17	0.17	0.66	0.75	0.57	0.21	0.22	0.15
300.00	n/a	n/a	n/a	0.62	0.71	0.52	0.17	0.19	0.13
306.75	0.10	0.10	0.10	0.44	0.62	0.37	0.13	0.16	0.09
330.00	0.07	0.06	0.06	0.06	0.10	0.40	0.06	0.10	0.04
360.00	0.04	0.04	0.04	0.02	0.03	0.02	0.04	0.07	0.02

Legend:

θ = angle in degrees measured from top of pipe, anticlockwise in the direction of flow
i) = case i)
m = main leg (inlet)
s = side arm
r = run arm
1 = average G'
2 = large G'
3 = small G'

Table A.2: *Continued*

θ	d).m.1	d).m.2	d).m.3	d).s.1	d).s.2	d).s.3	d).r.1	d).r.2	d).r.3
0.00	0.03	0.03	0.03	dry	0.01	dry	0.00	0.05	0.01
30.00	0.05	0.02	0.02	dry	0.01	dry	0.01	0.04	0.00
53.25	0.09	0.09	0.09	dry	0.05	dry	0.06	0.07	0.05
60.00	0.10	0.10	0.10	0.08	0.08	dry	0.08	0.10	0.08
66.75	0.12	0.13	0.12	0.10	0.08	dry	0.09	0.13	0.09
73.50	0.12	0.11	0.11	0.11	0.07	dry	0.10	0.19	0.09
80.25	0.13	0.13	0.13	0.14	0.09	dry	0.15	0.28	0.13
87.00	0.15	0.10	0.10	0.16	0.09	dry	0.21	n/a	0.17
93.75	0.17	0.10	0.11	0.17	0.12	dry	0.36	n/a	0.32
100.50	0.20	0.21	0.23	0.18	0.78	dry	n/a	n/a	1.97
107.25	0.21	0.16	0.17	0.19	0.38	dry	n/a	n/a	0.77
114.00	0.21	0.21	0.22	0.23	n/a	dry	n/a	n/a	n/a
120.75	0.39	0.38	0.40	0.36	n/a	0.06	n/a	n/a	n/a
124.23	0.86	0.87	0.91	0.92	2.17	0.57	3.97	5.66	2.73
156.82	13.82	14.06	14.45	1.51	0.87	1.09	14.41	14.07	13.03
180.00	19.14	19.65	19.81	0.67	0.54	1.42	17.51	13.54	16.58
203.19	14.16	14.75	14.87	1.56	2.16	1.11	12.82	7.49	13.08
235.77	1.31	1.40	1.34	3.70	5.09	2.44	1.19	1.09	1.21
239.25	0.61	0.66	0.65	1.30	1.58	1.09	0.30	0.21	0.37
246.00	0.28	0.30	0.31	n/a	n/a	n/a	0.18	0.19	0.16
252.75	0.20	0.21	0.21	1.01	1.21	0.96	0.17	0.21	0.14
259.50	0.18	0.13	0.14	n/a	n/a	0.89	0.17	0.17	0.10
266.25	0.15	0.15	0.15	0.61	0.82	0.71	0.17	0.20	0.12
273.00	0.15	0.11	0.12	0.46	0.67	0.62	0.17	0.16	0.09
279.75	0.14	0.13	0.14	0.37	0.49	0.47	0.17	0.20	0.11
286.50	0.13	0.11	0.11	0.24	0.34	0.33	0.16	0.17	0.10
293.25	0.12	0.11	0.12	0.17	0.23	0.26	0.15	0.19	0.12
300.00	0.10	0.10	0.10	0.10	0.14	0.14	0.11	0.16	0.10
306.75	0.08	0.08	0.08	0.04	0.06	0.05	0.10	0.13	0.07
330.00	0.05	0.05	0.05	dry	0.02	dry	0.04	0.07	0.02
360.00	0.03	0.03	0.03	dry	0.01	dry	0.00	0.05	0.01

Legend:

θ = angle in degrees measured from top of pipe, anticlockwise in the direction of flow
i) = case i)
m = main leg (inlet)
s = side arm
r = run arm
1 = average G'
2 = large G'
3 = small G'

Table A.2: *Continued*

θ	e).m.1	e).m.2	e).m.3	e).s.1	e).s.2	e).s.3	e).r.1	e).r.2	e).r.3
0.00	0.03	0.03	0.03	dry	0.02	dry	0.02	0.07	0.01
30.00	0.05	0.03	0.03	dry	0.01	dry	0.04	0.04	0.01
53.25	0.10	0.10	0.10	0.04	0.06	dry	0.06	0.10	0.06
60.00	0.12	0.12	0.12	0.10	0.08	dry	0.09	0.17	0.09
66.75	0.13	0.14	0.14	0.10	0.10	dry	0.10	0.18	0.09
73.50	0.14	0.13	0.13	0.12	0.09	0.06	0.12	0.24	0.08
80.25	0.15	0.15	0.15	0.14	0.08	0.06	0.17	0.35	0.11
87.00	0.15	0.12	0.12	0.14	0.07	0.05	0.24	n/a	0.13
93.75	0.14	0.14	0.14	0.19	0.13	0.05	0.41	n/a	0.24
100.50	0.17	0.34	0.35	0.30	1.09	0.10	n/a	n/a	1.53
107.25	0.19	0.20	0.20	0.48	0.51	0.11	0.80	n/a	0.60
114.00	0.21	0.21	0.21	n/a	0.78	0.10	n/a	n/a	n/a
120.75	0.30	0.31	0.31	1.08	0.56	0.11	n/a	n/a	n/a
124.23	0.82	0.83	0.83	1.43	1.91	0.63	2.35	3.97	2.90
156.82	9.20	9.61	9.46	0.83	0.65	1.49	9.38	10.49	8.29
180.00	13.97	14.25	14.13	0.36	0.23	0.63	12.41	9.52	12.50
203.19	9.45	9.70	9.49	0.86	1.30	0.87	8.10	3.29	9.10
235.77	1.17	1.19	1.18	2.00	3.41	1.63	1.15	6.38	1.22
239.25	0.41	0.39	0.40	0.68	1.02	0.61	0.20	0.21	0.26
246.00	0.24	0.24	0.24	0.58	n/a	0.58	0.18	0.22	0.16
252.75	0.21	0.21	0.21	0.54	0.83	0.51	0.17	0.23	0.15
259.50	0.20	0.16	0.16	0.53	0.73	0.50	0.16	0.21	0.10
266.25	0.19	0.18	0.19	0.47	0.63	0.45	0.16	0.24	0.12
273.00	0.18	0.14	0.14	0.39	0.55	0.38	0.16	0.20	0.09
279.75	0.16	0.16	0.17	0.37	0.48	0.32	0.17	0.23	0.12
286.50	0.15	0.12	0.13	0.25	0.34	0.23	0.17	0.20	0.10
293.25	0.14	0.14	0.14	0.20	0.23	0.18	0.17	0.22	0.13
300.00	0.12	0.11	0.11	0.11	0.34	0.09	0.13	0.19	0.11
306.75	0.09	0.09	0.09	0.05	0.07	0.04	0.11	0.16	0.08
330.00	0.05	0.05	0.05	dry	0.03	dry	0.04	0.11	0.01
360.00	0.03	0.03	0.03	dry	0.02	dry	0.02	0.07	0.01

Legend:

θ = angle in degrees measured from top of pipe, anticlockwise in the direction of flow
i) = case i)
m = main leg (inlet)
s = side arm
r = run arm
1 = average G'
2 = large G'
3 = small G'

Table A.2: *Continued*

θ	f).m.1	f).m.2	f).m.3	f).s.1	f).s.2	f).s.3	f).r.1	f).r.2	f).r.3
0.00	0.05	0.05	0.05	dry	0.02	dry	0.02	0.07	0.01
30.00	0.07	0.04	0.04	dry	0.01	dry	0.05	0.04	0.01
53.25	0.12	0.12	0.12	0.03	0.05	dry	0.07	0.12	0.07
60.00	0.15	0.14	0.14	0.07	0.08	dry	0.10	0.15	0.09
66.75	0.16	0.16	0.16	0.08	0.09	0.09	0.11	0.15	0.01
73.50	0.17	0.16	0.15	0.11	0.07	0.08	0.11	0.18	0.08
80.25	0.18	0.17	0.17	0.13	0.08	0.08	0.15	0.27	0.10
87.00	0.17	0.15	0.15	0.16	0.09	0.04	0.18	n/a	0.10
93.75	0.17	0.17	0.16	0.29	0.14	0.06	0.32	0.61	0.15
100.50	0.19	0.42	0.35	n/a	n/a	0.25	n/a	n/a	0.72
107.25	0.21	0.21	0.21	0.89	0.54	0.09	0.68	n/a	0.42
114.00	0.25	0.22	0.22	n/a	n/a	0.11	n/a	n/a	0.66
120.75	0.29	0.28	0.28	n/a	0.43	0.15	n/a	n/a	0.92
124.23	0.84	0.82	0.79	1.58	1.46	0.66	2.04	3.40	1.53
156.82	7.31	7.34	7.23	0.74	0.56	1.90	7.84	9.28	6.98
180.00	11.97	12.12	11.99	0.22	0.12	0.43	10.72	8.02	11.38
203.19	7.37	9.51	9.52	0.71	1.05	0.74	5.43	1.93	7.01
235.77	1.21	1.17	1.16	1.83	2.77	1.46	1.22	1.31	1.18
239.25	0.35	0.37	0.36	0.56	0.89	0.48	0.20	0.21	0.24
246.00	0.24	0.25	0.24	0.51	0.80	0.44	0.19	0.23	0.17
252.75	0.22	0.23	0.22	0.47	0.67	0.40	0.17	0.24	0.16
259.50	0.22	0.19	0.18	0.45	0.62	0.38	0.17	0.22	0.10
266.25	0.21	0.21	0.21	0.42	0.52	0.35	0.16	0.24	0.12
273.00	0.20	0.17	0.17	0.37	0.46	0.28	0.16	0.21	0.09
279.75	0.20	0.20	0.19	0.36	0.41	0.28	0.17	0.24	0.13
286.50	0.18	0.15	0.16	0.28	0.30	0.18	0.17	0.20	0.10
293.25	0.17	0.17	0.16	0.22	0.22	0.14	0.17	0.22	0.13
300.00	0.15	0.14	0.14	0.13	0.13	0.07	0.15	0.19	0.11
306.75	0.12	0.12	0.12	0.06	0.08	dry	0.12	0.16	0.09
330.00	0.08	0.08	0.08	dry	0.02	dry	0.05	0.12	0.01
360.00	0.05	0.05	0.05	dry	0.02	dry	0.02	0.07	0.01

Legend:

θ = angle in degrees measured from top of pipe, anticlockwise in the direction of flow
i) = case i)
m = main leg (inlet)
s = side arm
r = run arm
1 = average G'
2 = large G'
3 = small G'

Table A.3: *Film thickness (mm) for the six cases, measured at a station 0.9 m downstream of the mixing section.*

θ	a)	b)	c)	d)	e)	f)
0.00	0.30	0.10	0.18	0.06	0.09	0.11
30.00	0.30	0.15	0.19	0.10	0.10	0.11
53.25	0.42	0.20	0.27	0.16	0.18	0.19
60.00	n/a	0.20	0.29	0.17	0.19	0.20
66.75	0.47	0.21	0.30	0.18	0.20	0.21
73.50	n/a	0.22	0.32	0.19	0.21	0.22
80.25	0.51	0.24	0.33	0.20	0.21	0.23
87.00	n/a	0.25	0.38	0.18	0.20	0.24
93.75	0.54	0.26	0.38	0.19	0.21	0.25
100.50	n/a	0.27	0.38	0.20	0.22	0.27
107.25	0.68	0.30	0.41	0.22	0.24	0.28
114.00	n/a	0.42	0.42	0.25	0.26	0.31
120.75	n/a	n/a	0.44	0.43	0.34	0.39
124.23	1.68	1.17	0.97	0.85	0.74	0.80
156.82	10.18	9.48	10.08	11.11	5.51	5.08
180.00	20.57	14.14	13.77	14.87	10.55	7.42
203.19	9.71	11.21	10.71	10.18	6.35	5.32
235.77	2.45	2.35	1.47	1.26	1.23	1.29
239.25	0.92	0.76	0.40	0.30	0.26	0.26
246.00	0.74	0.36	0.35	0.20	0.21	0.23
252.75	0.75	0.27	0.34	0.20	0.20	0.23
259.50	0.69	0.24	0.30	0.15	0.19	0.22
266.25	0.65	0.22	0.31	0.17	0.18	0.21
273.00	0.63	0.21	0.32	0.17	0.18	0.22
279.75	0.61	0.21	0.31	0.16	0.18	0.21
286.50	0.57	0.21	0.30	0.16	0.18	0.21
293.25	0.57	0.19	0.28	0.15	0.17	0.20
300.00	0.51	0.18	0.26	0.13	0.16	0.19
306.75	0.50	0.18	0.25	0.12	0.15	0.17
330.00	0.40	0.18	0.25	0.12	0.17	0.20
360.00	0.30	0.10	0.18	0.06	0.09	0.11

θ = angle in degrees measured from top of pipe, anticlockwise in the direction of flow

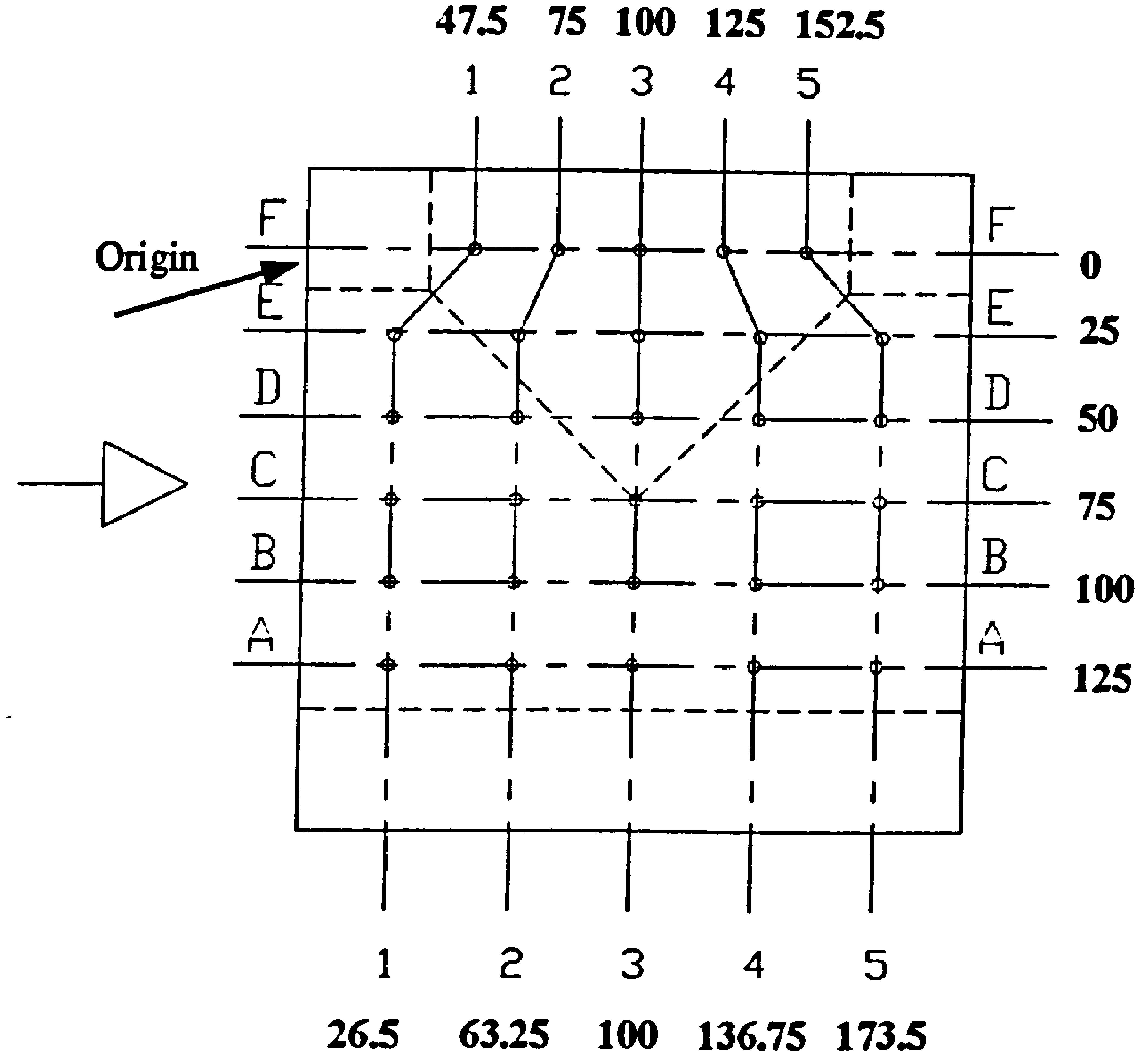

Figure A.1: *Map of wire probes fitted for measurements within the T. Each point is individuated by the co-ordinates of the grid (bold characters), from the indicated origin.*

Table A.4: *Film height from pipe bottom in the T-block (mm). To use in conjunction with figure A.1 for co-ordinates of probes.*

case A1	1	2	3	4	5
F	31.67957	5.520225	0.91301	6.810935	31.07256
E	28.56549	15.01454	8.149756	15.12432	26.86686
D	19.68162	18.53652	11.7376	17.76346	18.77452
C	16.45039	17.56354	17.91419	16.86422	17.35591
B	19.10085	19.08607	19.19657	18.96649	19.93355
A	27.45049	26.7493	26.96293	27.75595	28.07617

case A2	1	2	3	4	5
F	30.69768	5.573398	1.381411	6.603947	31.87044
E	29.13619	17.80427	6.246266	20.81309	27.4899
D	20.92883	19.37223	12.62688	17.73091	18.48289
C	17.5355	17.82996	18.54325	17.20401	17.09822
B	19.95823	20.12588	20.09931	20.45224	21.42504
A	28.77965	27.52475	27.05156	27.41351	27.65852

case A3	1	2	3	4	5
F	28.48139	5.891603	0.684509	7.069668	30.83676
E	28.8317	17.29249	5.983684	20.9029	26.87066
D	20.29437	19.42346	12.15492	19.64486	20.50746
C	17.2982	17.97504	18.75623	17.79767	18.08932
B	20.05419	20.2238	19.95492	19.4871	19.96944
A	28.67731	27.30765	27.35478	27.45199	27.83858

Table A.4: *Continued*

case B1	1	2	3	4	5
F	28.58383	5.639825	1.43992	5.853573	30.72563
E	25.52995	14.39332	3.150937	17.79134	27.39543
D	19.66642	19.41963	11.59987	17.5845	18.57137
C	19.12732	16.67413	18.82013	17.67873	18.42478
B	19.06007	19.83483	19.34962	19.47564	19.51662
A	25.79497	25.06973	25.15618	25.57508	25.8304

case B2	1	2	3	4	5
F	29.14467	5.699633	1.748757	6.060981	31.46097
E	25.63855	14.52661	4.089842	18.8789	28.59373
D	19.90476	19.08135	13.36728	17.09691	19.2944
C	19.34818	16.13657	18.8221	17.16948	17.06021
B	19.81789	19.22767	18.81176	18.10252	17.19095
A	25.88408	24.91861	25.21194	25.49076	25.53194

case B3	1	2	3	4	5
F	27.91104	6.080681	0.934567	5.758675	29.62379
E	25.36528	14.3151	2.52671	17.22104	26.77613
D	19.88802	19.87608	12.47264	17.81499	18.72254
C	18.93464	16.44895	18.26554	17.51846	18.48344
B	19.6644	19.87621	20.10518	20.02628	20.43445
A	26.07666	25.07876	25.13039	25.64143	26.03069

Table A.4: *Continued*

case C1	1	2	3	4	5
F	29.37793	5.554662	1.16438	5.627478	30.43516
E	26.23566	14.39659	2.494264	17.15763	27.21555
D	15.20257	14.6035	9.388496	12.97862	13.99242
C	14.74171	15.44241	15.33322	14.02264	13.7364
B	15.27774	15.13011	14.83721	14.23623	14.11246
A	26.02986	25.15373	25.29764	25.73661	26.03885

case C2	1	2	3	4	5
F	29.47468	5.592036	1.272172	6.127555	31.21937
E	25.84839	14.42188	3.242003	17.97137	27.24935
D	14.77003	13.975	10.4239	12.60909	14.57761
C	13.935	14.9363	14.78212	13.10465	13.26078
B	14.43082	14.45713	13.89924	13.34532	13.12645
A	26.52545	25.73006	25.7532	25.99314	26.01381

case C3	1	2	3	4	5
F	28.70439	5.741218	1.219026	5.649859	30.1982
E	25.85776	14.42164	2.32476	17.10198	27.05435
D	14.88108	14.40668	9.461472	13.56412	14.16062
C	14.83275	14.53679	14.68776	13.67697	14.08464
B	15.25168	15.25235	15.15557	14.72378	14.73081
A	26.36428	25.32066	25.39854	25.72344	26.01903

Table A.4: *Continued*

case D1	1	2	3	4	5
F	28.01329	6.032256	2.041264	6.75337	32.99284
E	24.91663	14.32388	4.968992	19.21535	28.301
D	18.72664	19.08598	14.26925	18.00761	19.74815
C	19.19353	18.59699	21.00818	18.10833	17.47168
B	19.52771	19.71209	19.16202	18.41458	17.7392
A	25.48967	24.96781	25.21906	25.6114	25.76439

case D2	1	2	3	4	5
F	32.29225	8.659878	2.269801	7.732845	33.33225
E	25.41381	14.25983	1.070132	14.37106	30.28611
D	19.30352	19.43576	13.42811	20.16031	19.11327
C	19.85579	18.33823	19.24923	14.96298	13.60213
B	19.7961	18.91838	17.06533	14.0234	12.52137
A	25.73177	25.1004	25.01915	25.19708	25.32856

case D3	1	2	3	4	5
F	27.84461	5.65783	1.953229	6.041414	31.03234
E	25.03879	14.0188	3.532327	18.26592	27.34467
D	19.78523	19.23184	14.77245	17.52548	18.18653
C	19.66099	18.26629	20.49915	17.16131	16.6812
B	20.08335	19.58496	19.14295	18.33511	18.09373
A	25.99577	25.22156	25.16803	25.37922	25.37436

Table A.4: *Continued*

case E1	1	2	3	4	5
F	28.18385	5.693891	1.182144	6.02172	30.81766
E	25.02484	13.94516	2.500878	17.56065	26.99585
D	14.41409	14.03382	9.376636	12.59844	14.426
C	13.9681	13.61067	15.21356	12.83476	12.39187
B	14.77878	14.3902	14.73687	13.96292	13.34267
A	25.55864	24.90317	25.15622	25.5655	25.73125

case E2	1	2	3	4	5
F	28.78291	5.56617	1.478771	6.377603	31.4741
E	24.97737	13.94732	3.648639	18.37841	28.21144
D	14.99276	14.63358	9.849038	15.38901	15.54448
C	14.40325	13.91535	13.71966	10.55271	9.707312
B	14.53572	13.70663	12.51006	10.05698	8.316882
A	25.44531	25.9905	27.41741	29.1169	30.68515

case E3	1	2	3	4	5
F	27.89841	5.741991	1.215945	5.740448	29.88009
E	24.93194	13.87302	1.866558	16.49807	27.55844
D	14.82884	14.36088	9.989137	12.25518	13.22617
C	13.96727	13.69131	14.79054	12.7434	12.6012
B	14.35436	14.44769	14.50962	14.23068	14.40169
A	25.68674	24.98866	25.18631	25.55494	25.81363

Table A.4: *Continued*

case F1	1	2	3	4	5
F	28.34426	5.443722	1.016897	6.496903	30.37748
E	25.24681	14.00087	2.038959	16.53435	26.36997
D	12.28798	12.17413	8.752536	11.35426	12.84458
C	11.72003	9.429269	8.60633	10.13687	10.6066
B	12.38027	12.38983	13.54663	10.95948	10.68609
A	25.54887	25.77141	25.63313	25.70814	25.48533

case F2	1	2	3	4	5
F	28.70828	5.495404	1.212097	7.155446	32.14555
E	25.45727	13.86374	2.801629	19.27787	27.9902
D	12.75176	13.3847	10.93123	13.43918	14.44015
C	11.92622	4.452147	5.821682	7.70244	7.872613
B	14.88395	13.8684	11.80112	9.175919	6.994519
A	25.6682	25.29424	25.36092	25.67365	25.75352

case F3	1	2	3	4	5
F	27.91782	5.770275	1.102373	5.63941	29.44507
E	25.44457	13.82983	1.481788	15.99454	25.98774
D	12.12063	12.20728	7.066761	11.01223	12.00092
C	12.13702	10.00589	11.20817	11.17569	11.39414
B	14.54669	14.13322	13.56454	12.73215	12.11975
A	25.35298	24.83323	25.0809	25.53118	25.77905

Appendix B

Table B.1: *split data for the vertical T-junction, 0.076 m ID.*

U_{gs} (m/s)	U_{ls} (m/s)	Series	Run length (m)	G'	L'
3.8	0.8	B	1.9	0.93	1.00
				0.91	1.00
				0.85	0.77
				0.69	0.33
				0.15	0.08
				0.91	1.00
				0.89	1.00
				0.64	0.41
				0.46	0.21
				0.22	0.13
				0.55	0.27
				0.65	0.31
				0.71	0.41
				0.78	0.51
				0.80	0.62
				0.89	0.88
				0.91	1.00
				0.49	0.23
				0.32	0.16
				0.52	0.25
				0.69	0.41
				0.68	0.43
				0.26	0.15
				0.66	0.32
3.8	1.56	B	1.9	0.86	0.63
				0.82	0.60
				0.75	0.39
				0.55	0.24
				0.15	0.06
				0.80	0.62
				0.75	0.51
				0.63	0.31
				0.41	0.21
				0.28	0.13
				0.83	0.63
				0.85	0.67
				0.88	0.63
				0.85	0.64
				0.83	0.62
				0.85	0.67
				0.94	0.86
				0.96	0.95
				0.85	0.64

Table B.1: *Continued*

U_{gs} (m/s)	U_{ls} (m/s)	Series	Run length (m)	G'	L'
2.2	0.8	B	1.9	0.94	1.00
				0.90	1.00
				0.84	0.93
				0.78	0.70
				0.71	0.53
				0.64	0.42
				0.59	0.43
				0.57	0.43
				0.51	0.36
				0.41	0.25
				0.33	0.21
				0.18	0.07
				0.07	0.01
2.2	1.56	B	1.9	1.00	0.98
				0.91	0.92
				0.89	0.85
				0.83	0.63
				0.75	0.43
				0.63	0.37
				0.48	0.25
				0.39	0.21
				0.27	0.12
				0.20	0.08
				0.15	0.04
				0.53	0.34
				0.64	0.43
				0.77	0.53
				0.84	0.68

Table B.1: *Continued*

U_{gs} (m/s)	U_{ls} (m/s)	Series	Run length (m)	G'	L'
10	0.8	B	1.9	0.64	0.23
				0.62	0.28
				0.56	0.26
				0.58	0.18
				0.54	0.19
				0.47	0.21
				0.47	0.18
				0.43	0.18
				0.34	0.17
				0.10	0.08
				0.37	0.16
				0.44	0.21
				0.50	0.23
				0.58	0.26
				0.63	0.26
				0.65	0.27
				0.64	0.26
				0.71	0.35
				0.86	0.38
				0.92	0.64
				0.92	0.70
				0.94	0.86
				0.93	0.86
				0.92	0.69
				0.76	0.28
				0.65	0.26
				0.63	0.28
				0.60	0.19
				0.46	0.22
				0.31	0.15

Table B.1: *Continued*

U_{gs} (m/s)	U_{ls} (m/s)	Series	Run length (m)	G'	L'
3.8	0.8	B	0.7	0.74	0.33
				0.73	0.31
				0.67	0.29
				0.52	0.23
				0.40	0.20
				0.12	0.09
				0.93	0.87
				0.91	0.72
				0.86	0.59
				0.81	0.45
				0.77	0.35
				0.72	0.31
				0.38	0.21
				0.49	0.22
				0.65	0.29
3.8	1.56	B	0.7	0.78	0.31
				0.77	0.31
				0.71	0.26
				0.48	0.21
				0.23	0.12
				0.78	0.33
				0.80	0.33
				0.84	0.44
				0.90	0.58
				0.93	0.68
				0.58	0.24
				0.42	0.20
2.2	0.8	B	0.7	0.9	0.77
				0.89	0.73
				0.74	0.46
				0.51	0.28
				0.44	0.26
				0.13	0.08
				0.95	0.96
				0.95	0.92
				0.94	0.91
				0.93	0.86
				0.93	0.87
				0.93	0.86
				0.80	0.60
				0.61	0.33
				0.30	0.19
				0.92	0.83

Table B.1: *Continued*

U_{gs} (m/s)	U_{ls} (m/s)	Series	Run length (m)	G'	L'
10	0.8	B	0.7	0.64	0.25
				0.62	0.24
				0.57	0.24
				0.42	0.21
				0.08	0.10
				0.93	0.81
				0.91	0.64
				0.88	0.45
				0.78	0.35
				0.70	0.29
				0.65	0.26
				0.20	0.15
				0.89	0.47
				0.86	0.36
				0.34	0.19
3.8	0.04	D	0.7	0.50	1.00
				0.50	1.00
				0.49	1.00
				0.46	0.97
				0.18	0.76
				0.39	0.96
				0.07	0.16
				0.11	0.41
				0.13	0.42
				0.24	0.92

Table B.1: *Continued*

U_{gs} (m/s)	U_{ls} (m/s)	Series	Run length (m)	G'	L'
10	0.04	D	0.7	0.49	0.44
				0.47	0.46
				0.40	0.42
				0.10	0.35
				0.50	0.38
				0.54	0.42
				0.89	0.87
				0.04	0.21
				0.25	0.35
				0.49	0.45
				0.77	0.85
				0.78	0.73
				0.67	0.56
				0.52	0.44
				0.52	0.45
				0.49	0.47
				0.54	0.52
				0.34	0.41
				0.55	0.39
				0.10	0.31
				0.94	1.00
				0.02	0.10
10	0.02	D	0.7	0.54	0.51
				0.54	0.42
				0.52	0.43
				0.45	0.43
				0.16	0.23
				0.03	0.09
				0.37	0.33
				0.60	0.44
				0.77	0.79
				0.79	0.88
				0.66	0.57
				0.67	0.60
				0.23	0.20
				0.91	1.00

Table B.1: *Continued*

U_{gs} (m/s)	U_{ls} (m/s)	Series	Run length (m)	G'	L'
3.8	0.02	D	0.7	0.07	0.42
				0.08	0.43
				0.11	0.61
				0.29	0.96
				0.43	1.00
				0.20	0.96
				0.11	0.64
				0.06	0.29
				0.06	0.23
				0.14	0.85

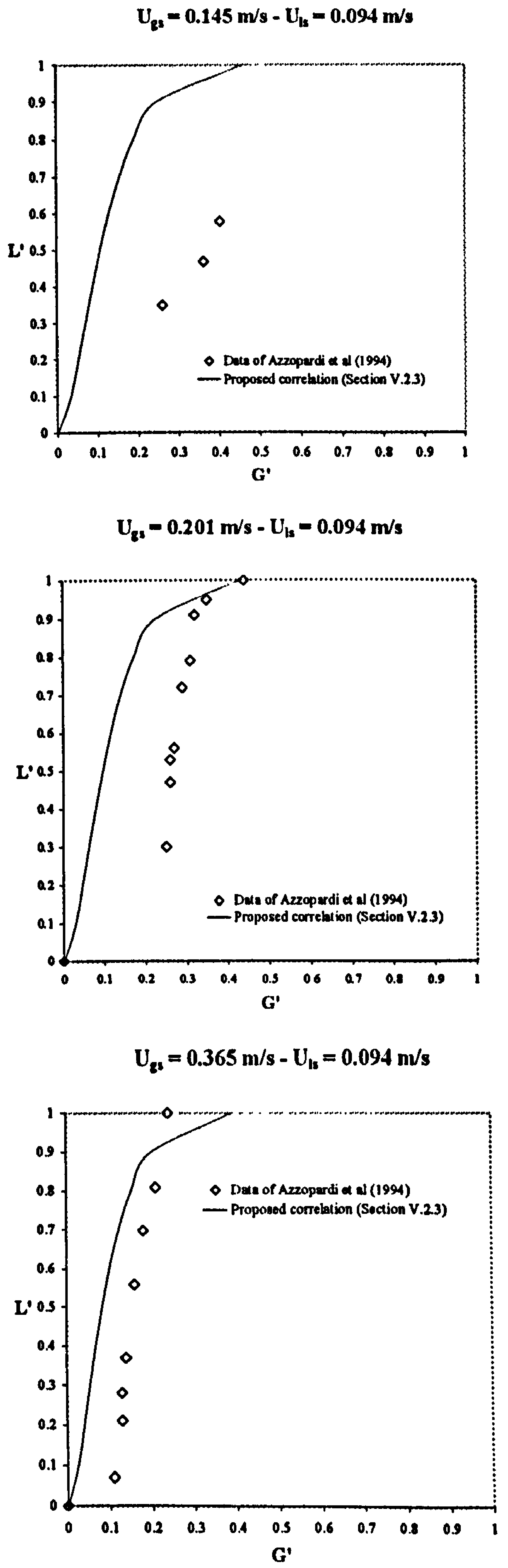

Figure: B.1: *Comparison of data from Azzopardi et al (1994) in the slug flow regime, with the correlation developed in section V.2.3.*

U_{gs} = 0.896 m/s - U_{ls} = 0.091 m/s

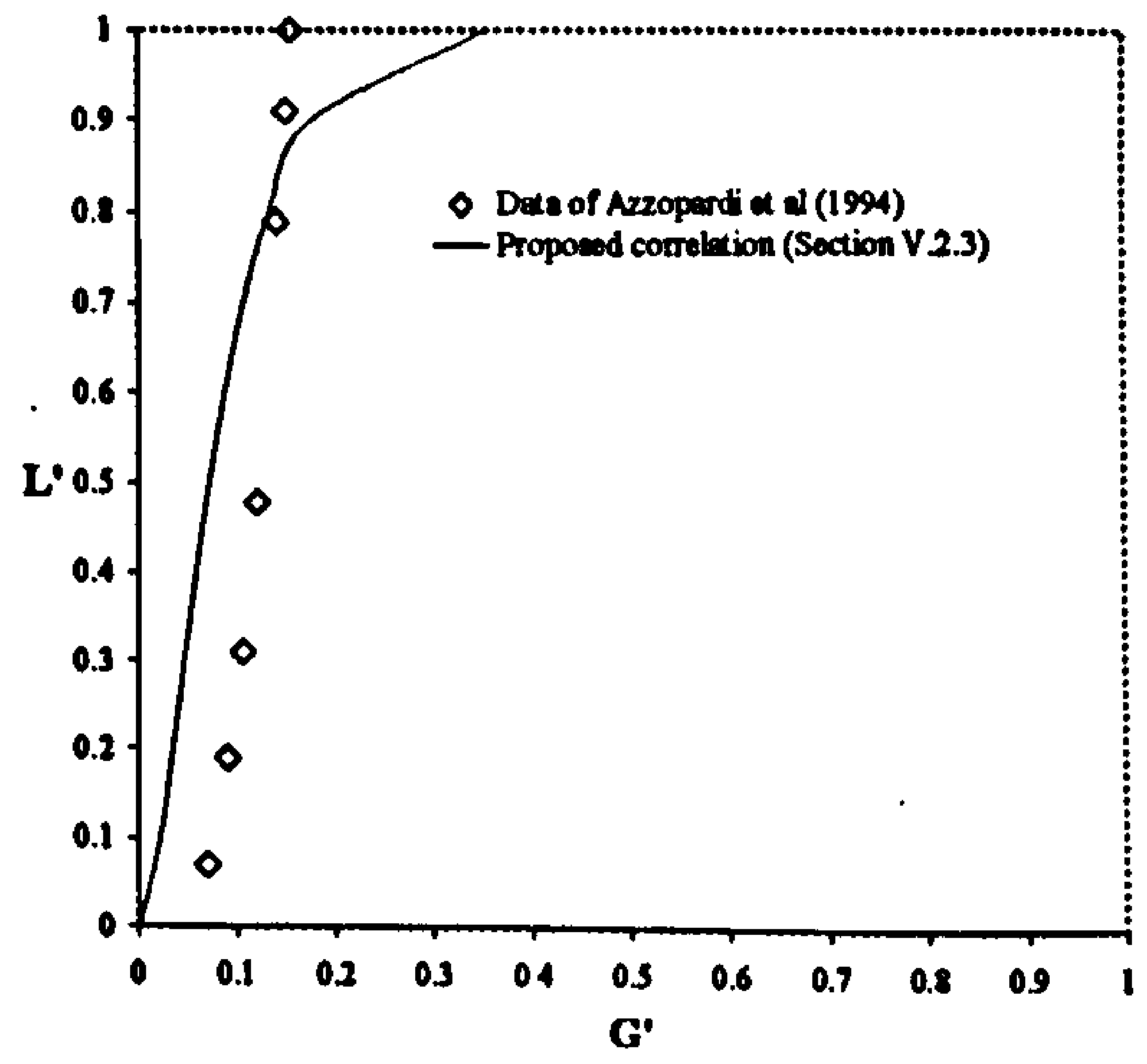

U_{gs} = 1.110 m/s - U_{ls} = 0.094 m/s

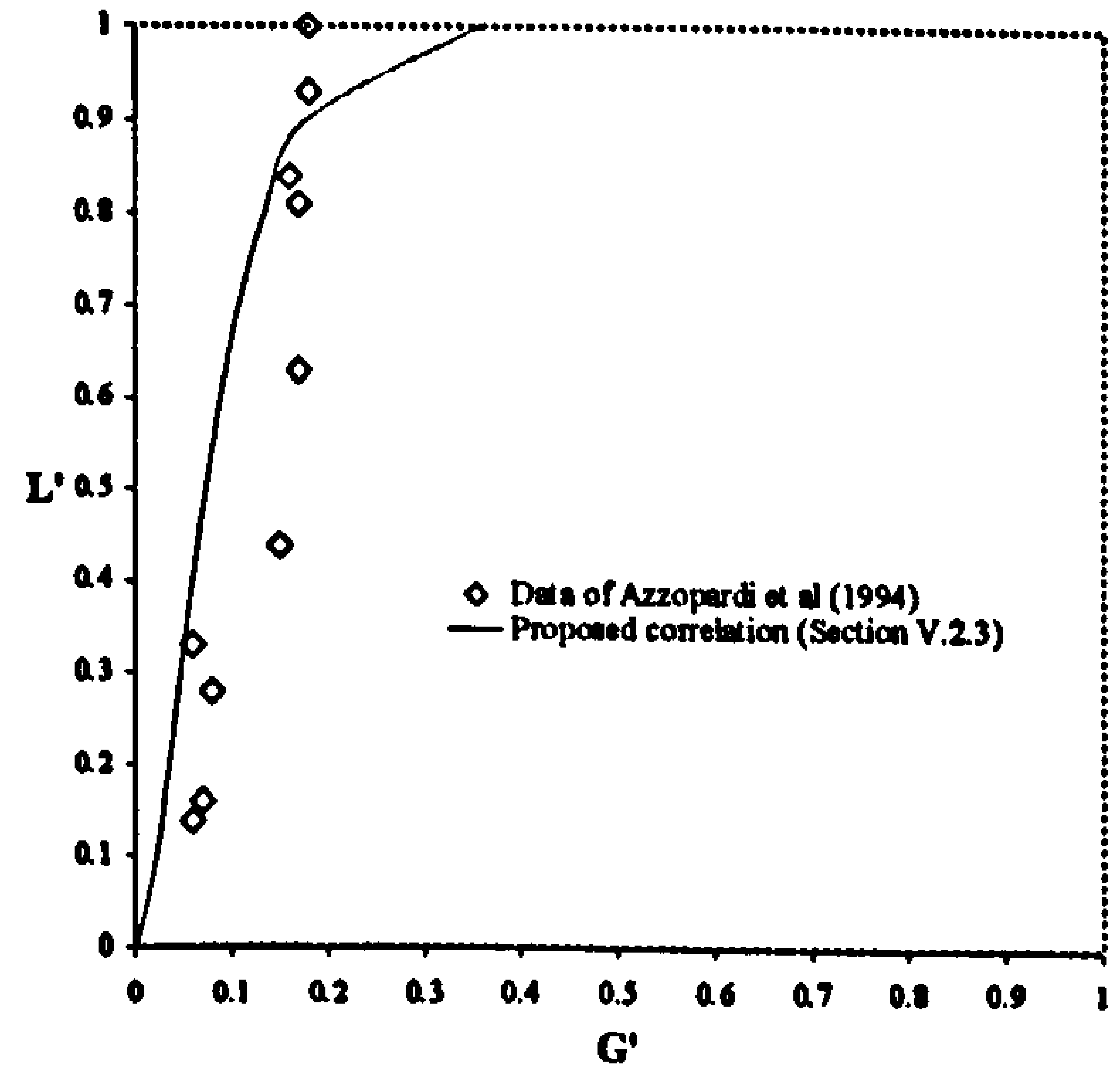

U_{gs} = 0.633 m/s - U_{ls} = 0.094 m/s

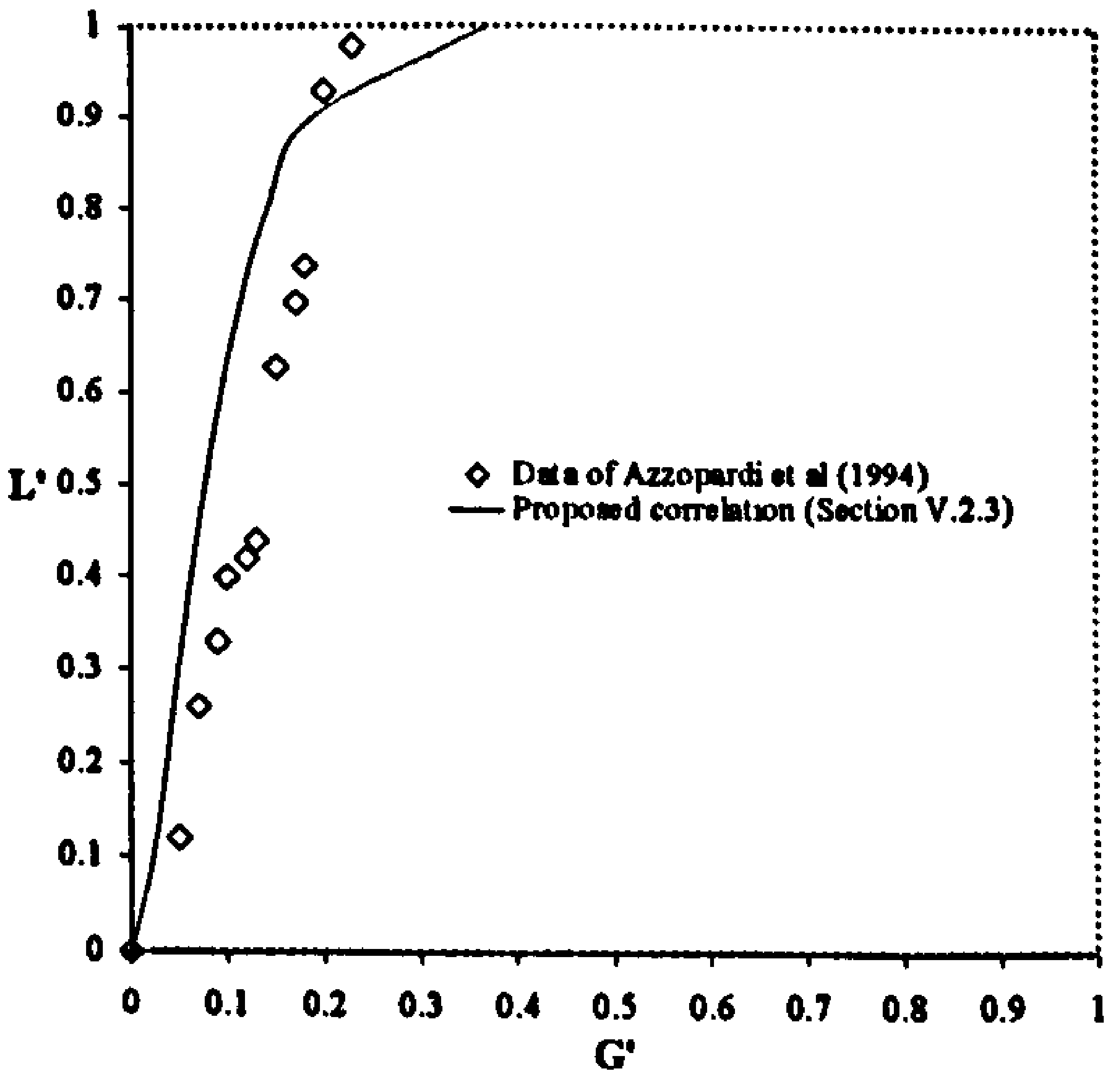

Figure B.1: *Continued*

U_{gs} = 0.164 m/s - U_{ls} = 0.204 m/s

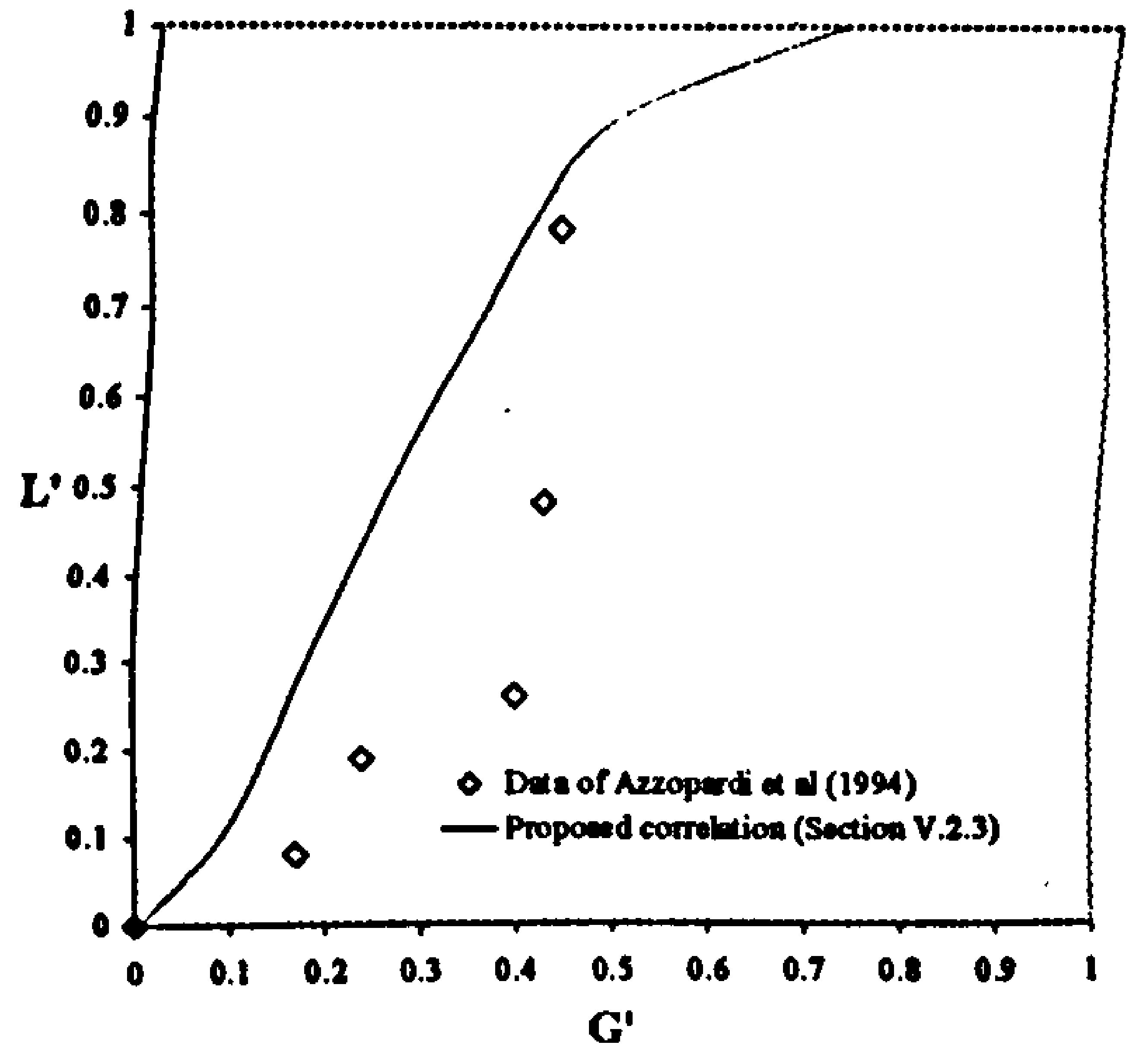

U_{gs} = 0.201 m/s - U_{ls} = 0.204 m/s

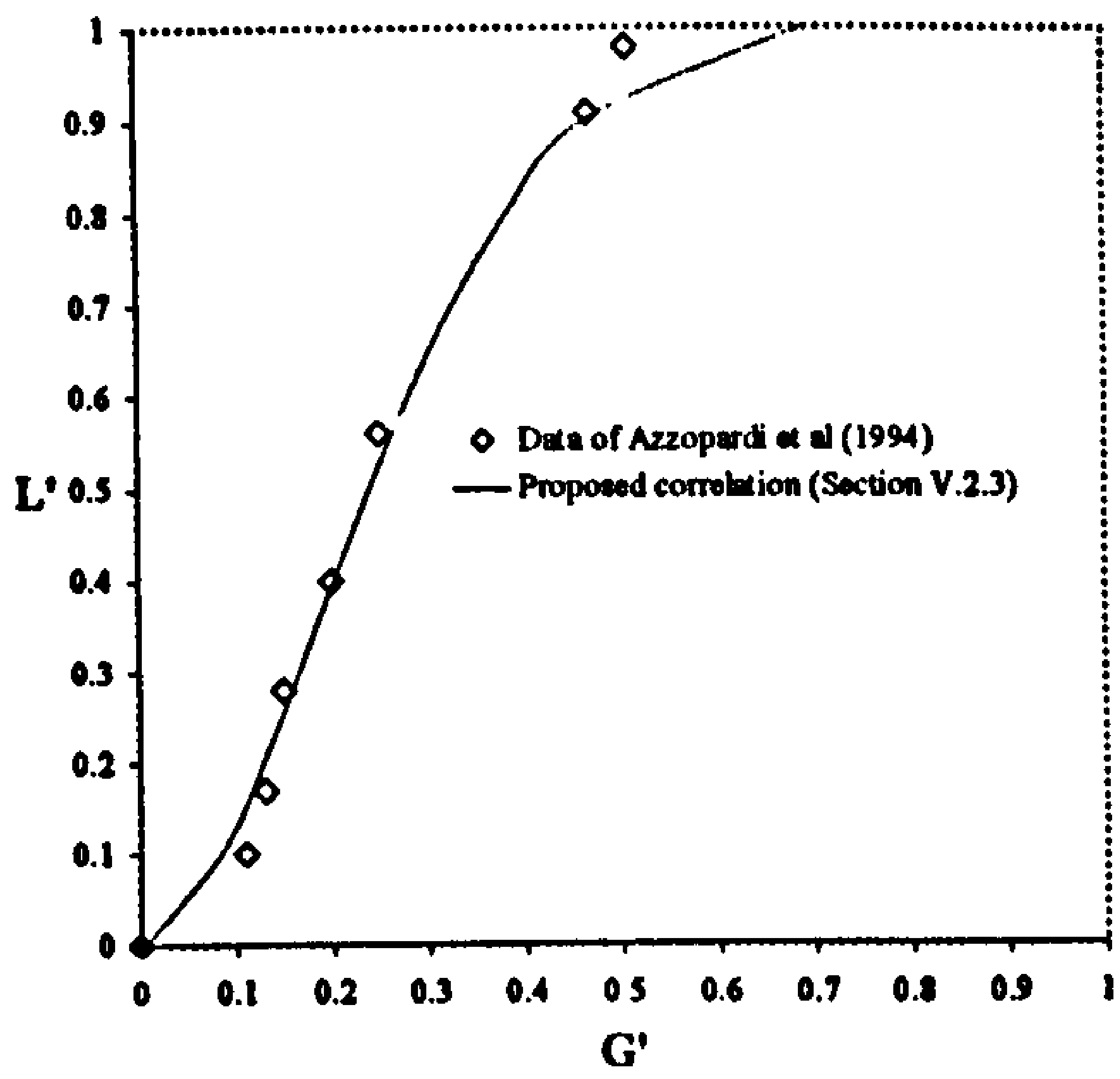

U_{gs} = 0.365 m/s - U_{ls} = 0.204 m/s

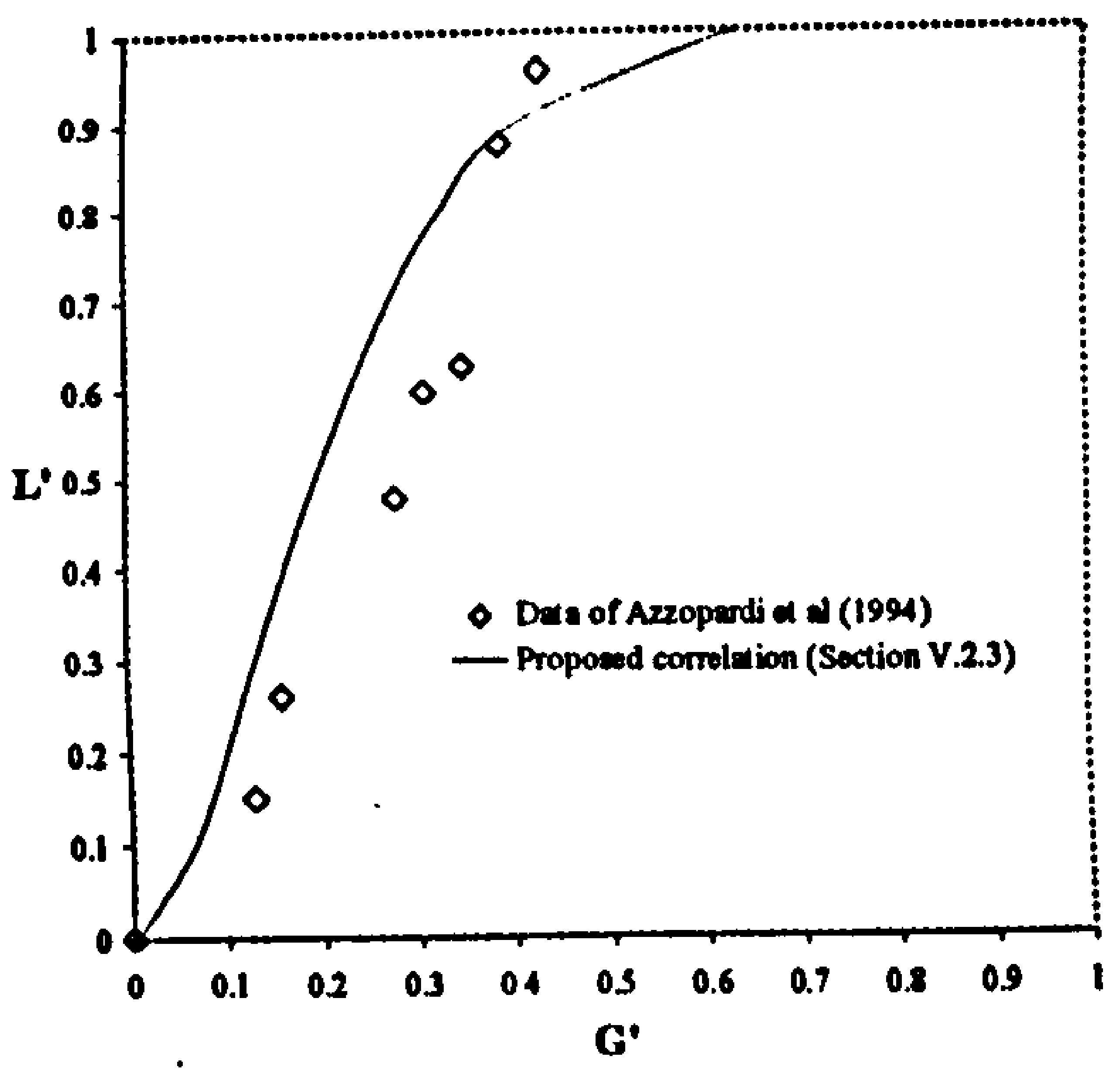

Figure B.1: *Continued.*

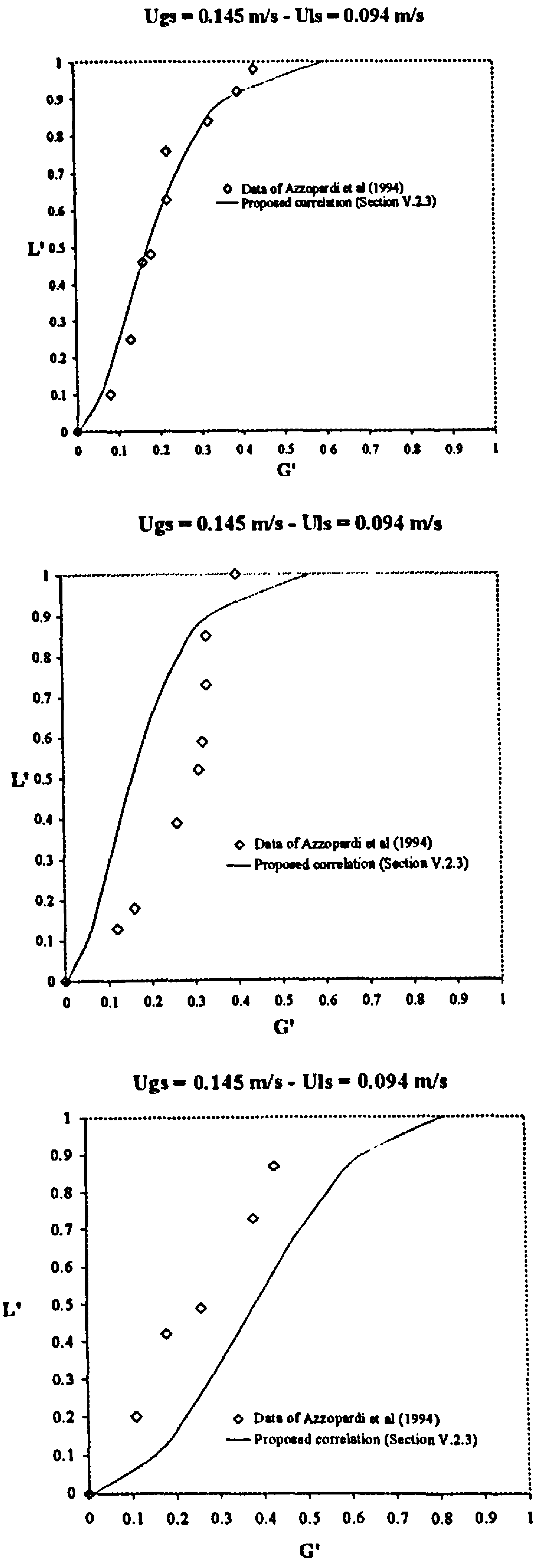

Figure B.1: *Continued.*

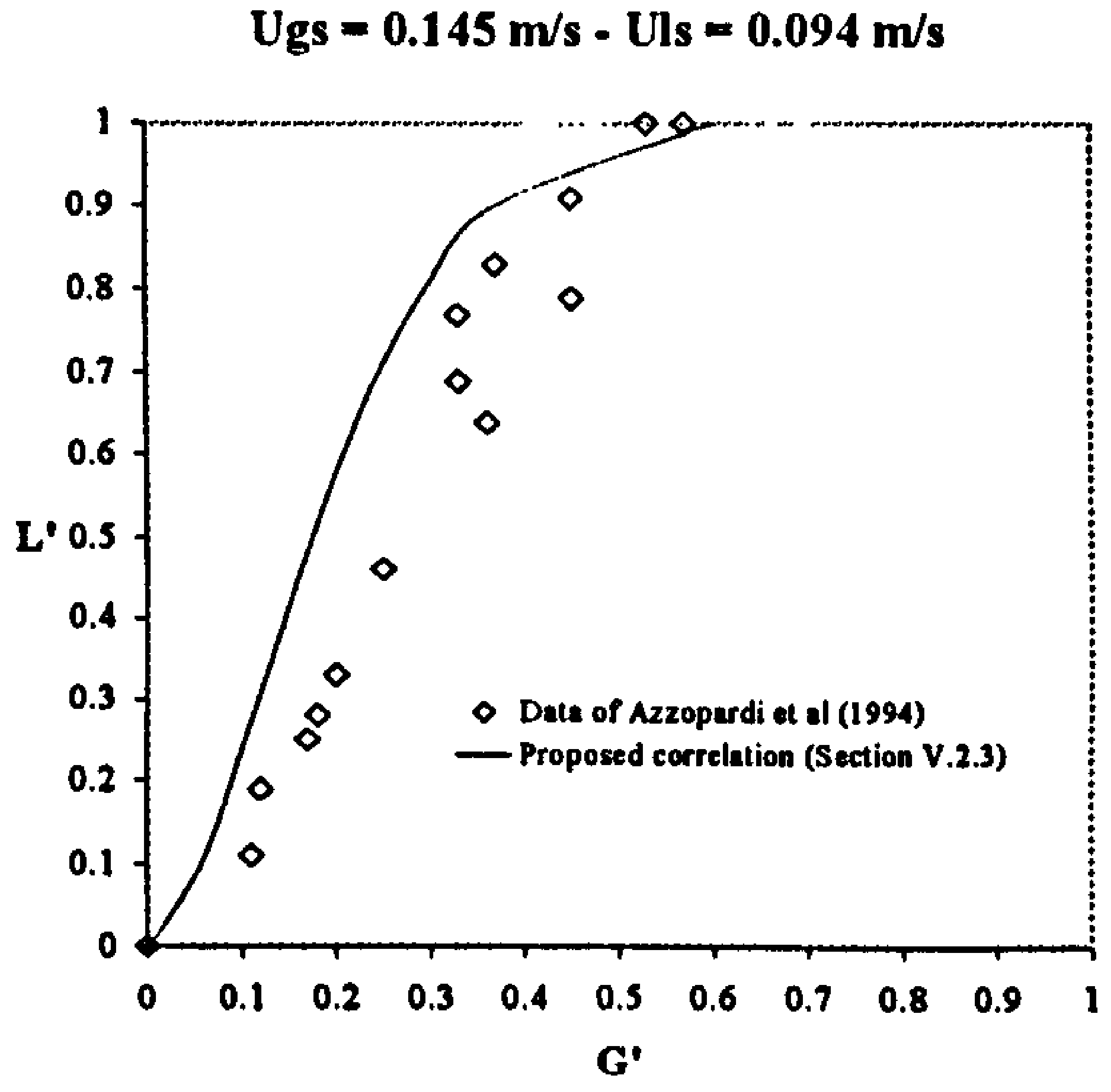

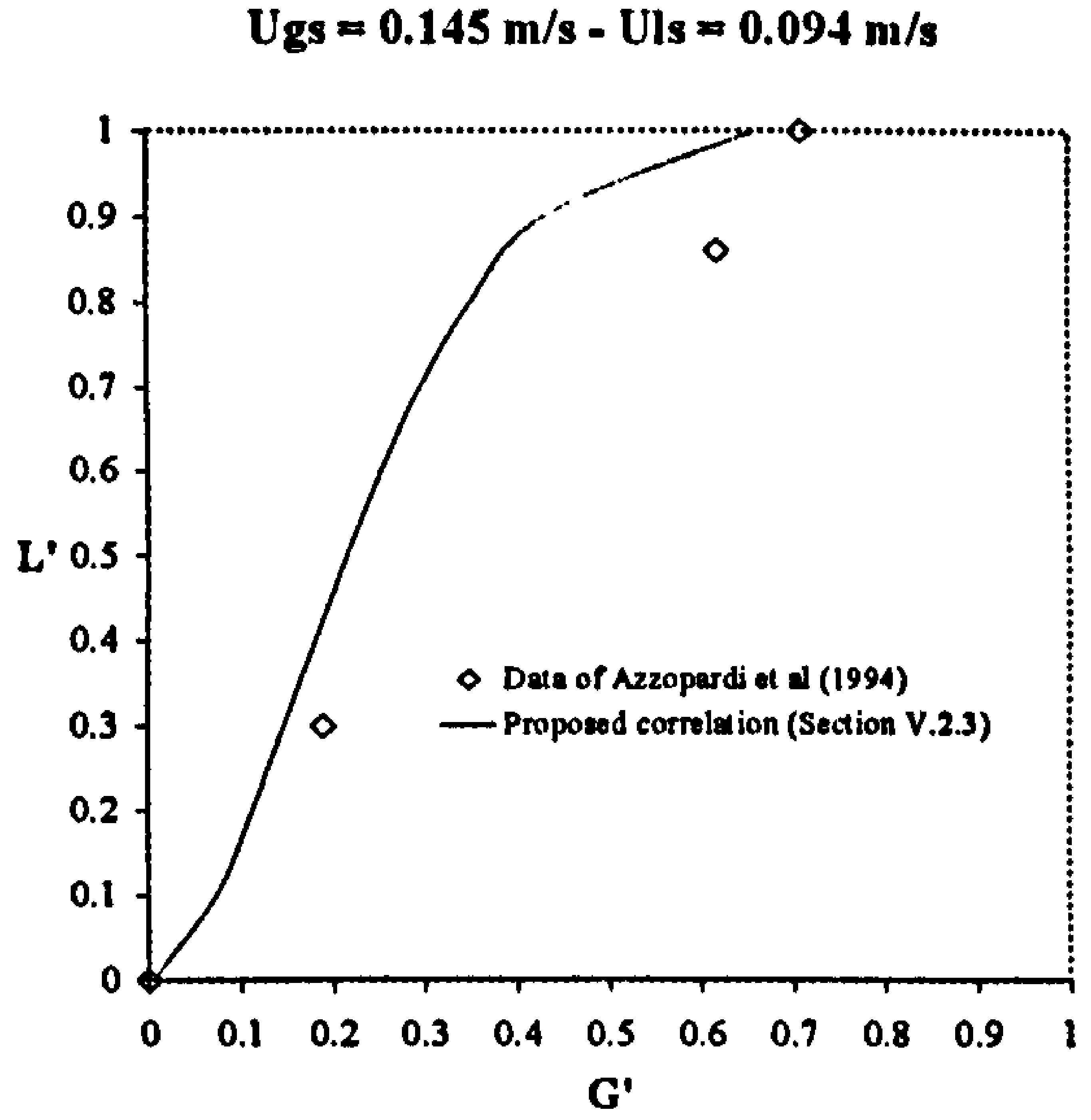

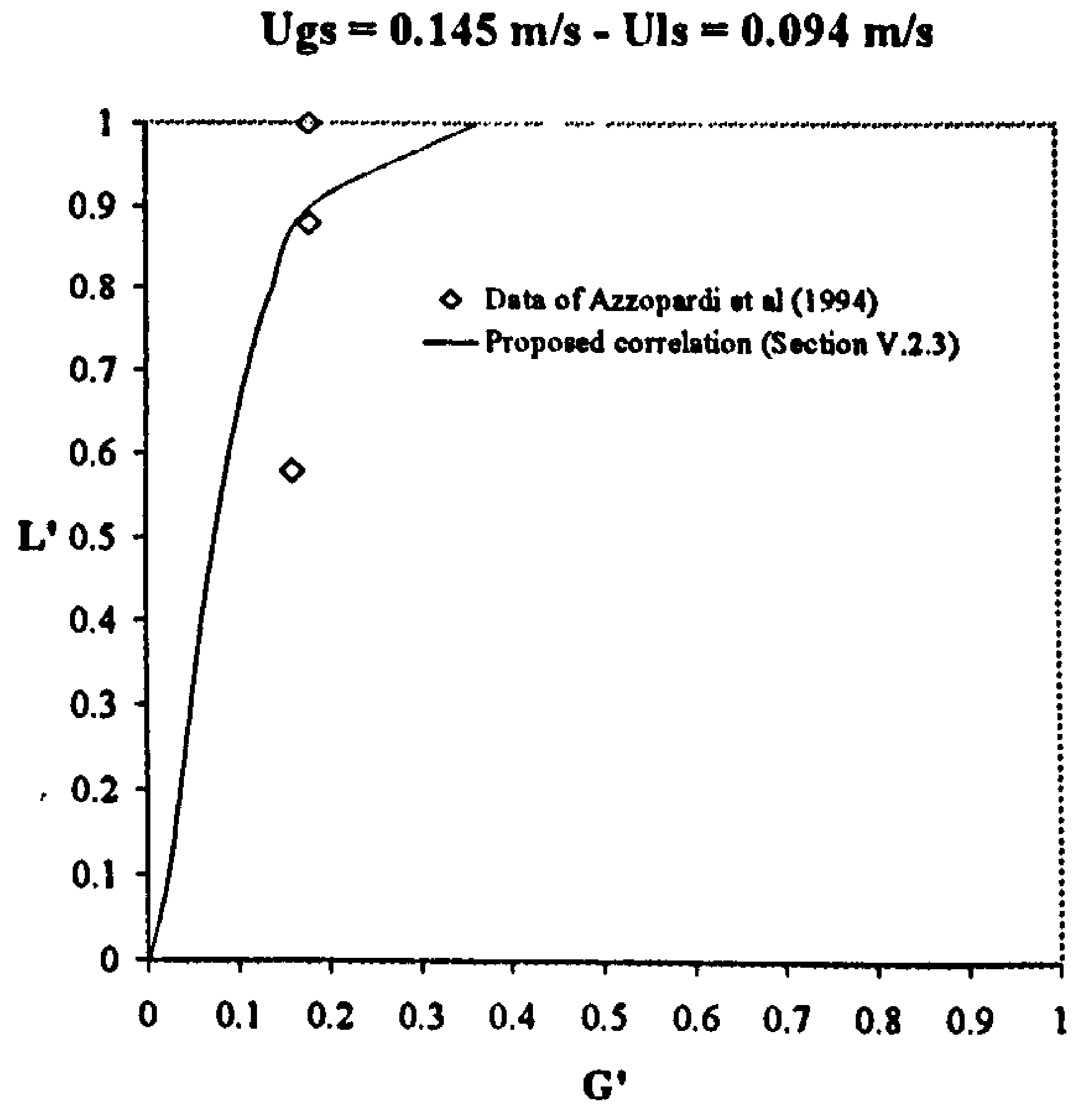

Figure B.1: *Continued.*

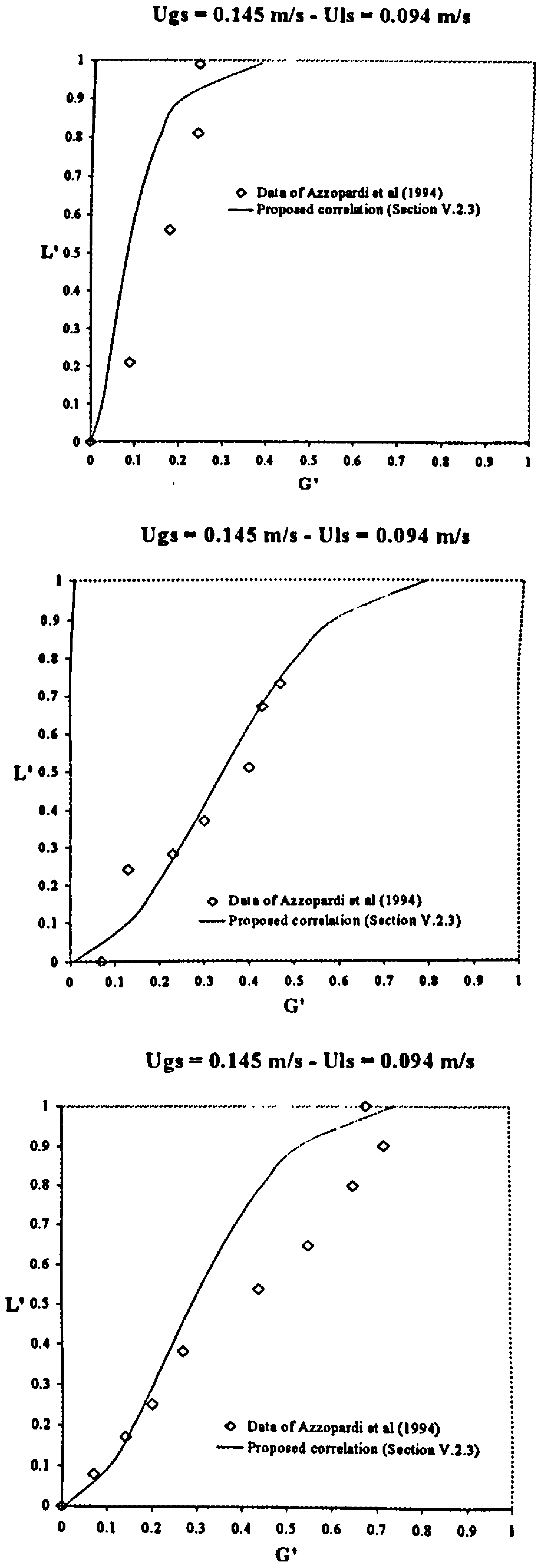
Ugs = 0.145 m/s - Uls = 0.094 m/s

Ugs = 0.145 m/s - Uls = 0.094 m/s

Ugs = 0.145 m/s - Uls = 0.094 m/s

Figure B.1: *Continued.*

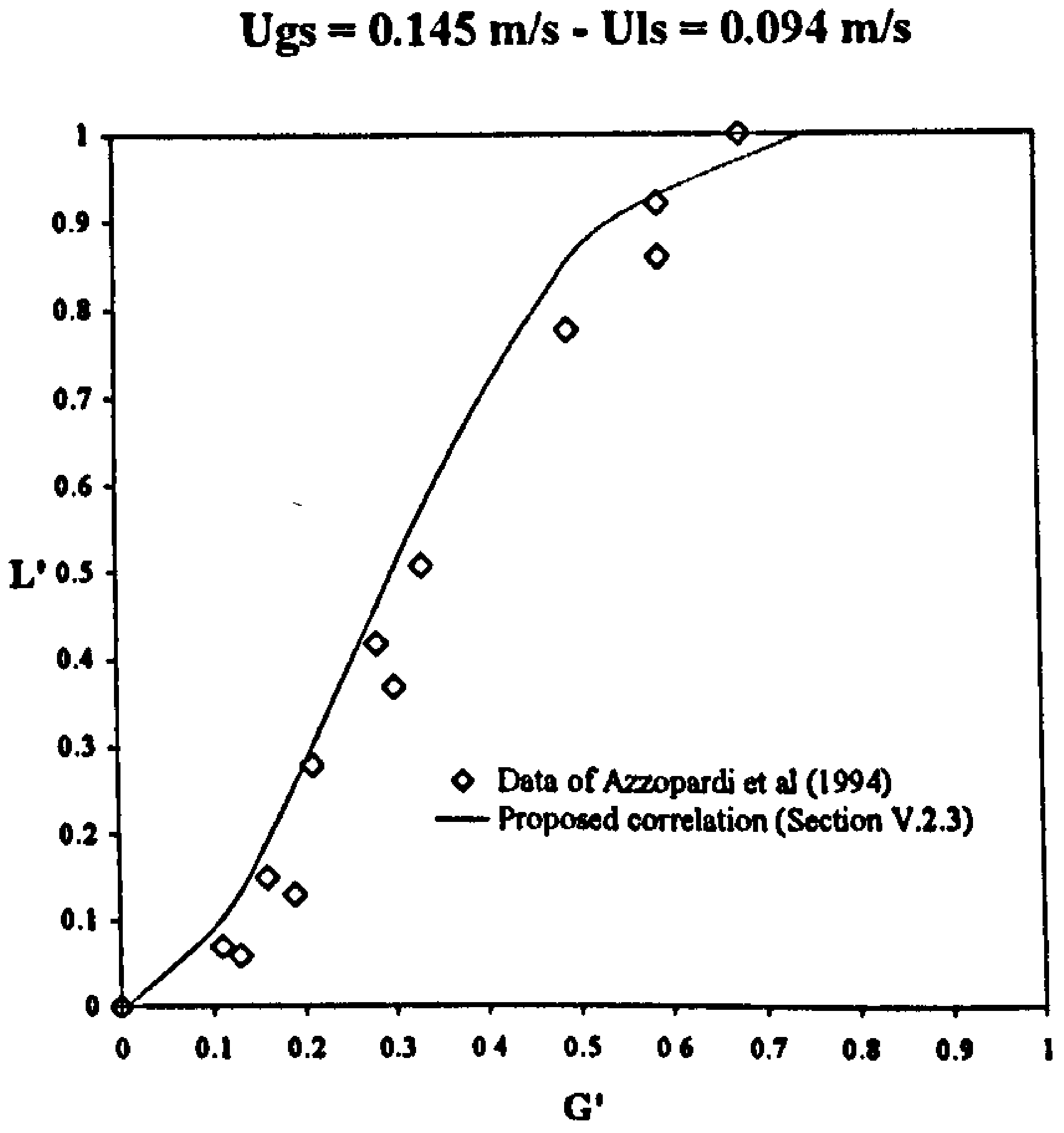

Figure B.1: *Continued.*